UNIVERSITÀ DEGLI STUDI DI TRIESTE

XXXVI CICLO DEL DOTTORATO DI RICERCA IN

BIOMEDICINA MOLECOLARE

HELP-based recombinant biopolymers: a versatile platform to realise antimicrobial interfaces for orthopaedic applications

Settore scientifico-disciplinare: BIO/11

Dottoranda:

Laura Colomina Alfaro

Coordinatore:

Prof. Alessandro Tossi

Supervisore di tesi:

Dr. Antonella Bandiera

Co-supervisore di tesi:

Prof. Alessandro Tossi

ANNO ACCADEMICO 2022/2023

"One never notices what has been done; one can only see what remains to be done"

Marie Curie

A mima y a pipo

Abstract

The work presented in this thesis was done within the MSCA-ITN Horizon 2020 AIMed project, which aims to develop materials with antibacterial properties suitable for use on the surfaces of orthopaedic implants.

Implant-associated infections are one of the major issues in orthopaedic procedures, often leading to implant failure. The materials employed to manufacture implants do not possess antimicrobial (AM) properties, and they are often modified to enhance osteointegration with the bone tissue, raising the likelihood of microorganism colonisation. Bacterial adhesion to the surface facilitates biofilm formation, which is highly resistant to antibiotic treatment and immune responses. In addition, bacterial resistance has been observed for almost all antibiotics, becoming an alarming threat, mainly due to the emergence of multidrug resistance phenotypes. To withstand bacterial infections, antimicrobial peptides (AMP) are currently considered potential next-generation antimicrobials, with mechanisms of action less prone to induce resistance. Thus, novel strategies rely on AMP employment to contrast infections and overcome AM resistance. Nevertheless, AMP clinical use is still limited, mainly due to several constraints of their production by chemical synthesis, such as high costs, low yields, and toxic reagents and waste. In the last two decades, several AMPs have been produced by recombinant expression and among the proposed fusion carriers, Elastin-like Polypeptides (ELPs) represent a biotechnological platform that offers valuable advantages, allowing a simple purification strategy resulting in high yields and reduced costs. Thus, the Human Elastin-like Polypeptide (HELP) was chosen as the carrier for AMP production due to this platform's advantages. For instance, unlike other ELPs, HELP mimics tropoelastin, possessing the cross-linking domains that allow the production of stable hydrogel matrices and composites. Furthermore, they are the preferred target for elastase degradation, which can trigger the release of the functional fusion domains.

Herein, we describe the design, production and characterisation of a fusion construct of HELP with indolicidin (named HIn). This work aimed to ascertain the potential of the HELP carrier for AMP production and realise 2D and 3D biomaterials endowed with AM activity. The indolicidin domain did not affect HIn production in *Escherichia coli* nor the thermo-responsive behaviour of HELP, which was employed to purify the fusion protein. HIn AM activity assessment showed that the fusion construct was strongly active toward *Pseudomonas aeruginosa* and that the HIn-based coatings could extensively disrupt the bacterial cells. In addition, despite the intact HIn-matrices being permissive to bacterial growth, the release of the AMP domain, either by specific endoproteinases or due to elastase degradation of the HELP moiety, restored the AM capacity of indolicidin. Thus, the HIn construct served as a model for producing AMPs and derived materials endowed with AM properties exploiting the HELP fusion carrier.

Further, we explored the HELP carrier to produce the difficult-to-synthesise sequence of the human β-defensin 1 (hBD1). This HELP fusion construct, named HhBD1, was successfully produced in *E. coli*, purified employing the HELP transition properties and physico-chemically characterised. HhBD1 carries six cysteines crucial for its activity since the redox state of the macromolecule determines its AM capacity. Thus, the AM potential of the fusion biopolymer and its release products against *E. coli* was evidenced using a radial diffusion assay under redox conditions. Unexpectedly, HhBD1-derived materials, such as coatings and matrices, showed a strong cell adhesion-promoting activity, a property that, to our knowledge, has not been described for hBD1 yet.

Finally, the possibility of improving the HELP carrier performance was explored. A new ELP carrier sequence (named UELP) was designed by aligning several vertebrates' tropoelastin primary structures, and a new synthetic gene was inserted in a plasmid vector for its recombinant expression in *E. coli*. Its physico-chemical characterisation showed enhanced transition capacity compared to HELP. Intriguingly, UELP displayed a strong potential to induce cell adhesion. Future work will aim to ascertain the suitability of UELP as a carrier for AMP production.

These results confirmed that the HELP carrier represents a versatile, environmentally friendly, multitasking platform for cost-effectively producing smart fusion constructs and derived materials endowed with AM capacity. The fusion with the hBD1 showed the potential of the HELP system for functional studies, using the unmodified HELP as the non-functional control. Compared to HELP, the UELP carrier showed enhanced thermo-responsive behaviour and the capacity to promote cell adhesion. These properties highlight its potential for producing AMPs and developing smart AM materials and surfaces.

Table of Contents

Glossary

This section provides a non-exhaustive glossary of the most relevant acronyms for the work presented in this thesis. Their full terms and brief definitions are included for clarity. In addition, throughout the thesis, all acronyms are introduced as full terms upon their first occurrence in each chapter.

Acronym	Term	Definition
AM	Antimicrobial	Agent that kills microorganisms or inhibits their growth.
AMP	Antimicrobial Peptide	Short peptides, mainly cationic, that possess antimicrobial properties, targeting bacteria, fungi, viruses, and even cancer cells (section 1.2)
MDR	Multidrug Resistance	The ability of microorganisms or cells to withstand the effects of multiple drugs, often leading to treatment challenges
ELP	Elastin-like Polypeptides	Stimuli-responsive, genetically engineered biopolymers based on elastin and characterised by their peculiar property of coacervation (section 1.4)
ELP-AMP	ELP fused to an AMP	Fusion protein where an antimicrobial peptide is produced at the C-terminal of an elastin-like polypeptide (Chapter 3)
AMP-ELP	ELP fused to an AMP	Fusion protein where an antimicrobial peptide is produced at the N-terminal of an elastin-like polypeptide (Chapter 3)
ELP-AMP-ELP	ELP fused to an AMP	Fusion protein where an antimicrobial peptide is produced between two elastin-like polypeptides (Chapter 3)
HELP	Human Elastin-like Polypeptide	Elastin-like polymer composed of the hexapeptidic repeat found in human tropoelastin (VAPGVG) as well as its hydrophilic (cross-linking) domain, closely resembling the native tropoelastin primary structure (section 1.4.5)
In	Indolicidin	A well-characterised antimicrobial peptide derived from bovine neutrophils belonging to the family of cathelicidins (section 1.2.2.2 offers a brief overview of the cathelicidins family and in section 1.2.2.2.1 the main properties of indolicidin are summarised)
HIn	HELP-indolicidin	Recombinant fusion protein designed, produced and characterised in the present thesis, where indolicidin was fused at the C-terminal of the Human Elastin-Like Polypeptide (Chapter 4)
hBD1	human β-defensin 1	An antimicrobial peptide from the defensin family, part of the innate immune system, with antimicrobial activity and immunomodulatory properties (section 1.2.2.1 offers a brief overview of the defensin family and in section 1.2.2.1.1 the main properties of human β-defensin 1, mainly regarding its antimicrobial capacity, are summarised)

oxhBD1	Oxidised form of the human β-defensin 1	The form of human β-defensin 1 where the disulfide bridges are arranged in the pattern C1-C5, C2-C4, and C3-C6, stabilizing its 3D structure. This form is active against some Gram-negative bacteria and fungi (section 1.2.2.1.1)
Trx	Thioredoxin	A key component of the antioxidant system. Thioredoxin plays a crucial role in the reduction of human β-defensin 1 in the epithelial lumen (section 1.2.2.1.1)
redhBD1	Reduced form of the human β-defensin 1	The form of human β-defensin 1 where all cysteines are in a reduced state (without disulfide bonds). This is the most active form against Gram-positive bacteria (section 1.2.2.1.1)
HhBD1	HELP-human β-defensin 1	Recombinant fusion protein designed, produced and characterised in the present thesis, where the human β-defensin 1 was fused at the C-terminal of the Human Elastin-Like Polypeptide (Chapter 5)
UELP	Universal Elastin-like Polypeptides	New elastin-like polypeptide developed during this thesis (Chapter 6)
MIC	Minimum Inhibitory Concentration	The lowest concentration of an antimicrobial agent that inhibits the growth of a microorganism (section 1.2.1.6)
LCST	Lower Critical Solution Temperature	The temperature below which a polymer solution is miscible and above which it separates into two phases (section 1.4.2)
Tt	Temperature transition	The temperature at which a phase change occurs, such as a transition from a solid to a liquid state (section 1.4.2)
ITC	Inverse Transition Cycling	Purification method that exploits the phase transition properties of the elastin-like polypeptides (section 1.4.3)
TGase	Transglutaminase enzyme	Enzyme that catalyses the formation of covalent bonds between the γ-carboxamide group of glutamine and the free amine group of lysine in proteins or peptides. In this work, it was employed to covalently cross-link HELP-based biopolymers into stable hydrogel matrices (sections 1.4.4.2 and 1.4.5, chapters 4 and 5)
Glu-C	Glutamyl endopeptidase	Serine proteinase which preferentially cleaves peptide bonds C-terminal to glutamic acid residues (chapters 4 and 5)
Asp-N	Endoproteinase Asp-N (flavastacin)	Zinc metalloendopeptidase which selectively cleaves protein and peptide bonds N-terminal to aspartic acid residues (chapters 4 and 5)
NP	Non-treated Polystyrene	Type of polystyrene surface used in this work as a non-adhesive surface. It was coated with the biopolymers developed to study their adhesion properties (chapters 5 and 6)
TP	Tissue culture-treated Polystyrene	Polystyrene surfaces treated to improve cell attachment and growth in culture (chapters 5 and 6)

Chapter 1. Introduction

1.1 The problem of antibiotic resistance

1.1.1 Antibiotics discovery and the emergence of resistant phenotypes

More than a hundred years after the discovery of the first antibiotics, the golden molecules that revolutionised medicine have often become ineffective due to the development of resistance mechanisms that minimise or void their efficacy.[1]

Antibiotics are molecules used to treat bacterial infections. The term "antibiotic" - against life - has its origins in the 19th century from the Greek words *ἀντι* and *βίος,* meaning "anti" and "life", respectively. Nevertheless, there is strong evidence to believe that antibiotic-producing microorganisms were used thousand years ago in China, Greece, and Egypt to prevent and cure conditions that modern medicine considers infections; it is well-known that these ancient civilisations employed traditional poultices of mouldy bread, herb extracts and medicinal soil to treat for instance open wounds.[2] Nevertheless, the nature of the infectious diseases was unknown at that time, thus, the specific cure. Pioneering studies by Louis Pasteur and Robert Koch established the basics for modern bacteriology, and in the late ninetieth and beginning of the twentieth centuries, several pathogenic bacteria were characterised and recognised as the agents of many infectious diseases.[2] Thus, the first natural antibiotic was discovered in 1893 by Bartolomeo Gosio, who obtained from *Penicillium brevicompactum* a crystalline product active against *Bacillus anthracis*, the causative agent of anthrax.[2] Later, in 1909, Paul Ehrlich developed the first synthetic anti-infection drug, salvarsan, and then neo-salvarsan, both synthetic arsenic-based pro-drugs toxic to the bacterium *Treponema pallidum* and considered the first scientific and effective cure for syphilis as well as against trypanosomiasis.[3]

In 1928, Alexander Fleming made the discovery that marked "the birth of the antibiotic era". The observation that "around a large colony of a contaminating mould, the *Staphylococcus* colonies became transparent and were obviously undergoing lysis" led to the discovery of penicillin.[4] A few years later, the sulfonamide pro-drug Prontosil was developed, and it was indeed the first broad-spectrum antimicrobial in clinical use, and it is still in use nowadays.[5]

The large-scale production of penicillin, about a decade after its discovery, and its introduction in the health system for treating infections marked the start of the "GOLDEN AGE" of antibiotics. Most current antibiotic classes were discovered in the following years.[6] Antibiotics made it possible to treat common infections and carry out complex surgeries, sparing millions of lives and spanning the average life in more than two decades. These molecules interfere with bacterial physiology and biochemistry, leading to microbial cell death or arresting cell growth by interacting with intracellular targets; to date, around 30 bacterial targets have been described for commercially available antibiotics, and they can be grouped into six target categories. A significant number of these antibiotics i) interfere with bacterial cell wall biosynthesis (β-lactams and glycopeptides) and ii) disrupt bacterial membrane structures (colistin, daptomycin); several others iii) affect protein biosynthesis by binding to the 30S and 50S ribosomal subunits (aminoglycosides, macrolides, tetracyclines, oxazolidinones, streptogramins); other groups include antibiotics that iv) hamper DNA replication and repair (fluoroquinolones), v) RNA synthesis (ansamycins) and vi) interfere with metabolic pathways (sulfonamides, antifolates) (Figure 1A).[7]

Nevertheless, soon after the introduction of penicillin in the market, Fleming predicted that the misuse and overuse of the antibiotics could lead to the development of resistance phenotypes and, indeed, just a few years after the large-scale production of penicillin, bacterial resistance to the drug designed to kill them, started to emerge reducing or annulling the efficacy of penicillin.[8] This began the race between the scientific community, which seeks novel antibiotic molecules, and the microorganisms, which develop, acquire and spread new mechanisms that render the antibiotics ineffective against them. Thus, resistance has been observed for almost all available antibiotics two or three years after their introduction in clinical treatments.[9] It is a complex phenomenon that can be driven either by biochemical processes such as enzymatic degradation of antibiotic drugs, alteration of bacterial proteins that are antibiotic targets, changes in membrane permeability to antibiotics or activation of efflux pumps (Figure 1B) as well as by genetic aspects such as spontaneous and adaptative mutations, hypermutations or horizontal gene transfer.[10]

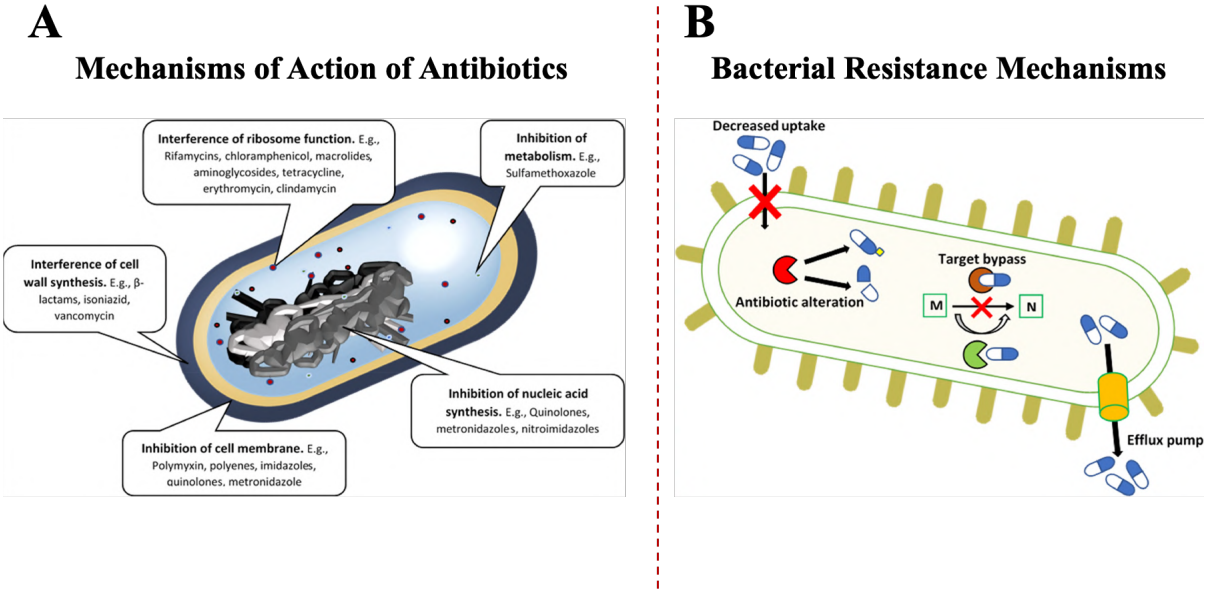

Figure 1. Schematic representation of the most common mechanisms of action of antibiotics against bacteria **(A)** and the most common mechanisms of bacterial antibiotic resistance **(B)**. Reproduced with permission from ref.[10] under a Creative Commons Attribution-NonCommercial-NoDerivs 4.0 International (CC BY-NC-ND 4.0 DEED). *Copyright © 2022* by *Thiruchelvi Pulingam, Thaigarajan Parumasivam, Amirah Mohd Gazzali, Azlinah Mohd Sulaiman, Jiun Yee Chee, Manoj Lakshmanan, Chai Fung Chin, Kumar Sudesh. Published by Elsevier B.V.*

In addition, bacterial antibiotic resistance has become a significant concern of modern medicine, especially after the emergence of methicillin-resistant *Staphylococcus aureus* (MRSA), vancomycin-resistant *S. aureus* (VRSA) and vancomycin-resistant *Enterococci* (VRE).[11] Multidrug resistance (MDR) phenotypes have also been observed, posing a new challenge for global health and making it more difficult to treat common infectious diseases. Moreover, most efforts have been dedicated to controlling and treating multidrug-resistant Gram-positive bacteria. With time, drug-resistant tuberculosis and new Gram-negative bacteria strains have started to outnumber common Gram-positive infections. It is estimated that the resistant Gram-negative may now be even more worrying and costly than Gram-positives, primarily due to their structural characteristics, with outer membranes challenging to penetrate and a higher number of efflux pumps, which render them intrinsically resistant to many drugs. The main Gram-negative threats are MDR and pan-drug resistant *Escherichia coli*, *Pseudomonas aeruginosa*, *Acinetobacter, Klebsiella pneumoniae*, *Enterobacter*, and *Neisseria gonorrhoeae*.[12]

Further, the discovery and the clinical translation of conventional antibiotic compounds belonging to novel classes and with new mechanisms of action have been challenging in recent years; the discovery of new antibiotics and novel antimicrobial mechanisms has quickly dropped, and the interest of pharmaceutical companies in antibiotic research has decreased.[12] Thus, new resistant strains are continuously emerging and spreading worldwide, ending in more extended hospital stays, increased morbidity, and mortality. The golden age of antibiotics is now a distant past, and society is again threatened at alarming levels by infectious diseases. It is estimated that, only in Europe, 25,000 people die each year due to hospital infections caused by resistant bacteria, which result in extra healthcare and societal costs as well as productivity losses of at least EUR 1.5 billion each year.[13, 14] Moreover, statistic suggests that by 2050, more than 10 million people will die due to bacterial infections.[1, 15] In addition, the resistance crisis does not affect only the health system but also the food, veterinary and agricultural industries and society in general.

Thus, the increasing rates of bacterial resistance development to the last-line antibiotics have highlighted the urgent need to obtain non-conventional antibacterial agents with strong antimicrobial activities that are less prone to induce new resistance mechanisms. So thus, several antimicrobial alternatives have been studied, among them the combination of antibiotics, antibiotic adjuvants, antibodies, probiotics, vaccines, immune stimulation, nucleic acids, metal chelation compounds, bacteriophages, predatory bacteria, nanoparticles, and antimicrobial peptides (AMPs).[16] Among them, AMPs are outstanding antimicrobial candidates with great potential, broad-spectrum activity, and flexibility for designing antimicrobial therapies. Their multifaceted mode of action makes them promising candidates for treating infections and mitigating the growing threat of antimicrobial resistance in clinical settings.[17, 18]

1.2 Antimicrobial peptides: promising antimicrobial drug candidates

AMPs are a diverse class of naturally occurring molecules produced by all living organisms. Microbial AMPs are produced to eliminate other bacteria competing for the same environment. At the same time, in higher organisms, they are essential effectors of the innate immune system, constituting their first line of defence against pathogens. AMPs display a strong and broad-spectrum activity against bacteria, fungi, parasites, and viruses, not only directly killing the invading pathogens but also targeting biofilm formation, initiating and modulating immune responses, and having anti-inflammatory properties.[18, 19] Thus, in recent years, the AMPs' potentialities for developing innovative non-traditional anti-infective therapies and "modern antibiotics" have gained significant attention in different fields, including medicine, biotechnology, and agriculture.[17, 18]

1.2.1 Main characteristics and properties. AMPs classification

Lysozyme, identified in body secretions by Alexander Fleming in 1922,[20] and gramicidin, produced by the soil bacterium *Bacillus brevis* and discovered by René Jules Dubos and Rollin Hotchkiss in 1939, are among the earliest examples of natural molecules with potent antimicrobial properties.[21, 22] Nevertheless, the discovery of penicillin, the so-called "golden age of antibiotics", as well as the low stability, toxicity and high cost of AMP production shelved their exploration as clinical agents in the last century,[23] even though a considerable number of AMPs from a variety of organisms were isolated and characterised. Nowadays, mainly driven by the rising antimicrobial resistance to antibiotics, the AMP landscape has changed drastically, and more than 4100 AMPs with demonstrated antimicrobial activities, *in vitro* or *in vivo*, have been manually curated and annotated in the *Antimicrobial Peptide Database* (APD3, as of December 2023 updates).[19]

Comparative analysis of AMP primary structures has shown significant differences regarding their sequences and length; thus, it has been difficult to predict a shared consensus sequence or a short domain among all of them that is required to exert antimicrobial properties; nevertheless, shared structural properties have been identified. According to APD3, AMPs are oligopeptides that can vary in length from 2 to 200 amino acids (aa). More than 88% of the AMPs are small, with less than 50 aa, while only 10% of them have a size ranging from 50-100 aa, so thus, the average length for the 4175 AMPs annotated in the APD3 is 31.67 aa.[19, 24] Even though AMPs are in majority cationic (88%), 6% of the AMPs are neutral, and another 6% carry a negative charge; thus, their net charge spans from -12 to +30, with a net charge that on average is +3.59,[19] which explains their selectivity towards microbial membranes usually negatively charged due to their phospholipidic composition and their inactivity towards the neutral membrane of mammalian cells.

All the 20 natural aa are represented in AMPs; nevertheless, hydrophobic aa such as glycine (11.97%), leucine (8.62%), alanine (7.52%), isoleucine (5.91%) and valine (5.71%), the hydrophilic positively charged aa arginine (9.99%) and lysine (6.58%) as well as the hydrophilic uncharged cysteine (6.33%) and serine (5.8%) are more commonly found on their primary structure and contribute to the cationic charge, hydrophobicity, and amphipathicity needed for their potent antimicrobial activities.[19] Thus, many AMPs are amphipathic (87%),[19] with both cationic and hydrophobic aa, with a hydrophobic content varying from 31% to 70%. In contrast, a few AMPs are entirely hydrophobic (baceridin[25] and lugdunin[26]) or hydrophilic (SAAP).[27] In addition, some AMPs are rich in particular aa (more than 25% of their content), including histidine-rich, tryptophan-rich, proline-rich, arginine-rich, and glycine-rich.[28]

Besides the association of AMPs by size, charge, hydrophobicity, and aa composition, several criteria have been employed to classify the AMPs, for instance, biological source, structure, peptide bonding pattern, mechanism of action, as well as function, and they are briefly described herein.

1.2.1.1 Biological source

As stated in previous sections, AMPs have been identified in all the six kingdoms of life. Their classification based on source discriminates first among natural, predicted and synthetic peptides. To date, APD3 contains 3146 natural AMPs, 190 AMPs predicted using computational approaches or *in silico* modelling, and 314 synthetic peptides inspired by natural AMPs or *de novo* peptides designed based on AMP knowledge. Natural AMPs are further classified based on the organisms that produce them (Figure 2A). Thus, APD3 contains 383 peptides from bacteria, 5 from archaea, 8 from protists, 29 from fungi, 250 from plants, and 2463 from animals. Intriguingly, amphibians are the largest source of AMPs, with more than thousands of AMPs identified between toads and frogs, followed by insects (Figure 2B).[19]

AMPs from bacteriophages have also been identified; among them are endolysins (lysins), virion-associated peptidoglycan hydrolase, depolymerases, and holins. The phages use these enzymes during their viral cycle and affect the integrity of the cell wall and the bacterial membrane, with great potential for developing antibacterial and antibiofilm agents.[29]

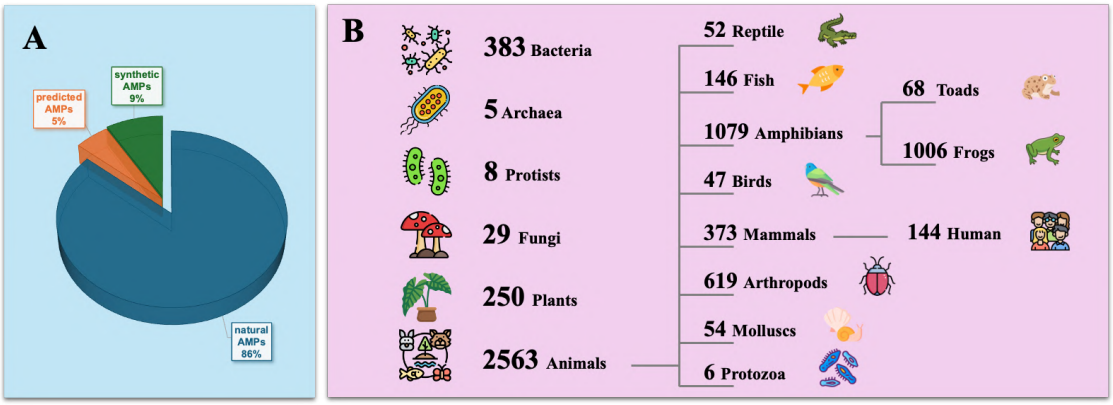

Figure 2. Current statistics on the origins of AMPs are reported in the APD3 **(A)**. Classification of AMPs based on their source **(B)**. Images on panel B were taken from FLATICON.

1.2.1.2 Peptide biosynthesis

AMPs can be obtained through ribosomal mRNA translation or non-ribosomal peptide synthesis.[30] While ribosomally synthesised peptides are predominant (97%) and have been identified in all organisms, a few non-ribosomal peptides have been discovered, mainly in bacteria and fungi. Typically, the latest contain non-standard aa and particular chemical bonds.[19]

1.2.1.3 Structure

To date, APD3 contains the 3D structure of 490 AMPs (429 resolved by NMR and 61 by x-ray diffraction), representing around 12% of the AMPs annotated in the database. Thus, the classification of AMPs based on their 3D structure is limited to the fact that only for a few of the identified AMPs, the 3D structure has been resolved; therefore, this criterion of classification groups only those AMPs with known or partially known 3D structure. This classification is based on the presence of secondary structure elements and distinct the AMPs into four families: α, β, αβ and non-αβ (Figure 3).[19]

AMPs in the α family adopt a predominantly α-helical secondary structure, and so far, the AMPs belonging to this family are the most common and well-studied.[19, 31] The members of this family are usually unstructured in an aqueous solution, while the α-helical structure is adopted upon interaction with the bacterial membrane. Thus, the AMPs often assume an amphiphilic structure, with the hydrophobic aa segregated from hydrophilic aa, allowing them to interact with and disrupt the bacterial membranes, leading to cell lysis and death.[32]

Further, the C-terminal of α-helical peptides is often amidated, enhancing the electrostatic interaction between the AMPs and the negatively charged bacterial membrane and stabilising the helical structure.[33] AMPs within the α helical family include cecropin P1 (Figure 3),[34] magainins, LL-37, and melittin.[35]

The AMPs belonging to the β family form β-sheet structures, with at least a pair of two β-strands, stabilised by hydrogen bonds,[31] and contain conserved cysteine residues that form disulfide bridges often critical for their conformation and functions.[29] Similarly to α-helical, they can also be amphiphilic, but β-sheet structures are more rigid and ordered in aqueous solution; thus, upon membrane interaction, they do not change conformation drastically.[18] Typical examples of this family are bovine lactoferrin B (Figure 3)[36] and defensins, found in diverse organisms, among them humans.[29]

A combination of α-helical and β-sheet structures within the same peptide molecule are the structural characteristics of the αβ family, and they intensely target the bacterial membrane.[29] For instance, β-defensins

[human β-defensin 1 (hBD1) Figure 3][37] contain both α-helical and β-sheet regions, potentially enhancing their antimicrobial activity or broadening their spectrum of targets.[29]

The non-αβ family comprises peptides with extended structures, random coiled, turns, and spiral structures[31] lacking secondary structure and often contains a high arginine, proline, tryptophan, and/or histidine content. These AMPs have broad mechanisms of action, including pore formation, interference with intracellular processes, or inhibition of essential enzymes.[29] Among them is indolicidin (Figure 3).[38]

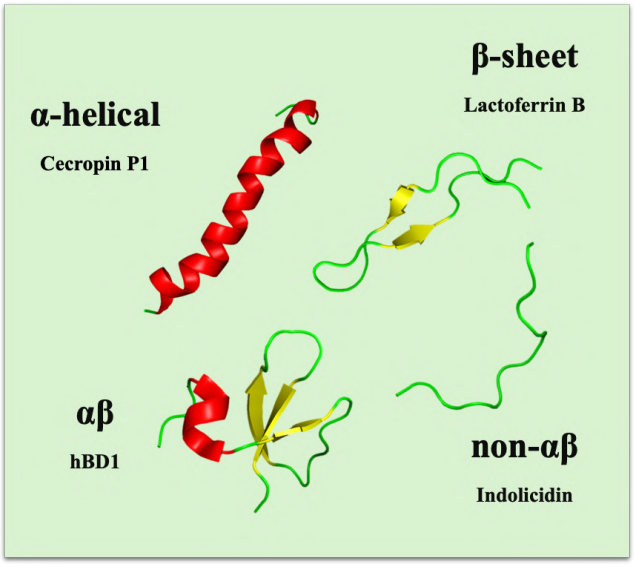

Figure 3. AMP classification based on structural features. The 3D structures of the AMPs were downloaded from the Protein Database Bank (cecropin P1: 7DEH; lactoferrin B: 1LFC; hBD1: 1E4S; and indolicidin: 1G89) and visualised using PyMOL 2.5.8; α-helix are shown in red, β-sheets in yellow and non-structured regions in green.

A deep analysis of these AMP families has shown that the lysine/arginine ratio (K/R ratio) is different for each structural family, and this could be an essential parameter for classifying an AMP into a particular family, even if its 3D structure is unknown. Lysines predominate in the α-helical family, while arginines are more abundant in the β-family as well as the non-αβ families, and the αβ family present a K/R ratio of ~1.2.[31]

1.2.1.4 Peptide bonding pattern

Unlike other classifications, sequence-based categorisation is more universal and based on peptides' covalent bonding patterns. It does not consider the 3D structure, source, mechanism of action, or activity of AMPs. Recently, this classification has been introduced to universally classify the AMPs based on the peptide connection pattern, which directly determines the peptide structure and function. Four groups have been distinguished and named UCBB, UCSB, UCSS and UCLL (Figure 4, UC stands for universal classification); each group can be further classified based on chain number and type of chemical modifications.[31]

UCBB are cyclic peptides with a seamless backbone where the N-terminal and C-terminal are chemically bound (head-to-tail connection); among them are bacterial enterocin AS-48, plant cyclotides and primates θ-defensins.[31] UCSB are also cyclic peptides through any chemical bond between the side chain of one aa and the backbone of another aa,[31] such as in lassos.[39] UCSS family is characterised by a chemical linkage between different side chains, for instance, lantibiotics (thioether rings) and defensins (disulfide bonds).[31] Peptides in the UCLL family have one or two linear peptide chains not covalently connected, with no branches or cyclic structures; nevertheless, they can

have chemical modifications such as amidation, sulfonation, phosphatisation, bromination, or glycosylation; examples of this family are indolicidin, LL-37 and magainins.[24]

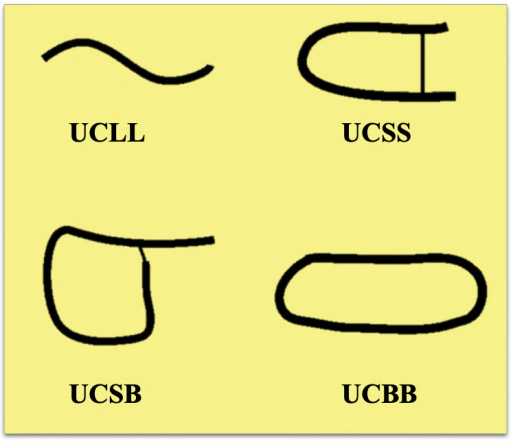

Figure 4. Classification of AMPs based on the connection patterns of the polypeptide chain. Adapted from ref.[31] Guangshun Wang, *"Improved Methods for Classification, Prediction and Design of Antimicrobial Peptides"* Methods Mol. Biol., Vol. 1268, Page 57, (2015). Reproduced with permission from Springer Nature. *Copyright © 2015, Springer Science Business Media New York.*

1.2.1.5 Antimicrobial mechanism of action

Based on their direct killing antimicrobial mechanism of action, AMPs are classified as membrane-targeting and non-membrane-targeting. Membrane-targeting AMPs exert their antimicrobial activity primarily by interacting with and disrupting the microbial cell membrane, leading to increased membrane permeability, membrane integrity loss, and cell death. In non-membrane mechanisms, the AMP targets are the cell wall or intracellular processes (Figure 5).[33]

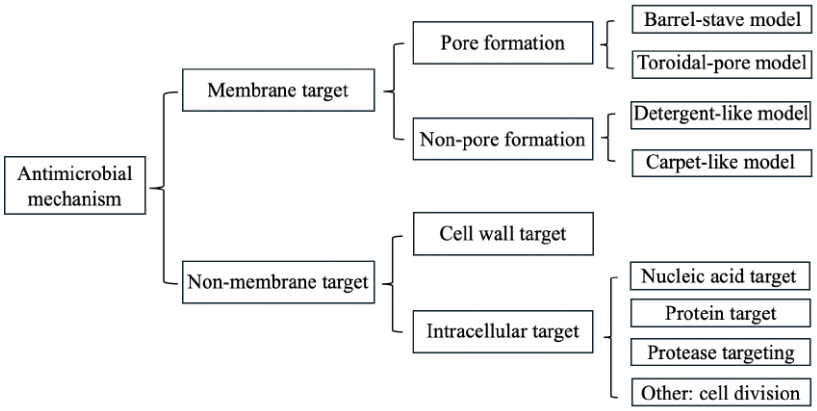

Figure 5. Antimicrobial mechanisms of AMPs. Reprinted from ref.[33] Na Chen and Jiang Cheng, *"Antimicrobial peptides: Structure, mechanism, and modification"*, European Journal of Medicinal Chemistry, Vol 255, Page 115380, (2023), with permission from Elsevier. *© 2023 Elsevier Masson SAS. All rights reserved.*

1.2.1.5.1 Membrane targeting mechanism of action

Independently of the microbial cells and the AMP, the first step of the AMP-mediated activity is its attraction to the microbial cells via electrostatic interactions. These interactions are primarily driven by the cationic nature of AMPs and anionic moieties on the bacterial membrane, such as lipopolysaccharides (LPS) in Gram-negative bacteria and teichoic acids in Gram-positive bacteria.[40] Once attracted to the bacterial membrane, AMPs attach or

bind to the lipid bilayer, favoured by the distribution of AMP's polar and hydrophobic residues, resulting in pronounced interactions of the peptides with the phospholipid membranes.[41] Upon binding to the membrane surface, AMPs adopt an energetically advantageous secondary structure determined by their hydrophobicity. For instance, α-helical peptides typically exhibit consistent hydrophobicity along their α-helical axis, compelling them to adopt orientations relative to the membrane that are either parallel or perpendicular to its surface.[42]

Further, the AMP/lipid ratio dictates the orientation of the AMPs on the membrane. Low AMP/lipid ratios cause AMPs to embed parallel to the lipid head groups, stretching the membrane. As the ratios increase, pores start to form due to membrane thinning. Pores become more prominent at high AMP/lipid ratios, and the peptides insert themselves perpendicularly into the bilayer.[43]

After attachment, membrane-targeting AMPs exert their antimicrobial activity by disrupting the integrity of the lipid bilayer. The mechanism of AMP membrane disruption involves two main models: the transmembrane pore models and the non-porous models. The transmembrane pore models are the barrel-stave and toroidal-pore, while the non-porous models are carpet-like and detergent-like.[33] Figure 6 schematically represents these models.

In the barrel-stave model, as the concentration of the monomer peptides aggregated on the membrane increases, they oligomerise and insert vertically into the hydrophobic core of the lipid bilayer. Then, upon oligomerisation and insertion in the membrane, the AMPs adopt an α-helical structure where the hydrophobic side of the peptide aligns with the central lipid region, arranging themselves in a cylindrical fashion with the hydrophilic side facing the inner surface of the water-soluble pore. Further peptide recruitment increases the size of the pore, forming a stable channel (barrel) through which cytoplasmic contents can flow out, leading to membrane collapse and rupture and resulting in cell death.[44]

The toroidal-pore model suggests that the AMPs attach to the lipid bilayer at low concentrations and vertically insert into the membrane at higher concentrations. The hydrophilic segments of the peptide interact with the phospholipid's polar portion, inducing the lipid monolayers to bend and form annular pores.[45] During pore formation, the peptide's hydrophilic region aligns with the lipid's hydrophilic head group. Thus, the toroidal pore model involves creating a pore where the AMPs and bacterial membrane contribute to the pore structure; the AMPs and the lipid head groups form the pore lining, with the lipid tails pointing outward. Nevertheless, the pores formed by this model are temporary and less stable than those formed by the barrel-stave model.[29]

In the carpet-like model, the AMPs aggregate on the membrane surface as monomers or oligomers and cover it in a carpet fashion. As the concentration of the AMPs increases, the aggregated AMPs spread out and cover the entire membrane surface with hydrophobic regions of the AMPs interacting with the hydrophobic lipid tails of the membrane. In contrast, the hydrophilic areas face outward towards the aqueous environment. Once the peptide concentration reaches a threshold, the aggregated peptides induce membrane permeation, leading to membrane rupture.[43]

On the other hand, the detergent-like model is similar to the carpet-like model since it involves the AMPs binding to phospholipid heads and aligning on the membrane surface. As the concentration of AMPs increases, more peptides bind to the membrane surface and induce further lipid bilayer distortion, forming transient defects or pores in the lipid bilayer, similar to the action of detergent molecules in disrupting lipid membranes. These pores disrupt the membrane's integrity, allowing cellular contents to leak and leading to cell death.[33]

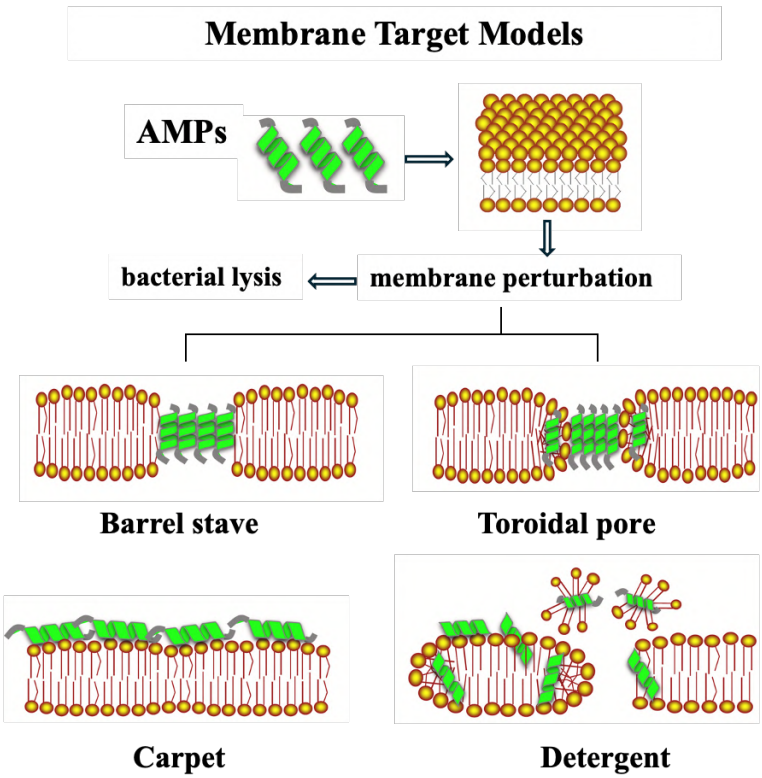

Figure 6. The membrane-targeting mechanisms of action described for AMPs are based on AMPs' interaction with the membrane and membrane perturbation followed by bacterial lysis. Adapted from ref.[33] Na Chen and Jiang Cheng, *"Antimicrobial peptides: Structure, mechanism, and modification"*, European Journal of Medicinal Chemistry, Vol 255, Page 115380, (2023), with permission from Elsevier. *Copyright © 2023 Elsevier Masson SAS. All rights reserved.*

Thus, the carpet-like and detergent-like models involve the initial binding of AMPs to the membrane surface, followed by peptide-induced distortion of the lipid bilayer and membrane disruption. The carpet-like model involves spreading peptides across the membrane surface like a carpet. In contrast, the detergent-like model consists of the formation of transient pores due to peptide-induced membrane distortion.

1.2.1.5.2 Non-membrane targeting mechanism of action

Regarding non-membrane mechanisms, AMP activity can target the cell wall components or intracellular processes without affecting membrane stability (Figure 7).

AMPs targeting the bacterial cell walls inhibit their formation and destroy their already formed structure. This mechanism of action is based on the interaction of certain AMPs with lipid II, an important component of peptidoglycan. Lipid II is essential for transporting cell wall-building blocks across the bacterial plasma membrane. AMPs such as bacitracin, vancomycin and plectasin have been proven to bind to lipid II and inhibit cell wall formation.[43]

AMPs can interact with microbial cells through mechanisms other than direct membrane disruption; AMPs may permeate the bacterial membrane through various mechanisms depending on the specific characteristics of the AMP and the microbial cell type; some mechanisms are energy-independent, such as the formation of instantaneous pores and translocation across the cell membrane while others involve energy-dependent endocytosis. Thus, upon penetration of the bacterial membrane and accumulation in the cytoplasm, AMPs directly

interfere with diverse and critical cellular activities, including DNA replication, transcription, translation, protein synthesis, folding, and cell division.[33] A few examples of AMPs targeting intracellular processes are:

- Indolicidin has been shown to bind and wrap duplex DNA, leading to the subsequent inhibition of DNA replication and transcription,[46]
- Buforin II inhibits cellular processes by interrupting DNA and RNA metabolisms,[47]
- Microcin B17 inhibits type II DNA topoisomerase,[48]
- Pleurocidin inhibits protein, DNA, and RNA synthesis,[49]
- Lactoferrin B interferes with the phosphorylation of a two-component system to suppress bacterial growth,[50]
- Histatin 5 is a potent protease inhibitor,[51]
- Human α-defensin 5 disrupts cell division by forming bleb, cellular elongation, and clumping.[52]

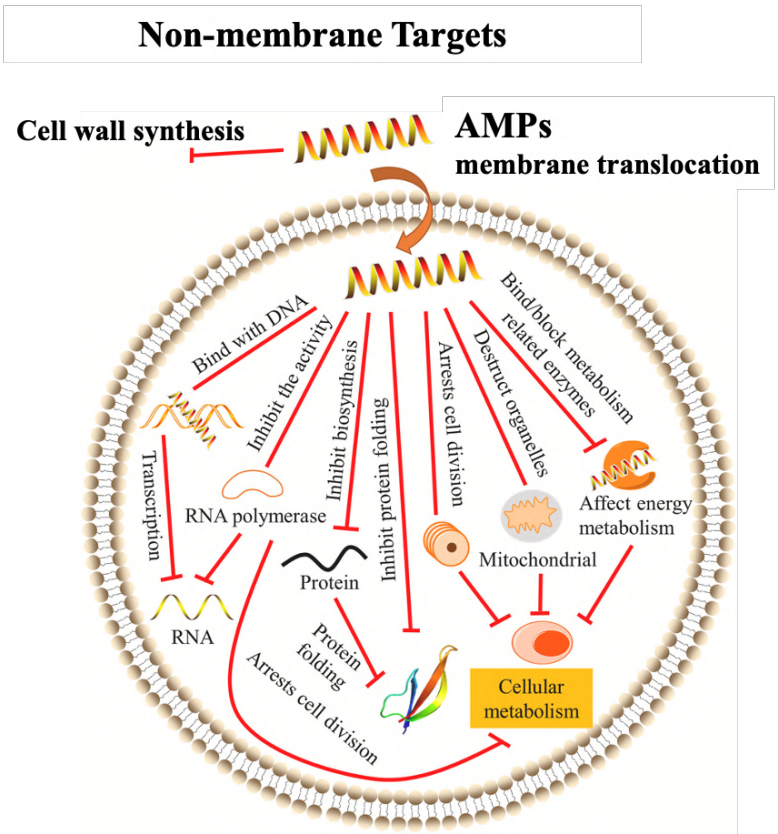

Figure 7. The main mechanisms of action described for AMPs for non-membrane targeting include inhibition of cell wall formation and membrane translocation to reach intracellular targets. Adapted from ref.[33] Na Chen and Jiang Cheng, *"Antimicrobial peptides: Structure, mechanism, and modification"*, European Journal of Medicinal Chemistry, Vol 255, Page 115380, (2023), with permission from Elsevier. *Copyright © 2023 Elsevier Masson SAS. All rights reserved.*

These mechanisms illustrate the diverse manners in which non-membrane disrupting AMPs exert their antimicrobial activity by targeting intracellular components or critical processes for microbial survival; nevertheless, there is a lot of evidence indicating that a particular AMP can exert its function through different mechanisms of action and each AMP triggers a unique bacterial response.[53]

1.2.1.6 Biological function

Nowadays, the understanding of the biological function of AMPs goes far beyond their direct antimicrobial activity, and Table 1 resumes the biological activities reported so far for natural, predicted and synthetic AMPs annotated on APD3.

Table 1. AMP functions within biological environments. AMP examples and statistics were taken from APD3.

Biological Function	Selected AMP examples	Amount (%)
Antibacterial	lactoferrin B, indolicidin, hBD1, LL-37, GL13K	3588 (**85.94**)
Anti-MRSA	indolicidin, lactoferrin B, HNP1, nisin (Z and A), hBD3, LL-37	446 (**10.68**)
Anti-Tuberculosis	LL-37micrococcin P1, hBD10, laterosporulin 10	15 (**0.36**)
Antibiofilm	indolicidin, temporin B, LL-37, hBD3, BMAP (27 and 28)	112 (**2.68**)
Antifungal	dermaseptin B-2, indolicidin, hBD1, aurein, lactoferrin B	1399 (**33.51**)
Anti-Candida	dermaseptin B-2, hBD1, lactoferrin B	825 (**19.76**)
Antiviral	alloferon 1, lactoferrin B, indolicidin, hBD1, cecropin A, melittin	244 (**5.84**)
Anti-HIV	lactoferrin B, indolicidin, hBD1	136 (**3.26**)
Anti-endotoxin	bactenecin, lactoferrin B, cecropin (A, P1, 2), magainin 2	93 (**2.23**)
Anti-toxin	HNP (1-4), hBD (1-5)	17 (**0.41**)
Protease inhibitors	HNP (1-3), LL-37, microcin H47, elafin	37 (**0.89**)
Ion channel inhibitors:	hBD (1-4), microcin, bldesin	11 (**0.26**)
Antiparasitic	cecropin A, bombinin H4, brevenin, temporin (A, B, F, L)	152 (**3.64**)
Insecticidal	esculentin-1, magainin 2, melittin, poneticin (W1, W3-W6)	44 (**1.05**)
Spermicidal	maximin (1, 3, 4), magainin 2, dermaseptin (S1, S4), LL-37	14 (**0.34**)
Chemotactic	bactenecin 7, temporin (A, B), HPN (1-3), hBD (2, 3, 4), LL-37	71 (**1.70**)
Wound healing	temporin A,indolicidin,magainin 2, hBD (2, 3, 5), HNP1, LL-37	28 (**0.67**)
Antioxidant	thrombocidin, lunasin, hispidalin	33 (**0.79**)
Anti-inflammatory	hBD3, citropin 1.1, chicken CATH-1, cathelicidin-PY, GL13K	62 (**1.49**)
Anticancer (antitumor)	dermaseptin-B2, alloferon (1, 2), lactoferrin B, indolicidin, hBD1	290 (**6.95**)
Anti-diabetic	pseudin-2, amolopin, magainin-AM2, dermaseptin-B4	20 (**0.48**)
Surface Immobilized	cecropin (B, P1), indolicidin, LL-37, dermaseptin, GL13K	31 (**0.74**)
Two-chain peptides	gallocin A and D, formicin, haloduracin	39 (**0.93**)
Synergistic peptides	gramicidin S, nisin A, hBD1, hBD3, LL-37	52 (**1.25**)

AMPs exert a broad-spectrum activity against microorganisms, including Gram-positive and Gram-negative bacteria,[54] fungi,[55] and viruses.[56] AMPs such as defensins, cathelicidins, and magainins directly kill or inhibit the growth of microbial pathogens by disrupting microbial cell membranes, interfering with intracellular processes, or

targeting essential microbial components. AMP antimicrobial activity is usually reported as Minimum Inhibitory Concentration (MIC) with values ranging from 1 to 100 μM for most peptides against Gram-positive and Gram-negative bacteria as well as fungi such as *Candida albicans*.[57] In addition, several AMPs have been found active towards MRSA,[58, 59] while others effectively prevent or disrupt biofilm formation.[44, 59]

AMPs with antiviral activity target viruses by disrupting viral membranes and targeting multiple steps in viral pathogenesis, including viral entry and replication or modulating host immune responses to fight viral infections.[60] Moreover, several AMPs have been examined for their potential as drugs for treating infections by human immunodeficiency virus (HIV), influenza A and herpes viruses and SARS-CoV-2.[60, 61]

At concentrations below their MIC, AMPs have been found to modulate the immune response by regulating the activity of immune cells, such as macrophages, neutrophils, and dendritic cells and promoting inflammation, enhancing phagocytosis, or modulating cytokine production and complement activation. Certain AMPs participate in wound healing and tissue repair by promoting cell proliferation, migration, and angiogenesis while exhibiting antimicrobial activity to prevent wound infections.[62, 63] Moreover, AMPs exert anti-inflammatory properties by modulating inflammatory signalling pathways, reducing cytokine production, inhibiting neutrophil activation, and regulating the balance between inflammation and immune responses.[44, 62] Human cathelicidin and defensins are among the most studied immunomodulatory AMPs.[63]

AMPs with antioxidant activity scavenge free radicals and protect cells from oxidative damage, contributing to cellular homeostasis and reducing inflammation.[64] Some AMPs exhibit cytotoxic effects against cancer cells by inducing apoptosis, disrupting cell membranes, or inhibiting angiogenesis. They hold great potential as novel anticancer drugs or adjuvants to conventional cancer therapies, including cationic peptides and lactoferrin. Moreover, recent findings suggest that β-defensins and the cathelicidin peptide LL37 are richly expressed in carcinoma, and both pro-tumoral and antitumoral activities have been described for these AMPs and their roles in tumour development and progression remain poorly understood; nevertheless, their overexpression in this kind cancer holds potentialities as biomarkers for diagnosis.[63]

1.2.2 Families of AMPs in vertebrates

Defensins and cathelicidins are the most prominent families of AMPs found in vertebrates.[65] Nevertheless, other families have been identified across vertebrates, among them histatins from the saliva of humans and other primates; bombinins, buforin, dermaseptins, esculentins, fallaxin, magainins, maximins, phylloseptins, phylloxin, plasticins, plasturins, pseudins, and ranateurins from amphibians; hepcidins, piscidins, and histone-derived peptides from fish; platelet antimicrobial proteins, hepcidins, and dermcidin from mammals as well as other peptides derived from large proteins, such as lysozyme.[29, 65] Each family encompasses several members with unique structures, functions, and modes of action, with essential roles in the innate immune system, collectively contributing to the host's defence against microbial pathogens.[65]

1.2.2.1 Defensins

Defensins have been identified in a wide range of organisms, including vertebrates, invertebrates, plants, and fungi. They are cationic (+1 to +11) cysteine-rich AMPs with a unique 3D structure composed of β-sheets stabilised by three disulfide bridges. Thus, they adopt amphipathic conformations, with one face of the molecule being hydrophobic and the other being hydrophilic, critical structural characteristics for defensins' ability to interact with and disrupt microbial membranes.[65]

Defensins are produced primarily by epithelial cells, immune cells, and specific specialised tissues in response to microbial infection, inflammation, or other stimuli and are often constitutively expressed at low levels. They are produced as pre-pro-defensins, composed of an N-terminal hydrophobic signal pre-sequence, a conserved pro-sequence, and a mature peptide (Figure 8A). Thus, defensins are produced as inactive forms to avoid their potential toxicity during protein processing and intracellular transport; in pre-pro-defensins, negative charges balance the positive charge of the mature defensins. The pre-sequence directs the pre-pro-peptide to the endoplasmic reticulum, where it undergoes cleavage to remove the signal sequence. The pro-defensin peptide then undergoes further processing, including proteolytic cleavage and disulfide bond formation, to generate the mature defensin that is packaged into secretory vesicles and transported to the cell membrane for its extracellular activity, or they are directly released in the cytoplasm in response to cellular stress or damage.[65-68]

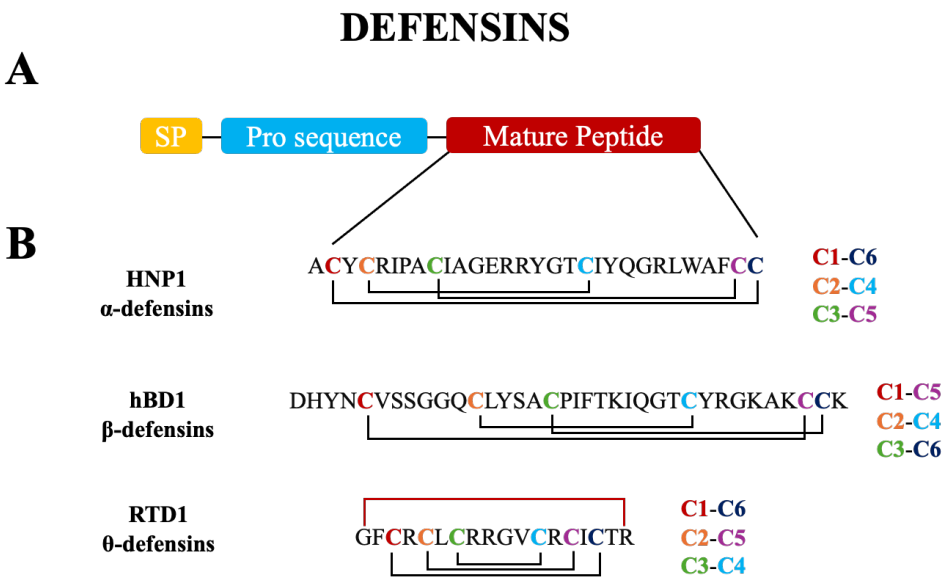

Figure 8. Schematic representation of preprodefensins (**A**). Disulfide bridge pattern characteristic of α-, β- and θ-defensins (**B**).

Defensins are potent AMPs effective against bacteria, fungi, and some viruses. They disrupt microbial membranes through electrostatic interactions, leading to cell lysis, or they penetrate the microbial cells, hindering DNA replication and protein synthesis. Moreover, they possess immunomodulatory functions, recruiting immune cells, modulating inflammation, and aiding in wound healing.[65]

Three main defensin subfamilies can be distinguished based mainly on the pattern of their disulfide bridge connectivity (Figure 8B):

- α-defensins are characterised by "C1-C6, C2-C4, C3-C5" disulfide bridge pattern. They are often constitutively expressed and primarily found in mammals' neutrophils, macrophages, and epithelial cells. In humans, six α-defensins have been identified; α-defensins 1 to 4 are produced by myeloid cells and are known as human neutrophil peptides (HNP from 1 to 4), while α-defensins 5 and 6 (HD5 and HD6) are expressed in paneth cells of the intestine and the epithelial cells of the genitourinary tract.[69, 70]
- β-defensins are characterised by "C1-C5, C2-C4, C3-C6" disulfide bridge pattern. Different from the α-defensins and θ-defensins, β-defensins have been identified across the animal kingdom, with a highly variable number of gene-encoding defensin among vertebrates and functionalities that go beyond their antimicrobial capacity.[65] Their expression is mainly localised to epithelial and mucosal surfaces and

immune and reproductive tissues and is highly upregulated by pathogens.[71] In humans, more than 30 β-defensin genes have been identified; nevertheless, only a few have been studied at the protein level, particularly human β-defensins (hBD) from 1 to 4.[72]

- θ-defensins are cyclic peptides formed from two truncated α-defensin joined through a post-translational head-to-tail cyclisation process and with a "C1-C6, C2-C5, C3-C4" disulfide bridge pattern. Each truncated chain contains nine aa, including the three cysteines.[73] They are unique AMPs from neutrophils and bone marrow of some non-human primates, such as rhesus macaques[74] and olive baboons.[75]

1.2.2.1.1 Human β-defensin 1

hBD1 is an essential AMP for epithelial defence against infection. It is the only β-defensin that is constitutively expressed, and it is produced across several epithelial cells, including skin, kidney, respiratory, reproductive, and urogenital tract. Additionally, its expression can be upregulated in microbial infection or due to inflammation.[71, 76] hBD1 exhibits a broad-spectrum antimicrobial activity, effectively preventing microbial colonisation and proliferation within epithelial tissues, thus maintaining tissue integrity and homeostasis. In antiviral defence, hBD1 has been shown to directly reduce HIV infectivity up to 50% *in vitro* and indirectly upregulate the expression of human β-defensin 3 (hBD3), which has a more potent antiviral activity. Moreover, it plays multifaceted roles beyond antimicrobial defence, such as modulating the local immune response, acting as a selective chemoattractant factor, and promoting the activation and maturation of immune cells. It participates in glucose metabolism, with a crucial function in hypoinsulinemia. In addition, hBD1 regulates keratinocyte differentiation and acts as a tumour suppressor in most carcinomas, inhibiting cell growth and migration and promoting apoptosis. It is relevant in male fertility, increasing sperm motility and egg-penetrating ability. Thus, in the scientific literature, hBD1 is known as the "restless warrior" due to its constitutive expression and defensive role against external threats like infections and internal challenges like cancer (Figure 9). However, deficiencies in hBD1 production have been linked to various diseases, particularly those involving epithelial barrier dysfunction and increased susceptibility to microbial infections such as inflammatory bowel disease, atopic dermatitis, cystic fibrosis, periodontal disease, urinary tract infections, susceptibility to MRSA infections as well as infertility.[77, 78]

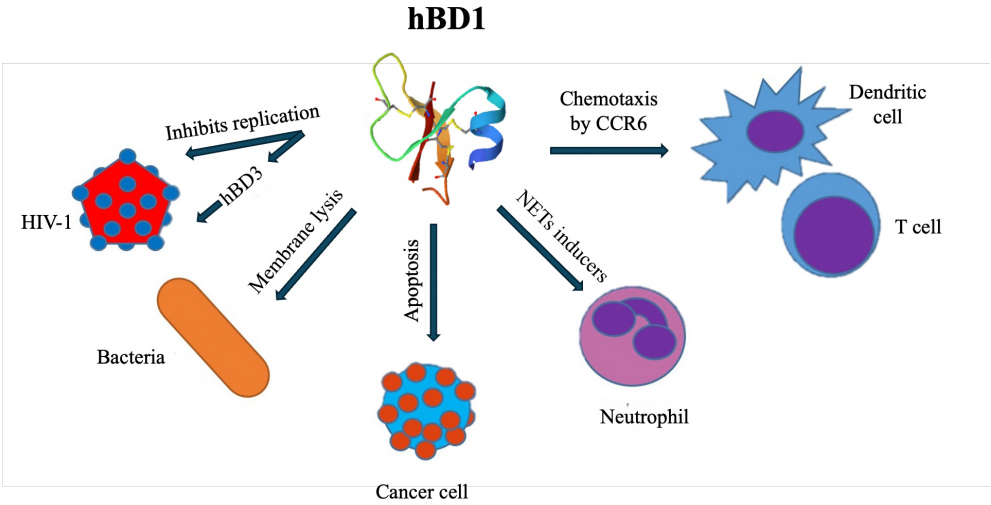

Figure 9. The multifunctional role of hBD1 in preserving epithelial integrity, inhibiting microbial infiltration, coordinating immune responses, and maintaining tissue homeostasis. Reprinted from ref.[77] Ángel H. Álvarez, Moisés Martínez Velázquez, Ernesto Prado Montes de Oca, *"Human β-defensin 1 update: Potential clinical applications of the restless warrior"*, The

hBD1 is the product of the gene *DEFB1*, and it is produced as a pre-pro-peptide of 68 aa, carrying a signal peptide, an N-terminal pro-peptide and the mature AMP.[79] Its post-translational modifications (PTMs) include the proteolytic cleavage of the signal peptide and the pro-peptide and disulfide bridge formation. Further, the mature peptide is often truncated at the N-terminal, producing hBD1 active forms that range in size from 36 to 47 aa and with different microbicidal capacities.[71, 79] Similarly to other β-defensins, hBD1 is an αβ peptide composed of three antiparallel β-sheets and an α-helix at the N-terminal stabilised by three disulfide bridges (Figure 3). Thus, it adopts an amphipathic structure crucial for its antimicrobial and immunomodulatory properties.[71, 80, 81]

The antimicrobial mechanism of action of hBD1 is based on the interaction of its cationic side with the negatively charged microbial membranes, disrupting their integrity and leading to leakage of cellular contents and eventual microbial cell death. In laboratory conditions, hBD1 has a weak antimicrobial activity compared to other human AMPs; yet, it is effective against some Gram-negative bacteria and some fungi but less potent toward Gram-positive bacteria.[71, 82] Nevertheless, laboratory conditions do not adequately reflect the physiological environment of epithelial cells where hypoxia and reducing conditions are dominant; thus, for some microorganisms, including fungi and Gram-positive bacteria, the activity of the peptide has been reported to be significantly influenced by its redox state (herein we will use the terms redhBD1 and oxhBD1 to refer to the reduced and oxidised hBD1 forms, respectively).[83, 84]

Natural and recombinant forms of hBD1 are antimicrobial against laboratory and clinical *E. coli* strains at micromolar concentrations, and their activity is not affected at low pH but is impaired at high salt concentrations; only the 36 aa hBD1 variant retains its microbicidal capacity in urine.[79] Similarly, salt-sensitive antimicrobial activity has been reported towards *P. aeruginosa*.[85, 86] In addition, hBD1 (47 aa peptide) inhibited the growth of *S. aureus* (methicillin-sensitive *S. aureus* and MRSA) clinical isolates with a MIC of 0.5 mg/L and topical gels with the peptide encapsulated in silica nanoparticles showed significantly improved wound healing when evaluated *in vivo* in an MRSA-infected wound model in rats.[87] Later, the same Authors reported that among several clinical isolates, the MIC of hBD1 (36 aa peptide) against *S. aureus* is 8 (4-8) mg/L, while for *E. coli,* they found that the peptide was inactive for 10 out of the 24 strains with a MIC of 32 (14-32) mg/L against susceptible strains.[88]

Schroeder *et al.* (2011) showed that the cysteines at the C-terminal of the peptide are critical for its bactericidal activity and that the reduction of the disulfide bridges turned hBD1 into a potent agent against the opportunistic pathogenic fungus *C. albicans* and anaerobic Gram-positive bacteria from *Bifidobacterium* spp. and *Lactobacillus* spp..[83] In addition, their study revealed the ability of the thioredoxin system to reduce hBD1 *in vitro.* Thioredoxin (Trx) co-localises with redhBD1 in human epithelia, highlighting the critical cooperation between redox systems and innate immune defence in protecting human epithelia.[83, 89] Nevertheless, despite the redox state, antimicrobial activity has been reported against *Salmonella enteritidis, E. coli* and *P. aeruginosa*.[82] Intriguingly, other Authors have reported that oxhBD1 is bacteriostatic while redhBD1 has a bactericidal mechanism of action against *E. coli*; in addition, oxhBD1 was active only against some Gram-negative bacteria while redhBD1 was strongly active against Gram-negative (*S. enteritidis* and *E. coli*) and Gram-positive bacteria (*Bacillus subtilis* and *S. aureus*).[84]

In addition, Kraemer *et al.* (2010) described a novel bactericidal mechanism of hBD1 in human platelets; they indicated that upon recognition of pathogen toxins, platelets release hBD1, which induces polymorphonuclear leukocytes to extrude neutrophil extracellular traps (NET) that trap and kill *S. aureus*.[90]

More recently, redhBD1, but not oxhBD1, has been shown to induce cysteine-dependent self-net formation that entraps bacteria and prevents bacterial translocation independent of bacterial killing; *E. coli* entrapped in redhBD1 nets showed extensive membrane disruption while in the case of *K. pneumoniae,* the nets reduced its migration without exerting a bactericidal activity. Moreover, they proved that free cysteines are critical for net formation since their substitution by α-amino butyric acid impaired the net formation capacity of the reduced peptide.[84]

Interestingly, proteolysis of the redhBD1 by gastrointestinal proteases and human duodenal secretions produces an octapeptide composed of hBD1 C-terminal active against pathogenic and antibiotic-resistant microorganisms, including *E. coli*, *P. aeruginosa*, and *C. albicans.* Moreover, mutant peptides derived from the octapeptide where alanines substituted cysteines displayed no antimicrobial activity against the microorganisms tested, reinforcing previous observations that cysteines are essential for hBD1 activity.[91]

Given its multifunctional properties and broad-spectrum antimicrobial activity, hBD1 holds immense potential as a therapeutic agent for combating infectious diseases and addressing various pathological conditions associated with epithelial barrier dysfunction and microbial susceptibility.

1.2.2.2 Cathelicidins

Cathelicidins are a family of small, cationic, amphipathic AMPs extensively studied in cattle and pigs; nevertheless, they are likely to be found in all vertebrates, and indeed, they have been identified in other organisms, including humans, reptiles, birds, amphibians, and fish. They are produced as precursor peptides, stored in neutrophils and macrophages' secretory granules, and upon leukocyte activation, they are processed to active AMPs and released. The precursor peptides are characterised by the presence of three main domains: an N-terminal signal peptide (29-30 aa), a highly conserved cathelin-like domain (94-114 aa) and a variable AMP that is released from the precursor peptide by the action of proteases (Figure 10A).[65] Different from defensins, cathelicidins are more heterogeneous, with sizes ranging from 12 to 80 aa, variable aa sequences and folding into α-helix and β-sheet structures, loops, and unstructured linear peptides (Figure 10B). Thus, their production as precursor peptides carrying the cathelin domain is the unifying characteristic of this family of AMPs.[70, 92]

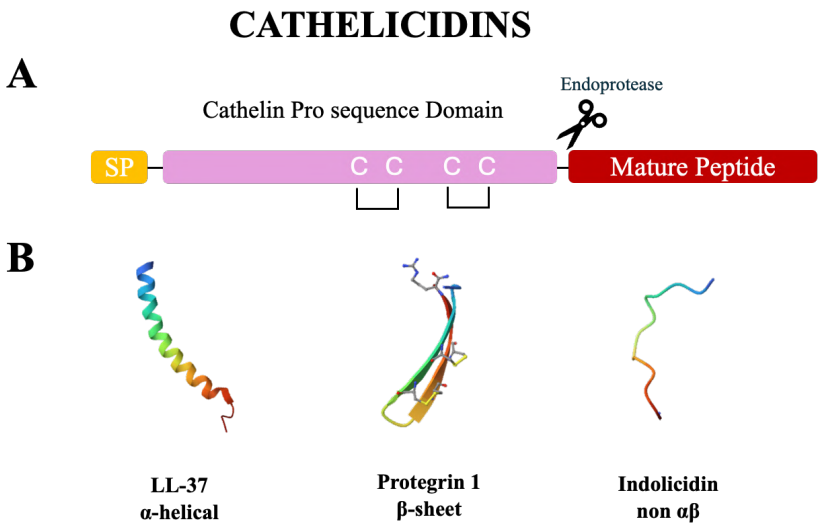

Figure 10. Schematic representation of cathelicidin precursors **(A).** Mature cathelicidin AMPs show diverse 3D structures **(B).** The 3D structures of the AMPs were taken from the Protein Database Bank (LL-37: 2K6O; Protegrin 1: 1PG1; and indolicidin: 1G89).

1.2.2.2.1 Indolicidin

Indolicidin (ILPWKWPWWPWRR-NH2) is a short (13 aa) cationic (+4) AMP isolated from bovine neutrophils. Half of the aa in its primary structure are hydrophobic; among them, five tryptophans that contribute to its antimicrobial and hemolytic activities.[93] Indolicidin's ability to adopt different secondary structures is crucial for its antimicrobial activity; this flexibility enables indolicidin to adapt to various environmental conditions, making it a broad antimicrobial agent able to recognise several targets.[94] It exhibits a random coil unordered structure in aqueous solutions, as confirmed by NMR spectroscopy and circular dichroism.[95] However, molecular dynamics simulations indicate it assumes a boat-shaped conformation when interacting with negatively charged lipid bilayers.[93, 96]

Indolicidin is active against planktonic Gram-positive and Gram-negative bacteria, among them MRSA, and has antibiofilm activity.[97, 98] The antimicrobial mechanism of action of indolicidin involves transient perturbation of the bacterial membrane, without inducing cell lysis, to reach intracellular targets and inhibit protein and DNA synthesis (Figure 11A).[93] Furthermore, indolicidin structural plasticity and the presence of a high content of aromatic residues allow this AMP to bind and neutralise LPS, being the potential mechanism through which indolicidin exerts antisepsis and antibiofilm activities (Figure 11B).[93] Moreover, the hemolytic activity of indolicidin may be attributed to its capacity to operate as an organic anion carrier (Figure 11C).[93] In addition, antifungal, antiparasitic and antivirus activities have also been described for this AMP. Nevertheless, the mechanism of action remains unclear.[93, 99-101] Table 2 resumes the activity of indolicidin against several microorganisms of interest.[93]

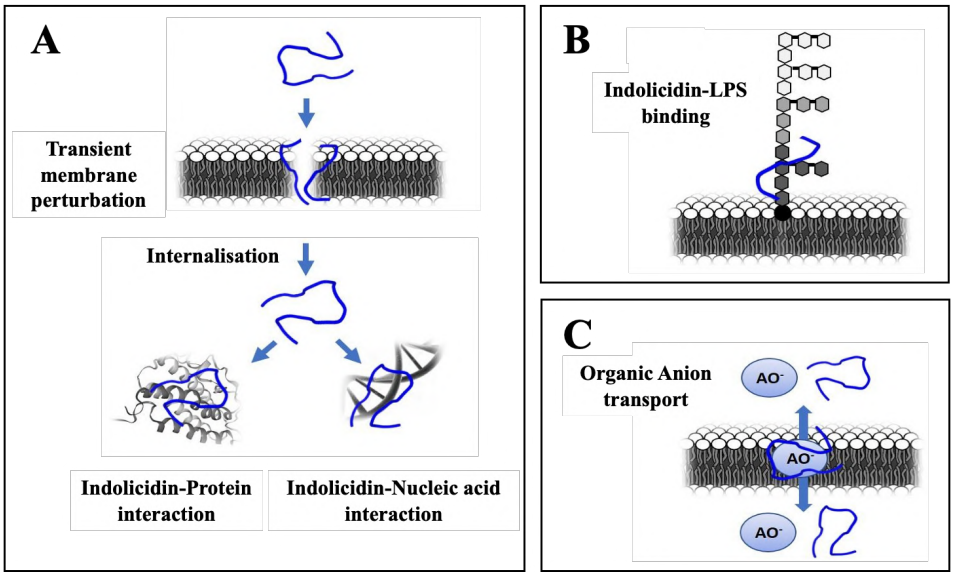

Figure 11. Mechanisms of action described for indolicidin: antimicrobial activity via interaction with intracellular targets (**A**), interaction with LPS for its antisepsis and antibiofilm activities **(B)**, and anion carrier mechanism to explain hemolytic activity (**C**). Adapted from ref.[93] Batista *et al., "Indolicidin revisited: biological activity, potential applications and perspectives of an antimicrobial peptide not yet fully explored"*, World Journal of Microbiology and Biotechnology Vol. 38, Page 6. Reproduced with permission from Springer Nature. *Copyright © 2022, by Jaqueline Batista Araujo, Guilherme Sastre de Souza and Esteban Nicolas Lorenzon, under exclusive licence to Springer Nature B.V.*

Considering the potentialities of indolicidin as a therapeutic agent and the possible drawbacks for its translation into clinical environments, several peptides inspired by the indolicidin sequence have been developed to enhance

the antimicrobial and antifungal capacity while reducing its hemolytic activity and increasing the resistance to proteases. Among the designs outstands:

- CP-11 (ILKKWPWWPWRRK-NH_2), an indolicidin analogous with a higher content of lysine and arginine that showed higher activity against bacteria and yeasts as well as less toxicity than the parental AMP,[102]
- cycloCP-11 (I**C**LKKWPWWPWRR**C**K-NH_2), a cyclic disulfide-bonded peptide with higher resistance to proteases while retaining the same antimicrobial and low hemolytic activity of the linear CP-11,[103]
- Omiganan (ILRWPWWPWRRK-NH_2, DRAMP18160) analogue of indolicidin with potent antimicrobial activity against a broad spectrum of bacteria, including drug-resistant strains and various *Candida* spp.. Its rapid bactericidal and fungicidal effects have been well-documented. At least sixteen clinical studies, currently in phase II or III, are being conducted to explore its efficacy as a topical gel formulation for rosacea treatment, its ability to prevent catheter-related infections, its effectiveness in managing genital warts, and its role in addressing acne vulgaris,[104-106]
- Ld-indolicidin analogue (IlPwKwPwWpWrR-NH_2) containing L and D aa alternated in its primary structure showed high resistance to enzymatic degradation, tolerance in mice and better capacity than indolicidin to enhance cell-mediated immune responses,[107]
- an indolicidin pseudo-peptide containing two reduced amide bonds displaying less hemolytic activity and improved stability without a decrease in its antimicrobial activity.[108]

Thus, indolicidin is a versatile peptide holding great promise in combating multidrug-resistant microorganisms, fungi, parasites, and certain viruses. Its multifaceted targets and ease of production position it as a strong candidate for diverse medical, biomedical, and food preservation applications.[93]

Table 2. Indolicidin activity against microorganisms of interest to the present thesis. *IC50* half maximal inhibitory concentration. Extracted from ref.[93] Batista *et al., "Indolicidin revisited: biological activity, potential applications and perspectives of an antimicrobial peptide not yet fully explored"*, World Journal of Microbiology and Biotechnology Vol. 38, Page 4. Reproduced with permission from Springer Nature. *Copyright © 2022, by Jaqueline Batista Araujo, Guilherme Sastre de Souza and Esteban Nicolas Lorenzon, under exclusive licence to Springer Nature B.V.*

Microorganism	Activity (µg/mL)
Gram-positive bacteria	
S. aureus	MIC 2-30
MRSA	MIC 8-15
Gram-negative bacteria	
E. coli	MIC 5-30
P. aeruginosa	MIC 8-100
Fungi	
C. albicans	MIC 15-200
Virus	
HIV	IC50 70-110
Herpes simplex virus	IC50 10-50

1.2.3 Development of resistance to AMPs

The paradigm that bacterial resistance to AMPs is highly improbable has changed in recent years. Bacteria encounter AMPs in their natural environment; thus, by selective pressure, they can develop several induced resistance mechanisms to overcome AMP activity. Among them are AMP sequestration or degradation by proteases, modification of the cell surface charge and composition, modification of the AMP target, overexpression of efflux pumps, and biofilm formation affecting AMP interaction with the microbial cells (Figure 12).[17]

A very well-studied mechanism of resistance consists of the modification of the bacterial cell surface by incorporating positively charged molecules to reduce or abolish the electrostatic interactions and binding affinity of positively charged AMPs. For instance, Gram-positive bacteria, such as *S. aureus,* modify their cell surface by inducing D-alanylation of teichoic acids, incorporation of lysyl phosphatidylglycerol as well as the addition of L-lysine to membrane phospholipids, reducing their overall negative charge. Similarly, Gram-negative bacteria also abolish electrostatic interactions with AMPs by modification of their lipopolysaccharide via conjugation of lipid A with 4-aminoarabinose, palmitate and phosphoethanolamine, as well as its monophosphorylation and glycylation.[109, 110]

Another common mechanism is the employment of efflux pumps to deplete the bacterial cells of the AMPs. *S. aureus* and *B. subtilis* efflux pump systems, such as ABC transporters, actively expel the LL-37 from the bacterial cell.[111] Efflux pumps that act on AMPs have also been identified in *N. gonorrhoeae* and *Yersinia* spp..[109]

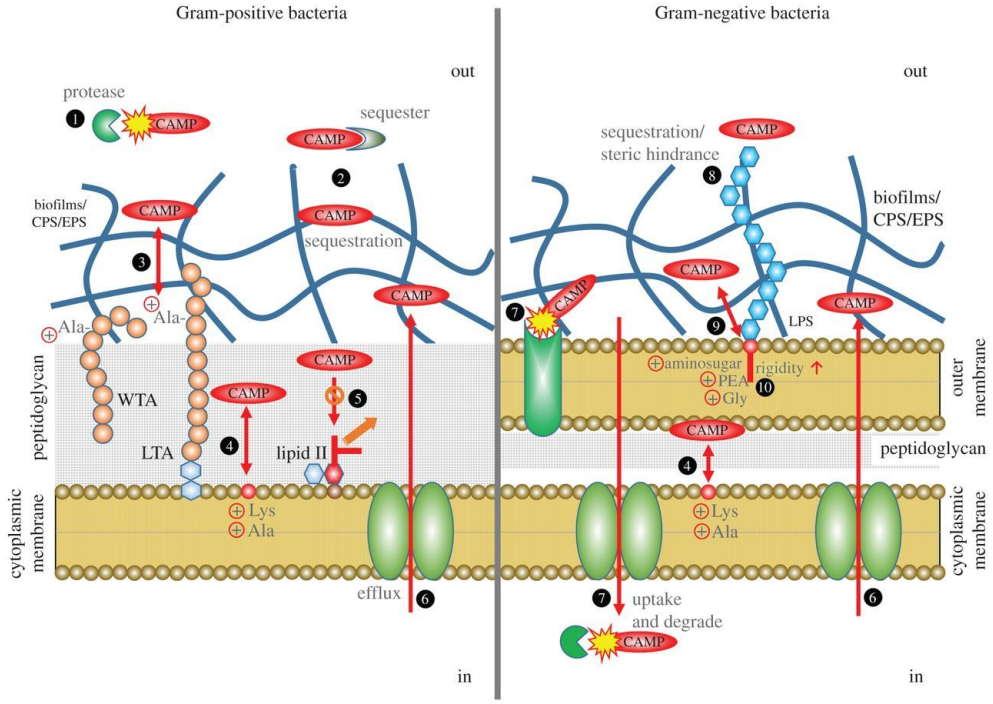

Figure 12. Mechanisms of bacterial resistance to AMPs. Adopted from ref.[112] Joo *et al.*, *"Bacterial strategies of resistance to antimicrobial peptides"*, Phil. Trans. R. Soc. B. Biological letters, Vol 371, Page 20150293. Reproduced with permission from The Royal Society (U.K.). *Copyright © 2016, by Hwang-Soo Joo, Chih-Iung Fu, and Michael Otto, published by the Royal Society. All rights reserved.*

P. aeruginosa, Enterococcus faecalis, Proteus mirabilis and *Streptococcus pyogenes* secrete proteases that degrade AMPs, rendering them ineffective.[113] *S. aureus* extracellular metalloproteinase aureolysin has been reported to cleave and inactivate LL-37,[114] while a *P. mirabilis* extracellular metalloprotease has been reported to degrade hBD1 and LL-37.[115] In addition, cytosolic proteases can contribute to AMP resistance; for instance, in *E. coli*, a

serine peptidase's overexpression reduces bacterial cells' susceptibility to proline-rich AMPs.[116] Moreover, some microorganisms produce non-proteolytic sequestering proteins that bind to the AMPs and render them ineffective. For instance, *S. aureus* secretes staphylokinase, which can bind and inactivate cathelicidin murine AMPs and α-defensins.[117]

In addition, another common strategy employed by microorganisms to bypass AMP activity is the production of an anionic polysaccharide capsule that surrounds the cell, acting as a physical barrier between the microorganisms and the AMPs.[118] *P. aeruginosa* has been reported to produce such a capsule to restrict the access of AMPs to the outer membrane and sequester AMPs through electrostatic interactions.[119]

Several microorganisms, including *E. coli,* contrast AMP activity by forming biofilms, providing a protective environment where AMPs, such as LL-37, struggle to penetrate and exert their antimicrobial effects.[120] For instance, it has been reported that in *P. aeruginosa* biofilm, extracellular DNA causes cation chelation, inducing LPS modification genes and resistance to antimicrobial agents such as polymyxin B and colistin.[121]

Nevertheless, their unique mechanisms of action involve the interaction with multiple low-affinity targets rather than a particular one with high-affinity (characteristics of conventional antibiotics), which renders the AMPs less prone to induce resistance compared to traditional antibiotics. AMPs have a broad-spectrum activity targeting multiple microbial structures or processes, which makes it harder for bacteria to develop resistance by modifying a single target. They kill microbial cells quickly through membrane disruption or casing lethal intracellular effects within minutes, which reduces the capability of bacteria to adapt and develop resistance mechanisms. There is an excellent diversity of AMP structures and mechanisms of action; thus, developing a single resistance mechanism effective against all AMPs is highly challenging.[33, 62, 122] In addition, bacterial adaptation and resistance development to AMPs is not a result of an accelerated mutation rate, as observed for antibiotics.[110] Moreover, AMP functions span from antimicrobial to immunomodulatory, activating the host cell to combat the pathogens through a wide range of mechanisms involving immune cells, cytokines and complement effectors.[57, 62] While bacterial resistance to AMPs can occur, the multifaceted nature of AMPs and multitarget action mechanisms make them less susceptible to induce resistance mechanisms.

1.2.4 Clinically approved and submitted for approval AMPs

Several synthetic and natural AMPs are currently under clinical trials for their potential applications as antimicrobial, antifungal, anticancer and immunomodulatory drugs. The *Data Repository of Antimicrobial Peptides* (DRAMP) database reported that at least 96 AMPs have been developed by pharmaceutical companies and submitted so far for clinical investigation, representing around 0.43% of the total AMPs listed on DRAMP (this database reports a total of 22528 natural and synthetic AMPs). Among them, 49 are intended for antibacterial applications; four for antibacterial and antifungal properties; seven are described to have antifungal capacity, being one of them active against *Candida* spp., and other two have anti-HIV activity; four have anticancer properties; two are potential chemokine inducers, and only one has a broad-spectrum activity (this information is based on the last DRAMP updated information of clinical entries from May 17th, 2023).[123]

However, most of those AMPs are still under preclinical trials (31) and between phase I and II clinical trials (32). Only 18 AMPs have reached phase III clinical trials, and at least four of them have been withdrawn from the AMPs pipeline because they did not show apparent efficacy and superiority over conventional treatments (MSI-78 DRAMP18057, iseganan DRAMP18059 and rBPI21 DRAMP18069) or they induced severe adverse effects

(murepavadin DRAMP20774). In addition, DP178 (T20, Enfuvirtide & Fuzeon DRAMP18181), a potent inhibitor of viral infection, has been approved by the FDA as an antiviral therapy for the human immunodeficiency virus (HIV).[123]

Furthermore, 11 AMPs are currently on the market for treating bacterial infections. For instance, daptomycin (DRAMP18058, lipopeptide),[124] dalbavancin (DRAMP18067, semisynthetic lipoglycopeptide derivate of teicoplanin),[125, 126] telavancin (DRAMP18086, semisynthetic glycopeptide antibiotic derived from vancomycin),[126] oritavancin (DRAMP18159, glycopeptide),[126, 127] vancomycin (DRAMP29330, glycopeptide),[128] and bacitracin (DRAMP29315, homodetic cyclic peptide) have been employed for the treatment of Gram-positive bacterial infection. In contrast, colistin (DRAMP29317, polymyxin antibiotic)[129] and polymyxin B (DRAMP29328, polymyxin antibiotic)[130] have been introduced against Gram-negative bacteria. Moreover, other AMPs such as gramicidin D (DRAMP29333, heterogeneous mixture of gramicidins A, B and C, alternating D and L aa)[131, 132] are active against most Gram-positive and some Gram-negative bacteria. Gramicidin S (DRAMP29332, cyclic peptide biosynthesised from gramicidin in *B. brevis*)[132] and tyrothricin (DRAMP29329, polypeptide antibiotic mixture obtained from *B. brevis*),[133] in addition, have antifungal activity.

These statistics suggest that despite the vast number of AMPs discovered, designed, and characterised mainly *in vitro* in recent years, there are still many challenges and a long way to go before they can be broadly employed as human drugs instead of conventional antibiotics.

1.2.5 Design of peptides with improved properties

Many challenges still limit AMP production and widespread use as a clinical drug. For instance, high production costs, low stability, low bioavailability, low activity in physiological conditions, and the potential to induce undesired immune responses are often highlighted as critical concerns.[33, 134] AMP development and production are reported to be costly processes compared to antibiotic production; while a gram of aminoglycoside production costs less than $1, the chemical synthesis of a gram of an AMP costs $50 - 400;[135] therefore, there is an urgent need to develop other strategies for commercial-scale production. Moreover, due to low selectivity, AMPs are often hemolytic and cytotoxic to eukaryotic cells at antimicrobial concentrations.[136] Another obstacle to the clinical introduction of AMPs is related to their reduced activity and stability in clinically relevant environments; some AMPs may be sensitive to physiological salt conditions, displaying a reduced or abolished bactericidal activity, serum proteins such as albumin and host cells may interact with AMPs interfering with their activity as well as the high susceptibility of AMPs to proteases degradation.[137] The following sections (1.3) will cover the aspects of AMP production platforms to improve production yields while reducing costs. Herein, we briefly summarise the main strategies to enhance AMP activity, toxicity, and pharmacokinetics *in vivo* (Figure 13).

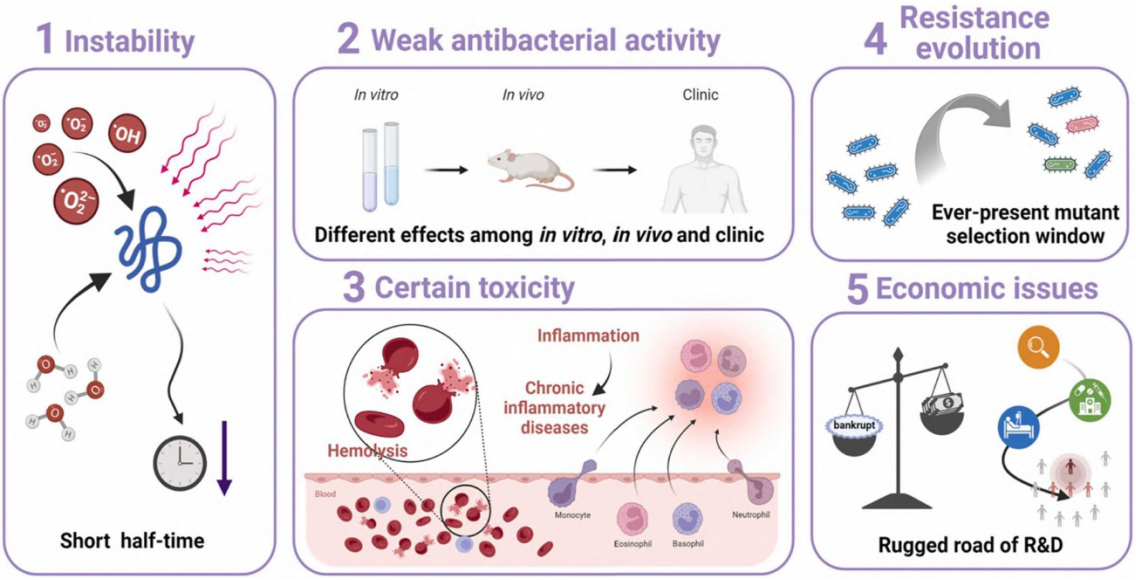

Figure 13. The main challenges for AMP translation into clinical and therapeutical agents. Reprinted from ref.[138] under a Creative Commons Attribution-NonCommercial-NoDerivs 4.0 International. Copyright © *2023 by Jiaqi Xuan, Weiguo Feng, Jiaye Wang, Ruichen Wang, Bowen Zhang, Letao Bo, Zhe-Sheng Chen, Hui Yang, Leming Su. Published by Elsevier Ltd.*

1.2.5.1 Modification of peptide sequence and length

The length of AMPs is crucial for antimicrobial activity and stability; it is very well characterised that at least 22 aa are needed to form an α-helical structure to cross the bacterial lipid bilayer for the barrel-stave model, while only eight aa are required for β-sheet AMPs; thus, the AMP length affects its secondary structure and mechanism of action. Most of the AMPs annotated so far are made of 10-50 aa, indicating that a considerable number of aa may not contribute to their antibacterial activity. Thus, one of the common strategies is to determine the optimal AMP length to obtain a balance between stability and activity while contributing to lowering the cost of production; nevertheless, there is no predetermined or consensus manner to establish the optimal length of the peptide and the implications of C-terminal or N-terminal truncation on the activity of a particular peptide.[33]

In addition, modification of the peptide hydrophobic or charged aa content could also contribute to AMP activity while reducing its toxicity. For instance, introducing positively charged aa into indolicidin and magainin-2 has significantly potentiated antimicrobial activity.[102, 139] On the other hand, super hydrophobic AMPs can also lead to decreased antibacterial activity and increased mammalian toxicity.[140]

C-terminal amidation and N-terminal acetylation are common PTMs found in a wide variety of peptides and proteins; N-terminal acylation has been reported to increase AMP stability against protease degradation in human serum, while C-terminal amidation may and may not improve peptide stability. Moreover, fluorinated aa can enhance the stability of synthetic peptides, which is explained by the increase in size or hydrophobicity.[141] In addition, N-methylation of backbone and side chains is reported to improve AMP activity.[33]

1.2.5.2 Structural modifications

Three main cyclisation patterns are known in natural AMPs (backbone-backbone, backbone-side chain, and side chain-side chain) and have been described above (section 1.2.1.4). In all cases, cyclic AMPs are more compact and less exposed; thus, they are expected to be more resistant to protease activity. Nevertheless, the cyclisation effect is only sometimes straightforward since either a decreased or increased protease susceptibility has been observed for cyclic peptides compared to their linear counterpart.[141] Cyclic AMPs derived from melittin (side

chain-side chain) displayed increased antibacterial activity and reduced hemolytic activity.[142] The cyclisation of arginine- and tryptophan-rich peptide (RRWWRF-NH2, backbone-backbone) showed higher antimicrobial activity and cell selectivity.[143] Moreover, a cyclic peptide made of the C-terminal domain (RRKK) of hBD3 and the internal domain of hBD1 (PIFTKIQGT) retained the antimicrobial and antiviral activity of the parent peptides, and its oxidised form was considerably more stable in human serum.[144] Conversely, a reduction of antimicrobial capacity and hemolytic activity has been reported for cyclic magainin 2 (side chain-side chain).[142]

Substituting L-aa with D-aa can increase resistance to protease degradation while maintaining antimicrobial activity. For instance, engineered GF-17 (derived from LL-37) containing 3 D-aa in replacement of L-aa was toxic to bacteria but not human cells and structural analysis showed that this peptide adopted a non-classical amphipathic structure.[145]

Moreover, introducing structural constraints such as α-helical or β-sheet motifs or substituting particular aa to modify the AMP structure can stabilise the peptide, improve its activity, and, in some cases, modulate hemolysis. Magainin-2 exerts its activity via amphiphilic α-helix. Thus, substituting glycine with alanine, an α-helix promoting aa, increased the AMP antibacterial activity.[146]

1.2.5.3 Hybrid peptide and peptidomimetic design

Chimeric peptides combine sequences from different naturally occurring AMPs to create hybrid peptides with improved stability, activity, selectivity and resistance to degradation. LM1, a hybrid peptide analogue obtained by the fusion of truncated melittin (11 aa) to LL-III (15 aa), has been reported to have high stability and great antimicrobial potential towards *Acinetobacter baumannii* and *S. aureus*.[147] Also, a hybrid peptide obtained from bovine lactoferricin and buforin II resulted in potential antifungal molecules for future therapeutic applications against *Cryptococcus neoformans var. grubii*.[148] Cecropin A-melittin hybrid peptide showed enhanced antimicrobial activity and selectivity against bacterial membranes.[149] Indolicidin-ranalexin hybrid peptides showed potent antibacterial activity against *S. pneumoniae* and very low toxicity against human red blood cells compared to parental AMPs.[150]

The hBD activities are often affected by their sensitivity to physiological salt concentration; a hybrid peptide composed of hBD2 and hBD3 not only showed higher efficacy in killing both *E. coli* and *S. aureus* but also showed improved antimicrobial behaviour in physiologic salt concentrations compared to the wild-type molecules, demonstrating that hybrid peptides may contribute to the search and development of novel-antibiotic agents with enhanced performance in physiological environment.[151] Similarly, Scudiero *et al.* (2010) designed two analogues of hBD1 and hBD3 with enhanced antimicrobial activity and no salt sensitivity without affecting its chemotactic activity. Their findings suggest that the hBD1 internal region and the hBD3 C-terminal region are critical for antibacterial activity at high salt concentrations. In contrast, deletion of the N-terminal region of hBD3 increases antibacterial activity. Moreover, the analogue carrying the hBD1 internal region and the hBD3 C-terminal region showed enhanced antiviral activity against herpes simplex virus.[82]

Moreover, in recent years, synthetic AMP analogues or "peptidomimetics" have been designed to mimic the AMP physico-chemical properties (cationic charge, hydrophobicity, amphiphilicity) and biological effects while being stable to enzymatic degradation, displaying potent activity against multidrug-resistant bacteria, and improved pharmacokinetic properties. Peptidomimetics contains in their backbones non-peptidic components;[152, 153] among peptidomimetics, there are β-peptides which are composed of β-aa instead of α-aa,[154] α -peptoids which are N-alkylated glycine oligomers (cyclic peptoids, peptide-peptoid hybrids),[155] β-peptoids which are N-alkylated β-

alanine oligomers,[155] AApeptides containing N-acylated-N-aminoethyl aa units derived from chiral PNA backbones,[156] β-turn mimetics,[157] as well as stapled peptides.[158]

1.2.5.4 Lipidation, glycosylation and PEGylation

Glycosylation involves the attachment of sugar moieties to AMPs through strategies like O-, N-, C-, and S-glycosylation. Glycosylation enhances proteolytic stability, solubility, aggregation ability, and AMP pharmacokinetic properties. However, it may reduce the hydrophobicity and the overall positive charge of the peptides, which may only sometimes improve their antimicrobial capacity. Moreover, glycosylation holds great promise for developing therapeutic AMPs with decreased immunoreactivity within the host by attaching bacterial-derived glycans like polysialic acid.[159] For instance, O-glycosylated formaecin and formaecin 2 potentiated the antimicrobial activity towards *E. coli.* In addition, a glycosylated analogue of indolicidin (βGlc-T9, K7) displayed potent antibacterial activity with reduced toxicity against erythrocytes and macrophage cells, thereby enhancing therapeutic selectivity; the inclusion of sugar moiety improved peptide solubility and interestingly, despite glycosylation, the peptide's mode of bacterial killing, functional stability, LPS binding, and cytokine inhibitory potential remained unaffected.[160]

Conjugation of AMPs to lipid moieties involves the attachment of a fatty acid moiety to the N-terminal or lysine side chains. Lipidation can increase peptide hydrophobicity and self-assembling ability, enhancing its interaction with the membrane and permeability and protecting the AMP against enzymatic proteolysis. Lipidated AMPs show an increased affinity for bacterial membranes, aiding their insertion and disrupting membrane integrity.[159] For instance, a nanobacterial agent developed by lipidation of HD5 with myristic acid followed by non-covalent self-assembly displayed higher antibacterial activity in the presence of nearly physiological salt concentration or serum. When tested *in vivo*, it showed a low toxicity in animals and protected mice from MRSA infection and *E. coli*-induced sepsis.[161] Moreover, a hybrid peptide derived from G3 with simultaneous lipidation (N-terminal conjugation to caprylic acid) and glycosylation (C-terminal conjugation to galactose) displayed enhanced antibacterial and anti-biofilm activities, as well as outer membrane permeability and reduced hemolytic activity.[162]

Among the advantages of PEGylation are the increase of peptide solubility and stability in aqueous solutions, prolonged circulation time by reducing renal clearance, and reduced immunogenicity. Recent studies indicate that PEGylation does not alter the AMP mode of interaction and maintains antimicrobial activity while minimising tissue toxicity and improving proteolytic resistance to trypsin and proteinase K.[163] Nevertheless, it remains one of the less explored AMP modifications.

1.2.5.5 Computational Design

Bioinformatics tools offer potent methods for designing and optimising AMPs, leading to the development of more effective and safer treatments for combating microbial infections. Over the past decade, several online databases and computational tools have emerged, making it easier to explore AMP diversity[17] and to design AMPs with increased selectivity and reduced adverse effects.[164-167] Thus, machine learning has become a popular approach for high-throughput molecular design of AMPs. Fueled by a deeper understanding of AMP mechanisms and the vast molecular datasets collected by researchers over decades, these algorithms learn from patterns in the data to identify promising candidates more quickly than traditional methods. Some commonly used machine learning algorithms include artificial neural networks, fuzzy K-nearest neighbour, logistic regression (LR), random forest (RF), support vector machine (SVM) and quantitative structure-activity relationship (QSAR),[168] being the latest

pointed as highly effective in predicting models based on biological behaviour.[169] Recently, the LR, RF and SVW algorithms were combined and successfully employed to accelerate the *de novo* design of valuable AMP candidates; out of the 180 peptides chemically synthesised, 18 showed antimicrobial activity against pathogenic bacteria, with 16 of them with MICs of less than 10 μg/mL against at least to one of the tested microorganisms.[170] QSAR is a modelling technique used to predict the biological activity of molecules based on their chemical structure, establishing mathematical relationships between the structural features of peptides and their activity. By analysing patterns in data from experimental assays, QSAR models can predict the potency, selectivity, and other properties of AMPs based on their structural characteristics. This approach facilitates the rational design and optimisation of AMPs with desired antimicrobial properties, accelerating the discovery and development process.[164] For instance, an *in silico* library containing a hundred thousand peptides derived from 1018 AMP was employed to predict using QSAR models the probability that a peptide would possess antibiofilm activity; the subset of predicted peptides was SPOT-synthesized, and the assessment of their activity revealed that QSAR methods resulted in about 85% prediction accuracy. Intriguingly, compared to the parental AMP, one of the predicted peptides showed an 8-fold increased antibiofilm activity *in vitro*, highlighting QSAR capabilities for predicting improved AMPs.[171]

1.3 Production of AMPs: chemical synthesis vs heterologous production

AMPs can be isolated from their natural sources, chemically synthesised, or produced in heterologous organisms (Figure 14). Nevertheless, using AMPs as clinical antimicrobial agents demands cost-effective large-scale production and purification methods.[172]

Isolation from natural sources ensures the obtention of the AMPs in their native conformation, often with PTMs essential for their biological activity or to enhance their functionality. However, it's a labour-intensive process that requires a large amount of material from natural sources since the peptides are often produced in low quantities and involve complex purification steps that yield very low amounts of AMPs. Moreover, ethical and environmental concerns may arise depending on the source, mainly if certain species produce them. Consequently, it is not cost-effective, hindering large-scale production and commercialisation efforts (Figure 14A). Therefore, chemical synthesis and recombinant technologies are the most promising platforms for AMP production for research purposes and translation into clinical products.[172, 173] The following subsections will cover each technology's peculiarities, highlighting its main advantages and drawbacks for the large-scale production of AMPs needed to meet clinical and biopharmaceutical requirements.

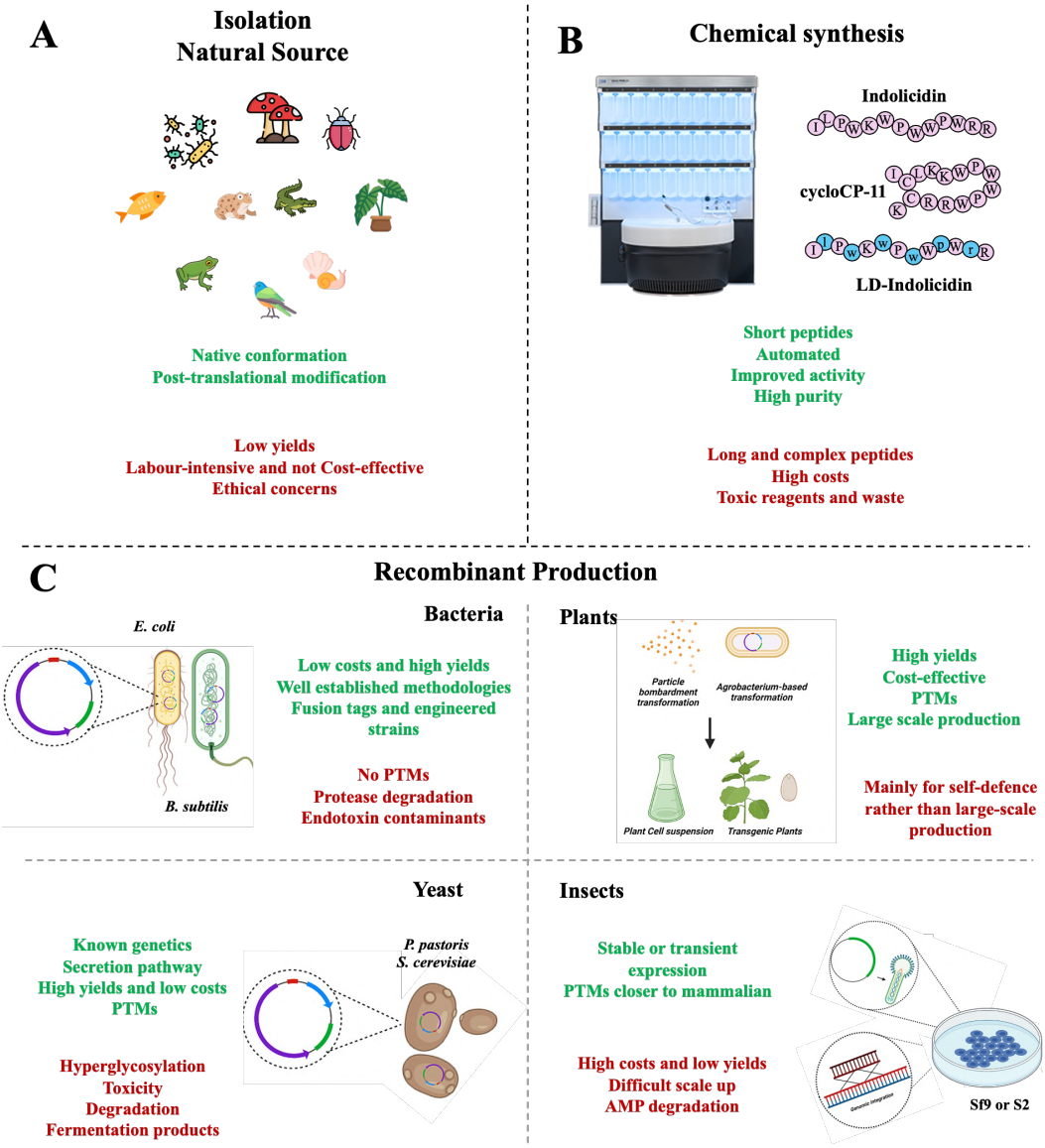

Figure 14. AMPs can be extracted from their natural source (**A**), chemically synthesised (**B**), or recombinantly produced in bacteria, yeast, fungi, plant, and insect cells (C). Each production platform has advantages and drawbacks, and their employment is directly correlated to the AMP's characteristics and properties. The scheme in C was adapted from ref.[174] Soumya Deo, Kristi L. Turton, Tajinder Kainth, Ayush Kumar and Hans-Joachim Wieden *"Strategies for improving antimicrobial peptide production"*, Biotechnology advances, Vol 59, Page 107972 (2022) with permission from Elsevier. *Copyright © 2022 Elsevier Inc.*

1.3.1 Chemical synthesis

Most of the peptides currently used as therapeutic agents and those already in clinical trials have been produced by chemical synthesis methods (Figure 15B).[175] The introduction of solid-phase techniques revolutionised the landscape of peptide synthesis, rendering it rapid, efficient, and reliable; nevertheless, large-scale peptide production is still expensive and constrained by the size of the peptides and their functional structure, among other factors.[176]

Chemical synthesis involves the stepwise assembly of peptide sequences in a laboratory setting, offering precise control over peptide design and modifications. The most used method for peptide synthesis is solid-phase peptide

synthesis (SPPS), introduced by Merrifield in 1963, allowing to obtain peptides of small to medium sizes (up to 50 aa).[177] In this methodology, the first residue of the peptide is immobilised onto a solid support, and each residue, in the form of protected aa, is sequentially added in a controlled manner, minimising side reactions and facilitating purification steps between each coupling process, leading to higher yields and purity compared to other synthesis methods. Moreover, it can be automated, allowing for high-throughput synthesis of peptide libraries or large-scale production of peptides with minimal manual intervention.[178] In addition, SPPS offers excellent flexibility in peptide design, enabling the incorporation of several modifications, such as the incorporation of non-proteinic aa and D-aa, as well as the production of hybrid, lipidated, PEGylated and cyclic AMPs, to tailor their properties and functions specifically.[173, 178-180]

Nevertheless, this technology still poses challenges for synthesising long (more than 50 aa) or highly complex peptide sequences due to the potential for aggregation, steric hindrance, and incomplete coupling reaction.[178, 180] Moreover, it requires expensive equipment, resins, and reagents and has relatively high purification costs, which are not viable for long AMPs.[180] In addition, peptides containing cysteines whose 3D structure is stabilised by disulfide bridges are, in most cases, difficult-to-synthesise and purify, thus hampering their production or increasing costs.[181] Peptides obtained through this method lack complex PTMs, such as glycosylation, often present in natural AMPs and are needed for their biological function.[182] In addition, it involves using large amounts of highly hazardous coupling reagents and solvents and generates highly toxic waste products with a detrimental impact on the environment.[179, 183] In summary, chemical synthesis is often employed to produce short AMPs with low complexity and cysteine content without PTMs.[172] Thus, it is imperative to find alternatives for the large-scale production of complex AMPs with reduced costs and more sustainable and greener chemistries.

1.3.2 Heterologous production

Advances in DNA recombinant technologies have enabled the development of optimised expression systems to meet the demands of translating AMPs into therapeutic agents. Thus, in recent years, heterologous production platforms in prokaryotic or eukaryotic host cells have gained popularity due to their flexibility, scalability, and sustainability. They have started to be considered the most efficient platforms for peptide production in terms of time and cost.[184, 185] Therefore, AMPs have been produced in bacteria, yeast, fungi, plants, insects, and mammalian cells.[184, 186] In addition, cell-free systems have been employed, in a few cases, to produce AMPs.[187-190]

Bacterial and yeast expression systems are the most suitable for AMP production due to their high yields, low costs, scalability, easy manipulation, and well-known genetics. Indeed, AMPs produced in bacteria and yeast represent more than 95% of the total heterologous-expressed AMPs; nevertheless, bacterial cells are more often used for AMP production than yeasts.[172, 185] Few AMPs produced in mammalian cells have been reported; however, this technology is too expensive, and for most AMPs, the reason for employing this system does not justify their high costs.[186] In addition, AMP production in plants has traditionally been used to protect themselves from diseases; nevertheless, they have become promising bioreactors for AMP production in recent years (Figure 15C).[174, 186]

1.3.2.1 Recombinant production in bacteria

Bacterial expression systems have been widely used for peptide and protein production since they offer the highest production efficiencies. *E. coli* stands out as the most commonly used microorganism for heterologous protein production in bacteria;[191] thus, it is the first choice as a host for AMP production and the one with the highest

reported yields.[172] In addition, other prokaryotes, such as *B. subtilis* and *Propionibacterium freudenreichii*, have also been used.[180]

E. coli offers many advantages for AMP production. It is a very well-studied bacterium in terms of genetics, biochemistry, and physiology; thus, it is easy to handle and manipulate for genetic engineering purposes. Indeed, several engineered *E. coli* strains have been developed to expand their biosynthetic capacities and produce, for instance, peptides stabilised by disulfide bridges (Origami and Rosetta-gami strains) and translate rare codons (Rosetta strains).[191] Further optimising parameters such as growth conditions, promoter strength, and codon usage maximises the yields.[172, 191-194] Its fast growth rate, the simple fermentation equipment needed, and the inexpensive media employed contribute to reduced production times and costs, making it cost-effective and efficient for industrial-scale production.[184]

E. coli and prokaryotes, in general, also face challenges for AMP production. Many AMPs exhibit toxicity not only against target microbes but also towards the host cells producing them, leading to decreased cell viability, lower yields, and difficulties in maintaining stable production lines. Moreover, AMPs, being short and highly cationic, are susceptible to endogenous protease degradation, further reducing production yields.[174, 180, 186, 195] Hence, several strategies have been developed over the last years to overcome these limitations and will be covered in the following subsection (1.3.2.1.1).

Moreover, compared to other expression platforms, *E. coli* lacks the machinery for most of the PTMs (particularly glycosylation), which may impact the efficacy of the AMP.[196] Nevertheless, PTMs do not seem critical for producing AMPs;[186] hence, AMPs that strictly depend on PTMs for their activity must be produced in other expression systems or through semi-synthetic approaches.[196]

Even though purification processes are generally straightforward, with several affinity tags available for AMP purification through chromatographic methods,[190, 191] they account for more than 70% of the costs of downstream processes for AMP production.[197] Thus, a promising solution to the high cost of chromatography techniques is the employment of Elastin-like Polypeptides (ELPs) and four-helix bundle protein DAMP4 carriers that allow protein isolation by non-chromatographic approaches.[184, 198-201] Due to the relevance of ELP for the present thesis, the particularities of these carriers will be covered in detail in the following section (1.4).

1.3.2.1.1 Strategies to hinder AMP toxicity and reduce protease degradation

1.3.2.1.1.1 Inclusion bodies

Overexpression of AMP as inclusion bodies (IBs) has proven effective for their production in *E. coli*. AMPs of considerable size and rich in cysteine residues are prone to aggregate and form IBs. While proteins' production as IBs may be detrimental and involve complicated purification and folding steps,[190, 191] producing AMPs as IBs is beneficial since they shield AMP toxicity and hinder protease degradation.[186] Moreover, in recent years, IBs have started to be considered active biomaterials, and several studies have highlighted the potential employment of AMP-based IBs against pathogenic bacteria.[186] In addition, using AMP-IBs can improve the half-life of AMPs *in vivo,* modulating their release and maintaining antimicrobial potency over time.[186, 202] For instance, lingual AMP and HD5 IBs have been reported to be strongly active against MRSA and *P. aeruginosa*, with antimicrobial activities comparable to the soluble AMPs.[202] Further, surfaces covered by AMP-IBs inhibited carbapenem-resistant *K. pneumoniae* biofilm formation.[203]

1.3.2.1.1.2 Production as fusion proteins

A widely used strategy to hinder AMP toxicity towards the host cells is their production as fusion proteins, which directly impacts the protein solubility and stability (herein, the AMP-fusion term will refer to the production of AMP fused to a carrier).[174, 180, 184, 204] The presence of carriers modifies the AMP properties, changing their overall charge and increasing their size, thus reducing their toxicity and protecting them from protease degradation.[204] In some cases, the employment of carriers resembles the physiological production and storage of AMPs as inactive pro-AMPs,[205] as described for defensins and cathelicidins in section 1.2.2. Thus, when exploring the designs for fusion AMPs, it is recommended to introduce a cleavage method to release the AMP from the AMP-fusion.[180, 184, 193, 204] Nevertheless, some AMPs must be released from the AMP-fusions to be active, while others retain their functionalities as fusion products.[204, 206] Further, once the AMPs are released from the carriers, they are often purified using cation-exchange chromatography since the isoelectric point of AMPs is usually higher than that of the carriers.[204]

Several carriers are available and have been proven to positively contribute to the successful production of AMP-fusions in *E. coli* (Figure 15).[184, 204, 193] They can be grouped into three main classes: solubility-enhancing, aggregation-promoting and self-cleavage carriers.[204] Consequently, diverse strategies have been developed employing one or multiple carriers fused to the AMP C-terminal and/or N-terminal;[184, 207] for instance, a solubility carrier, in combination with a purification tag, is a widely used design that facilitates AMP-fusion production and simplifies its purification. However, no general rules can guarantee maximum productivity when selecting carriers and designing AMP-fusion to produce a given AMP.[184]

Trx, glutathione transferase (GST) and small ubiquitin-related modifier (SUMO) belong to the solubility-enhancing carriers.[204] Trx is the most widely used carrier for producing AMPs,[180] accounting for more than 25% of the AMP-fusions; it does not only enhance the solubility of AMP-fusions produced in *E. coli* cytoplasm but also improves the AMP yields since, given its small size, allows obtaining higher ratios AMP/AMP-fusion.[208] GST dramatically improves the AMP-fusion solubility and can be employed simultaneously as a purification tag for affinity chromatography; nevertheless, in some cases, it has been found susceptible to protease degradation, thus ending in reduced yields.[195, 204] SUMO also allows for higher ratios of AMP/AMP-fusion. In addition, it offers an efficient release of the AMP since it is the target of a highly specific protease.[209] On the contrary, cleavage methods should be considered for releasing the AMP from Trx and GST fusions, and chemical or enzymatic release strategies have been employed. Moreover, Trx and SUMO are frequently combined with purification tags, mostly His_6-tag, to simplify the downstream processes.[184, 204]

For instance, active hBD1 has been recombinantly produced in *E. coli* N-terminally fused to a solubility tag and released from the carrier by incubation with a specific protease.[210] Moreover, Maiti *et al*. (2014) reported high levels of soluble protein when a His_6-Trx carrier was fused to hBD1 and hBD2, and AMPs released by incubation with enterokinase were active against *E. coli, S. aureus* and *Salmonella enterica serovar Typhi*.[211] In addition, hBD3 have also been produced in *E. coli* as a His_6-Trx fusion protein where optimisation of the culture conditions led to high expression levels of soluble His_6-Trx-hBD3, and the released AMP demonstrated antimicrobial activity towards *E. coli* K12.[212, 213]

Aggregation-promoting carriers are frequently combined with His_6-tag. Oppositely to the solubility-enhancing carriers, they allow the production of the AMP-fusion as IBs, which protect the AMP from degradation, mask their toxicity to the host cells and simplify purification steps.[204] The most common method for AMP release from

aggregation-promoting carriers is chemical cleavage using cyanogen bromide (CNBr), formic acid or hydroxylamine.[204, 214, 215] For instance, high expression levels of hBD1 have been reported when fused to the C-terminal of a His_6-tag and PaP3.30 combined carrier, and the release of the AMP from the fusion was achieved by chemical treatment with CNBr.[214] Also, high levels of fusion protein were detected when indolicidin was fused to PurF and produced in the cytoplasm of *E. coli* as IBs.[215]

Self-cleavage carriers, like intein and N^{pro}, allow for a simple self-cleavage strategy upon induction without harsh chemicals or expensive enzymes.[216] Intein carriers have also been employed with ELPs and chitin-binding protein (CBP) carriers. For instance, a CBD-intein N-terminal carrier fused to hBD2 was successfully produced regarding solubility and yields and allowed for the pH-dependent release of an active AMP domain.[217] Nevertheless, there are several limitations to their use at industrial levels, including the intein uncontrolled cleavage and N^{pro} incomplete release.[204]

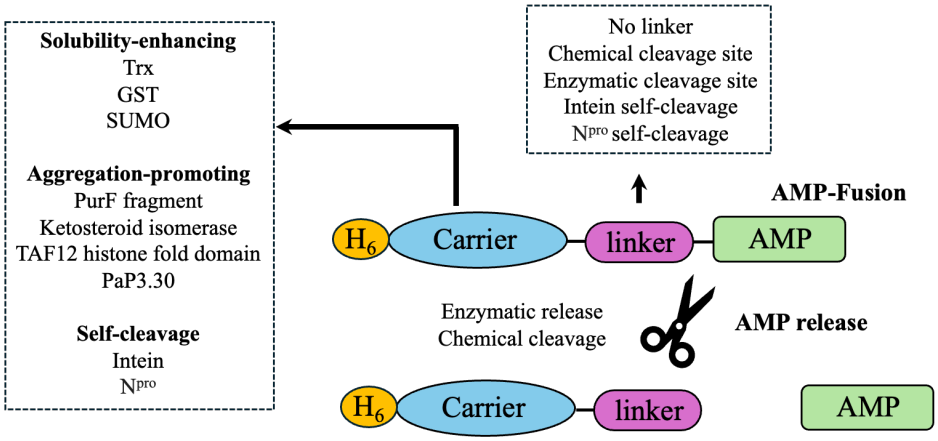

Figure 15. AMPs are commonly produced as fusion proteins to hinder their toxicity toward bacterial hosts. Several carriers and release systems have been described and employed when producing AMP-fusions.

Another approach is to use a toxicity quencher to hinder the detrimental effect of AMP on bacterial cells. In this strategy, the AMP is co-expressed with an anionic peptide that is highly prone to aggregation. Thus, like aggregation-promoting carriers, the AMP-toxicity quencher complex is produced in the cytosol of the bacteria as IBs, avoiding the lethal effect of AMP while reducing protease degradation. This system's main advantage is that it does not need further cleaving steps. The AMP and the quencher are not covalently linked; their complex relay only in electrostatic interactions. Thus, they can be easily separated by cation exchange chromatography once they are solubilised from IBs.[218]

1.3.2.1.1.3 Multimerization and hybridisation strategies

Multimeric expression has been demonstrated to improve the overall expression and yields of AMPs. This approach involves increasing the gene copy number to enhance transcription levels and express the AMPs as stable multidomain proteins.[219, 220] APMs are produced as multimeric proteins, and once isolated from the host proteins, the AMP monomers are often released by chemical cleavage and further purified. Nevertheless, the protein expression levels are not always directly correlated to the increase of the copies of the AMPs. Indeed, it has been observed that the expression levels reach a maximum with certain copies of the AMP and drop dramatically if the copy number is further increased. In addition, the effect of multimerisation is AMP-dependent and varies for different expression systems.[204]

Further, multimerisation strategies have been combined with solubility carriers, where several copies of the peptides also increase the AMP/AMP-fusion ratio. For instance, Xu *et al.* (2005) studied the effect of coding hBD2 in one, two, four and eight copies into four expression vectors and observed that the copy number, the vector choice and the presence of a solubility carrier impacted the expression of hBD2 multimers; in fact, expression was not detected from multimers cloned into pQE-30, pET-28a (one, two or four copies) and pBV220 (one or two copies) allowed the expression of the AMP but in low levels while only pGEX-4T-2, containing a GST carrier and one or two copies of hBD2, showed high expression levels. However, the Authors did not assess the antimicrobial activity of the monomers.[221] Later, Xu *et al.* (2006) reported that the tandem expression of His_6-Trx-2hBD2 (carrying two copies of the AMP) showed good solubility and volumetric productivity, and the released and pure AMP was efficient in inhibiting *E. coli* K12 growth.[222] Moreover, indolicidin multimers (three copies) have also been fused to Trx, improving the solubility of the AMP-fusion and final yield of the AMP monomer while retaining its antimicrobial capacity.[223]

On the other hand, hybridisation strategies aiming to improve expression levels and reduce toxicity towards the host cells have also been employed. Further, hybridisation strategies can increase the AMP selectivity, stability, antimicrobial capacity, and/or add other functionalities.[219] In addition, there are reports where hybrid proteins obtained with high yields have been cleaved, giving rise to monomeric active AMPs or used as a hybrid protein with potentially enhanced activities compared to parental peptides.[174] For instance, an N-terminal cecropin A (CecA) fragment has often been hybridised with other AMPs to reduce toxicity and improve selectivity.[224] A hybrid CecA-forlicidin-2 peptide exhibited excellent antibacterial activity and cell selectivity toward bacterial over mammalian cells compared to forlicidin-2, a highly cytotoxic AMP towards eukaryotic cells.[224]

Overall, *E. coli* offers numerous advantages for AMP production in terms of ease of handling, genetic engineering flexibility, rapid growth, high expression levels, simple purification, low production costs, stability, and simple scaling up. These advantages make it a popular choice for AMP production for research and industrial applications.[185] However, the production of clinical AMPs in *E. coli* can also encounter regulatory limitations due to contamination with endotoxins, particularly LPS, and the release of genetically modified organisms into the environment.[190, 225, 226]

1.3.2.2 Other production systems

1.3.2.2.1 Yeast and fungal expression systems

Pichia pastoris and *Saccharomyces cerevisiae* yeast expression systems are extensively used to produce proteins and peptides since they offer the advantages of unicellular organisms, including ease of genetic manipulation, rapid growth rates, and high protein yields as well as the secretory, post-transcriptional and PTMs machinery present in eukaryotes.[172, 186, 227, 228] Peptides are produced intracellularly or secreted to the extracellular milieu, simplifying downstream purification and processing, resulting in good yields and simple scale-up processes. [186, 229]Furthermore, yeast expression systems enable the production of correctly folded and functional AMPs, including disulfide bond formation, O- and N-glycosylation, and accurate processing of signal sequences.[193, 230, 231] Thus, expression systems employing *P. pastoris* have recently gained popularity for the extracellular production of folded and matured AMPs.[184] Several AMPs have been produced in yeast systems, among them the members of the family of hBD. Properly folded and active hBD1 and hBD2 were expressed in *S. cerevisiae*,[232, 233] and an anti-MRSA hBD2-derived AMP and HD5 were produced in *P. pastoris*.[234, 235]

Nevertheless, yeast expression systems present some challenges. Similarly to bacterial expression systems, producing AMPs may be toxic for the host cells, and yeast endogenous proteases may degrade them, reducing peptide production yields, stability and/or efficacy;[232] thus, fusion strategies have been implemented for this expression system.[174, 180, 184] Yeast glycosylation patterns, often hyperglycosylated peptides, differ from those found in mammalian cells, potentially impacting protein function or immunogenicity.[186, 196] Moreover, even when several AMPs have been produced with high yields in yeast, many others have been produced in very low quantities or/and as inactive molecules.[185]

Fungal expression systems are promising platforms for AMP production; however, they remain among the least explored platforms since developing fungus-based expression systems is complex and time-consuming. Among their advantages are their capacity to secret the AMPs to the media, their ability to produce disulfide bridges and superior PTMs than yeast and more similar to those of mammalian cells, their high yields (up to 25 g/L) and the low cost for their scalability.[174, 236]

1.3.2.2.2 Plant expression systems

Plant recombinant production systems are unique in terms of scalability, cost-effectiveness, and safety. These systems use plants, such as *Nicotiana benthamiana*, *Nicotiana tabacum, Oryza sativa* and *Arabidopsis thaliana*, as bioreactors to produce complex proteins at a large scale and a relatively low cost compared to traditional expression systems. Moreover, plant-based expression systems offer inherent safety benefits, as plants are not known to harbour human pathogens and do not produce endotoxins or other contaminants typically associated with microbial fermentation. Additionally, plants can perform many PTMs, such as glycosylation, which are essential for the functionality and efficacy of therapeutic proteins. AMPs overproduced in plants can often be easily extracted, facilitating downstream purification processes.[174, 237, 238] Nevertheless, certain drawbacks still need to be addressed, among them their variable efficacy, stability in successive generations, and potential toxicity of the AMPs to plant cells and tissues.[238] In addition, most plant expression systems developed so far to produce AMPs aim to enhance plant properties and protect themselves from diseases rather than to establish AMP production and purification platforms at a large scale.[172, 186, 238] However, their capacities have drawn the scientific community's attention, and several steps have been taken to convert plants into AMP molecular farming.[174, 237] An expression system for growing plant-derived cells in suspension combined with protein secretion and scaling up through bioreactors has been developed.[174]

1.3.2.2.3 Insect expression systems

Few AMPs, such as human defensins, have been successfully produced in insect cells.[79, 239-241] Insect expression systems offer several advantages for protein production and have been primarily employed to produce insect-derived AMPs, which can be highly toxic when expressed in bacteria and yeast hosts.[242] These systems exploit insect cells, typically derived from species such as *Spodoptera frugiperda* (Sf9, Sf21), *Trichoplusia ni* (High-Five) or *Drosophila melanogaster* (S2), for either transient or stable production of the desired AMP.[230, 242-244] Transient expression often involves infecting insect cells with recombinant baculovirus carrying the genes encoding the protein of interest. In contrast, the vector is inserted into the cell genome for stable expression.[230, 243] The main advantage of insect expression systems lies in their capacity to perform complex PTMs, including glycosylation patterns, since insect cells are higher eukaryotes.[243, 245] Nevertheless, insect cells produce shorter and less complex N-glycans than mammalian cells,[196, 243] and O-glycosylation is only feasible in stable expression systems.[230]

Additionally, they offer safety benefits, as baculoviruses are specific to insects and do not infect vertebrates, minimising concerns related to pathogenicity.[245] Still, their use for large-scale production of AMPs is limited as it encounters several limitations when compared to bacteria and yeast expression systems, including high production costs, low yields, scalability challenges, and susceptibility to infection. Moreover, another limitation is the long time required to go from DNA to target protein and the decay of baculovirus over time.[196] Furthermore, degradation due to protease activity may be problematic, mainly due to the lytic cycle of the baculovirus.[174, 243, 245]

1.3.2.2.4 Mammalian expression systems

Mammalian expression systems are the preferred choice for producing biopharmaceutical and other therapeutic proteins, including antibodies, hormones, and growth factors, due to their ability to generate proteins with high fidelity to their native counterparts and compatibility with regulatory requirements for human therapeutics. These systems employ mammalian cells, such as Chinese hamster ovary (CHO) and human embryonic kidney 293 cells, to produce proteins with the notable advantage of achieving proper protein folding and PTMs, including glycosylation, phosphorylation, and disulfide bond formation, since they closely mimic the native environment of human cells.[196, 246] However, mammalian expression systems' main limitations are the high costs, long production times, and potential cell line stability and variability issues;[186, 196] thus, they are not as popular as bacterial and yeast systems for recombinant AMP production.

1.3.2.2.5 Cell-free protein systems

Cell-free protein systems (CFPS) have been employed to produce and study AMPs, including hBD2.[187-189, 247, 248] These systems carry all the enzymes and proteins needed for gene transcription and protein translation without bacterial membranes or cell wall structure, affording the production of peptides with antibiotic activity.[249] They comprise bacterial lysates or purified components that work as peptide manufacturers assembled *in vitro*. Further, protein production can be operated in either batch or continuous mode. The batch system is simple and convenient but with low yield. In contrast, in the continuous exchange system, high quantities of protein can be obtained due to the continuous replacement of substrates and the removal of side metabolic products.[187, 250] Several CFPS have been developed in the last years based on *E. coli,*[187-189] *S. cerevisiae*,[251] *Vibrio natriegens,*[252] some *Streptomyces* spp.[253] and *Bacillus* spp.[254] and CHO cells;[255] however, only *E. coli* CFPS have been employed for AMP production.[187-189] hBD2 has been successfully produced employing either batch or continuous *E. coli* CFPS, but high productivity, up to 2 mg/mL, was achieved only using continuous mode.[187-189] Nevertheless, there is no report on the use of CFPS for large-scale production of AMPs, and it remains the least exploited method for peptide production.

1.3.3 Semi-synthetic approach

Semi-synthetic strategies for peptide production have emerged in recent years to overcome the difficulties faced during the chemical and biological production of AMPs. In this approach, recombinant or naturally produced peptides are modified using chemical or enzymatic methods to enhance their activity, stability, or other desired characteristics. This strategy is essential for peptides with difficult-to-synthesise sequences or when further modifications of the peptides are needed to enhance their biological activity and stability against proteases or to improve their pharmacokinetic properties. Moreover, it can simplify the synthesis process by modifying specific regions of a peptide rather than synthesising the entire sequence from scratch. It can be more cost-effective than

complete synthesis approaches, particularly for large or complex peptides. Among the peptides produced by semi-synthetic methods are vancomycin analogues, glycopeptide and lipopeptide antibiotics.[179]

1.4 Elastin-like polypeptides as carriers for AMP production

Artificial bio-inspired polymers possess many favourable features that allow their use in biomedical and biotechnological applications, spanning from tissue engineering to drug delivery and controlled release. They mimic the structure and properties of natural biological materials; thus, they are highly biocompatible and biodegradable without releasing toxic by-products. In addition, they can be finely tuned to achieve specific properties tailored to the intended application and allow for precise control over interactions with biological systems, such as cell adhesion and protein binding. At the same time, their smart properties, i.e., their response to different environmental stimuli, constitute an advantage during purification, self-assembling, and drug release, just to mention a few.[256] ELPs are among this class of biologically inspired protein-based materials.[257, 258]

1.4.1 ELP structural properties

ELPs are stimuli-responsive biopolymers based on elastin, a key extracellular matrix protein that provides resilience and elasticity to tissues and organs. Elastin, among the most hydrophobic proteins known, is the major component of elastin fibres, and it is produced by fibroblasts, smooth muscle cells, chondrocytes, keratinocytes, endothelial and airway epithelial cells as a soluble precursor, tropoelastin.[259-261] This precursor is composed of alternating hydrophobic and hydrophilic domains encoded by separate exons; thus, the protein domain structure reflects the exon organisation of the gene.[259, 262] The hydrophobic domains are rich in glycine, valine, proline and alanine; they are often organised in repeats of three to six residues, such as PGVGV, GGVP and PGVGVA,[263] and are responsible for the elastin coacervation properties, concentrating and aligning tropoelastin molecules prior to cross-linking. On the other hand, hydrophilic domains are typically rich in lysine and alanine,[263] and are often made of stretches of Lys separated by two or three Ala residues, such as AAAKAAKAA, and are involved in cross-linking during the formation of mature elastin.[259-261] Tropoelastin cross-linking through ε-(γ-glutamyl) lysine bonds is performed by lysyl oxidase enzymes, rendering elastin remarkably insoluble and stable, lasting up to 70 years.[259-261]

Thus, most of the ELPs are designed based on the repeated VPGXG motif derived from the hydrophobic domain of mammalian tropoelastin, where the four aa of the repeat, X, represents a guest residue that can be any natural or non-natural α-aa except proline.[264] Further, the X aa is often employed to enhance ELP functionalities without affecting their thermal behaviour. For instance, introducing aa with chemically reactive side chains such as cysteines, glutamines, and lysines facilitates cross-linking among ELP molecules, while introducing tyrosines allows for spectrophotometric analysis.[265, 266]

ELPs are often denoted as $[(X_iY_jZ_k)_n]$, where X, Y, and Z specify the guest residues; i, j, and k are their relative ratios, and n is the total number of pentapeptidic repeats, ranging from 20 to 330. Nevertheless, this designation does not specify the arrangement among repeats nor indicate possible additional residues at the N- or C-terminal ends of the ELP.[267, 268]

1.4.2 ELP thermo-responsive properties

The first reference to ELPs in the scientific literature dates to the pioneering studies by Urry and colleagues focused on understanding the unique properties of elastin-derived polymers carrying the basic VPGVG repeat, using first

synthetic and then recombinant ELP polymers. Overall, these studies significantly contributed to unveiling the most distinctive characteristic of this family of biopolymers: their thermo-responsive behaviour.[264, 269-276] Urry's experiments elucidated the temperature-dependent phase transition behaviour of ELPs, characterised by reversible coacervation above a critical temperature, which he called inverse temperature transition (Tt),[269, 273, 274] later recognised as lower critical solution temperature (LCST).[268] Thus, below a particular Tt, ELPs are soluble and adopt a typically disordered hydrophilic structure, while above it, they separate into an insoluble, biopolymer-rich, coacervate phase characterised by regular β-spiral structures.[277] He demonstrated that intermolecular hydrophobic interactions are predominant in the coacervate phase and revealed the effect of biopolymer concentration and molecular weight, among others, on temperature-response profiles.[264, 269, 270, 274] In addition, he investigated the impact of sequence composition, particularly of the guest residue of the basic repeat, on ELPs' thermal properties.[264, 275, 276]

These thermo-responsive properties are closely related to the ELP chain's interactions with H_2O molecules and are dictated by the entropy changes associated with these interactions (Figure 17). In an aqueous solution and at low temperatures, the change in Gibbs free energy is negative, allowing ELP and H_2O to mix spontaneously. Thus, the arrangement of H_2O molecules around the ELP chain is highly ordered, leading to negative entropy changes. However, as temperature increases, the mixing becomes energetically unfavourable, leading to the phase separation of ELPs from H_2O molecules. Above the Tt, hydrophobic interactions become favourable, causing ELP chains to aggregate and form a coacervate phase, expelling H_2O molecules and increasing entropy. This entropy gain drives the transition from a soluble to an insoluble state. Conversely, when the temperature decreases below the Tt, the hydrophilic interactions between H_2O molecules and the ELP chains become dominant again, causing the coacervate phase to dissolve back into the aqueous solution. This re-solvation process is associated with decreased entropy, as H_2O molecules reorganise around the biopolymer chains.[278, 279] In summary, the transition of ELP from soluble to insoluble in H_2O with increasing temperature is driven by changes in entropy and Gibbs free energy, reflecting the balance between ordered and disordered states in the system.

ELP aggregation turns optically transparent solutions into cloudy mixtures (Figure 16); thus, the Tt is often determined by ELP turbidimetry-temperature-dependent profiles at 350 nm in the concentration range and buffer condition desired. Plotting absorbance values at 350 nm versus temperature, a sigmoidal curve is obtained, and Tt is reported as the temperature at which the optical density (OD) reaches 50% of its maximum value. In addition, the shape of the curve also gives information about the transition.[280, 281]

The Tt at which the phase separation occurs is influenced by several parameters, such as the length of the repeat unit and the number of repeats, its molecular weight and concentration, as well as the composition of the guess residue, and the presence of specific motifs. The Tt decreases as the molecular weight and concentration in the solution increase; for instance, ELPs with high molecular weight show a sharper transition at lower Tt.[270] In addition, the guess residue cannot be proline because it disrupts conformation and LCST properties,[264, 282] and hydrophobic guest residues result in a lower Tt, while more hydrophilic residues increase the Tt.[264] Further, charged residues in position X made ELPs responsive to pH,[267] and they exhibit coacervation properties only when their charge is neutralised.[283] In addition, among other factors, the presence of co-solutes such as NaCl also modifies the Tt, which is shifted to lower values with increasing salt concentration; nevertheless, the type of salt also influences ELP assembly and aggregation.[278]

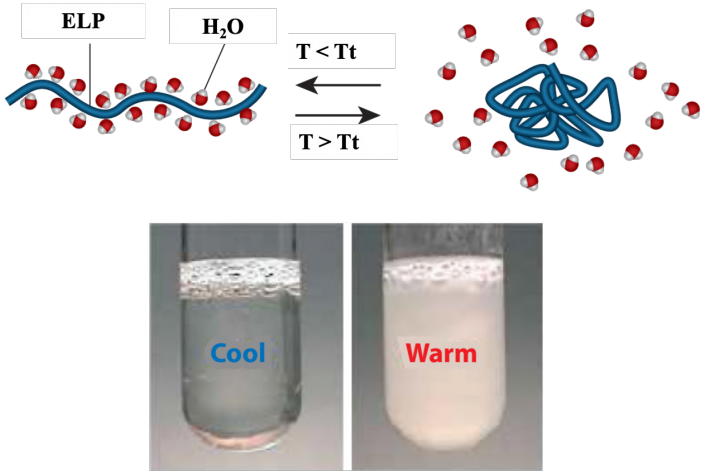

Figure 16. LCST behaviour of ELPs. Below the Tt, ELPs are hydrated and completely soluble, resulting in clear aqueous solutions. However, when the temperature exceeds the Tt, the ELPs undergo phase separation and form coacervates, causing the solution to become cloudy. Upon lowering the temperature, the ELPs re-dissolve and become soluble again. Reproduced from ref.[279] *Anastasia K Varanko, Jonathan C Su, Ashutosh Chilkoti, "Elastin-Like Polypeptides for Biomedical Applications"*, Annu Rev Biomed Eng, Vol 22, Page 348 (2020), with permission from Annual Reviews. *Copyright © 2020 by Annual Reviews. All rights reserved.*

1.4.3 ELP production and purification

Urry's studies were initially performed with small synthetic ELP peptides obtained through SPPS and polymerisation methods;[273, 284] nevertheless, these techniques were limited due to labour-intensive methodologies, reduced scalability, low yields, high costs, and macromolecular polydispersity of the polymers obtained. Hence, the emergence of DNA recombinant technologies addressed these issues, being considered a more practical and affordable way of obtaining ELPs, allowing the production of monodisperse polymers with larger molecular weights and suitable for industrial-scale production.[285]

Thus, Urry described, for the first time, the genetic engineering of ELPs by concatemerisation of a synthetic DNA sequence encoding the desired ELP monomer. Therefore, monomer genes are connected at overlapping sticky ends within a bacterial vector, forming an ELP oligomer.[285, 286] Nevertheless, due to the intrinsic limitations of the methods, i.e., the uncontrolled oligomerisation, this technique was later substituted by the recursive directional ligation (RDL) method.[267] This approach entailed the sequential assembly, in a stepwise manner, of an ELP gene monomer with a linear plasmid vector following a seamless cloning strategy employing a single restriction enzyme. Further, the same group refined this method and developed PRe-RDL (recursive directional ligation by plasmid reconstruction), which involves pairing two ELP-plasmid halves, each one containing an ELP monomer, to form a dimer ELP. This approach's advantage relies on using type II restriction enzymes to obtain linear ELP-plasmid halves with sticky ends, overcoming significant limitations of RDL, such as plasmid circularisation.[287] Altogether, these advancements laid the groundwork for the widespread recombinant production of ELPs using efficient and scalable platforms.

ELP recombinant production offers precise control over sequence design and allows tailoring their chemical reactivity and mechanical, thermodynamic, physico-chemical, and biochemical properties, influencing ELPs' behaviour and determining their suitability for particular applications. So far, there are reports of the production

of ELPs in several hosts, including yeasts (*P. pastoris*), fungi, and plants;[288, 289] nevertheless, due to the advantages of bacterial expression systems, ELPs have been primarily produced in *E. coli*.[257]

Further, ELPs are produced, either as IBs or as soluble biopolymers in the cytoplasm of *E. coli*, bacterial cells are lysed, and ELP thermo-responsive properties are used for their purification. This method, first used by Urry, exploits, in a clever manner, the reversible phase transition properties of ELPs for their isolation and purification from bacterial lysates, with excellent purity and low endotoxin levels.[290] Further, Meyer and Chilkoty (1999) successfully employed simple rounds of cold and warm centrifugations for the purification of ELP-based proteins, a method that they coined as "inverse transition cycling" (ITC, schematically represented in Figure 17).[291]

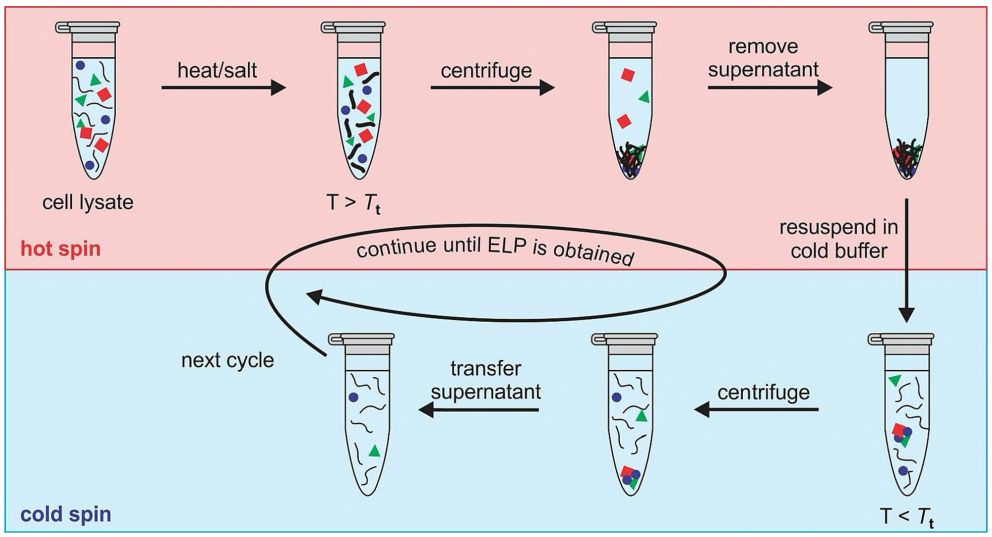

Figure 17. Schematic representation of one ITC cycle to purify ELP-based proteins. Reproduced from ref.[292] under a Creative Commons license CC BY 4.0. *Copyright © 2022 by Jolinde van Strien,Oscar Escalona-Rayo,Wim Jiskoot,Bram Slütter,Alexander Kros. Published by Elsevier B.V.*

ITC takes advantage of the reversible solubility of ELPs in response to changes in temperature and/or other external stimuli (i.e. salt concentrations) to efficiently separate ELPs from the host proteins by repeated centrifugation cycles below and above the Tt. LCST phase separation can be triggered by simple rising temperature above Tt and/or isothermally induced by adding salts in the Hofmeister series, such as NaCl and $(NH_4)_2SO_4$, with a neutral and strong propensity to promote protein aggregation, respectively. For instance, NaCl concentrations ranging from 2-3 M or a few hundred mM of $(NH_4)_2SO_4$, are sufficient to induce isothermal ELPs and ELP-based protein aggregation while having little or no impact on the host soluble contaminants.[293] Initially, the bacterial lysate supplemented with salt is heated above the Tt. This causes ELPs transition from a soluble state to an insoluble coacervate phase, while most *E. coli* proteins remain soluble. Subsequently, ELPs are pelleted by centrifugation at temperatures above the Tt; the supernatant containing most of the host protein is discarded, and the resulting pellet, predominantly composed of ELPs, is resuspended in a cold buffer. Then, a round of centrifugation at temperatures below the Tt allows the separation of the soluble ELPs from the host proteins that co-precipitated with ELP during the warm step and that were irreversibly aggregated and unable to resolubilise in the cold step. Further, this cycle of aggregation, warm centrifugation, re-solubilization, and cold centrifugation can be repeated as many times as needed to achieve the desired purity.[257, 291]

Altogether, these efforts extensively addressed the challenges in ELP synthesis and established a methodology for their purification employing a cost-effective method that does not involve expensive, complex and time-consuming

chromatographic steps. This enables the efficient and scalable production of ELP with uniform and desired properties, paving the way for developing ELP-based biomaterials with tunable thermo-responsive properties and highlighting their potential as protein carriers, purification tags and versatile biomaterials.

1.4.4 ELP applications

1.4.4.1 ELPs for producing therapeutic agents

1.4.4.1.1 ELP fusion carriers for bioactive domains production and delivery

Proteins and peptides employed as clinical drugs often have poor pharmacokinetic properties, low bioavailability and high immunogenicity. Recent studies have demonstrated the potentiality of fusing proteins and peptides to recombinant carriers to produce novel therapeutic agents with enhanced properties.[294] The high biocompatibility, lack of toxicity and thermo-responsive properties of ELP biopolymers make them ideal fusion carriers for producing materials for biological applications.[265, 291, 295, 296] It has been widely studied that ELP fusion to bioactive domains does not compromise their thermo-responsive behaviour;[291] nevertheless, their Tt is shifted depending on the surface hydrophobicity of the fusion domain, with more hydrophobic domains showing a decreased Tt.[280] Thus, several bioactive domains have been used to functionalise ELPs; consequently, the final fusion protein carries both the biological activity of the domain of interest and the ELP coacervation properties in response to diverse stimuli (Table 3).[289, 295, 297, 298] ELP fusions are often produced in *E. coli* due to the aforementioned properties of this platform for heterologous protein production or obtained by chemical conjugation using click chemistry.[289]

Table 3. Examples of bioactive domains fused to ELPs. Reproduced with permission from ref.[289] under a Creative Commons Attribution 4.0 International License CC BY 4.0 DEED. *Copyright © 2023 by Yingshu Guo, Shiwei Liu, Dan Jing, Nianzu Liu and Xiliang Luo.*

Protein composition	Tt (°C)	Half-life ($t_{1/2}$)/h	Bioactive Domain	Therapeutic effect
IFN-ELP_{90}	45.3	8.6	IFN	Inhibit tumour growth. Prolong the survival time of mice. No hemolysis.
IFN-$ELP(V)_{90}$	37	280 ± 0.5	IFN	Stimulate anti-tumour immune response. Inhibit the recurrence of glioblastoma.
IFN-α-MMPs-$ELP(V)_{90}$	< 37	422.2 ± 13.7	IFN-α	Improve anti-tumour efficacy. Increase intratumoral accumulation.
α-FLT3-$ELP(A)_{192}$	42.3	14.7	α-FLT3	The fusion protein has high stability and specificity. Effective therapeutic effect on AML.
α-CD99-$ELP(A)_{192}$	45.3	15.8	α-CD99	Reduces cell viability of AML cell lines. Reduced leukemia burden in mice.
DRA-$ELP(V)_{120}$	25	-	DRA	Eliminate DRA-sensitive tumour tissue
mini cry-$ELP(S)_{48}(I)_{48}$	30	2.8	miny cry	Inhibit RPE apoptosis and caspase-3 activation and protect the retina from cell death.
FGF-21-ELP_{120}	~ 30	16.6 ± 3.9	FGF-21	A single injection can control blood sugar for 5 days.
vRAGE-$ELP(V_{40}C_2)$	30	-	vRAGE	Reduce expression of pro-inflammatory factors. Accelerate wound healing in mice.

ELP fusions improve the stability and bioavailability of therapeutic proteins and peptides by protecting them from enzymatic degradation, denaturation, or aggregation in physiological environments, preserving their bioactivity and therapeutic efficacy and, at the same time, increasing their half-life due to the increase in size and helping to mask potential immunogenicity of the bioactive domain.[299, 300] In addition, their reversible phase transition behaviour in response to external stimuli, such as temperature or pH, can be exploited to produce, under physiological conditions, a therapeutic protein reservoir or depot that is slowly released in a controlled manner, exerting their therapeutic effects for longer times while minimising systemic side effects (Figure 18).[301-304] On the

other hand, the ELP moiety is biodegradable and can undergo enzymatic degradation in the body mainly due to elastase and collagenase activity, leading to the gradual release of the active molecule and the clearance of ELP by-products that have a high bioresorbability due to their biotic origin.[305, 306] This biodegradability minimises the accumulation of carrier materials and facilitates the elimination of exogenous substances from the body, enhancing the safety profile of ELP-based drug delivery systems.[279]

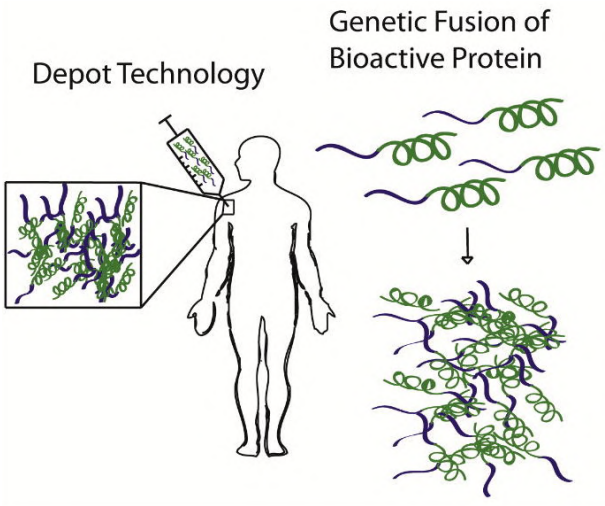

Figure 18. ELP fusion protein applications for the sustained release of bioactive molecules. Adapted from ref.[296] Stefan Roberts, Michael Dzuricky, and Ashutosh Chilkoti, *"Elastin-like polypeptides as models of intrinsically disordered proteins"*, FEBS letters Vol 589, Page 2481 (2015) with permission from John Wiley & Sons – Books.

Overall, producing therapeutic proteins and peptides as ELP fusion offers several advantages, including biocompatibility, tunable properties, stimuli-responsive delivery, enhanced stability, versatile delivery platforms, and biodegradability, making them promising candidates for advanced drug delivery applications.

1.4.4.1.2 ELPs as purification tag

In recent years, ELPs have attracted significant attention for protein purification due to ITC advantages compared to other methods relying on chromatography separation. Thus, ELPs have been employed as carriers to improve biological performance and deliver *in vivo* fused bioactive domains, as well as purification tags to allow the obtention of high-purity proteins and peptides using simple and cost-effective platforms.[266, 280, 291, 297, 307-310] ELP tags have been successfully employed to purify the domain of interest produced as ELP fusions in *E. coli, P. pastori* and plants.[288, 309]

Unlike other purification tags that involve chromatographic separation, which often requires expensive resins and specialised equipment, ELP purification primarily relies on simple reagents and equipment such as NaCl and a standard laboratory centrifuge. This simplicity reduces the overall cost of the purification process. It minimises the need for sophisticated instrumentation and reagents, making it accessible to a broader range of research laboratories and facilities, especially those with limited resources. Moreover, the method operates under mild conditions, preserving the native structure and bioactivity of the tagged proteins, making them suitable for biomedical applications. Furthermore, the scalability of ITC enables efficient purification of proteins at various production scales, from research laboratories to industrial and pharmaceutical settings, without significant additional cost or complexity. In addition, when needed, it can be combined with other purification techniques,

such as chromatography, allowing for customisation of the purification process based on specific requirements and desired purity levels.[280, 308-310]

In addition, when ELPs are employed as purification tags, the domain of interest is often released to avoid the ELP moiety's interference with its biological activity. Frequently, the release is achieved by incubation with a specific protease that targets the linker sequence between the domain of interest and the ELP macromolecule and then at least one more purification step is carried out to purify the released domain. In this sense, ELP tags offer another advantage since after cleavage of the fusion protein, the released ELP tag and unreacted ELP-fusion proteins can be separated from the bioactive domain by an ITC cycle, simplifying the downstream process; nevertheless, the proteases remain soluble and are co-purified with the domain of interest. Other innovative approaches involve the use of ELPs as the carrier for the proteases (ELP-tagged protease); thus, once the ELP fusion protein is purified from host contaminants by the ITC method, it is incubated with ELP-tagged protease for the release of the bioactive domain. Thus, a subsequent purification step, exploiting ELP's coacervation properties, allows for the selective separation of the bioactive domain from ELP-based macromolecules, including the ELP-tagged protease (Figure 19).[310, 311]

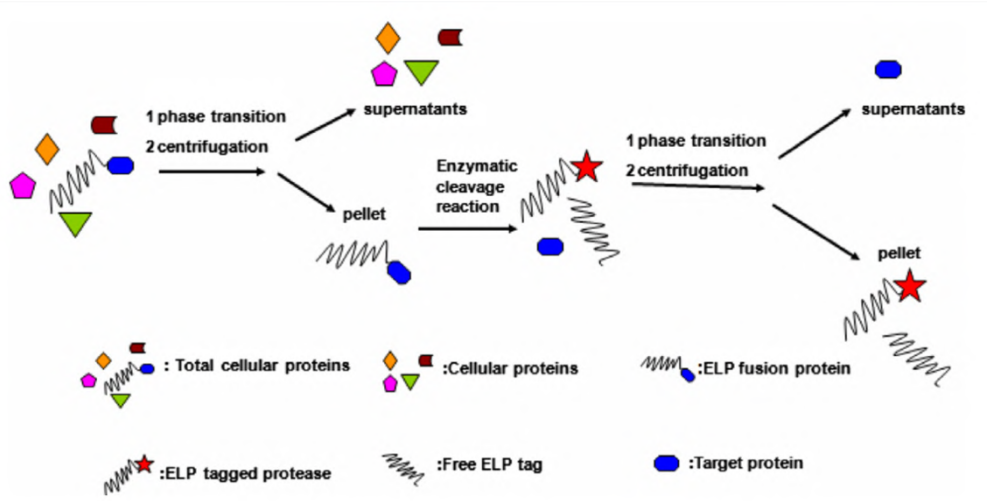

Figure 19. Schematic representation of purification of recombinant proteins using ELP-tagged proteases. Reprinted from ref.[311] Dongming Lan, Guangrui Huang, Hongwei Shao, Lichun Zhang, Lixin Ma, Shangwu Chen, Anlong Xu *"An improved nonchromatographic method for the purification of recombinant proteins using elastin-like polypeptide-tagged proteases"*, Analytical Biochemistry, Vol 415, Page 201 (2011), with permission from Elsevier. *Copyright © 2011 Elsevier Inc. All rights reserved.*

Moreover, ELPs are versatile tags that can be combined with other purification methods. For instance, an ELP-affinity tag carrying an affinity peptide was successfully employed to selectively purify the domains of interest by affinity precipitation (Figure 20). Briefly, this strategy involves the fusion of an ELP sequence with an affinity tag (ELP-affinity tag), creating a fusion protein where the ELP retains the thermo-responsive behaviour and serves as a carrier and purification tag, while the affinity tag facilitates the specific binding of the target domain. Thus, the fusion protein is recombinantly produced in *E. coli*, and the ITC is exploited for purification. Then, the pure ELP-affinity tag is incubated with a protein extract or cell lysate containing the domain of interest, which specifically binds to the ELP-affinity tag; thus, a stable complex (ELP-Protein) is formed. Right after, ELP's LCST properties are exploited to selectively precipitate the ELP-Protein complex, which is separated from the other contaminants by centrifugation. Further, the ELP-Protein complex is solubilised in a suitable buffer that allows the release of the

domain of interest from the fusion protein. Finally, the domain of interest is purified from the ELP-affinity tag exploiting ELP's thermal properties. Thus, this method allows for efficient protein purification via affinity precipitation, with high-affinity systems resulting in high purity and yield. At the same time, multivalency-based interactions may improve the performance of intermediate-affinity systems and low-affinity systems may pose challenges. Other factors, such as ELP and protein hydrophobicity and linkers between the ELP and affinity tag, also influence the process's success. This approach offers promises to produce new affinity strategies without involving complex and costly affinity chromatography procedures and allows for continuous precipitation processes. In addition, the interactions between the ELP-affinity tag and the domain of interest are non-covalent; thus, the release is achieved simply without using harsh chemical reagents or enzymes, which may complicate the process and increase the prices.[312, 313]

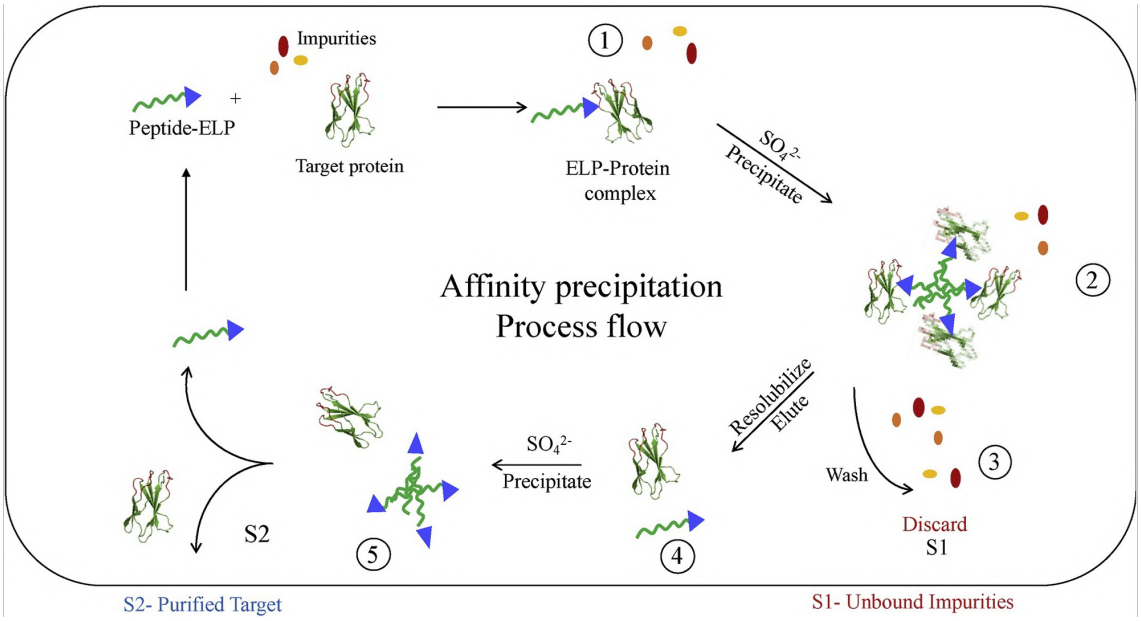

Figure 20. Schematic representation of the sequential steps employed for the affinity-precipitation using an ELP-affinity tag to purify a protein of interest. Reproduced from ref.[312] Akshat Mullerpatan, Divya Chandra, Erin Kane, Pankaj Karande and Steven Cramer *"Purification of proteins using peptide-ELP based affinity precipitation"*, Journal of Biotechnology, Vol 309, Page 62 (2019), with permission from Elsevier. *Copyright © 2019 Elsevier B.V. All rights reserved.*

Furthermore, other Authors have reported organic extraction-precipitation methods to obtain biologically active ELP fusion proteins. These Authors reported that this method further reduced the purification times to 2.5 h while removing major host cell contaminants and with LPS levels below 1 EU/mL, indicating the suitability of this method for producing materials for *in vivo* applications.[314]

More recently, a novel purification method combining aqueous two-phase flotation (ATPF) with ITC was efficiently used to purify recombinant β glucosidase-ELP-graphene binding fusion from cell lysis solution. The Authors demonstrated that the developed method overcame significant issues associated with non-specific adsorption and time-dependent denaturation in the purification of recombinant proteins by multistage chromatographic procedures; they did not find any adverse effect of the ATPF-ITC on the structure of the recombinant protein obtained.[315]

Thus, using ELPs as purification tags provides an efficient, straightforward, scalable, cost-effective, mild, versatile and environmentally sustainable method for obtaining high-purity proteins for biomedical and biotechnological

purposes. Nevertheless, there is no report on using ELP tags in industrial or pharmaceutical protein purification processes.

1.4.4.2 ELP application in tissue engineering and drug delivery

Due to their unique properties, ELPs have attracted significant interest in tissue engineering, drug delivery (Figure 21), regenerative medicine, and biosensing, among other applications. Their reversible phase transition behaviour allows for the development of dynamic stimuli-responsive biomaterials that can undergo reversible changes in mechanical properties, porosity, or shape *in situ*, enabling minimally invasive procedures and dynamic tissue engineering applications.[268, 279, 289, 298]

Similarly to other thermo-responsive polymers, ELPs can self-assemble into micelles, vesicles, and nanofibers.[288, 292] Moreover, they have low immunogenicity and low adhesion capabilities to platelets;[289] thus, engineered ELPs are excellent biopolymers for producing smart drug carriers that encapsulate therapeutic agents and release them in a controlled fashion in response to diverse stimuli, such as changes in temperature, pH, or enzyme activity.[292]

For instance, covalently linked ELP diblocks composed of a hydrophobic and a hydrophilic domain, each with a different Tt, have been employed to encapsulate bioactive molecules or cells. These diblocks are soluble below the critical micellar temperature, but above it, the hydrophobic domain self-assembles, creating spherical micelles where hydrophobic domains form the micelle core and are in contact with the drugs while hydrophilic domains are exposed; further, the modification of hydrophobic domain guest residue can make the diblock pH-responsive. Thus, controlling temperature or pH, sustained release kinetics and targeted delivery to specific tissues or cells can be achieved.[257, 268, 292, 296]

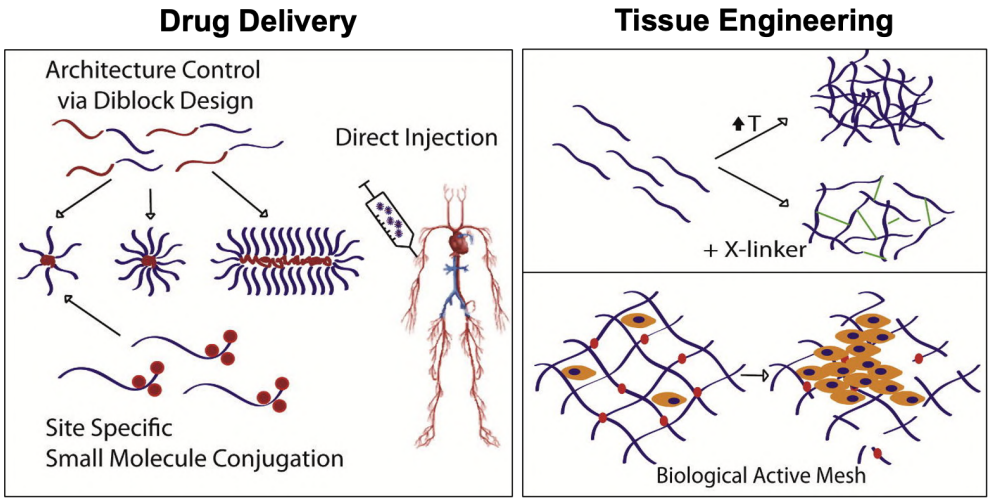

Figure 21. ELP biomedical applications for drug delivery and tissue engineering. Adapted from ref.[296] Stefan Roberts, Michael Dzuricky, and Ashutosh Chilkoti, *"Elastin-like polypeptides as models of intrinsically disordered proteins"*, FEBS letters Vol 589, Page 2481 (2015) with permission from John Wiley & Sons - Books.

Other strategies are based on the use of ELP recombinant chimeric peptides carrying small tags (i.e. cysteine residues) for the chemical conjugation of hydrophobic bioactive domains creating macromolecules that spontaneously self-assemble into nano micellar structures with the cargo drug sequestered in the core of the micelles.[316, 317] These structures have been extensively studied and proven efficient in delivering chemotherapeutic drugs, improving their aqueous solubility, plasma half-life, tumour-specific uptake and therapeutic potential.[257, 279]

For instance, in cancer therapy, ELP-based nanoparticles have been designed to co-encapsulate chemotherapeutic drugs and targeting ligands, such as antibodies against tumour-specific antigens, allowing for precise drug delivery to cancer cells and minimising systemic toxicity.[279, 292] In these micellar structures, drug toxicity is shielded in the micelle core by direct conjugation or interaction with the hydrophobic domain, while the conjugation of target ligands to the hydrophilic exposed domain can direct the drug to its site of action.[292, 318] Further, multiple drugs or therapeutic agents can be co-encapsulated within these structures, contributing to synergistic effects, personalised treatment, and improved therapeutic outcomes for various diseases, including cancer, infections, and inflammatory disorders.

ELP-based biomaterials have shown promising results in wound healing applications. ELP micelles-based dressings have been developed to deliver ELP-fused antimicrobial peptides, such as LL-37, and growth factors for re-epithelialisation and epidermal regeneration, such as KGF and SDF1, to combat infections in chronic wounds, promoting faster healing and tissue regeneration.[319]

ELPs can be engineered to mimic the extracellular matrix proteins, providing an ideal environment for cell adhesion, proliferation, and differentiation.[257, 279, 289] ELP-based scaffolds/hydrogels have been tailored to mimic the mechanical properties of specific tissues, providing a three-dimensional matrix and an ideal environment for cell growth and tissue regeneration.[289, 320-322] ELP-based hydrogels have been engineered to respond to temperature changes, allowing for minimally invasive delivery and in situ gelation for tissue repair. For instance, ELP thermal properties can be tuned to obtain in situ scaffolds upon injection, representing an advantage to *ex vivo* cells loading into pre-formed scaffold and implantation. Thus, cells are encapsulated on ELP scaffolds upon coacervation or due to covalent cross-linking in the presence of chemical stimuli. Depending on the application, the uncross-linked scaffold may not bear the desired rheological properties. Often, scaffold structures stabilised by cross-linking are employed to improve the behaviour of coacervation-driven scaffolds.[257, 323]

ELP scaffold properties can be tuned to mimic native tissue environments by modification of the guest residue, N- or C-terminal of ELP biopolymers, introducing aa with reactive side chains such as glutamine, lysine, serine, threonine, and cysteines as well as a linker that reacts with the functional groups on ELP side chains.[324] Chemical cross-linking of ELP chains using genipin or UV irradiation has also been reported.[325] Moreover, ELP biopolymers carrying lysine and glutamine can be efficiently cross-linked by transglutaminase enzymes (TGase), a mild reaction that does not affect cell encapsulation.[326] Thus, ELP-based cross-linked scaffolds have been helpful in encapsulating human mesenchymal stem cells (hMSCs) and delivering them to damaged tissues, enhancing cell survival and promoting tissue regeneration.[324]

Moreover, these scaffolds, similarly to elastin, are susceptible to elastase and collagenase enzyme activity, producing elastin-derived peptides similar to those produced during extracellular matrix remodelling and that may regulate critical cellular activities.[327]

Furthermore, ELPs may serve as contrast agents for biomedical imaging modalities such as magnetic resonance imaging, ultrasound, and optical imaging. By conjugating imaging probes to ELPs, enhanced contrast and specificity can be achieved for diagnostic purposes.[289, 328, 329]

In conclusion, ELPs represent a versatile class of components with unique thermal behaviour and tunable properties that make them attractive for a wide range of biomedical applications. From smart drug delivery systems to tissue engineering hydrogels and scaffolds, ELPs offer smart solutions to intricate biomedical challenges. However, significant research efforts are still needed to overcome existing hurdles and fully exploit the potential

of ELP-based materials in clinical practice. By addressing issues related to synthesis methods, structural characterisation, biocompatibility, long-term stability, and regulatory approval, ELPs hold promise for revolutionising various aspects of modern medicine. Future research directions may include the design of multifunctional ELPs capable of integrating multiple functionalities, such as targeting ligands, imaging probes, and therapeutic payloads and allowing combined and personalised therapy.

1.4.5 Human Elastin-like polypeptides: a platform to produce smart and functional biomaterials

Most ELPs described in the literature are built upon the mammalian pentapeptidic repeat VPGXG, with variable guest residues and minor modifications to fine-tune the properties of the resulting polymer to suit specific applications. However, there are numerous other ELPs with different repeats but similar thermal behaviour, such as those consisting of the pentapeptidic IPGVG, KGGVG, VGGVG, GVGVP, the heptapeptidic LGAGGAG, and nonapeptidic LGAGGAGVL repeat sequences.[265, 266]

Remarkably, another ELP has been inspired by the hexapeptidic repeat found in human tropoelastin (VAPGVG) and consequently named Human Elastin-like Polypeptide (HELP). Notably, the HELP polymer mirrors the structure of the human tropoelastin by incorporating most of the exon 24 of tropoelastin, encoding its hydrophobic domain, alongside the hydrophilic domain encoded by the second half of exon 23. Consequently, HELP comprises eight repetitions of a block alternating hydrophilic and hydrophobic domains, closely resembling the native tropoelastin primary structure (Figure 22). The main motivations behind constructing an ELP biopolymer based on the human elastin repeats were its expected low immunogenic potential and its role, upon release, in cell proliferation and other critical cellular functions. In addition, including the tropoelastin hydrophilic domains in this ELP sets it apart from the others. Firstly, the alanine-rich domain within the hydrophilic region serves as a target for elastase enzymes,[330, 331] facilitating their biodegradation and reabsorption within tissues, as well as enabling the release of any bioactive domains fused to the macromolecule, enhancing its versatility and allowing for the sustained and smart release of the domain of interest. Moreover, the presence of lysine and glutamine residues within the hydrophilic domain offers the potential for forming stable hydrogel matrices. In the presence of a TGase enzyme, these residues form an isopeptide bond, resulting in cross-linking; thus, herein, the alanine-rich hydrophilic domain will be referred to as the cross-linking domain, underscoring its role in facilitating the formation of stable hydrogel structures.[329, 332]

Hence, following an RDL method, eight repetitions of the PCR-amplified DNA fragment corresponding to the desired sequence from exons 23 and 24 were assembled in an expression vector, and restriction sites flanking the C-terminal of the HELP coding sequence were designed to insert any further domain of interest. The HELP biopolymer is routinely produced in *E. coli* and purified following an ITC method with high purity, yielding up to about 200 mg per litre of bacterial culture.[329, 333] The physico-chemical characterisation of HELP revealed that this new artificial protein retained the thermal behaviour characteristic of ELPs.[334] Furthermore, the biological characterisation of this macromolecule did not evidence any cytotoxicity when HepG2 cells were grown onto HELP-coated surfaces and demonstrated its capacity to support cell adhesion and growth, but with clearly different cellular morphologies with respect to the cells grown on tissue culture surface, at least for the assay conditions evaluated in those studies.[329] In addition, other studies evidenced that HELP-based coatings were permissive to the adhesion of the SH-SY5Y neuroblastoma cell, which maintained their phenotypic features and retained the potential to differentiate in response to proper stimuli.[334] Similarly, H9c2 myoblast cells seeded on HELP-coated

wells demonstrated improved cell adhesion, proliferation, and differentiation compared to tissue culture surfaces and collagen coatings.[335] Furthermore, these coatings showed a stimulatory role in the osteogenic differentiation of hMSCs.[336] Altogether, these results highlighted the potentialities of this polymer to produce cytocompatible 2D interfaces for biomedical applications.[329, 334-336]

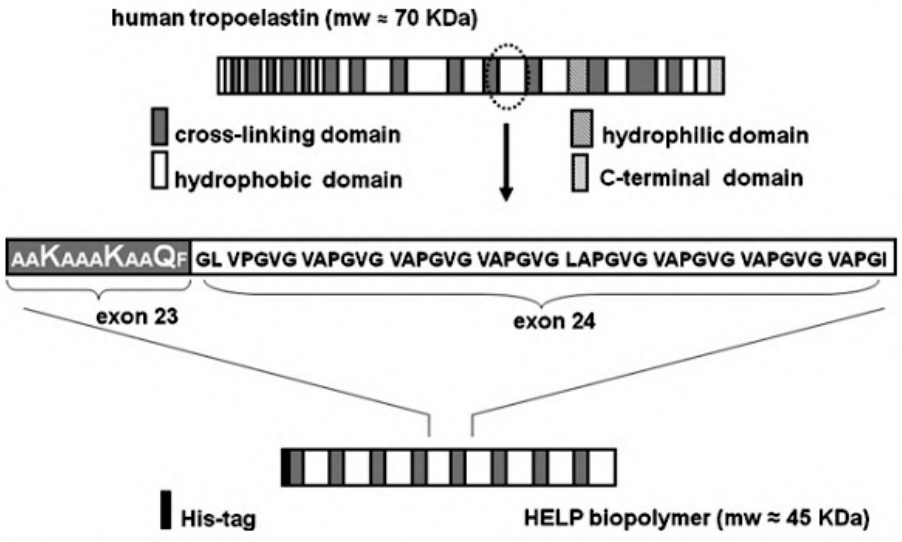

Figure 22. Schematic representation of the HELP biopolymer based on the gene of the human tropoelastin. Reprinted from ref.[332] Antonella Bandiera, *"Transglutaminase-catalyzed preparation of human elastin-like polypeptide-based three-dimensional matrices for cell encapsulation"*, Enzyme and Microbial Technology, Vol 49, Page 348 (2011) with permission from Elsevier. *Copyright © 2011 Elsevier Inc. All rights reserved.*

In addition, due to the presence of the cross-linking domains, HELP and HELP-based biopolymers can be stabilised by intra- and intermolecular bonds, allowing the formation of 3D hydrogel matrices. This reaction is catalysed by TGase and occurs under mild conditions, avoiding the use of harsh chemicals and potentially allowing for cell encapsulation. The hydrogel matrices obtained by this method have been extensively characterised and studied for cell seeding and encapsulation to develop biomimetic materials for tissue engineering and regenerative medicine applications.[332, 337] For instance, no toxicity has been observed when HELP matrices have been placed in contact with human umbilical vein endothelial cells, revealing their potential as biomaterials for vascular tissue engineering.[337] Nevertheless, when using HELP hydrogel matrices as support to seed HepG2 human hepatoblastoma and MCF-7 human breast cancer cells, even though cells were viable, morphological changes were clearly visible, with a tendency to form cell clusters, and a delay in cell adhesion and, consequently, in proliferation was observed compared to cells grown on the tissue culture surface (Figure 23A). Similarly, encapsulating these cell lines on HELP matrices leads to the formation of islets of proliferating viable cells (Figure 23B).[332] Overall, these results established the basis for developing cross-linked HELP biomaterials compatible with cell viability; nevertheless, the system's capacities may be further improved by tailoring specific domains that can improve cell adhesion or confer other functionalities.

Indeed, more recent studies explored the capacity of a HELP fusion biopolymer carrying a domain derived from type IV collagen, containing two RGD motives (named HELPc), to produce 2D and 3D biomaterials and evaluate their effect on myoblast viability and function. HELPc-based coatings improved C2C12 myoblast adhesion, proliferation, and differentiation,[338] while hydrogels greatly stimulated cell proliferation and partially inhibited

myogenic differentiation, revealing the potentialities of the latest for *in vitro* expansion of muscle stem cells and for developing novel biomaterials for muscle regeneration.[339]

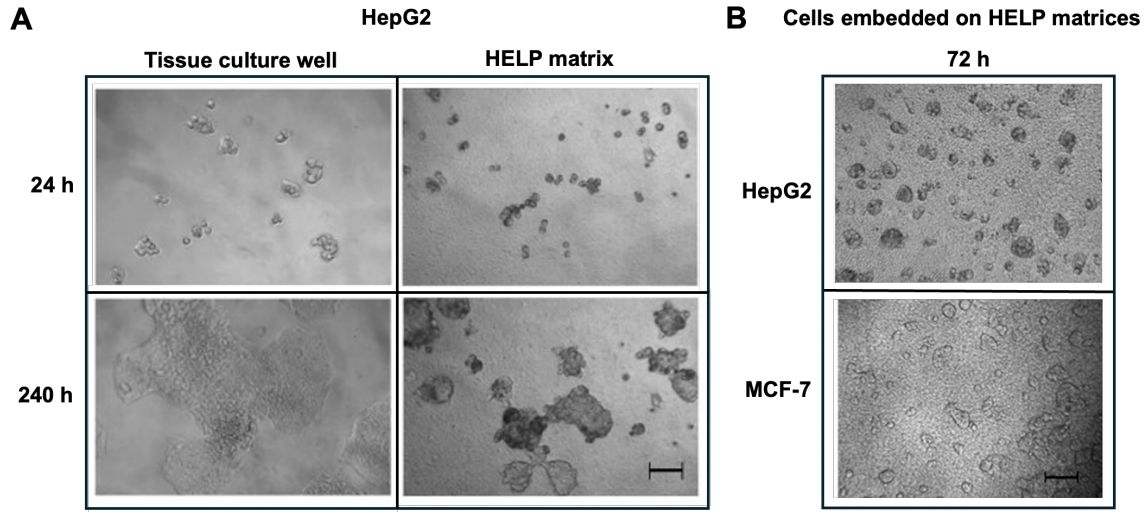

Figure 23. Phase contrast microscopy observation of HepG2 cells seeded on HELP matrices revealed different cell morphologies compared to cells grown on control surfaces **(A)**. HepG2 and MCF-7 cells embedded on cross-linked HELP-based matrices grew as islets **(B)**. The Bar is 100 µm. Reprinted from ref.[332] Antonella Bandiera, *"Transglutaminase-catalyzed preparation of human elastin-like polypeptide-based three-dimensional matrices for cell encapsulation"*, Enzyme and Microbial Technology, Vol 49, Pages 350 and 351 (2011) with permission from Elsevier. *Copyright © 2011 Elsevier Inc. All rights reserved.*

Further, HELP has been successfully employed as a carrier to produce functional recombinant fusion proteins that not only retain HELP's thermo-responsive characteristics and matrix-forming abilities but also preserve the biological activity of the bioactive domain. For instance, a fusion protein combining HELP with endothelial growth factor (HEGF) has been produced in *E. coli*, purified using the ITC method, and subsequently utilised to create HEGF-based coatings that stimulated myoblast proliferation and differentiation, increased the population of muscle stem cells, and facilitated the development of multinucleated myotubes, fostering the expansion of myoblasts while preserving their myogenic potential.[340] In addition, a recombinant fusion protein made of HELP and the bilirubin-binding protein UnaG have been shown effective in detecting bilirubin at the nanoscale and in samples with high noise background, unveiling the capacities of this family of biopolymers to develop analytical biosensors for the detection of toxicological biomarkers of clinical relevance.[341-343]

Additionally, HELP-based biopolymers have also been explored for drug delivery applications. For instance, magnetic HELP microparticles have been developed to encapsulate a drug of interest on spherical cross-linked HELP microparticles. This design enables controlled delivery through their magnetic properties and sustained drug release at the target site. This drug delivery platform has demonstrated efficacy in encapsulating nerve growth factor and effectively delivering it in an in vitro neuronal cell model.[344]

Other HELP-based drug delivery strategies take advantage of the ability of elastase enzymes to degrade the alanine-rich cross-linking domains and release short elastin motifs with known cellular activities, fused bioactive domains, or functional proteins embedded in HELP-derived materials.[330, 331] Elastase activity is widespread in both prokaryotic and eukaryotic organisms, and it is implicated in several significant pathological conditions, such as pulmonary emphysema, cystic fibrosis, infections, inflammation, chronic wounds, and atherosclerosis.[345] Moreover, it is well documented that some pathogenic microorganisms, such as *P. aeruginosa*, produce elastase

enzymes.[346] HELP biopolymer and matrices' susceptibility to elastase degradation have been extensively studied and proposed as an effective strategy for the smart control of the release of a domain of interest under specific stimuli, thus offering several advantages (Figure 24).[330, 331] Firstly, it enables targeted and site-specific drug release, particularly in response to elevated elastase levels associated with infections or inflammation. Secondly, the HELP carrier's gradual degradation prolongs the fused or embedded protein's release kinetics, resulting in sustained therapeutic effects.[330] Overall, leveraging elastase's enzymatic activity to trigger drug release from HELP-based carriers holds promise for developing more effective and precisely controlled drug delivery systems. For instance, elastase proteolytic activity has been proven to effectively and sustainedly release *in vitro* functional EGF domains from 3D-printed alginate scaffolds embedded with HEGF.[347]

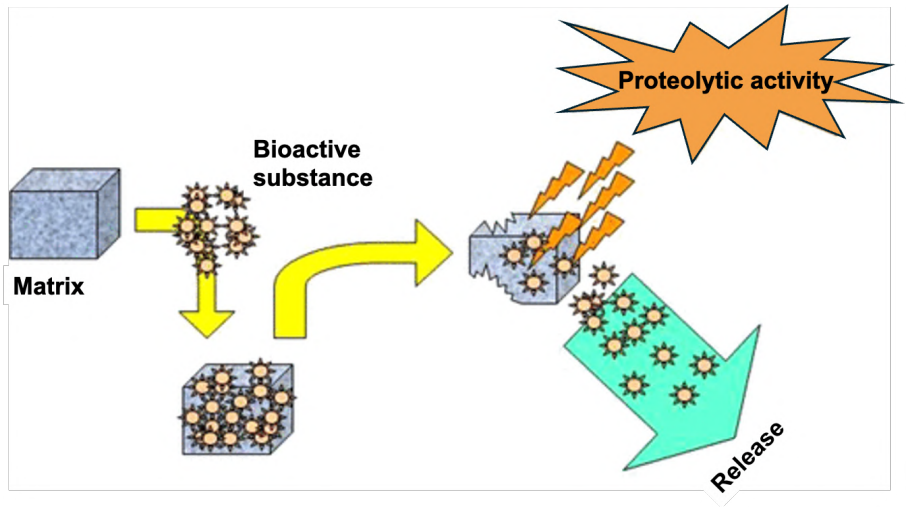

Figure 24. Schematic representation of the release of bioactive domains embedded on HELP matrices. The release is triggered by specific stimuli, such as high elastase concentrations, due to infections or inflammation. Notably, releasing the bioactive domain may counteract the stimulus that initiated the process. Reprinted from ref.[330] Antonella Bandiera, Ana Markulin, Lucia Corich, Francesca Vita, and Violetta Borelli, *"Stimuli-Induced Release of Compounds from Elastin Biomimetic Matrix"*, Biomacromolecules, Vol 15, Page 418 (2014) with permission from American Chemical Society. *Copyright © 2014, American Chemical Society.*

In summary, the family of HELP stimuli-responsive biopolymers represents a multifaceted platform for producing and delivering functional domains. HELP is an efficient carrier for producing and purifying functional recombinant fusion proteins, preserving the fused domains' biological activity and the HELP moiety's properties. Altogether, recombinant production and purification by the ITC method represent a simple, cost-effective, sustainable, and scalable approach for bioactive domain production that are easy to implement in almost all lab settings. In addition, HELP's ability to form stable hydrogel matrices further enhances its utility in tissue engineering and regenerative medicine applications. Extensive research has demonstrated the compatibility of HELP-based biomaterials with cell viability and function, paving the way for their use in developing cytocompatible interfaces and scaffolds for tissue regeneration. Furthermore, the susceptibility of HELP matrices to elastase degradation provides a smart strategy for regulating drug release kinetics, ensuring localised and sustained therapeutic effects in response to specific stimuli. Additionally, the release of the bioactive domain often counteracts the stimulus that initiated its release, thereby further regulating its activity and helping to prevent toxicity and drug resistance resulting from the prolonged and uncontrolled release of therapeutic agents. Finely tuning the unique properties of HELP-based

carriers holds immense promise for developing stimuli-responsive advanced biomaterials for tissue engineering and regenerative medicine.

1.5 Antimicrobial interfaces for preventing orthopaedic implant-related infections

1.5.1 Most common pathogens in orthopaedic infections

Implant-related infections (IRIs) are the major complication during orthopaedical procedures, accounting for a large number of all surgical site infections and ending in secondary and revision surgeries, failure of the implants, and, in the worst of cases, the death of the patient.[348] IRIs frequently stem from microbial contamination during surgical procedures or normal flora opportunistic pathogens,[349] and the signs of infection may manifest as early as the first few weeks or months post-surgery; however, in other cases, bacterial infections can emerge long after the surgical procedure.[350] Also, peri-operative antibiotic prophylaxis is inefficient in eradicating infections due to bacterial resistance to last-line antibiotics.[351]

The Gram-positive cocci *S. aureus*, coagulase-negative *Staphylococci* (*Staphylococcus epidermidis, Staphylococcus hominis* and *Staphylococcus haemolyticus*), *Enterococci* (*E. faecalis*), and the aerobic Gram-negative bacilli *P. aeruginosa*, are the most common microorganisms causing IRIs; among them, *S. aureus* is the most common pathogen and, altogether with *S. epidermidis*, accounts for up to two-thirds these infections.[352] In addition, MRSA, methicillin-resistant *S. epidermidis*, *E. coli*, *P. mirabilis*, and *Propionibacterium acnes* also contribute to implant infections.[353, 354]

IRIs are characterised by a multifaceted interplay involving the pathogen, the implanted biomaterial, and the host's immune response. Usually, the materials used to produce the implants are not antimicrobial themselves,[355] and often, their surfaces are modified to increase their osteoinductive, osteoconductive, and osteointegration properties, with the bone tissue rising at the same time the ability of bacteria to colonise and adhere to the implants and enhancing biofilm formation.[356] The theory known as the “race for the surface”, described by Gristina *et al.* (1988), suggests that, upon implantation, there is a competition between the host cells and bacteria for the colonisation of the implant surface and that the successful osseointegration with the host tissue depends on the balance between host cell integration and bacterial adhesion onto the implant surfaces.[357] If the host cell wins the race, the implant starts to integrate with the bone tissue, reducing the risk of infection and contributing to the success of the implant and the patient’s recovery.[349] In contrast, if bacteria win, they colonise the surface and begin to form complex and dynamic 3D structured communities of bacteria encapsulated in a self-produced extracellular matrix composed of proteins, polysaccharides and DNA, known as biofilm (Figure 25). If biofilm forms, bacteria in this configuration become highly resistant to antibiotics and to the host’s innate and adaptative immune responses.[358-360] Thus, biofilm turns into chronic infections in around 65% of all cases, leading to implant removal as the only efficient manner to eradicate it.[352, 360]

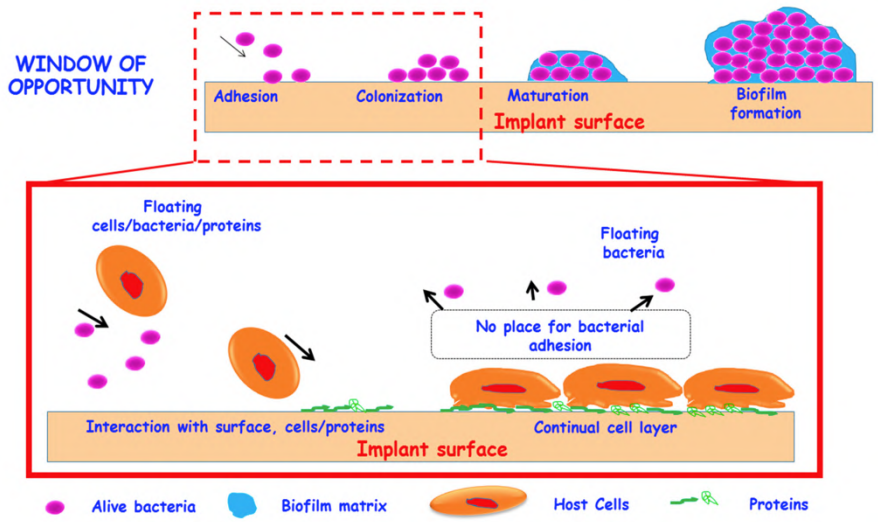

Figure 25. Schematic representation of the concept of "race for the surface" showing the competition among microorganisms and host cells for colonisation and dominance on a surface. Microbial colonisation of the surface will lead to biofilm formation impairing osteointegration. Reproduced with permission of ref.[361] under a Creative Commons Attribution (CC BY) license. *Copyright © 2018 Montserrat Colilla, Isabel Izquierdo-Barba and María Vallet-Regí. Licensee MDPI, Basel, Switzerland.*

1.5.2 Implant coatings: strategies to address bacterial adhesion and biofilm formation.

Implants are usually intended to replace and restore bone and joint functions. Among the most used materials to produce orthopedical implants are titanium (Ti) and Ti alloys due to their excellent mechanical, physical, and chemical properties and capacity to promote osteointegration. Nevertheless, they do not bear any antimicrobial capacity; therefore, bacterial adhesion and biofilm formation are the leading causes of Ti implant failure.[362] Thus, the design and manufacturing of new generation implant materials not only focus on the mechanical properties of the materials employed but also include the modification of the device surface to render them biocompatible, to promote integration with the host tissue where desired and to be able to control infections both, in the acute and latent conditions. A good balance among these requirements could significantly enhance the success of the implants; however, it is not always possible to achieve them because bacteria and host cells employ similar mechanisms to adhere to the implants, and many antibacterial and antibiofilm coatings prevent osteointegration.[363] Diverse implant coatings have been developed recently to achieve proper implant integration while avoiding bacterial infection. According to their mechanism of action, they can be classified into active and passive coatings. Due to their surface properties, passive coatings hinder bacterial adhesion or cause bacterial death upon contact. On the contrary, active coatings tackle infection using bactericidal agents, such as antibiotics, antiseptics, metal ions, and functional peptides (Figure 26).[352, 364]

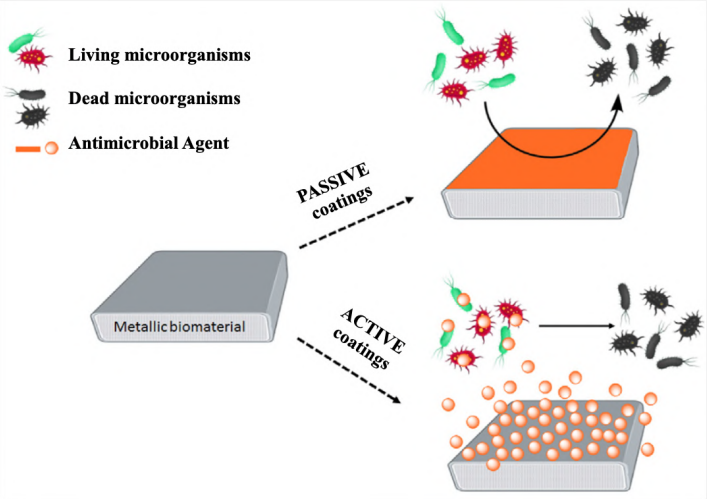

Figure 26. Active and passive antibacterial coatings protect implant surfaces from bacterial adhesion and colonisation. Active coatings release the antibacterial agents, while passive coatings create a physical barrier that impairs bacterial adhesion. Adapted with permission from.[364] under a Creative Commons (CC BY 4.0 DEED). *Copyright © 2023 Alireza Nouri, Anahita Rohani Shirvan, Yuncang Li, Cuie Wen. Published by Elsevier.*

1.5.2.1 Passive coatings

Parameters such as surface topography, roughness, chemistry and composition, hydrophilicity, surface energy and potential, and conductivity play crucial roles in initial bacterial adhesion to implants and biofilm formation afterwards.[352] Thus, passive coatings modify the implant's physico-chemical properties, creating anti-fouling and contact-killing surfaces that impair bacterial adhesion and proliferation, respectively (Figure 27).[363-366]

Modifying the crystalline structure of the surface oxide layer and ultraviolet irradiation of titanium dioxide (TiO_2) surfaces have been proven efficient in creating bacteria non-adhesive surfaces while preserving osteointegration.[355, 363]

Other strategies aim to create hydrophilic surfaces, which are quickly covered by water in aqueous environments, acting as a barrier or shield between the surface and the bacteria, thus hindering bacterial adhesion.[367] Anti-fouling polymeric coatings or "polymeric brushes" made of hydrophilic polymers [polyhydroxypropyl and polyhydroxyethyl methacrylate, polyethylene glycol (PGE) and its derivate], zwitterionic polymers (hosphatidylcholine, carboxybetaine, sulfobetaine, sulfonium ion and trimethylamine-N-oxide), as well as polysaccharides [hyaluronic acid (HA) and sodium alginate], have been proven effective in mitigating bacterial attachment on Ti substrates.[366, 368]

While hydrophilic surfaces hinder bacterial adhesion by creating a hydration barrier, hydrophobic surfaces promote the detachment and cleaning of loosely bound proteins or bacteria.[366] Surface laser and temperature treatments to produce micro- and nano-patternings modify the surface topology and its hydrophobicity, and they have been widely studied to generate bacteria-repulsive biomimetic surfaces, which impair biofilm formation even if a low number of bacteria can still attach.[369] For instance, biomimetic patterning inspired by nature-occurring surfaces renders Ti super-hydrophobic due to the introduction of micro- and nanoscale self-organised structures by femtosecond laser ablation that efficiently controlled the adhesion of *P. aeruginosa* but not *S. aureus*, suggesting that hydrophobicity and bacterial cell size may play an essential role in bacterial adhesion to super-hydrophobic materials.[370] Moreover, superhydrophobic Ti nanotube array surfaces created by chemical modification of the Ti

surface and attachment of hydrophobic groups have been proven more efficient in preventing bacterial colonisation than unmodified Ti nanotube array and super-hydrophilic surfaces.[371] Other Authors report that the combination of micro-nano topologies with super-hydrophobic surfaces, such as that achieved by the treatment of Ti with silane, significantly inhibited bacterial colonisation.[372]

On the other hand, nano surface topographies, including nanorods, nanopillars, and nano edges, grant the surfaces with inherent bacterial-killing properties, thus leading to bacterial cell lysis and/or bacterial growth inhibition.[327]

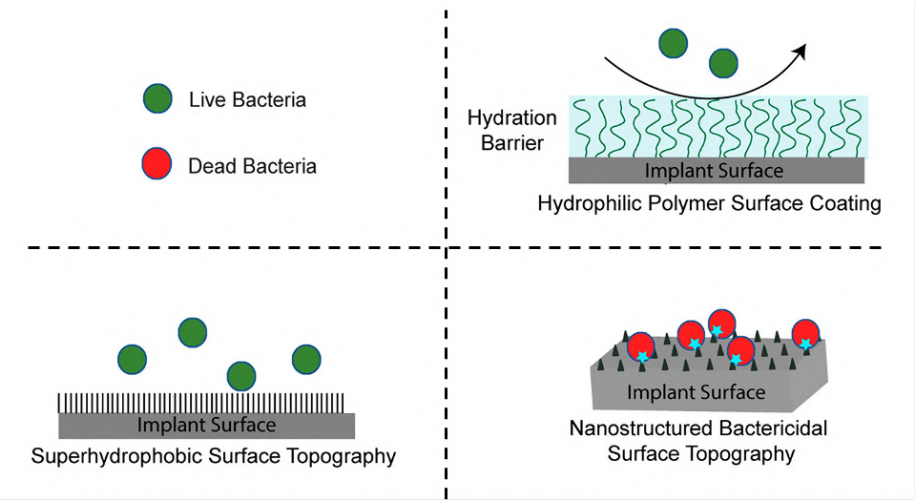

Figure 27. Hydrophilic, superhydrophobic, and nanostructure antifouling surfaces designed to impair bacterial adhesion, colonisation, and biofilm formation. Adapted with permission from ref.[366] Ghimire, Ananta, and Jie Song, *"Anti-periprosthetic infection strategies: from implant surface topographical engineering to smart drug-releasing coatings"*, ACS Applied Materials & Interfaces 13.18 (2021): 20921-20937. *Copyright © 2021, American Chemical Society*.

Nonetheless, these surface modifications impair bacterial adhesion and biofilm formation and, in some cases, affect osteoblast and fibroblast functionality. Thus, anti-fouling and bactericidal topographies can be improved by further functionalisation with RGD sequences that may enhance hMSCs adhesion while preserving bactericidal properties.[363, 373, 374]

1.5.2.2 Active coatings

Active coatings transform passive and inert implants into bioactive medical devices where the bactericidal agents are covalently attached to the implant surface or are passively released in the implant microenvironment. Any antimicrobial molecule can potentially coat surfaces, including metals (silver), organic and non-metal compounds (antibiotics, AMPs, chitosan), and their combinations (Figure 28).[352]

Antibiotic coatings create a bactericidal environment in the vicinity of the implant, and surfaces coated with covalently linked antibiotics have been extensively studied.[368, 375, 376] The most common antibiotics employed are vancomycin, gentamicin, tobramycin, amikacin, and rifampin, or a combination of them. Hydroxyapatite (HAp) coatings have been widely used as gentamicin and vancomycin carriers.[363, 365] Poly(methyl methacrylate) (PMMA) bone cement has been mixed with gentamycin, tobramycin, erythromycin, cefuroxime, vancomycin, and colistin.[377] Moreover, in recent years, antibiotics have been loaded onto implant surfaces in combination with biodegradable polymer materials and hydrogels that allow a localised drug delivery in the proper concentration and for the period necessary to avoid the infection while minimising antibiotic resistance as well as adverse unwanted effects in tissue integration and systemic side effects due to the formulation of the hydrogel.[365, 378] For instance, hydrogel coatings made of HA, named disposable antibacterial coating (DAC, composed of covalently

linked hyaluronan and poly-D, L-lactide) loaded with antibiotic, diminished bacterial colonisation and biofilm formation *in vitro* and *in vivo*.[378-380]

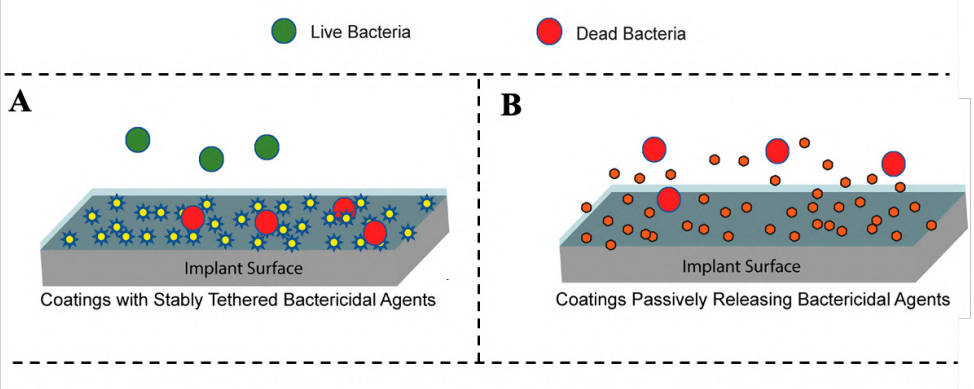

Figure 28. In active coatings, the bactericidal agents are covalently tethered to the surface through stable linkages (**A**) or physically encapsulated on the surface for their passive release in the implant microenvironment over time (**B**). Adapted with permission from ref.[366] Ghimire, Ananta, and Jie Song, *"Anti-periprosthetic infection strategies: from implant surface topographical engineering to smart drug-releasing coatings"*, ACS Applied Materials & interfaces 13.18 (2021): 20921-20937. *Copyright © 2021, American Chemical Society*.

The most commonly used metal for producing antibacterial coatings is silver, which has a broad-spectrum antibacterial activity, antifungal activity, a long-term antibacterial effect and a low risk of developing bacterial resistance; nevertheless, silver ions can also exert toxic effects towards eukaryotic cells at high concentrations, and besides the efforts to mitigate its toxicity its use in clinical devices is still limited.[365, 381]

Other excellent antimicrobial substances are chlorhexidine (CHX), chlorogenic acid (CGA), chloroxylenol, and poly-hexamethylene-biguanide. CHX-releasing coatings have been extensively used to provide long-lasting protection against bacterial infection.[363, 382] CHX-grafted phenolamine coating has been proven effective against bacterial colonisation, while CHX-hexametaphosphate coatings are effective against multi-species biofilm formation and display good cytocompatibility.[383] CGA is well known for its antimicrobial capacity;[384] for instance, a multifunctional functional surface modification strategy by coating zirconia surface with ethylene imine, HA and chitosan-CGA has been found to inhibit bacterial growth without affecting osteoblast cell adhesion, proliferation, differentiation, and calcification.[385]

In addition, Ti surfaces coated with chitosan have been proven to have excellent antimicrobial activity and can induce the growth and fixation of osteoblastic cells around the coated surface.[365] Moreover, chitosan-alginate films render the final Ti surface material biocompatible and effective against *E. coli*.[386] Chitosan gel alone or loaded with antimicrobial agents such as silver[387] and antibiotics[388-390] have also been studied to coat implant surfaces.

Further, quaternary ammonium compounds (QACs) have been employed to produce antimicrobial coatings for orthopaedic implants. For example, p(DEMMP-co-TMAEMA) polymers have shown outstanding antimicrobial activity with limited cytotoxicity towards C2C12 cells.[391] On the other hand, a self-assembly gelatin thin layer grafted with a mixture of diepoxide quaternary ammonium salt (QAS) and maleopimaric acid quaternary ammonium used to coat Ti surfaces has been demonstrated bacteriostatic and exhibited good biocompatibility and adhesion properties towards human cells.[392] Recently, Liu *et al.* (2023) have reported that a hydrogel made of a modified photocross-linkable gelatin-based polymer (GELMA) with cationic QAS showed great bactericidal activity towards *E. coli, S. aureus* and MRSA and high mammalian cells cytocompatibility.[393]

1.5.2.2.1 Antimicrobial peptide coatings

As stated above, AMPs have become promising novel drug candidates to fight against bacterial infection and antimicrobial resistance. Thus, many implant coating strategies have been developed, following the previously mentioned approaches and employing AMPs as bioactive and bactericidal agents. Therefore, AMPs have been directly immobilised onto the surfaces, using linkers, polymeric brushes, and chimeric peptides, as well as employed to design AMPs-releasing materials where AMPs are embedded into TiO_2 nanotubes (TNTs), bone cement and polymeric matrices, among others (Figure 29).[394]

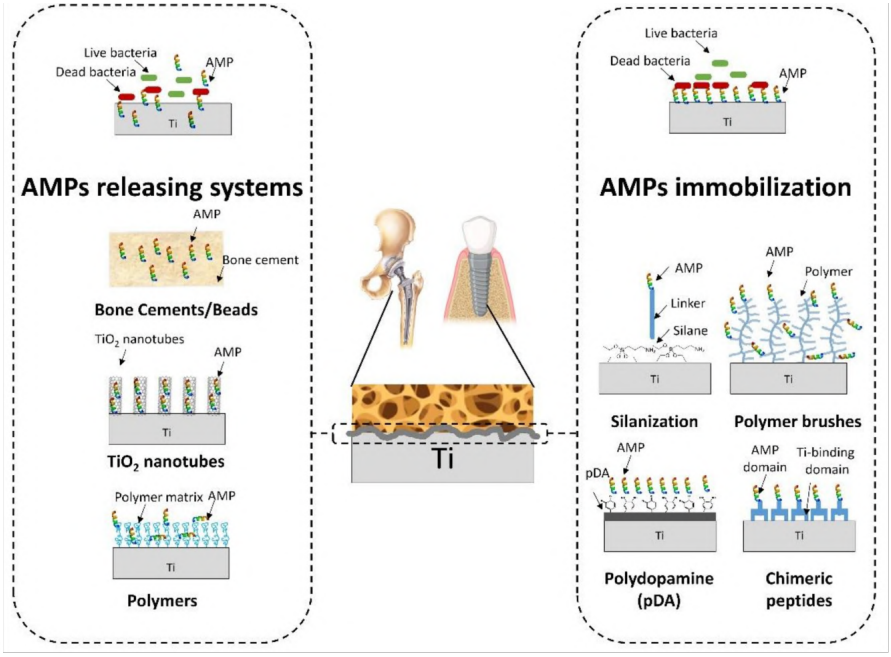

Figure 29: AMPs-based strategies for coating orthopedical implants. Reproduced with permission from ref.[394] Creative Commons Attribution (CC BY) license. Copyright © 2021 by Bruna Costa, Guillermo Martínez-de-Tejada, Paula A. C. Gomes, M. Cristina L. Martins, and Fabíola Costa. *Licensee MDPI, Basel, Switzerland*.

1.5.2.2.1.1 AMP immobilisation strategies

AMP-immobilised coatings offer long-lasting protection, as the peptides remain anchored to the surface, providing continuous antimicrobial efficacy. Nevertheless, their protection is only around the implant surface and covalently immobilised AMPs can be blocked by blood components, proteins, and dead bacteria, resulting in lower activities than AMPs in free form.[394]

For instance, several AMPs have been grafted/immobilised on implant surfaces following silanisation strategies, taking advantage of the functional groups present or introduced on the surface. AMPs such as LL-37 (and its derivate peptides),[395-397] GL13K,[398] human lactoferrin (hLF1-11),[399] melimine,[400] and JH8194,[401] among others, have been directly immobilised onto Ti surfaces[396, 397] or through polymeric linkers.[398] For instance, PEG linkers improve AMP flexibility, which, in some cases, has been reported to be essential for establishing proper interactions with bacterial cells.[395] In addition, Acosta *et al.* (2020) employed an ELP as a linker to covalently attach GL13K (L or D) to silanised Ti surfaces and compared the antimicrobial capacity of Ti, Ti-ELP and Ti-ELP-GL13K surfaces. They observed that the antibiofilm capacities of the Ti-ELP-GL13K surfaces were superior to that of Ti and Ti-ELP; nevertheless, the Ti-ELP surface hindered biofilm maturation, exhibiting a low-fouling behaviour. These results, combined with the excellent cytocompatibility towards primary gingival fibroblasts, pointed out the potentiality of ELP in the fabrication of advanced coatings.[398]

Silanisation processes are often complex and have low efficiencies.[402] Therefore, other coating approaches exploit chimeric peptides containing an AMP domain and either a Ti-binding domain[403-405] or an HAp-binding domain.[406, 407] When using chimeric peptides, the success of the final coatings depends not only on the AMP capacity to inhibit bacterial adhesion and growth but also on the structural flexibility of the linker, its configuration, the hydrophobicity of the AMP and the bacterial target.[394]

Further, polymers such as polydopamine (pDA), chitosan, and polymeric brushes have been extensively used to immobilise AMPs on material surfaces.[394]

Ti-pDA coatings, such as KR12, cecropin B (CecB), and bacitracin, have been developed for the covalent attachment of AMP. Ti-pDA-CecB surface inhibited bacterial adhesion and growth, improved cytocompatibility and reduced inflammation responses compared to non-functionalised surface.[408] On the other hand, *in vitro* studies of the Ti-pDA-bacitracin surface showed decreased *S. aureus* and MRSA colonisation while promoting hMSCs differentiation;[409] moreover, *in vivo* experiments demonstrated antibacterial activity for up to 3 weeks and osteointegration over 12 weeks.[410] Recently, Wang *et al.* (2021) have also employed pDA coatings to incorporate DJK-5 into porous Ti alloy; the final Ti-pDA-DJK-5 surface non only showed excellent antibacterial activity towards *S. aureus, S. epidermidis* and *P. aeruginosa* and reduced biofilm formation, but also improved macrophage capacity to uptake bacteria and suppressed inflammatory reaction.[411]

Other surface functionalisation approaches employ polymeric brush coatings. They offer several advantages for AMP immobilisation due to the presence of a high density of functional groups on the surfaces, which increases the AMP conjugation density while acting as flexible linkers.[394] For instance, Tet213 conjugated to different poly DMA-APMA [poly(N,N-dimethylacrylamide-co-N-(3-aminopropyl)methacrylamide hydrochloride)] copolymer brushes used to coat Ti surfaces highlighted that the conjugation of the AMP onto brushes strongly depended on the graft density of the brushes, further, the peptide density and graft density greatly influence their antimicrobial activity.[412] Similarly, Tet20 and hLF1-11 have also been immobilised on Ti surfaces employing DMA-APMA copolymer brushes. Ti-DMA-APMA-Tet20 surface had potent antimicrobial activity *in vivo* in a rat infection model.[413] In the case of Ti-DMA-APMA-hLF1-11 surface, a higher decrease in bacterial adhesion and biofilm formation by *S. sanguinis* and *Lactobacillus salivarius* was observed compared to hLF1-11 grafted on Ti by silanisation processes, highlighting the superiority of the polymeric brushes for grafting AMPs compared to silanisation approaches.[402]

In addition, gold substrates coated by a chitosan thin film covalently bound to the AMP MSI-78 (via a PEG spacer) have been proven to be bactericidal towards *S. epidermidis*, independently of the AMP tethering site (N- or its C-terminal).[414] Furthermore, hLF1-11 conjugated to chitosan through its C-terminal cysteine, with and without a PEG pacer, showed that AMP functionalisation on chitosan films significantly increases bacterial adhesion; nevertheless, the viability of adherent MRSA cells was decreased, especially when hLF1-11 was immobilised through the PEG spacer.[415] Moreover, these Authors develop Dhvar-5-chitosan conjugates using either C- or N-terminal AMP anchoring as well as different sizes spacers, demonstrating that Dhvar-5 N-terminal conjugation improved the coating capacity in preventing MRSA colonisation and longer spacers improved this activity regardless their flexibility. Moreover, N-terminal conjugation did not modify bacterial adhesion to chitosan, while randomly oriented Dhvar5 (physically adsorbed) induced bacterial adhesion,[416] reinforcing the influence of AMP orientation on its activity. Anoplin-chitosan conjugates displayed enhanced antibacterial activity compared to free anoplin peptide, especially against Gram-positive bacteria, while exhibiting a non-hemolytic behaviour, even when

the free AMP was reported to have hemolytic activity; so thus, in this case, the chitosan conjugation potentiated not only the antimicrobial activity of the AMP but also its cytocompatibility.[417] In addition, Barbosa *et al.* (2019) developed ultra-thin coatings composed of Dhvar-5-chitosan conjugates, revealing that when Dhvar-5 was C-terminally, the coating displayed a superior antimicrobial activity against Gram-positive bacteria and reduced adhesion of Gram-negative bacteria, without being toxic for eukaryotic cells.[418] All these studies reinforced the role of the spacers and the AMP orientation on their antimicrobial activity; nevertheless, no rule can be established for designing AMP immobilised coatings since their outcome varies for different coatings and are highly dependent on the AMP, the spacers and the bacterial target.

1.5.2.2.2.2 AMPs releasing systems

In recent years, AMP-releasing coatings have emerged as a novel approach to fight microbial infections. They offer dynamic protection through continuous AMP release at bactericidal concentrations for several days after implantation.[381] Common strategies to deliver AMP in the implant's surrounding tissues include embedding into TNTs, bone cement, polymeric, and hydrogel matrices.

Broad spectrum activity AMPs such as GL13K[419] and HHC-36[420] have been successfully loaded onto TNTs, displaying good antimicrobial properties and outstanding biocompatibility. Other approaches employ mesoporous titania-covered Ti implants to deliver AMPs (RRP9W4N) and successfully inhibit biofilm formation to a greater extent than traditionally used antibiotics (cloxacillin) without influencing osteointegration *in vivo*.[421] Further, a more complex strategy was followed by Kazemzadeh-Narbat *et al.* (2013); they developed a coating where HHC-36 was embedded in a multilayer coating made of three layers of vertically oriented TNTs, a thin layer of calcium phosphate (CaP) and a phospholipid film. This coating was highly effective against Gram-positive and -negative bacteria without being toxic to host cells.[422]

The most employed bone cement for AMP loading are CaP and PMMA. Andrea Volejníková *et al.* (2019) reported that AMP-loaded PMMA bone cement can protect or significantly reduce surface colonisation and biofilm formation by Gram-positive and -negative bacteria.[423] In addition, different studies have demonstrated the potential of hLF1-11 incorporated into CaP[424, 425] and calcibon bone cement in reducing bacterial growth and enhancing osseointegration;[426] moreover, *in vivo* studies did not show any toxicity associated with the release of hLF1-11 and vascular ingrowth into the CaP cement was observed indicating the potentialities of the coatings for complete bone remodelling.[427] Other Authors studied the combination of CaP with Tet213 to develop Ti coatings by electrolytic deposition of CaP, showing that none of them had any cytotoxicity for osteoblast-like cells while displaying antimicrobial activity against Gram-positive and Gram-negative bacteria.[428] Later, they compared the cytotoxicity of coatings made of CaP loaded with Tet213 or HHC-36, demonstrating that CaP-HHC-36 coatings have superior biocompatibility.[429] Furthermore, one of these studies demonstrated the antibacterial superiority of CaP-Tet213 coatings compared to CaP-MX226, CaP-hLF1-11 or even CaP-tobramycin.[428] Another research group reported that CaP and PMMA loaded with AMPs were able to control MRSA and *S. epidermidis* infections to a greater extent compared to gentamicin and vancomycin, highlighting once more the superiority and the potential of AMPs in the treatment and control of infections caused by antibiotic resistance bacteria compared to conventional-antibiotics.[430]

Many polymers and hydrogels have been reported as potential antibacterial coatings for titanium surfaces. Several cases described embedding the AMPs into polymeric matrices; in others, the AMPs are covalently attached to the polymers. Moreover, in some cases, besides being the AMP carrier and creating the matrix structure, the polymers

also bear antimicrobial properties that contribute in an additive or synergetic manner to the antimicrobial capacity of the final coatings.[394] It has been reported that hydrogel coatings for Ti alloy surfaces comprised of a mixture of alginate and Pluronic polymer with the AMP cateslytin displayed strong antimicrobial activity against *Porphyromonas gingivalis* with no sign of toxicity towards human fibroblasts.[431] In addition, hydrogels made of gelatin methacrylate chemically conjugated to dopamine (GelMA-DOPA) loaded with HHC-36 and silica nanoparticles have been described as efficient in preventing bacterial infection and promoting osteogenesis of hMSCs.[432]

A multi-layer PLEX-coating (Polymer-Lipid Encapsulation MatriX) has been described to be an efficient polymeric matrix to encapsulate and then sustainably deliver bioactive molecules for up to 4 weeks; thus, PLEX-coatings containing an AMP derivated from LL-37 reduced bacterial growth up to 38 % in an infection model *in vivo*.[433] Other Authors have reported the employment of polyelectrolyte multilayer to cover Ti discs and deliver the antimicrobial molecule. For instance, a stable β-aa-based peptidomimetic AMP embedded in cross-linked layer-by-layer chitosan-HA hydrogels reduced about 60% of *S. aureus* biofilm formation without impairing preosteoblast cell function.[434]

Even though the use of AMP-releasing systems has clear advantages and provides good antimicrobial solutions to contrast infections, they face several concerns, mainly due to their transient antibacterial activity, which may primarily prevent early post-surgical infection caused by contamination during the surgical procedures but may not be very effective for preventing secondary infections due to opportunistic bacteria. Additionally, developing coatings that can consistently load and release the AMPs at bactericidal concentrations throughout the implant's lifetime remains challenging.[381]

1.5.2.3 "Smart release" coatings

Nowadays, the concept and the use of "smart coatings" or "self-defensive" coatings have become popular due to their high sensitivity and responsiveness to diverse stimuli, including the presence of bacteria and innate immune system factors. Moreover, physical stimuli, such as pH, temperature and ionic strength, and photothermal and photodynamic therapy, have been used to trigger the release of bactericidal agents (Figure 30).[366, 368] These coatings are designed to optimise the delivery of the antimicrobial agent, enhance its stability, and avoid undesired side effects on the patients. In most cases, "smart release" coatings are designed to have no anti-infection properties under physiological conditions. In contrast, they release the bioactive molecule upon the proper stimulus and tackle the infections.[435-439] These coatings exploit the implant microenvironment changes produced due to bacteria colonisation and biofilm formation, such as the reduction in the pH and the increase in the concentration of specific enzymes or virulence factors.[440, 441] In addition, some others are produced to maintain the implant surface sterile before implantation and to block the release of potentially toxic antimicrobial compounds into the body upon surgery.[442]

In this sense, smart coatings made of branched PEG-poly-propylene-sulfide have been designed to passively and actively deliver tigecycline and vancomycin and have been proven effective against *S. aureus*.[435-437] Other strategies employ enzyme-sensitive peptide linkers to covalently attach antibiotics to the Ti surface and achieve an infection-dependent drug release behaviour in the presence of an *S. aureus* protease.[439]

For instance, a novel antibacterial Ti surface to sense hyaluronidase-secreting bacteria has been developed. The coatings were made of TNTs loaded with CecB and then coated, layer by layer, with five layers of chitosan/sodium hyaluronic [(CH/SH)5] or chitosan/sodium hyaluronic-CecB [(CH/SH–CecB)5]. In this design, CecB remains

trapped within the TNTs due to the presence of CH/SH and CH/SH–CecB layers; CecB release was triggered by the presence of *S. aureus* and exogenous hyaluronidase that degraded the blocking layers, thus facilitating the release of CecB from TNTs. Both surfaces had good short- and long-term bactericidal capacity against *S. aureus* and *S. epidermidis* and osteoblast compatibility, even in the presence of *S. aureus* co-cultures.[443]

Yan *et al.* (2016) developed a pH-responsive hierarchical surface based on multilayer polymeric brushes made of polymethacrylic acid (PMAA). While the PMAA outer layer granted the coating with antifouling surfaces, the PMAA inner layer contained CecB covalently immobilised. In this design, the PMAA hydration layer renders the surface resistant to initial bacterial attachment and biocompatible under physiological conditions. Still, if bacteria colonise the surface, the pH of the surrounding microenvironment is reduced, inducing outer PMAA chains collapse and exposure of inner layers containing the bactericidal AMP. Moreover, once bacteria are dead, the pH returns to physiological values and the hydrophilicity of the PMAA is restored, releasing dead bacteria due to its anti-fouling properties. This strategy demonstrated the capabilities of reversible and on-demand antibacterial coatings to prevent bacterial colonisation (anti-fouling layer) and biofilm formation (pH-triggered exposure of PMAA-CecB layer) for producing non-leaching surfaces without additional reloading of the antibacterial agents. Nevertheless, no studies have indicated its employment in implant coatings, even when this surface had excellent biocompatibility.[444]

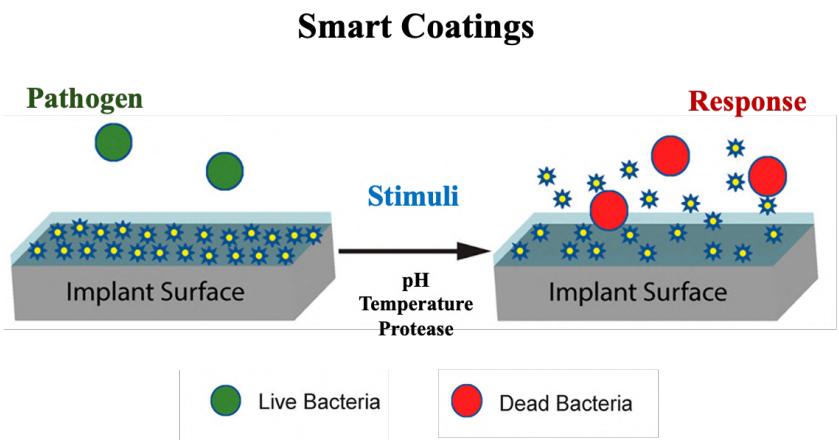

Figure 30. Smart coatings ensure local protection by releasing bactericidal agents in response to stimuli generated by the microorganism. Adapted with permission from ref.[366] Ghimire, Ananta, and Jie Song, *"Anti-periprosthetic infection strategies: from implant surface topographical engineering to smart drug-releasing coatings"*, ACS Applied Materials & interfaces 13.18 (2021): 20921-20937. *Copyright © 2021, American Chemical Society*.

A novel strategy to encapsulate an AMP for its subsequent smart release was described by Chen *et al.* (2020). They created a sort of "Pandora Box" made of TNTs loaded with HHC-36 closed with a gate made of a pH-responsive PMMA that, under physiological conditions (pH 7.4), swells and blocks HHC-36 release from TNTs but in the presence of bacterial infections (pH below 6) collapses and releases the AMP. The "Pandora box" was bactericidal against the most common pathogens associated with implant infections, *S. aureus, E. coli, P. aeruginosa,* and MRSA, and at the same time, promoted osteogenic differentiation of hMSCs.[438]

Zhan *et al.* (2018) developed a different strategy for the smart release of an AMP based on temperature and before implantation to avoid cytotoxicity due to the AMP release after implant allocation in the body. They developed a Ti-pDA coating conjugated with a temperature-sensitive polymer, poly(N-isopropylacrylamide) (pNIPAM), followed by AMP conjugation through a click chemistry reaction. The temperature-sensitive property of pNIPAM

allowed the release of the AMP domain, preferably at room temperature (25 °C) rather than at body temperature (37 °C). Thus, Ti-pDA-pNIPAM-AMP coating strongly inhibited the bacterial growth of *S. aureus* and *E. coli*. The Authors demonstrated that the smart behaviour improved the surface biocompatibility of the surface *in vitro* and *in vivo* at body temperature when compared to the substrates unmodified or modified by AMPs or pNIPAM alone.[442]

Thermo-responsive bactericidal surfaces employing pNIPAM have also been developed by Wang *et al.* (2017). These Authors develop a hierarchical structure containing an antifouling outer layer made of vancomycin covalently immobilised on pNIPAM and an inner layer composed of poly(sulfobetaine methacrylate) (pSBMA) polymeric brushes. At room temperature, the pNIPAM-based layer was stretchable, allowing vancomycin-mediated contact killing of bacteria. In contrast, the pNIPAM-based layer collapsed at physiological temperature, triggering vancomycin occlusion and exposing zwitterionic pSBMA brushes. This hierarchical surface effectively killed bacteria at room temperature and, at physiological temperature, turned into a zwitterionic anti-fouling surface, releasing dead bacteria and inhibiting subsequent planktonic bacteria adhesion and improving surface biocompatibility. Once more, the potentiality of hierarchical surfaces with switchable bioactivity was demonstrated, and the door was opened for their use in manufacturing infection-resistant medical devices.[445]

Overall, AMP coatings provide practical strategies to contrast orthopaedic implant infections, biofilm formation and antimicrobial resistance. However, challenges such as limited protection over time and susceptibility to biological interference persist. Even though immobilisation strategies demonstrate promising outcomes, they encounter issues due to the in vivo interaction of AMPs with host proteins, which affects their activity. On the other hand, AMP-releasing systems provide sustained antimicrobial efficacy, but face challenges related to their transient activity and loading-release profiles. Thus, “smart release” coatings hold promise in addressing these challenges by delivering antimicrobial agents in response to environmental stimuli or bacterial presence, improving implant safety and efficacy. Nevertheless, the strategies reported have been mainly studied in laboratory conditions; their clinical evaluation is still limited and further studies about long-term effectiveness and safety are needed. In addition, collaborations among multidisciplinary academic and medical teams as well as industrial partners are mandatory to develop advanced implantology techniques that, for instance, incorporate 3D printing for manufacturing personalised and functionalised orthopedical implants.

Chapter 2. Aims and Objectives

As stated in the previous sections, antimicrobial peptides (AMP) are a promising alternative to traditional antibiotics, mainly due to their broad-spectrum activity and low propensity to induce resistance mechanisms. Moreover, their recombinant production has gained relevance in recent years as it is a more sustainable and environmentally friendly technology than chemical synthesis. Thus, taking advantage of the recombinant Human Elastin-Like Polypeptides (HELP) platform developed in our laboratory, and its employment as a carrier for the production in *Escherichia coli* of functional and bioactive domains, we decided to explore its capabilities for the production of antimicrobial domains as well as derived materials that could be employed to coat implant surfaces and improve their antimicrobial properties.

Thus, the first aim was to define the strategies already employed to produce antimicrobial peptides fused to Elastin-Like Polypeptide (ELP) carriers. The objectives were to analyse the AMPs and ELPs employed, the AMP orientation, the characteristics of the expression system, the production yield, and the methods for releasing the AMP from the fusion proteins.

A second aim was to obtain a proof-of-concept related to the use of HELP as a multifunctional and antimicrobial delivery platform to produce biomimetic materials endowed with antimicrobial activity. The objectives were to design, produce and functionally test a HELP-Indolicidin (HIn) fusion construct. The production of 2D and 3D HIn-derived materials would allow the assessment of their functionality and their capacity for the "smart release" of the antimicrobial domain. This fusion biopolymer will serve as a model for subsequent constructs.

The third aim was to employ the HELP functionalisation model already developed. The objectives were to produce a fusion construct carrying the difficult-to-synthesise sequence of human β-defensin 1 and assess the biological properties of the fusion biopolymer as well as those of the derived materials.

The final aim was to develop a new ELP with optimised compatibility while maintaining the potential as a fusion carrier. Thus, the objectives were to design, produce, characterise, and biologically test a universal ELP obtained from an elastin consensus sequence and following a biomimetic strategy. The physico-chemical and biological properties of the new ELP will be compared to those of HELP.

Chapter 3. Smart tools for antimicrobial peptides expression and application: the elastic perspective

This chapter introduces a review article published in the Biotechnology and Bioengineering Journal (Wiley). **Colomina-Alfaro, L.**, Marchesan, S., Stamboulis, A., & Bandiera, A. (2023). **Smart tools for antimicrobial peptides expression and application: The elastic perspective.** *Biotechnology and bioengineering, 120*(2), 323–332. https://doi.org/10.1002/bit.28283. Reproduced with permission from John Wiley and Sons. *Copyright © 2023.*

The first aim of the thesis was to evaluate the strategies already employed and described to produce antimicrobial peptides fused to the ELP carriers. Thus, a literature research was performed to identify the approaches adopted to recombinantly fuse and chemically conjugate different AMPs with several ELPs. The nature of the AMPs and the ELPs was examined, as well as the main features of the expression and production systems. In total, 20 ELP-AMP constructs were analysed and classified as C-terminal ELP-AMP fusion proteins, N-terminal AMP-ELP fusion, ELP-AMP-ELP fusion proteins, and ELP-AMP conjugated by chemical methods. In all cases, the recombinant fusion proteins were successfully expressed with variable yields, and the presence of the ELP carrier was reported to increase the final construct solubility and mask the toxic effect of the AMPs on the expression hosts. Moreover, some AMPs conferred antimicrobial activity to the whole fusion constructs irrespective of the N-terminal or C-terminal position of the AMP. In contrast, in some cases, the antimicrobial activity was displayed only after their release and purification of the AMP from the carrier. Nevertheless, the use of ELP as carriers for functional AMP production is still limited. So far, a few ELP sequences and production systems have been employed and described. At the end of this process, beyond acquiring the functional information for designing a novel HELP-AMP fusion to achieve the following objectives, we realised that the information collected could be helpful for other researchers in the field. Thus, we decided to use the data collected to write a review paper to define the state-of-the-art in this cutting-edge technology and address its possible future development directions. My contribution to this journal article is as follows: systematic literature research, data collection for graphical representation, preparation of schemes, figures and tables, as well as original and revised draft writing.

Received: 7 July 2022 | Revised: 4 October 2022 | Accepted: 5 November 2022

DOI: 10.1002/bit.28283

MINI-REVIEW

BIOTECHNOLOGY BIOENGINEERING WILEY

Smart tools for antimicrobial peptides expression and application: The elastic perspective

Laura Colomina-Alfaro[1] | Silvia Marchesan[2] | Artemis Stamboulis[3] | Antonella Bandiera[1]

[1]Department of Life Sciences, University of Trieste, Trieste, Italy

[2]Department of Chemical and Pharmaceutical Sciences, University of Trieste, Trieste, Italy

[3]School of Metallurgy and Materials, Biomaterials Research Group, University of Birmingham, Edgbaston, Birmingham, UK

Correspondence
Antonella Bandiera, Department of Life Sciences, University of Trieste, Via Licio Giorgieri 1, I-34127, Trieste, Italy.
Email: abandiera@units.it

Funding information
Horizon 2020 Innovative Training Network AIMed, Grant/Award Number: 861138

Abstract

In recent years, antimicrobial peptides (AMPs) have become a promising alternative to the use of conventional and chemically synthesized antibiotics, especially after the emergence of multidrug-resistant organisms. Thus, this review aims to provide an updated overview of the state-of-the-art for producing antimicrobial peptides fused or conjugated with the elastin-like (ELP) peculiar carriers, and that are mostly intended for biomedical application. The elastin-like biopolymers are thermosensitive proteins with unique properties. Due to the flexibility of their modular structure, their features can be tuned and customized to improve the production of the antimicrobial domain while reducing their toxic effects on the host cells. Both fields of research faced a huge rise in interest in the last decade, as witnessed by the increasing number of publications on these topics, and several recombinant fusion proteins made of these two domains have been already described but they still present a limited variability. Herein, the approaches described to recombinantly fuse and chemically conjugate diverse AMPs with ELPs are reviewed, and the nature of the AMPs and the ELPs used, as well as the main features of the expression and production systems are summarized.

KEYWORDS
antimicrobial peptides, conjugation, elastin-like polypeptides, recombinant expression

1 | INTRODUCTION

In the last decades, the sudden rise of bacterial resistance against conventional chemically synthesized antibiotics has boosted the seek for novel molecules and strategies to fight infections. This defensive response of bacteria underpins the occurrence of the so-called superbugs that cause infections that are hard to treat and eradicate, mainly due to the emergence of new resistance mechanisms that quickly spread globally. Alternative treatments based on innovative antimicrobial mechanisms are urgently required to withstand the threat of multi-drug resistant (MDR) bacterial and nosocomial infections.

Antimicrobial peptides (AMPs) naturally occur as a component of innate immunity, and are widely produced by many diverse organisms. They represent the earliest physiological response of living entities (animals and plants) and were evolved by them in the fight for survival (Magana et al., 2020). For this reason, they seem to be less prone to give rise to bacterial resistance. Thus, using these peptides instead of chemically synthesized antibiotics is considered a powerful tool to counteract the phenomenon of bacterial resistance.

There is a general agreement that AMP's multiple site-targeting mechanisms of action, together with the rapid microorganism killing capacity, hinder the development of resistance, in contrast to what happens for conventional antibiotics. In addition, some AMPs exhibit

other favorable properties, such as anti-inflammatory, regenerative and anticancer capacities that extend their opportunity to be employed in many other clinical applications (Rai et al., 2022; Ramazi et al., 2022).

However, there are still several concerns that hinder the introduction of AMPs into the market soon, such as the risk of toxicity and adverse reactions, often linked to the issue of finding an adequate delivery route to the infection site as well as the high costs for their production on a commercial scale (Wibowo & Zhao, 2019). The feasibility of AMP employment as antibiotics is strictly connected with the peptide availability in an appropriate amount, and in a cost-effective manner (Li, 2011). Moreover, to optimize the therapeutic use of AMPs, the conjugation and functionalization with other polymers or macromolecules have been proven as effective strategies able to fully exploit their antimicrobial activity, the mode of action, the route of delivery as well as the half-life (Bellotto et al., 2022) minimizing their systemic toxicity (Cui et al., 2021). Many AMP conjugation strategies based on chemical and biotechnological approaches have been described and were recently reviewed (Silva et al., 2022).

The recombinant approach is considered an efficient alternative for peptide production on a large scale, offering several advantages with respect to conventional methods, such as the labor-intensive isolation from natural sources and costly chemical synthesis (Li, 2011). Most of the described recombinant systems are based on expression in *Escherichia coli* and AMPs are often expressed as fusion proteins, with several advantages ranging from masking the potentially lethal effects on the host microorganism to protecting the peptides from proteolytic degradation (Li, 2009). However, an ideal platform for AMP functionalization and large-scale production is not established yet. Among those described, the recombinant elastin-like polypeptides (ELPs) fusion technology still appears the least exploited. ELPs are macromolecules modeled after elastin first described by Urry (1988).

ELPs primary structure is characterized by the presence of repeated motifs, typically the pentapeptidic VPGVG sequence found in the bovine elastin homolog, where the fourth position can be replaced by any "guest" amino acid except proline (Luan et al., 1992). They retain several biophysical properties peculiar of the native tropoelastin, mainly the lower critical solution temperature (LCST) phase behavior. Above their LCST, also known as the inverse transition temperature (Tt), these polypeptides coalesce, forming insoluble, aggregates that result in a coacervate phase (McDaniel et al., 2013). The Tt is a function of several intrinsic and extrinsic factors that can be controlled, like the amino acid composition of the "guest" residue position, the chain length as well as the polypeptide concentration, and the concentration of other solutes in the buffer. This feature allowed to set up of a procedure designated as the inverse transition cycle (ITC) that is a time-saving and cost-effective way of purifying the recombinant ELP-based proteins (Figure 1). The unique ELPs properties, including their minimal immunogenicity, make them ideal candidates for a variety of biomedical applications, since they benefit from recombinant synthesis and genetically encoded design that enable control over their size, sequence, and consequently, thermo-responsive behavior (Varanko et al., 2020).

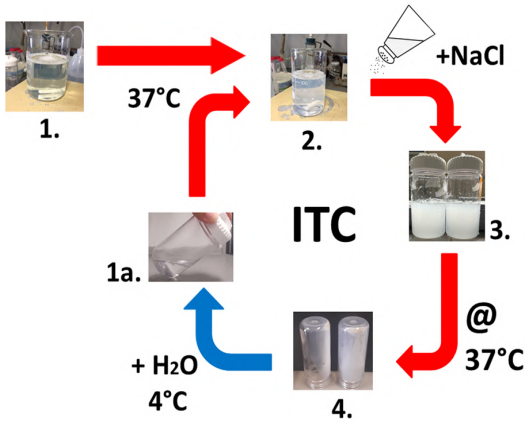

FIGURE 1 Schematic representation of the purification process based on the ITC. The use of ELPs as a purification tag exploits the thermo-responsive properties of the elastin-like domain. 1. Supernatant obtained after centrifugation of bacterial cell lysate; 2. Phase transition after heating to 37°C and 3. after NaCl addition; 4. Pellet obtained after centrifugation at 37°C; 1a. Pellet resuspension in cold water.

Currently, ELPs are considered a strategic fusion partner for components of biological origin (Yeboah et al., 2016).

This review aims to provide an updated overview of the described AMP fusion proteins that use ELP carriers. All the constructs reported were analyzed, keeping into account the structure, the features of the expression systems, the antimicrobial activity, and the potential applications of this approach. This analysis will be functional to define the state-of-the-art in this cutting-edge technology and, thus, identify its possible future development directions.

2 | AMP SEQUENCES SELECTED FOR RECOMBINANT FUSION WITH ELPS

Antimicrobial peptide research is currently one of the most active fields of investigation, as witnessed by the huge number of reviews on this topic in the last decade. It is reported that approximately 6000 of AMPs have been either isolated from natural sources or chemically synthesized. Less than 100 peptide drugs have reached the market, but several hundreds of novel therapeutic peptides have undergone the route for drug development (Boparai & Sharma, 2020). However, according to the FDA database, less than 10 are currently approved for clinical applications (Rai et al., 2022).

Many approaches were described for biotechnological AMP production routes, such as the fusions with many different carriers (reviewed in Li, 2009), expressed mainly in the *E. coli* bacterial system (Li, 2011). The first report of a recombinantly AMP expressed as an ELP fusion dates back to 2008, and from 2010 to the present 20

constructs of this kind have been successfully produced mainly using bacterial recombinant systems, whereas five of them were produced in a plant expression system (see Table 1).

An analysis of the AMP sequences that were selected as ELP fusion partners reveals that their size ranges from 12 to 69 amino acids, and with respect to the total fusion protein, they represent from about 1/70 to 1/3 of the whole macromolecule mass (Table 1). The majority of the selected AMP sequences were cationic as most of the AMPs, with the net charge ranging from +1 to +7. Among them, about half presented the amphipathic α-helical structure and the others are cathelicidin and defensin-like peptides (Table 1).

All the anionic AMPs described as ELP fusion partners are characterized by the presence of intra-chain disulfide bonds, showing a cysteine knot, which is typical for defensin-like structures. Only one was expressed as an ELP fusion in a bacterial recombinant system (Table 1, #5), whereas the other negatively charged AMPs were successfully expressed as ELP fusions in a plant system, (Table 1, #14 to #18) according to the finding that, in general, AMPs of plant origin are significantly less cationic than the others (Ghidey et al., 2020).

3 | STRATEGIES EMPLOYED FOR ELP FUSION AND ELP FUNCTIONALIZATION WITH AMP

Three main approaches for positioning the AMP domain within the ELP fusion construct were described (Figure 2a–c).

Seven AMPs were placed at the C-terminus of the ELP region (ELP–AMP). Five of them were placed after an intein domain to trigger their release from the expressed construct by self-splicing of the intein (Figure 2a, Table 1, #1). Inteins are indeed widely used as auto-processable tools for protein splicing so that adjacent domains are post-translationally linked together with the extrusion of the intein domain (Shah & Muir, 2014). The other two were preceded by the enterokinase proteolytic domain, to be enzymatically released without additional amino acids at their N-terminus (Figure 2a).

Several ELP fusion constructs carrying the AMP at the N-terminal end (AMP–ELP) were described (Figure 2b). Three of them were placed before a chemical cleavage site to release the AMP (Table 1, #2a, #8, and #9) whereas two were fused to functionalize the ELP moiety for the realization of biomaterial endowed with antimicrobial properties (Table 1, #10 and #11). The last four fusion constructs were based on a modified ELP domain containing alternate blocks of silk-derived repeats (Table 1, #2b, #9a–11a). In addition, other N-terminal AMP–ELP fusion constructs produced in a plant expression system were described (Table 1, #14–#18).

In the third approach, the AMP domain was embedded in the middle of the ELP moiety (ELP–AMP–ELP). In this configuration, the N-terminal ELP domain is intended as a protective "sacrificial block" which is subsequently cleaved by CNBr to release an N-terminal AMP fusion with ELP (Figure 2c and Table 1, #12, #13, and #13a).

In addition, ELP conjugation with AMPs was reported (Figure 2d). Two different chemical methods were employed. In one of them, a synthesized D-AMP enantiomer was covalently bonded to the expressed ELP by "click chemistry" (Table 1, #19) and in the other ELP was functionalized with the AMP by the EDC/NHS chemistry (Table 1, #20).

Overall, it emerges that AMPs belonging to different classes and spanning the entire range of length were successfully expressed as N-terminal and C-terminal ELP fusions, as well as in the middle of the ELP moiety (Figure 2). Most of the described constructs were aimed to obtain the AMP without any modification as an alternative route to the chemical synthesis. The maximum yield reported for purified AMPs released from the ELP fusion construct was almost 100 mg/L (Table 1, #4).

Interestingly, in some cases, the whole ELP fusion construct showed to possess the antimicrobial activity conferred by the AMP domain, (Table 1, #5, #14–#18). On the other hand, in several cases, the ELP fusion protein was designed with the aim of obtaining a bioactive component endowed with antimicrobial properties for the realization of biomaterials, matrices, and surfaces (Table 1, #10, #11, #13, and #13a).

The yield of the AMPs that were released by different means and purified ranged from 0.5 mg/L to above 100 mg/L under optimized expression conditions (Table 1). However, it should be noted that all of the reported recombinant fusions (except those expressed in plants) were produced by the T7 expression system using vectors of the pET series. From this point of view, there is likely room for further improvement in production.

4 | ELP SEQUENCES EMPLOYED AS FUSION PARTNERS

The interest that AMPs rise as an alternative approach to antibiotics of chemical synthesis is linked to their potential application as novel antimicrobial therapeutics. However, this implies that they should be produced cost-effectively. The recombinant expression is still considered one of the most appealing routes to meet the needs for large-scale peptide manufacturing. Although the AMPs recombinant expression is described, the strategy of the antimicrobial domain fusion with a carrier protein has been largely adopted to circumvent toxicity towards the bacterial host and to prevent proteolytic degradation of the peptides themselves (Li, 2009). In this regard, ELPs with their peculiar properties, represents a still underexploited fusion partner for the AMPs. Among the reported ELP constructs with AMPs, it is interesting to analyze the elastin-like sequences that were employed.

The five ELP-AMP fusion constructs based on intein as the system to release the bioactive domain were constituted by an N-terminal ELP region of the VPGXG pentapeptidic repeats ranging from 300 to 550 aa where X was V, G, and A or L. These constructs ranged from about 50–72 kDa, carrying an intein domain of about 200 amino acids (Figure 2a). Successful expression was reported for each construct (Table 1, #1–#5). The ELP carrier was expected to facilitate the purification of the AMP domain after intein cleavage.

TABLE 1 Antimicrobial peptides were selected as fusion partner for an ELP carrier

No	AMP domain	AMP sequence and information	AMP source and main features	Construct reference and main features
#1	human b-defensin 4 (hBD4) 50aa	EFELDRICGYGTARCRKKCRSQEYRIGRCPNTYACCLRKWDESLLNRTKP https://dbaasp.org/peptide-card?id=18490	From *Homo sapiens* cationic (+6), disulfide bonds Gram+, Gram-, Cancer, Mammalian Cell	**#1:** DOI: 10.1016/j. micres.2010.01.002 Intein-based release Released AMP yield: 1.8 mg/L Tt below 30°C in high-salt solution
#2 **#2a** **#2b**	Moricin CM4 ABP-CM4, 35aa	RWKIFKKIEKVGQNIRDGIVKAGPAVAVVGQAATI https://dbaasp.org/peptide-card?id=3460	From *Bombix mori* cationic (+6) Active against Cancer, Fungus, Mammalian Cell	**#2:** DOI: 10.1016/j. micres.2010.01.002 Intein-based release Released AMP yield: 0.6 mg/L Tt below 30°C in high-salt solution **#2a:** DOI: 10.1021/bm5016706 Chemical cleavage (formic acid) - Released AMP yield: 1.5 mg/100 mg fusion protein Tt 31.6°C **#2b:** DOI: 10.3390/app11125352 Active fusion yield: 120 mg/L Tt below 37°C
#3	Oxysterlin1 39aa	GSKRWRKFEKRVKKIFEETKEALPVVQGVVAVATAVGRR https://dbaasp.org/peptide-card?id=10889	From *Oxysternon conspicillatum* Cationic (+7), amphiphilic Gram +, Gram-, Fungus, Mammalian Cell	**#3:** DOI: 10.13345/j. cjb.200625 Intein-based release Released AMP yield: 1.2 mg/L Tt below 37°C in high-salt solution
#4	Pa-MAP2 28aa	LKAAAAAAKLAAKAAKAALKAAAAAAKL https://dbaasp.org/peptide-card?id=9012	Synthetic (inspired from *Pleuronectes americanus* Pa-MAP) Cationic (+6) Gram+, Gram-, Virus, Cancer, Mammalian Cell	**#4:** DOI: 10.1016/j. jbiotec.2016.07.021 Intein-based release Released AMP yield: 96 mg/L Tt below 30°C in high-salt solution
#5	IMPI Insect Metalloprotease Inhibitor (mutant I38V) 69aa	IVLICNGGHEYYECGGACDNVCADLHIQNKTNCPIIN**V**RCNDKCYCEDGYARDVNGKCI-PIKDCPKIRS NCBI Reference Sequence ID: XP_031769425.1	Mutant from *Galleria mellonella* Anionic (−1) 5 Disulfide bonds	**#5:** DOI: 10.3389/fbioe.2019.00150 Intein-based release Active fusion yield: 5 to 20 mg/L of bioactive fusion construct Tt not reported
#6	Cecropin AD 37aa	KWKLFKKIEKVGQRVRDAVISAGPAVATVAQATALAK https://dbaasp.org/peptide-card?id=6471/	Synthetic cationic (+7) amphipathic Gram+, Gram-, Mammalian Cell	**#6:** DOI: 10.1016/j. pep.2012.04.007 Enzymatic release Released AMP yield:1.2 mg/100 ml Tt below 30°C in high-salt solution

TABLE 1 (Continued)

No	AMP domain	AMP sequence and information	AMP source and main features	Construct reference and main features
#7	Pt5e (phosvitin C-term - derived mutant) 55aa	SRMSKTATIIEPFRKFHKDRYLAHHSATKDTSSGSAAASFEQMQKQNRFLGNDIP https://pubmed.ncbi.nlm.nih.gov/24028820/	Mutant from *Danio rerio* phosvitin Cationic (+4) Gram+, Gram-	**#7:** DOI: 10.1016/j. fsi.2016.09.044 Enzymatic release Released AMP yield: 1.47 mg/100 ml Tt below 30°C in high-salt solution
#8	Halocidin (subunit A) 18aa	WLNALLHHGLNCAKGVLA https://dbaasp.org/peptide-card?id=3	From tunicate *Halocynthia aurantium* cationic (+1), α-helical structure Gram+	**#8:** DOI: 10.1007/s12010-009-8850-2 Chemical cleavage (hydroxylamine) Released AMP yield: 1.7 mg/69 mg total protein Tt below 40°C in high-salt solution
#9 **#9a**	Synoeca MP 14aa	INWIKIGKKIIASL https://dbaasp.org/peptide-card?id=18234	From *Synoeca surinama* Cationic, and amphiphilic α-helical Gram+, Gram-, Fungus, Mammalian Cell	**#9:** DOI: 10.3390/ph14100956 Chemical cleavage (formic acid) Released AMP yield: 0.5 mg/100 mg of fusion Tt ~ 33°C **#9a:** DOI: 10.3390/app11125352 Active fusion yield: 73 mg/L Tt not reported, T increase accelerates gelation
#10 **#10a**	Hep25C (Hepcidin) 25aa	DTHFPICIFCCGCCHRSKCGMCCKT https://dbaasp.org/peptide-card?id=2042	Human cationic (+2), disulfide bonds Gram+, Gram-, Cancer, Fungus	**#10:** DOI: 10.1016/j. nbt.2018.07.001 Active fusion yield: 50 mg/L. Tt 32.3°C in H2O, 29.7°C in PBS **#10a:** DOI: 10.3390/app11125352 Active fusion yield: 90 mg/L Tt not reported, T increase accelerates gelation
#11 **#11a**	BMAP-28(1-18),18aa	GGLRSLGRKILRAWKKYG https://dbaasp.org/peptide-card?id=11938	Synthetic, truncated derivative of myeloid antimicrobial peptide 28 from *Bos taurus* Cationic (+7) Gram+, Gram-, Fungus	**#11:** DOI: 10.1021/acsbiomaterials.0c01262 Active fusion yield:108 mg/L Tt 32.7 in H_2O, 29.0°C in PBS **#11a:** DOI: 10.3390/app11125352 Active fusion yield: 70 mg/L Tt not reported, T increase accelerates gelation
#12	1018 12aa	VRLIVAVRIWRR https://dbaasp.org/peptide-card?id=7111	Synthetic Cationic (+5) Gram+, Gram-, Mammalian Cell	**#12:** DOI: 10.1021/acs. biomac.0c00865 chemical cleavage (CNBr) Active fusion yield: 380 to 600 mg/L Tt (heating) 17.5 ± 0.6 (cooling) 13.0 ± 0.6

(Continues)

TABLE 1 (Continued)

No	AMP domain	AMP sequence and information	AMP source and main features	Construct reference and main features
#13 **#13a**	GL13K 14aa	GKIIKLKASLKLL https://dbaasp.org/peptide-card?id=13151	Synthetic Cationic (+5) Gram+, Gram-, Insect, Mammalian Cell	**#13:** DOI: 10.1021/acs. biomac.0c00865 Chemical cleavage (CNBr) Fusion yield: 380 to 600 mg/L Tt (heating) 19.6 ± 0.5 (cooling) 13.1 ± 0.4 **# 13a:** DOI: 10.1021/ acsbiomaterials.9b00247 Fusion yield: 270 mg/L Tt not reported
#14	ADP-2 (Amblyomma defensin peptide 2), 41aa	YENPYGCPTDEGKCFDRCNDSEFEGGYCGGSYRATCVCYRT https://dbaasp.org/peptide-card?id=5176	From *Amblyomma hebraeum* Anionic (−3), non-cationic defensin-like Gram+, Gram-, Fungus	**#14 to #18:** DOI: 10.1016/j. nbt.2019.12.001 Enzymatic release Active fusion yield: 4 – 113 mg/200 g of plant tissue Tt below 37°C in high-salt solution
#15	DefensinTK 41aa	SPAIWGCDSFLGYCRLACFAHEASVGQKECAEGMLCCIPNVF https://dbaasp.org/peptide-card?id=8441	From *Theloderma kwangsiensis* Anionic (−2) disulfide bonds, defensins Gram+, Gram-, Fungus, Mammalian Cell	
#16	PopuDef, 44aa	GASPALWGCDSFLGYCRIACFAHEASVGQKDCAEGMICCLPNVF https://dbaasp.org/peptide-card?id=8198	From *Polypedates puerensis* Anionic (−2) non-cationic defensin Gram+, Gram-, Mammalian Cell	
#17	Laterosporulin 49aa	ACQCPDAISGWTHTDYQCHGLENKMYRHVYAICMNGTQVYCRTEWGSSC https://dbaasp.org/peptide-card?id=5743	From *Brevibacillus sp* Anionic (−1) non-cationic defensin Gram+, Gram-	
#18	SpliDef 50aa	VSCDFEEANEDAVCQEHCLPKGYTYGICVSHTCSCIYIVELIKWYTNTYT https://pubmed.ncbi.nlm.nih.gov/22067477/	Anionic (−5) non-cationic defensin HQ603825, APD3	
#19	D- enantiomer of GL13K 13aa	gkiiklkaslkll https://dbaasp.org/peptide-card?id=13152	Synthetic Cationic (+5) Gram+, Gram-, Insect, Mammalian Cell	**#19:** DOI: 10.1039/d0bm00155d ELP functionalization by click chemistry high yield ELP fusion Tt not reported

TABLE 1 (Continued)

No	AMP domain	AMP sequence and information	AMP source and main features	Construct reference and main features
#20	RRP9W4N 13aa	RRPRPRPRPWWWW-NH2 https://dbaasp.org/peptide-card?id=9325	Synthetic Cationic (+6), Proline-rich Gram+, Gram-, Mammalian Cell	**#20:** DOI: 10.1016/j. actbio.2018.10.039 ELP functionalization by EDC/NHS coupling Tt below 37°C

Note: Numbers refer to the ELP fusion constructs bearing the AMP. References and the main features of the fusion constructs are also reported. Information about peptides, when available, was obtained from the DBAASP (https://dbaasp.org) which is an open-access AMP data resource supported by I. Beritashvili Center of Experimental Biomedicine (IBCEB) Tbilisi, Georgia, and the National Institute of Allergy and Infectious Diseases (NIAID) Office of Cyber Infrastructure and Computational Biology (OCICB) in Bethesda, MD. These data were collected and submitted by members of the DBAASP team.

It was removed by the ITC (Inverse Transition Cycling) procedure, without the need for further downstream processing (Table 1, #1–#4). Intriguingly, one of these ELP-AMP fusion proteins was described as endowed with antimicrobial activity (Table 1, #5).

Two of the other ELP-AMP reported fusions carried the cationic elastin-like polypeptide (CELP) made of 36 pentapeptidic repeats adjacent to an enterokinase proteolytic site for the AMP release (Figure 2a). In both constructs, the composition of the ELP domain was the same, where the X guest residue was V, F, and K (7:1:1) and, the presence of lysine conferred the cationic feature to the ELP backbone. The yield of the released and ITC-purified AMPs per 100 ml of culture were comparable (Table 1, #6, and #7).

Analyzing the described AMP–ELP constructs (Figure 2b), one of them showed an ELP backbone of 90 pentapeptidic repeats where X was V, A, and G (Table 1, #8, and Figure 2b). It was reported that the ELP length had a dramatic effect on the fusion protein products and, in this case, the longest ELP domain was selected (Hu et al., 2010). The yield of this fusion protein was 69 mg/L of culture and the AMP recovery after the hydroxylamine chemical cleavage and purification was 1.7 mg/L (Table 1, #8).

The other four AMP-ELP fusion constructs were designed and produced with a very long ELP backbone of 1000 aa made of 200 pentapeptidic repeats where X was A (Figure 2b). Two of them carried the formic acid chemical cleavage site to release the N-terminal AMP (Table 1, #2a, and #9). Thus, ELP was used as the purification tag as in the previous examples. However, in this case, after the chemical cleavage and the ITC purification, a chromatographic step was required to improve the recovery of the AMPs (Pereira et al., 2021). This approach showed a yield about 2-times higher for the Moricin CM4, relative to that obtained with the ELP-intein-AMP fusion setup (Table 1, #2 and Figure 2a). The other two AMP-ELP fusion proteins were intended as a kind of AMP "conjugates" to obtain materials endowed with antibacterial activity, such as micro-particles and free-standing films since it was described that the whole AMP-ELP macromolecules possessed antibacterial activity when tested by a modified agar diffusion method. The yield was 50 and 108 mg/L for each fusion protein, respectively (Table 1, #10, and #11).

The last approach for ELP fusion with AMP consisted in placing the AMP between two ELP blocks (Figure 2c). The N-terminal ELP is described as a "sacrificial" 50 repeats pentapeptidic block that is expected to protect the host from the toxic side-effects of the AMP while increasing the expression levels as well as enabling the site-specific CNBr cleavage (Table 1, #12 and #13). In this block, the X guest residues were V and E conferring an acidic nature to this domain. Following this strategy, these authors designed and produced several constructs, bearing this sacrificial block followed by the AMP. Two different C-terminal ELP domains were selected for the fusion, one with an amphiphilic di-block structure and the other with a cationic nature (Figure 2c). These products were expressed at higher yields compared to the other reported fusion constructs, ranging from 380 to 600 mg/L (Table 1, #12, #13, and #13a).

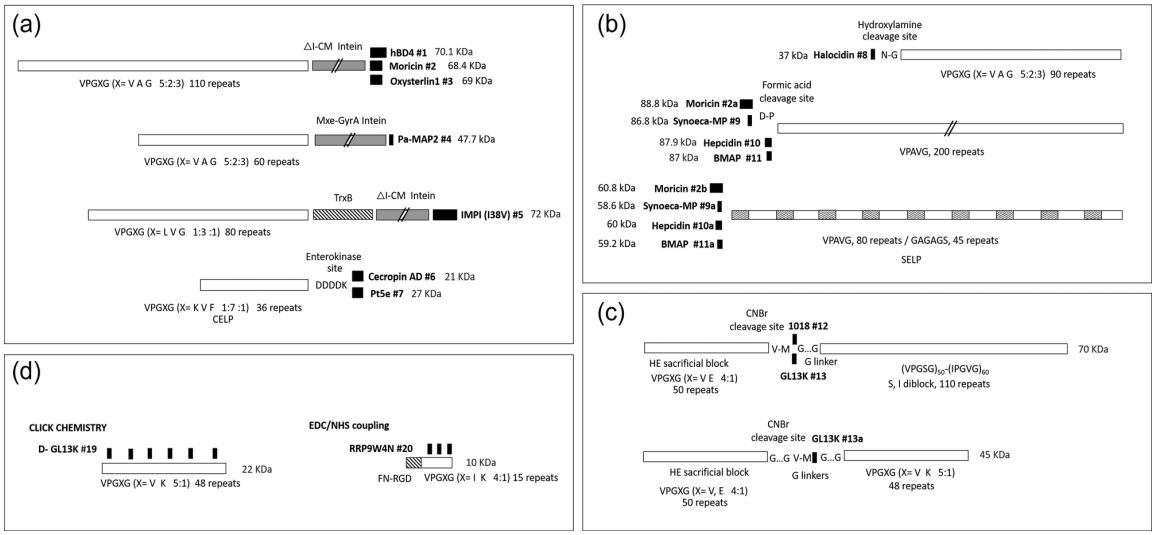

FIGURE 2 Schematic representation of the recombinant elastin-like polypeptide (ELP) fusion constructs and ELP conjugation with antimicrobial peptides (AMPs) that are reported in the literature. (a) C-terminal ELP–AMP fusion proteins, (b) N-terminal AMP–ELP fusion proteins, (c), ELP–AMP–ELP fusion proteins, and (d) ELP conjugated by chemical methods. Black box, antimicrobial domain; white box, elastin-like domain; gray box, intein domain; hatched box other domains. The name of AMP and the respective construct number correspond to those reported in Table 1.

The last strategy consisted of the chemical conjugation between ELP and AMP by click chemistry and by EDC/NHS coupling (Figure 2d). In both cases, a cationic ELP was selected for conjugation and it was employed as a scaffold on which the chemically synthesized AMP was covalently bound to confer antimicrobial properties to the derived material (Table 1, #19, and #20).

The AMP-ELP fusion expressed in plants had the shortest ELP domains corresponding to 28 repeats (Table 1, #14 to #18). Unexpectedly, only the uncleaved AMP-ELP fusions showed antimicrobial activity, whereas after enzymatic cleavage no activity was detected. The authors ascribed the loss of activity of the released AMP to a loss of structural integrity maintained by the ELP fusion partner close to the smaller AMP (Ghidey et al., 2020).

5 | CONCLUSION AND FUTURE PERSPECTIVE

Most of the studies described the use of the ELP as a tag either to purify the whole fusion protein or to selectively isolate the AMP from the ELP itself exploiting the ITC. Different strategies to release the AMP from the fusion protein were described, e.g., the intein-based excision as well as the chemical and the enzymatic cleavage (see Table 1). The employment of the ELP carrier as an alternative and effective route for active AMPs production was proposed in most cases. The other expected applications are related to the employment of the ELP fusion proteins as the basic components for new biomaterials endowed with antimicrobial activity. Table 2 briefly summarizes the possible applications.

Several AMPs with diverse features were selected from different authors for the fusion with the ELP carrier. Their lengths span from one to six dozens of amino acids. Most of them are cationic and they show different secondary and tertiary structures. Almost all the described recombinant fusions of AMPs with ELPs were successfully expressed in T7-based expression systems.

In the described constructs, the bioactive AMP domain was placed at either the N-terminus or C-terminus end of the ELP, as well as in the middle of two ELP blocks. All these fusion proteins were successfully expressed with a variable yield, depending on the recombinant construct and culture conditions. Most of them resulted in the active AMP domain recovery and, intriguingly, some fusion proteins showed antimicrobial activity too, irrespective of the N-terminal or C-terminal placement of the AMP. All the AMP-ELP uncleaved fusion constructs that were expressed in plants demonstrated strong antibacterial activity.

In summary, the structure of the ELPs employed for the fusion with AMPs consisted of repetitions of the pentapeptidic motif VPGXG from bovine elastin ranging from 36 to 200 repeats and resulting in fusion constructs of the total mass varying from about 20–90 KDa. From the point of view of the amino acid composition, only a few types of ELP carriers were employed. The guest X amino acid was mainly V, G, and A, sometimes L and F were introduced, and K and E were used to confer basic or acidic nature to the ELP block, as well as to allow for chemical conjugation. Other described variations in the pentapeptidic motif were VPAVG, VPGSG, and IPGVG. A hybrid ELP containing blocks of silk-derived repeats (SELP) was also described as the carrier for AMPs.

ELPs were reported to be effective to avoid the adverse effect of the fused AMPs on the expression host as well as to improve the

TABLE 2 Potential applications of the ELP-based fusion constructs carrying the AMPs

No	Applications
#1	Production of hBD4
#2	Production of moricin
#2a	Production of cast film for skin application
#2b	Production of free-standing films
#3	Model for large-scale production of antimicrobial peptides
#4	Production of Pa-MAP 2
#5	Scale-up production active IMPI containing multiple disulfide bonds using minimal medium
#6	Production of Cecropin AD
#7	Production of antibiotic for MRSA-resistant bacteria
#8	Production/purification of Halocidin
#9	Up-scalable biotechnological platform for AMP production
#9a	Production of free-standing films
#10	Production of AMP, use in microbial infections, advanced drug-delivery systems
#10a	Production of free-standing films
#11	Production of cast film for skin application, candidates for new drug-free polymers endowed with antimicrobial properties.
#11a	Production of free-standing films
#12	Molecular tools in the development of self-assembling nanosystems with potential use for biotechnological and biomedical applications
#13	
#13a	Self-assembled monolayers for realization of advanced, medical devices to prevent infection
#14	AMP fusions expression in plants in high yield, easy purification of fusion peptides with high antimicrobial activity without the need for a peptide cleavage step
#15	
#16	
#17	
#18	
#19	Multifunctional coatings for implants to be employed in regenerative medical applications
#20	Antimicrobial coatings for implants and medical devices

Note: The number of the constructs corresponds to those indicated in Table 1 and Figure 2.

Abbreviations: AMPs, antimicrobial peptides; ELP, elastin-like polypeptide.

expression yield. However, the length of the ELP domain was recognized as a key parameter affecting the yield of the fusion proteins. The presence of the ELP domain was described to facilitate protein solubility, avoiding inclusion body formation.

Overall, ELPs have been shown to be a versatile platform to express different kinds of AMPs and recover their functionality. However, the reported examples showed little variability regarding both the ELP sequences that were employed and the expression systems that were used for their production. The interesting finding that some AMP domains conferred antimicrobial activity to the whole fusion construct points to ELP as a versatile scaffold to support the AMP itself, opening the way to the realization of new materials endowed with antimicrobial properties.

From this point of view, the potential of ELPs as modular carriers for AMPs appears still underdeveloped so there is room for the design of unexplored combinations to improve the production and the performance of new constructs and their derived materials. New approaches offer intriguing opportunities, such as machine-learning algorithms, to optimize the antimicrobial sequences by improving the activity and avoiding microbial resistance. New technologies such as 3D printing are also attractive to make a qualitative leap in manufacturing. The adoption of such modern techniques spanning from in silico to experimental production holds the key to the wide application of this kind of versatile recombinant fusions in the field of active materials and coatings for medical devices and beyond.

ACKNOWLEDGMENTS

The authors are grateful to Prof. Giorgio Manzini that critically reviewed the manuscript. This study was supported by the Horizon 2020 Innovative Training Network AIMed under Marie Skłodowska-Curie, grant agreement No 861138.

CONFLICT OF INTEREST

The authors declare no conflict of interest.

DATA AVAILABILITY STATEMENT

Data sharing is not applicable to this article as no new data were created or analyzed in this study.

ORCID

Antonella Bandiera http://orcid.org/0000-0002-0376-9291

REFERENCES

Bellotto, O., Semeraro, S., Bandiera, A., Tramer, F., Pavan, N., & Marchesan, S. (2022). Polymer conjugates of antimicrobial peptides (AMPs) with d-amino acids (d-aa): State of the art and future opportunities. *Pharmaceutics*, *14*(2), 446. https://doi.org/10.3390/pharmaceutics14020446

Cui, Z., Luo, Q., Bannon, M. S., Gray, V. P., Bloom, T. G., Clore, M. F., Hughes, M. A., Crawford, M. A., & Letteri, R. A. (2021). Molecular engineering of antimicrobial peptide (AMP)-polymer conjugates. *Biomaterials Science*, *9*(15), 5069–91. https://doi.org/10.1039/d1bm00423a

Ghidey, M., Islam, S. M. A., Pruett, G., & Kearney, C. M. (2020). Making plants into cost-effective bioreactors for highly active antimicrobial peptides. *New Biotechnology*, *56*, 63–70. https://doi.org/10.1016/j.nbt.2019.12.001

Hu, F., Ke, T., Li, X., Mao, P. H., Jin, X., Hui, F. L., Ma, X. D., & Ma, L. X. (2010). Expression and purification of an antimicrobial peptide by fusion with elastin-like polypeptides in *Escherichia coli*. *Applied Biochemistry and Biotechnology*, *160*(8), 2377–87. https://doi.org/10.1007/s12010-009-8850-2

Kaur-Boparai, J. (2020). Mini review on antimicrobial peptides, sources, mechanism and recent applications. *Protein & Peptide Letters*, *27*(1), 4–16. https://doi.org/10.2174/0929866526666190822165812

Li, Y. (2009). Carrier proteins for fusion expression of antimicrobial peptides in *Escherichia coli*. *Biotechnology and Applied Biochemistry*, *54*(1), 1–9. https://doi.org/10.1042/BA20090087

Li, Y. (2011). Recombinant production of antimicrobial peptides in *Escherichia coli*: A review. *Protein Expression and Purification*, *80*(2), 260–267. https://doi.org/10.1016/j.pep.2011.08.001

Luan, C. H., Parker, T. M., Gowda, D. C., & Urry, D. W. (1992). Hydrophobicity of amino acid residues: Differential scanning calorimetry and synthesis of the aromatic analogues of the polypentapeptide of elastin. *Biopolymers*, *32*(9), 1251–61. https://doi.org/10.1002/bip.360320914

Magana, M., Pushpanathan, M., Santos, A. L., Leanse, L., Fernandez, M., Ioannidis, A., Giulianotti, M. A., Apidianakis, Y., Bradfute, S., Ferguson, A. L., Cherkasov, A., Seleem, M. N., Pinilla, C., de la Fuente-Nunez, C., Lazaridis, T., Dai, T., Houghten, R. A., Hancock, R. E. W., & Tegos, G. P. (2020). The value of antimicrobial peptides in the age of resistance. *The Lancet Infectious Diseases*, *20*(9), e216–30. https://doi.org/10.1016/s1473-3099(20)30327-3

McDaniel, J. R., Radford, D. C., & Chilkoti, A. (2013). A unified model for de novo design of elastin-like polypeptides with tunable inverse transition temperatures. *Biomacromolecules*, *14*(8), 2866–72. https://doi.org/10.1021/bm4007166

Pereira, A. M., Costa, A., Dias, S. C., Casal, M., & Machado, R. (2021). Production and purification of two bioactive antimicrobial peptides using a two-step approach involving an elastin-Like fusion tag. *Pharmaceuticals*, *14*(10), 956. https://doi.org/10.3390/ph14100956

Rai, A., Ferrão, R., Palma, P., Patricio, T., Parreira, P., Anes, E., Tonda-Turo, C., Martins, M. C. L., Alves, N., & Ferreira, L. (2022). Antimicrobial peptide-based materials: Opportunities and challenges. *Journal of Materials Chemistry B*, *10*(14), 2384–2429. https://doi.org/10.1039/d1tb02617h

Ramazi, S., Mohammadi, N., Allahverdi, A., Khalili, E., & Abdolmaleki, P. (2022). A review on antimicrobial peptides databases and the computational tools. *Database*, *2022*, 0. https://doi.org/10.1093/database/baac011

Shah, N. H., & Muir, T. W. (2014). Inteins: nature's gift to protein chemists. *Chemical Science*, *5*(1), 446–461. https://doi.org/10.1039/c3sc52951g

Silva, A. R. P., Guimarães, M. S., Rabelo, J., Belén, L. H., Perecin, C. J., Farías, J. G., Santos, J. H. P. M., & Rangel-Yagui, C. O. (2022). Recent advances in the design of antimicrobial peptide conjugates. *Journal of Materials Chemistry B*, *10*(19), 3587–3600. https://doi.org/10.1039/d1tb02757c

Urry, D. W. (1988). Entropic elastic processes in protein mechanisms. I. Elastic structure due to an inverse temperature transition and elasticity due to internal chain dynamics. *Journal of Protein Chemistry*, *7*(1), 1–34.

Varanko, A. K., Su, J. C., & Chilkoti, A. (2020). Elastin-Like polypeptides for biomedical applications. *Annual Review of Biomedical Engineering*, *22*, 343–69. https://doi.org/10.1146/annurev-bioeng-092419-061127

Wibowo, D., & Zhao, C. X. (2019). Recent achievements and perspectives for large-scale recombinant production of antimicrobial peptides. *Applied Microbiology and Biotechnology*, *103*(2), 659–71. https://doi.org/10.1007/s00253-018-9524-1

Yeboah, A., Cohen, R. I., Rabolli, C., Yarmush, M. L., & Berthiaume, F. (2016). Elastin-like polypeptides: A strategic fusion partner for biologics. *Biotechnology and Bioengineering*, *113*(8), 1617–27. https://doi.org/10.1002/bit.25998

How to cite this article: Colomina-Alfaro, L., Marchesan, S., Stamboulis, A., & Bandiera, A. (2023). Smart tools for antimicrobial peptides expression and application: The elastic perspective. *Biotechnology and Bioengineering*, 120, 323–332. https://doi.org/10.1002/bit.28283

Chapter 4. A Versatile Elastin-Like Carrier for Bioactive Antimicrobial Peptide Production and Delivery

This chapter introduces a research article published in the Journal of Macromolecular Bioscience (Wiley).

Colomina-Alfaro, L., Sist, P., Marchesan, S., Urbani, R., Stamboulis, A., & Bandiera, A. (2024). **A Versatile Elastin-Like Carrier for Bioactive Antimicrobial Peptide Production and Delivery.** *Macromolecular bioscience*, *24*(3), e2300236. https://doi.org/10.1002/mabi.202300236.

The second objective of the present thesis was to develop a model to employ the HELP carrier to produce AMP fusions. For this purpose, indolicidin, a fluorescent and well-characterized AMP, was chosen as an example of an antimicrobial functional domain to be produced as a C-terminal fusion of the HELP carrier. In the coding sequence design, a linker was added between indolicin and HELP coding sequences, and just before the indolicidin coding sequence, a triplet coding for a unique glutamic acid was introduced. This was expected to allow the specific release of the AMP domain from the fusion protein since glutamic acid is the target site of Glu-C, a highly specific endoprotease. The treatment of the fusion protein with this protease will trigger the release of the AMP domain for further characterisation. Following established procedures, indolicidin was cloned in the *E. coli* HELP expression vector, and the fusion protein, named HIn (HELP-indolicidin), was produced as a soluble protein in the bacterial cytoplasm and purified, exploiting the thermo-responsive properties that characterise the HELP moiety. Then, the physico-chemical and antimicrobial properties of the biopolymer in solution, as well as the antimicrobial behaviour of the 2D and 3D derived materials, were assessed. In addition, the proteolytic release of bioactive AMP from the 3D materials was evaluated either by incubating with a specific endoprotease or in the presence of elastase, an enzyme that can be secreted by bacteria or that is produced during the inflammation process in response to infections and other stimuli.

My contribution to this journal article is as follows: investigation, conceptualisation, methodology, formal data analysis and validation, graphical representation, and original & revised draft writing. The following experiments were carried out by myself:

- Antimicrobial HELP cloning, expression, and purification
- Assessment of antimicrobial activity of the HIn biopolymer and of the derived materials
- Antimicrobial activity of HIn coatings
- Antimicrobial capacity assessment of the HIn matrix
- Specific release of the In antimicrobial domain by Glu-C endoprotease from the HIn biopolymer
- Specific release of the In domain by Glu-C endoprotease from the HIn matrix
- Release of the In domain from the HIn biopolymer by elastolytic activity
- Release of the In domain from the HIn matrix by elastolytic activity

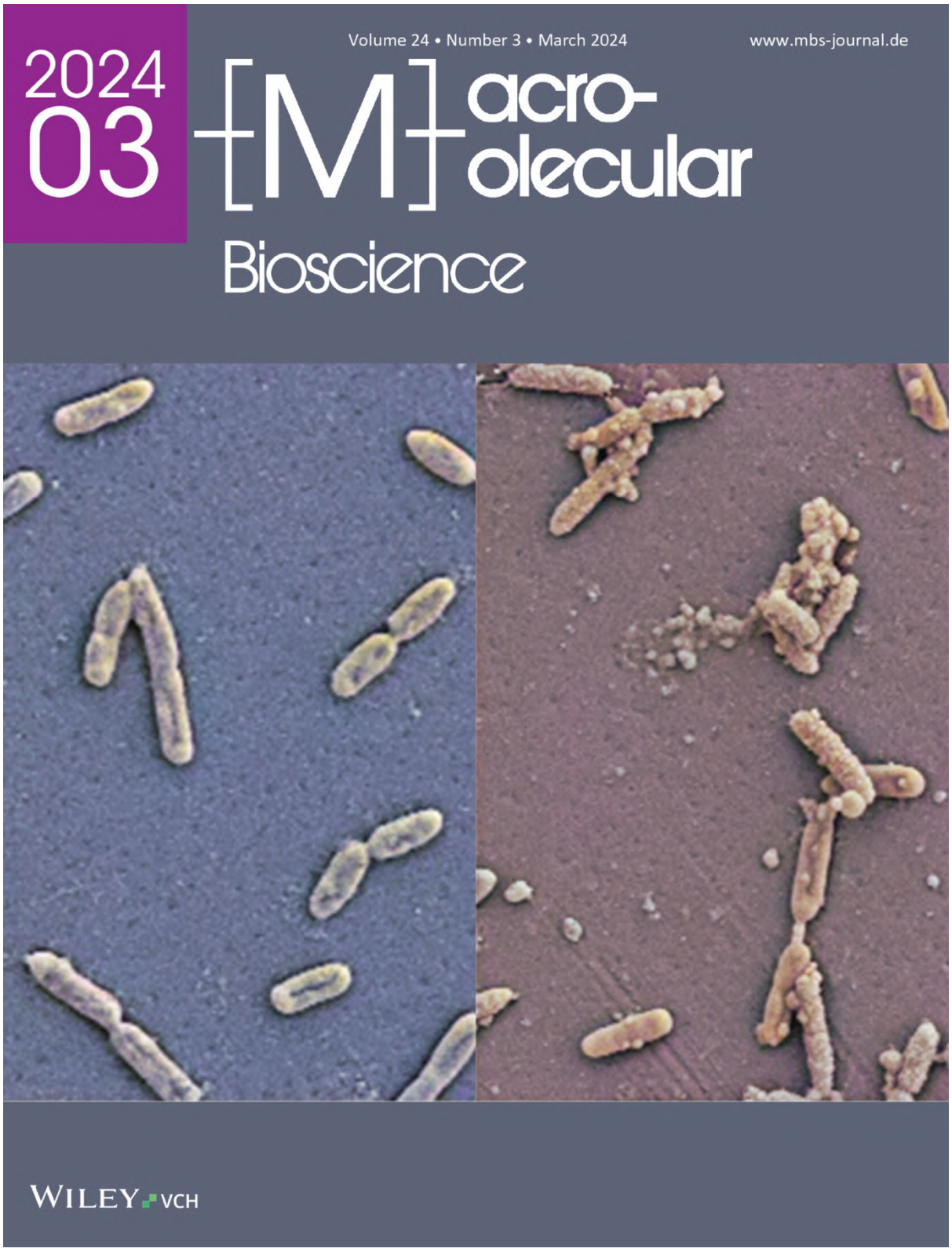
2024
03
Volume 24 • Number 3 • March 2024
www.mbs-journal.de
Macromolecular
Bioscience
WILEY VCH

RESEARCH ARTICLE

Macromolecular Bioscience
www.mbs-journal.de

A Versatile Elastin-Like Carrier for Bioactive Antimicrobial Peptide Production and Delivery

*Laura Colomina – Alfaro, Paola Sist, Silvia Marchesan, Ranieri Urbani, Artemis Stamboulis, and Antonella Bandiera**

Elastin-like polypeptides are biotechnological protein and peptide carriers that offer a vast scope of applicability. This work aims to build a model for the expression of antimicrobial peptides (AMPs) by genetically engineering the Human Elastin-like Polypeptide platform developed in the lab. The well-characterized AMP indolicidin is selected as an example of an antimicrobial domain for the recombinant fusion at the C-terminus of the carrier. The fusion construct has been designed to allow the release of the antimicrobial domain. The expression product has been purified and its physicochemical and antimicrobial properties has been characterized. Taking advantage of the self-assembling and matrix-forming properties of the recombinant biopolymer, the materials that are obtained have been evaluated for antimicrobial activity toward bacterial-strain models. This approach represents a cost-effective strategy for the production of smart components and materials endowed with antimicrobial capacity triggered by external stimuli.

1. Introduction

The issue of antimicrobial resistance is considered a major threat to human health and new strategies as well as multidisciplinary approaches are necessary to face this global emergency.[1,2] The host defense peptides, which are part of the innate immune response and are widespread throughout all living organisms, constitute the first barrier against attack by pathogens. These naturally occurring peptides, also known as antimicrobial peptides (AMPs), were selected by evolution and have recently raised great interest as a promising alternative to synthetic antibiotics.[3]

They have broad-spectrum activity against multiple types of microorganisms, yet there are several limitations to their employment as drug candidates, mainly related to their stability, solubility, cytotoxicity, and bioavailability.[4] One strategy to improve the delivery of these biodrugs is the conjugation with polymers that may extend their half-life, protect them from degradation, and increase their solubility.[5–7] The recombinant fusion approach offers several advantages, being a cost-effective means for large-scale peptide manufacturing. Among the described fusion partners, the elastin-like polypeptides (ELPs) carriers are still underexplored and offer a wide scope in terms of applicability.

ELPs are protein-based biopolymers inspired from mammalian tropoelastin. They can be chemically synthesized, however, the expression of recombinant products coded by easily customizable synthetic genes is preferred to overcome chain length limitations. They are generally comprised of repetitive VPGXG motifs, X being any amino acid except proline, which characterizes the bovine homolog.[8] They display a reversible thermoresponsive behavior, similar to tropoelastin, that renders them promising candidates for the development of advanced materials for controlled drug delivery, tissue engineering, and regenerative medicine.[9]

Up to now, roughly twenty ELP fusion constructs with AMPs have been described, and recently reviewed.[10] These ELP carriers are substantially based on the artificial repetitions of the canonical pentapeptidic motif. In our lab, synthetic genes coding for ELPs inspired by the sequences of the human homolog and thus named HELPs (Human Elastin-like Polypeptides) were assembled and expressed in *Escherichia coli*.[11] Compared to the other described ELPs, our HELP biopolymer contains not only the hydrophobic elastin-like sequences, but also the elastin-derived cross-linking domains, mimicking the human tropoelastin structure.[12] This feature enabled the setup of an enzymatic method to cross-link the biopolymer chains to yield a stable

L. Colomina – Alfaro, P. Sist, A. Bandiera
Department of Life Sciences
University of Trieste
via L. Giorgieri, 1, Trieste 34127, Italy
E-mail: abandiera@units.it
S. Marchesan, R. Urbani
Department of Chemical and Pharmaceutical Sciences
University of Trieste
via L. Giorgieri, 1, Trieste 34127, Italy
A. Stamboulis
School of Metallurgy and Materials
Biomaterials Research Group
University of Birmingham
Edgbaston, Birmingham B15 2TT, UK

The ORCID identification number(s) for the author(s) of this article can be found under https://doi.org/10.1002/mabi.202300236

DOI: 10.1002/mabi.202300236

ADVANCED SCIENCE NEWS
www.advancedsciencenews.com

Macromolecular Bioscience
www.mbs-journal.de

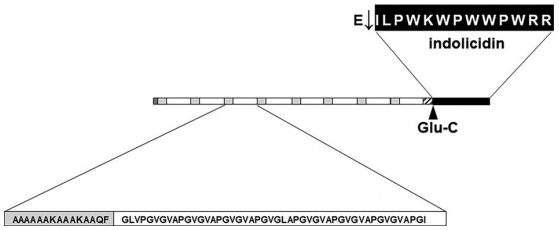

Figure 1. Schematic representation of the HIn construct structure. The theoretical molecular mass is 49 kDa. Dark grey, His-tag; hatched, linker; black, In domain; light grey, cross-linking domains; white, elastin-like hexapeptidic repeats.

hydrogel matrix.[13] Thus, our HELP carrier is a multifunctional fusion partner that strategically displays thermo-responsive behavior with dual function. First, it simplifies the purification of the expression product, and second it endows the resulting matrix with responsivity to release the bioactive motif upon proteolytic stimuli.

The aim of the work described in this paper is to apply our technology to produce AMPs therefore establishing a model for bioactive AMP production. Indolicidin (In) is a thirteen amino acids long cationic peptide belonging to the cathelicidin family, first isolated from bovine neutrophils.[14] Showing a broad spectrum of biological activity against a wide range of targets, it was often chosen as a model.[15] We selected this AMP as the antimicrobial domain and the fusion partner of HELP. The synthetic gene was specifically tailored, introducing some functional elements like the proteolytic cleavage site and the linker, thus giving an example of the broad range of customization options that our platform offers.

We report the new construct expression, purification, and characterization of its biochemical properties as well as the realization of the derived matrix and the evaluation of the antimicrobial activity toward *Staphylococcus aureus, Pseudomonas aeruginosa* and *Escherichia coli* strains.

2. Results and Discussion

2.1. Antimicrobial Help Fusion Construct Production and Characterization

Indolicidin (In) is a well-described and characterized 13-residue cationic AMP that is often selected as a model peptide, since it has a broad spectrum of biological activity, and is effective against a wide range of bacteria.[15,16] Moreover, its high tryptophan content confers it with fluorescence, facilitating its localization. We selected this AMP as the bioactive fusion domain with HELP for these reasons. In **Figure 1**, the schematic structure of this new construct named HIn is shown, and a short linker region was placed between HELP and the In domain. We decided to insert a glutamic acid residue just before the In sequence to obtain a unique specific proteolytic cleavage site to release the AMP, since neither In nor HELP possess this amino acid in their sequence. However, different specific proteolytic sites, like those for the TEV protease and factor Xa, rather than amino acids for specific chemical cleavage as well as linkers, spacers, and other functional

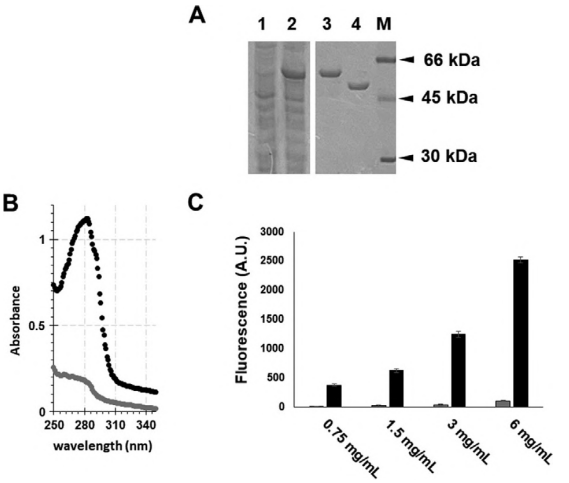

Figure 2. Production and characterization of the HIn construct. A) Representative SDS-PAGE analysis of the HIn construct. Lane 1, total protein content of the bacterial lysate before IPTG induction; lane 2, total protein content of the bacterial lysate 5 h after IPTG induction; lane 3, HIn construct purified by inverse phase transition cycling; lane 4, purified HELP biopolymer. Molecular masses of the protein markers (M) expressed in kilodaltons (kDa), are bovine serum albumin (66 kDa), ovalbumin (45 kDa), carbonic anhydrase (30 kDa). Coomassie blue staining. B) Absorbance spectra of HELP (grey) and HIn (black) biopolymers. C) Spectrofluorimetric analysis of aqueous solutions of different concentrations of HELP (grey bars) and HIn (black bars). The values represented the mean ± SD, $n = 4$.

sequences may be introduced depending on the requirements of the desired application.

HIn was expressed on a lab scale with a high efficiency of the purified product obtained by exploiting the reversible thermo-responsive behavior that characterizes HELP and that was maintained by this construct (**Figure 2**A and Supporting Information). Due to the presence of tryptophan in the antimicrobial domain, the absorbance spectrum of HIn showed a peak centered at 280 nm, that is considerably reduced in HELP (Figure 2B). This was confirmed by the fluorescence analysis, where HIn showed clear dose-dependent signals relative to HELP, which did not show such behavior, as expected (Figure 2C).

Table 1 reports the features of the secondary structure of HELP and HIn biopolymers obtained with the Expasy tools.[17] The physicochemical parameters for the biopolymers were calculated from their primary structure. Only a slight difference in the hydropathy index (Table 1) between the two biopolymers was predicted. In the same table, the results of the deconvolution of the CD spectra of **Figure 3**A for HIn and HELP are shown, and they are consistent with the theoretical predictions. The CD spectra of HELP and HIn did not show any significant change when 0.15 M NaCl was added to both biopolymer solutions (Figure S1, Supporting Information). However, despite these similarities between HIn and HELP, HIn showed a significant difference in the thermal transition properties with respect to HELP. Turbidity measurements were performed to investigate the thermo-responsive behavior of the biopolymers undergoing

ADVANCED SCIENCE NEWS
www.advancedsciencenews.com

Macromolecular Bioscience
www.mbs-journal.de

Table 1. Chemico-physical parameters were obtained using Expasy Tools (ProtParam on-line software) and the prediction of secondary structure using GOR IV was compared to the values obtained from CD measurements.

	p.I.	Hydropathy Index (GRAVY)	% Polar a.a.	% Charged a.a.		A (%)	β (%)	Random coil (%)
HIn	12.2	0.97	2.5	4.4	GOR IV	27	5	68
					CD	30	6	74
HELP	11.7	1.10	1.9	3.2	GOR IV	26	4	70
					CD	29	10	61

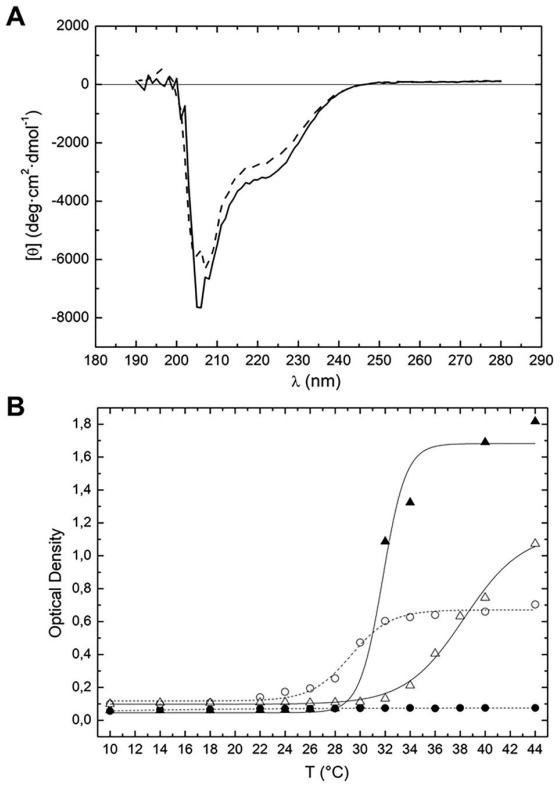

Figure 3. Physicochemical characterization of the HIn biopolymer. A) CD spectra recorded at 25 °C for HIn (black line) and compared with that of the HELP biopolymer (dashed line) in NaPi buffer solution at 0.1 mg mL^{-1}. B. Optical density profiles of 2 mg mL^{-1} solutions of HIn in NaPi buffer (black circle) and NaPi/0.15 M NaCl buffer (black triangle) solution as a function of temperature. HELP behavior in NaPi buffer (open circle) and in NaPi/0.15 M NaCl buffer (open triangle) is also reported for comparison.

the inverse temperature transition in the absence and in the presence of near-physiological salt concentration. It has to be taken into account that HELP, different from most of the other ELPs, possesses also cross-linking domains, mimicking the tropoelastin structure. It is described that the optimal tropoelastin coacervation occurs in the presence of the near-physiological salt concentration.[18] We already reported that the presence of the cross-linking domains in the HELP biopolymer affected its phase transition behavior and that the presence of a nearly physiological salt concentration fully restored the transition capacity.[19]

Figure 3B shows the turbidity profiles of 2 mg mL^{-1} HIn in buffer solution with and without 0.15 M NaCl as a function of temperature. HIn showed no thermal transition up to 45 °C in the absence of salt, while in the presence of 0.15 M NaCl, a sharp increase in turbidity ≈31.8 °C was observed. In the presence of NaCl, HIn showed a sharper transition curve that occurred 10 °C earlier with respect to HELP (Figure 3B).

DSC peaks and onset temperatures of the inverse transitions are listed in **Table 2** (see also Supporting Information) and were in agreement with those observed in the turbidity analysis. As already reported, the transitions of HELP and its modifications are always characterized by a broad peak extending over 10 °C or more[19,20] In the analysis presented here, especially in the presence of NaCl, the two biopolymers showed significant differences, confirming those observed in the turbidity experiments. Again, HIn in the absence of salt did not show any transition, even when heated at 90 °C (Table 2), confirming the results reported above by turbidimetric analyses. The possible explanation is based on the observation that the In domain contains several highly hydrophobic tryptophans and charged lysine and arginine. Being these amino acids endowed with diametrically opposed properties, the HIn hydropathy index resulted diminished respect to HELP (Table 1). In general, the T_t of the ELPs is lowered when the hydrophobicity of the chain is raised, for example, by substitution of the fourth, "guest" residue of their pentapeptidic motif.[21] On the other hand, an analogous but distinct effect was also observed, consisting of the decrease of the ELP T_t by the fusion with hydrophobic moieties.[22] Consistent with these observations, the increased sharpness of the HIn transition profile as well as the decreased transition temperature suggested that HIn responded more promptly than HELP to temperature rise, likely due to the hydrophobicity increase of the macromolecule. However, due to the presence of the cross-linking regions in HELP domain, this behavior is evidenced only when the charges are shielded avoiding repulsion, such as in the presence of salt.

In summary, the HIn construct carrying the antimicrobial domain placed at the C-terminus of HELP was successfully produced by recombinant methods. This construct was fluorescent, due to the presence of the tryptophan-rich In domain. This convenient feature allowed the tracking of the domain after its release from the HIn biopolymer. The phase transition behavior conferred by the HELP domain was maintained and even enhanced in the fusion construct, as demonstrated by the physicochemical characterization. Consequently, the purification of the construct by exploiting this property resulted in an average yield on the lab scale of more than 200 mg per liter of bacterial culture.

ADVANCED SCIENCE NEWS
www.advancedsciencenews.com

Macromolecular Bioscience
www.mbs-journal.de

Table 2. DSC onset and peak inverse transition temperatures for the 8 mg mL^{-1} solutions of HIn and HELP biopolymers in the absence and in the presence of 0.15 M NaCl.

	T [°C]	NaPi buffer	NaPi buffer / 0.15 M NaCl
HIn	onset	–	19.4
	peak	–	29.8
HELP	onset	16.2	31.4
	peak	29.5	35.6

2.2. Antimicrobial Activity of HIn

Around 10 ELP fusion constructs carrying the AMP at the N-terminus have been described to possess antimicrobial activity without the need to leave the antimicrobial domain ([10] and references herein). By contrast, only one ELP fusion carrying the AMP at the C-terminal was described to be active.[23] In our system, the In domain is placed at the C-terminal part of the fusion protein exploiting the features of the HELP vector (see Supporting Information). Thus, we assayed the whole construct for the activity against bacterial models that are commonly used as reference strains for antibiotic susceptibility testing.

The activity of the purified HIn biopolymer, as well as that of the HELP alone, was assayed toward *S. aureus*, *P. aeruginosa*, and *E. coli*. The results are presented in **Figure 4**A. At the concentration of 20 µM, HELP did not affect the growth of the tested microorganisms. On the contrary, efficient antimicrobial activity of the HIn biopolymer was observed at this concentration against *P. aeruginosa* (Figure 4A). One possible explanation is that *P. aeruginosa*, under certain growth conditions, can secrete elastolytic enzymes,[24] that may trigger In release in the medium, thus hindering the microorganism growth. This observation prompted us to select this microorganism as the model for this study, and we performed the mInimum inhibitory concentration (MIC) assay with the HIn biopolymer (Figure 4B). No significant effect was observed for any concentration of HELP relative to the untreated control, whereas HIn displayed the inhibitory effect on this strain at the concentration of 1.25 µM.

After the finding that HIn biopolymer maintained the activity conferred by the fusion AMP, we explored the opportunity to prepare antimicrobial surfaces. To coat the surface, aqueous solutions of HIn and HELP were deposited and dried on the bottom of 24-well plates. *P. aeruginosa* cells re-suspended in NaPi buffer (detailed in the Materials and Methods section) were deposited on each coating or on the untreated control surface. HELP-coated surfaces did not affect bacterial growth compared to the uncoated surfaces, whereas HIn-coated surfaces showed a bacterial growth reduction of ≈30%, suggesting a bactericidal activity due to the presence of the In domain (**Figure 5**A). SEM analysis was performed on these samples to observe any effect of the contact between the bacteria and the coated surface (Figure 5B). The bacteria deposited and incubated on HELP coating showed the morphology expected for healthy growing cells (Figure 5B left panel) whereas most of the bacteria deposited on the HIn-based coating showed extended membrane blebbing, indicating that cells underwent disruption (Figure 5B right panel). These results clearly showed that In, although in fusion with HELP, was able to display its effect at least toward *P. aeruginosa*, opening the possibility to employ HIn to realize materials and surfaces endowed with antimicrobial activity.

2.3. Specific Release of the In Domain from the HIn Biopolymer

Our model for AMP production in fusion with an ELP carrier was designed to allow the specific release of the bioactive domain using a specific endoprotease, the Glu-C enzyme that cleaves the proteins after the glutamic acid (Figure 1). Since HELP does not contain any glutamic or aspartic acid, no cleavage of the HELP domain is expected after the treatment with this enzyme, and this was confirmed by the SDS-PAGE analysis (not shown). When the reaction was performed in solution, the release of In could not be followed by fluorescence since HIn shares the same fluorescence

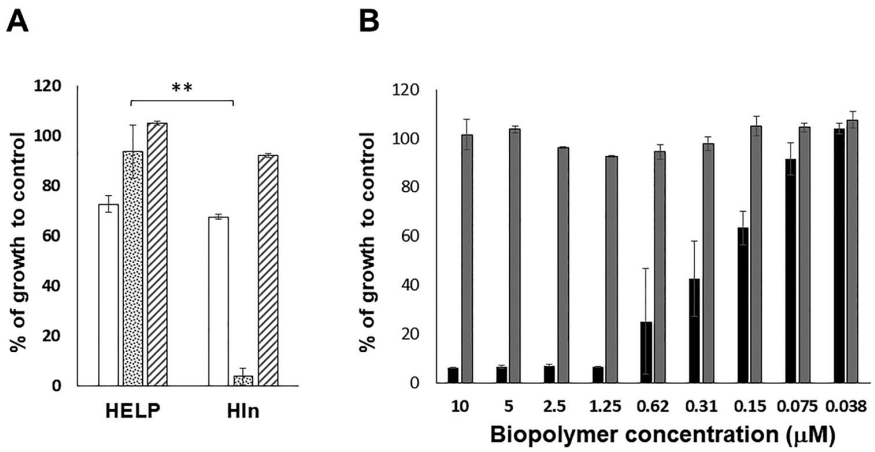

Figure 4. Antimicrobial activity of the HIn biopolymer. A) Comparison of the effect on bacterial growth of 20 µM of HELP and HIn biopolymers toward three bacterial strains. White, *S. aureus*; dotted, *P. aeruginosa* and hatched, *E. coli*. B) Antimicrobial activity evaluation of the HIn (black) fusion protein compared to the HELP (grey) biopolymer toward *P. aeruginosa*. The values were expressed as the percent respect the growth of the untreated control and represented the mean ± SD, $n = 4$; $^{**}p \leq 0.001$.

ADVANCED SCIENCE NEWS
www.advancedsciencenews.com

Macro-olecular Bioscience
www.mbs-journal.de

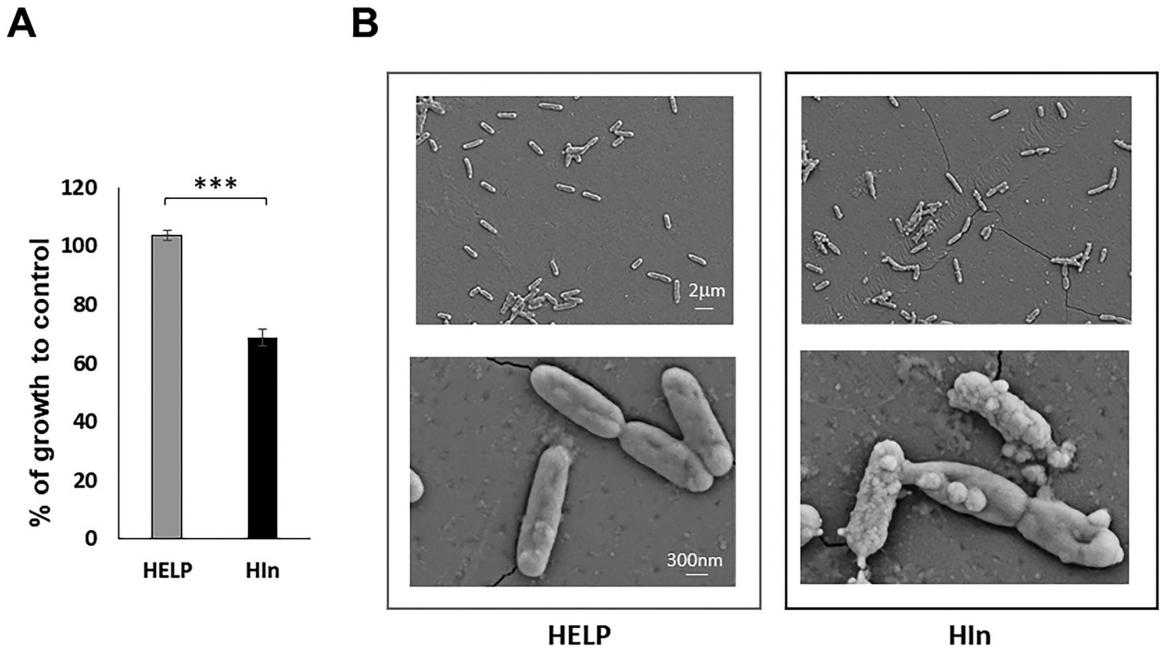

Figure 5. Antimicrobial capacity of HIn-based coatings. A) Effect of HELP and HIn coatings *on P. aeruginosa* growth. Results were expressed as the percent respect the growth of the control on the uncoated surface and represented the mean ± standard deviation (SD) of at least three replicates. ***$p \leq 0.0001$. B) Representative images of the SEM analysis of *P. aeruginosa* deposited on the HELP and HIn-based coatings.

property of In. For this reason, SDS-PAGE analysis was performed to assess the release of In. After Glu-C reaction, an electrophoretic band migrating faster than the front was clearly visible, suggesting the release of the In domain (**Figure 6**A, lane 2).

At first, the thermo-responsive behavior of HELP was employed for the Inverse Transition Cycling (ITC) purification of the released In domain (Figure 6B). However, after the addition of NaCl and warming to 37 °C to elicit the phase transition of HELP, and with subsequent centrifugation, no electrophoretic signal was detected in the supernatant (Figure 6A, lane 3) whereas both HELP and In were found in the pellet (Figure 6A, lane 4). This indicated that, in these conditions, the highly hydrophobic, tryptophan-rich, poorly soluble In domain remained in the pellet, likely due to hydrophobic interaction with the HELP moiety. In fact, when the phase transition was induced in the presence of detergent, after the centrifugation, the band corresponding to the In domain was clearly visible in the supernatant (Figure 6A, lane 5) and it was totally absent in the pellet constituted by HELP alone (Figure 6A, lane 6). Quantification of In in the supernatant with the BCA assay resulted in an average of 35 µg of In per mg of HIn, very close to the theoretical yield value, keeping into account that In represents ≈1/27 of the whole macromolecule. However, due to the presence of the detergent, it was not possible to assess the antimicrobial activity.

2.4. HIn Hydrogel Matrix Production and Bioactivity

The matrix-forming property of HELP has already been described. The method is based on the covalent binding of the biopolymer chains.[13] Since the HELP cross-linking domains are the main target of the transglutaminase enzyme that forms the matrix network, it is likely that any domain in fusion with HELP will not significantly affect the reaction, since most probably it is not the preferred substrate of the enzyme, even if it contains a few lysines and glutamines. Thus, the enzymatic cross-linking of a solution of 4% of HIn was performed, showing the same macroscopic aspect of the 4% HELP matrices that were prepared in parallel as the control (**Figure 7**A, see Materials and Methods for details).

The use of the specific endoprotease Glu-C was expected to trigger the release of the In domain from the HIn matrix. Following the cross-linking and extensive washing, and after assessing the absence of any unreacted substrate by fluorescence, the HIn matrix was treated with Glu-C. After the proteolytic reaction, all the matrices were macroscopically intact, indicating that the cleavage was specific, as expected (Figure 7A). The supernatant was collected and analyzed by fluorescence, SDS-PAGE, and mass spectrometry. Comparing the wash of the matrix before Glu-C addition with the supernatant after the proteolytic reaction, a fluorescence signal was detected in the latter, suggesting the presence of the In domain in the solution (not shown). The ESI-MS confirmed the presence of one predominant component of 1907.02 Da in the supernatant, corresponding to the expected value of 1907.30 Da calculated based on the amino acid sequence of In (Figure S3, Supporting Information). The supernatant was then tested for antimicrobial activity against *P. aeruginosa*, and a MIC value of 3 µM was determined, corresponding to the same order of magnitude of the data reported in the literature for In.[25]

ADVANCED SCIENCE NEWS
www.advancedsciencenews.com

Macro-olecular Bioscience
www.mbs-journal.de

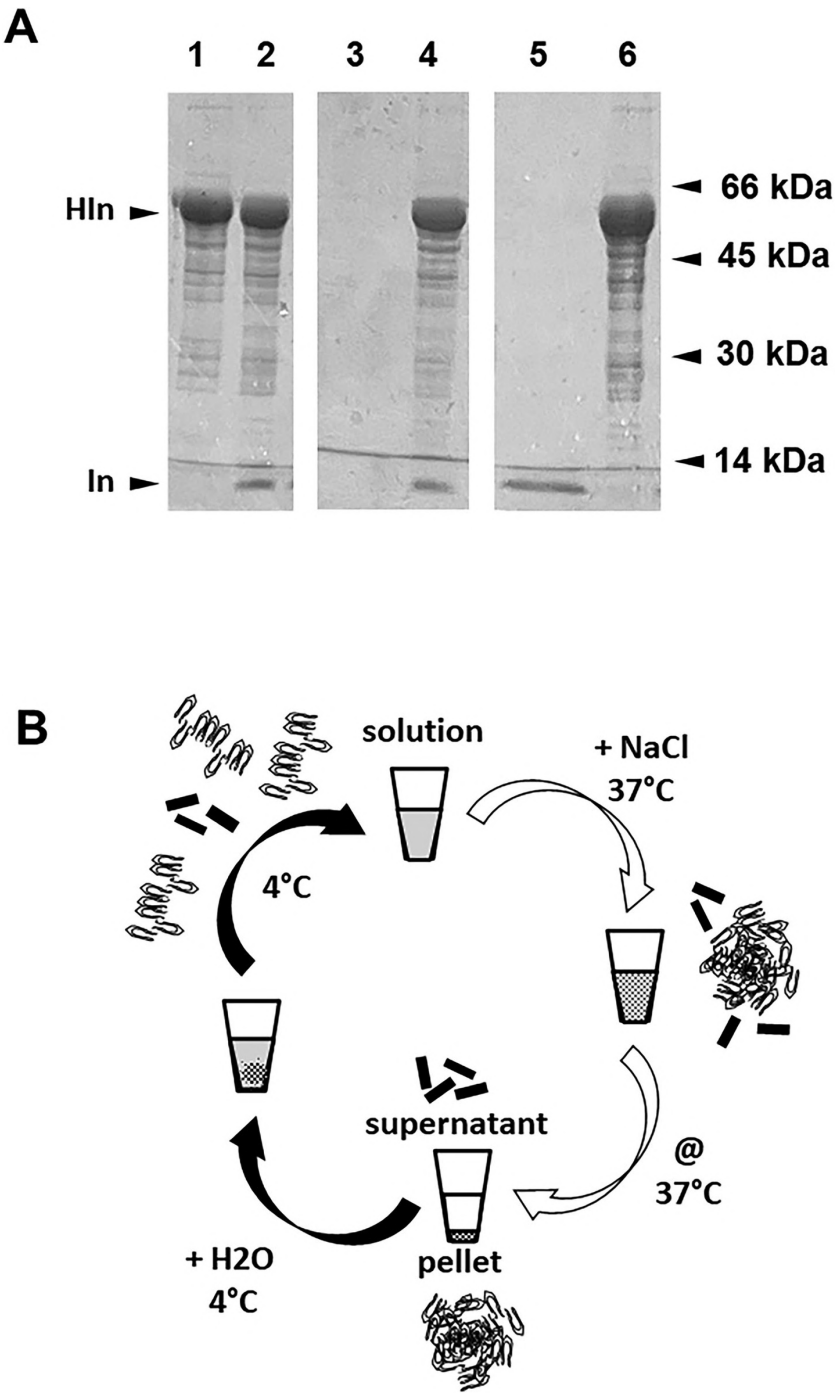

Figure 6. Release of In domain by specific enzymatic cleavage of HIn. Representative image of SDS-PAGE analysis of the HIn biopolymer treated with the Glu-C endoprotease. Lane 1, untreated HIn biopolymer; lane 2, HIn biopolymer treated with Glu-C; lane 3, supernatant after the precipitation and centrifugation at 37 °C; lane 4, pellet after the precipitation and centrifugation at 37 °C; lane 5, supernatant after the precipitation and centrifugation at 37 °C in the presence of detergent; lane 6, pellet after the precipitation and centrifugation at 37 °C in the presence of detergent. B. Scheme of the purification process based on the ITC method of the HELP biopolymer, which is soluble in a cold solution and precipitates after temperature and ionic strength increase. Molecular masses of the protein markers are indicated on the right. Bovine serum albumin (66 kDa), ovalbumin (45 kDa), carbonic anhydrase (30 kDa), lysozyme (14 kDa). Coomassie blue staining.

ADVANCED SCIENCE NEWS
www.advancedsciencenews.com

Macromolecular Bioscience
www.mbs-journal.de

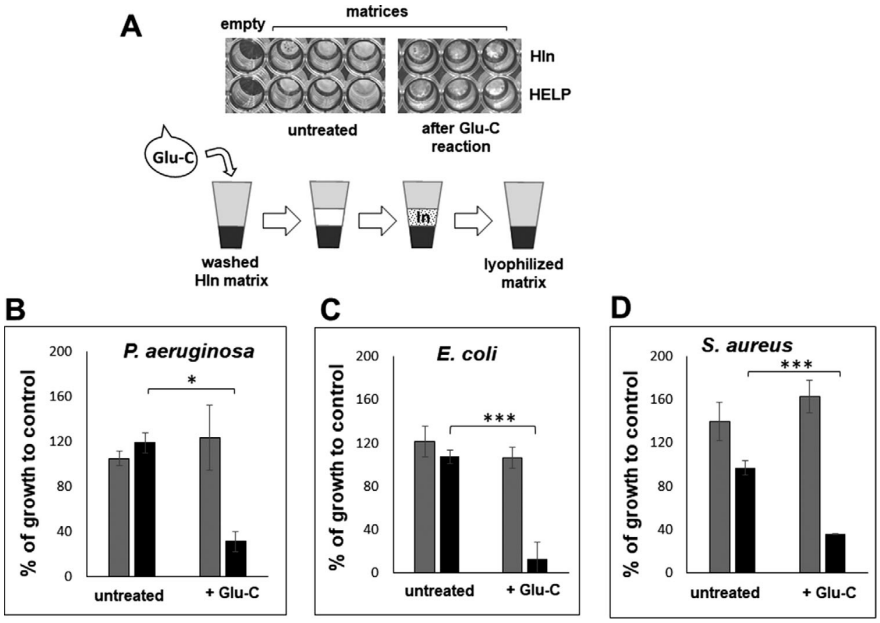

Figure 7. Antimicrobial activity of the HIn matrix. A) Macroscopic aspect of the HIn and HELP matrices before and after Glu-C reaction (top) and schematization of matrix treatment to test the activity toward the bacteria (bottom). B) Antimicrobial activity of the HELP (grey) and HIn (black) matrix toward *P. aeruginosa*. C. Antimicrobial activity of the HELP (grey) and HIn (black) matrix toward *E. coli*. D. Antimicrobial activity of the HELP (grey) and HIn (black) matrix toward *S. aureus*. The values were expressed as the percent respect the growth of the untreated control and represented the mean ± SD, $n = 4$; *$p \leq 0.01$, ***$p \leq 0.0001$.

The antibacterial capacity of HIn matrices was assayed. After the cross-linking reaction, both 4% HELP and HIn matrices were extensively washed with water to remove any unreacted substrate and then they were lyophilized (Figure 7A). The matrices were re-hydrated in bacterial culture, maintaining the same conditions of the MIC assay (detailed in the Materials and Methods section). Despite the fact that the uncleaved HIn biopolymer displayed antimicrobial activity toward *P. aeruginosa* (Figure 4), both HELP and HIn matrices allowed bacterial growth, suggesting that tethering of the In domain in a matrix may inactivate it. This was described for cationic peptides, since it was observed that peptide immobilization on a surface could result in a pronounced activity decrease.[26] Thus, the cleavage with Glu-C was performed on the HIn as well as the HELP matrix. All the samples were lyophilized, to be re-hydrated in the presence of *P. aeruginosa*, as described above for the undigested matrices. The results are shown in Figure 7B. The untreated and the Glu-C treated HELP matrices as well as the untreated HIn matrix did not show any significant effect on bacterial growth. On the contrary, the HIn matrix treated with Glu-C drastically reduced the growth of *P. aeruginosa*, suggesting the release of the active antimicrobial domain from the HIn matrix. Since it is described that In has a broad activity toward bacteria, we repeated the same assay with *S. aureus* and with *E. coli*. The results in Figures 7C,D clearly showed that the In activity toward these two strains was restored after the cleavage with Glu-C of the HIn matrix.

Overall, the fusion of In with HELP has demonstrated the versatility of this peculiar elastin-like domain as a valuable carrier. First, the cleavage of In from the matrix and its release was successfully performed representing a convenient and smart alternative option with respect to ITC to obtain the bioactive AMP domain. Second, although the matrix resulted not active after the cross-linking, we demonstrated that the antimicrobial property was restored after the specific proteolytic cleavage. Since In to exert its effect has to penetrate inside the bacterial cell, the antimicrobial activity was just hindered when the AMP resulted immobilized within the matrix.

This is consistent also with the observation that the HIn coating was toxic for bacterial cells. In the coating HIn is not cross-linked, thus it is likely that it could re-dissolve in aqueous solution to some extent and, in consequence, it can be internalized by the bacteria exerting the observed growth inhibition (Figure 5).

The features of the HELP fusion with an AMP domain can be exploited to realize smart stimuli-responsive materials with antimicrobial properties that can be triggered on/off on demand.

2.5. Release of the Antimicrobial Activity by Elastase

An interesting feature of HELP biopolymer is its elastin-mimicking structure, which is composed of both elastin-like and cross-linking domains. It has already been reported that HELP is particularly susceptible to elastase activity, likely due to the presence of the cross-linking domains that represent one of the main targets of this enzyme.[27]

This property is valuable to realize stimuli-responsive systems for the sustained release of active AMPs, especially in the presence of elastolytic activity, a condition occurring during

ADVANCED SCIENCE NEWS
www.advancedsciencenews.com

Macromolecular Bioscience
www.mbs-journal.de

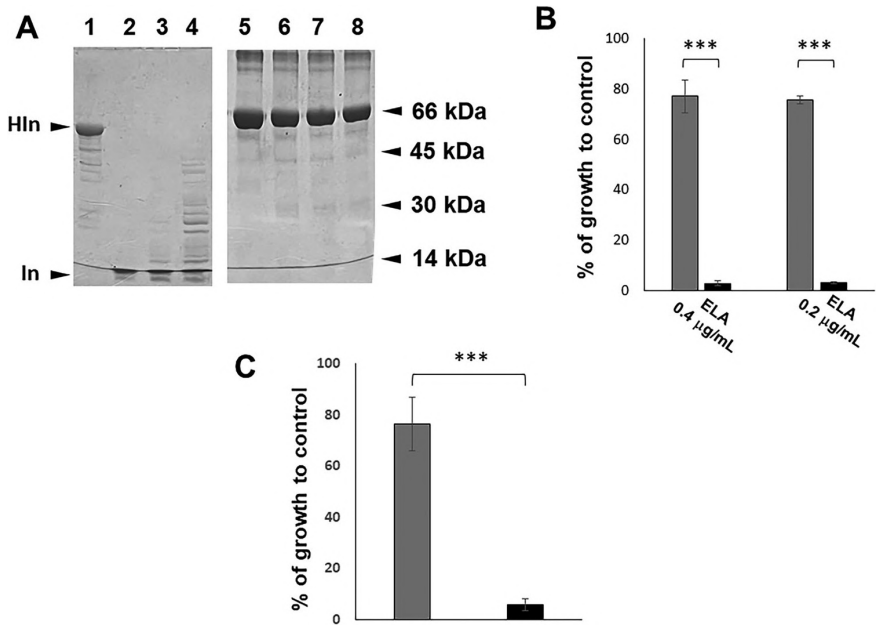

Figure 8. HIn biopolymer and HIn matrix degradation by elastase and release of the antimicrobial activity. A) Representative SDS-PAGE analysis of elastolytic degradation of the HIn biopolymer. HIn (lane 1) was treated with 0.4, ng μL^{-1} of elastase (lane 2), 0.2, ng μL^{-1} of elastase (lane 3), and 0.1, ng μL^{-1} of elastase (lane 4). In the same conditions, BSA (lane 5) was treated with equal amounts of elastase, 0.4, ng μL^{-1} of elastase (lane 6), 0.2, ng μL^{-1} of elastase (lane 7) and 0.1, ng μL^{-1} of elastase (lane 8). Molecular masses of the protein markers expressed in kilodaltons (kDa) are indicated on the right, Coomassie blue staining. B. Effect on bacterial growth of HELP (grey) and HIn (black) biopolymer solution treated with 0.4 and 0.2 ng μL^{-1} of elastase (ELA). C. Effect of HELP (grey) and HIn (black) matrix degradation by elastase on bacterial growth. The values were expressed as the percent respect the growth of the untreated control and represented the mean ± SD, $n = 4$; ***$p \leq 0.0001$.

neutrophil activation due to inflammation processes, for instance. Therefore, we assessed the release of In by elastase by first testing the HIn biopolymer in solution (**Figure 8**A). Elastase concentrations of 0.4 and 0.2 µg mL^{-1} were necessary to degrade all the HELP domain of the HIn biopolymer, releasing the In product (Figure 8A, lanes 2 and 3), whereas the same enzyme concentrations did not degrade bovine serum albumin (BSA) at all (Figure 8A, compare lane 5 with lanes 6–8), confirming the reaction specificity.

The antimicrobial activity of these reactions' products was assessed against *P. aeruginosa* and the data showed that the presence of the products of the elastolytic degradation of HIn biopolymer resulted in a marked inhibition of bacterial growth. In contrast, the degradation products of HELP had only a minor effect (Figure 8B).

Moreover, the 4% matrix of HIn and that of HELP, were treated with elastase. The reaction completely degraded the matrices, as already reported.[27] The obtained supernatants were then assayed with *P. aeruginosa*, showing that HIn matrix degradation was sufficient to allow the release of an amount of In that was effective in inhibiting bacterial growth (Figure 8C).

These data showed that our HIn construct might be employed to obtain smart materials that, upon the proper stimuli, trigger the release of a bioactive compound that may interfere with the process that provoked the release, possibly leading to the attenuation of the process itself. The concentration of the enzyme that showed to be sufficient to release an amount of bioactive domain, was ineffective on the BSA, suggesting that the high susceptibility of HELP to elastase is a valuable feature to exploit for the production of antimicrobial materials that may be well tolerated by the tissues.

3. Conclusion

The HELP fusion platform described in this work was successfully employed to produce a model construct bearing the bioactive antimicrobial domain indolicidin. The synthetic gene was further tailored to introduce a specific cleavage site, giving an example of the versatility of our system. The HIn recombinant biopolymer retained both the properties of the elastin-like carrier, as demonstrated by the physicochemical characterization, and those of the antimicrobial domain, displaying growth inhibitory activity at least towards one of the model strains tested. The exploitation of the HIn thermo-responsive behavior allowed its production with very good purity and yield on a lab scale and can be further scaled up. The matrix-forming property of HELP was also maintained by HIn. Two ways were evaluated to produce indolicidin by a specific enzymatic cleavage route. To purify the In released from the reaction the ITC was exploited to deplete the supernatant of the HELP moiety. Although this method showed some limitations due to the high hydrophobicity and poor water solubility of In itself, the bioactive AMP was successfully recovered by cleaving the HIn matrix and recovering the supernatant. Overall, the recombinant platform described

ADVANCED SCIENCE NEWS
www.advancedsciencenews.com

Macromolecular Bioscience
www.mbs-journal.de

herein showed valuable versatility and opened the door to the production of materials endowed with antimicrobial properties that might be integrated into engineered multifunctional bio-systems capable of sensing and actively responding to their surrounding environment. Due to the strict control of the amino acid sequences, this platform can also be exploited to better elucidate the still poorly characterized mechanism of action of the AMPs at the molecular level.

4. Experimental Section

Antimicrobial HELP Cloning, Expression, and Purification: The sequence coding for indolicidin (In, GenBank: AAB21494.1) was in-frame cloned at the C-terminal region of HELP gene exploiting the unique *DraIII – HindIII* restriction sites.[12] The positive clones were sequenced to verify the open reading frame and then the *E. coli* C3037I (New England Biolabs Inc., Ipswich, MA) expression strain was transformed with the plasmid carrying the new HIn construct. The expression and purification of the recombinant HELP and HIn biopolymer were performed in standard conditions, as described previously.[28]

The purified biopolymers were analyzed by a 9% acrylamide SDS-PAGE stained by Coomassie blue using a reported procedure.[19] The purified products were lyophilized for long-term storage.

Physicochemical Characterization: The spectrophotometric analysis of 2 mg mL^{-1} aqueous solution of the pure samples was performed in the range of $\lambda = 250 - 300$ nm using a Jenway scanning spectrophotometer (Model 7205, Jenway, Staffordshire UK). The fluorescence of aqueous solutions of the biopolymers at different concentrations was measured in a 96-well black polystyrene microplate (Nunc, Sjelland, Denmark), analyzing 50 µL $well^{-1}$ and detecting the emission fluorescence at $\lambda = 350$ nm, following excitation at $\lambda = 280$ nm by a microplate reader (Synergy H1, BioTek, Winooski, VT).

The secondary structure was evaluated using the ProtParam (Expasy) program available on the SIB Swiss Institute of Bioinformatics website. The grand average of hydropathy value (GRAVY) for proteins was calculated as the average of hydropathy values of all the amino acids in the sequence. The prediction of secondary structures of HIn was based on the primary amino acid sequences of the polypeptides by using GOR IV software from the Expasy Web site (http://www.au.expasy).

Circular dichroism (CD) spectra were recorded on protein solutions with a concentration of 0.1 mg mL^{-1} in NaPi (10 mM sodium phosphate pH = 6.8) or NaPi / NaCl (10 mM sodium phosphate/ 0.15 M NaCl pH = 6.8) buffers. The CD Spectra were recorded at 25 °C in a 200- to 500-nm thermostatic cell on a Jasco J-710 spectrometer under constant nitrogen flow, and the data were expressed as the mean molar ellipticity [θ] of the residue (mdeg-cm^2-$dmol^{-1}$).

By using a turbidimetric method, the optical density (OD) of HIn samples was measured at $\lambda = 350$ nm in the range of temperature 20–50 °C at a heating scan rate of 0.2 °C min^{-1} on a Jenway 6300 spectrophotometer. The inverse transition temperature (T_t) was obtained as the temperature corresponding to 50% of the maximum OD value. The purified proteins were dissolved in NaPi buffer to a final concentration of 2 mg mL^{-1}. The solutions were equilibrated at 4 °C for 16 h before analysis.

The thermal properties of lyophilized proteins in solution were evaluated by Differential Scanning Calorimetry (DSC) using a Setaram MicroDSC III DSC model. Stainless steel cells were filled by weight with protein samples (4 mg mL^{-1}, in NaPi or NaPi /NaCl buffers) and then hermetically sealed and equilibrated for 16 h at 4 °C. The calorimeter was pre-equilibrated at 5°C for 10 min, followed by heating from 5 to 70 °C at a scan rate of 0.5 °C min^{-1}. The solvent was used as a reference. The calorimetric area, the onset, and the peak inverse transition temperatures (T_t) were determined by a homemade software written in Fortran code.

Assessment of Antimicrobial Activity of the HIn Biopolymer and of the Derived Materials: The bacterial strains used to assess the antimicrobial activity of the HIn recombinant biopolymer were *S. aureus* ATCC 25 923, *P. aeruginosa* ATCC 15 692, and *E. coli* ATCC 25 922. The antimicrobial activity was assessed using a modification of the broth microdilution method, according to Bera et al.[29] using 2.1% (w/v) Mueller-Hinton broth (Merck Millipore, Massachusetts, USA). The bacterial cells were incubated with the biopolymers in the NaPi buffer (10 mM sodium phosphate, pH 6.8) before broth addition and incubation at 37 °C. The minimum inhibitory concentration (MIC) was taken as the lowest concentration of the biopolymer that completely inhibited the growth of microorganisms was assessed as follows. Briefly, 300 µL of overnight bacterial culture were diluted in 10 mL of 2.1% (w/v) Mueller-Hinton broth and incubated at 37 °C with continuous shaking (150 rpm) for ≈2–2.5 h, until OD ≈ 0.5 was reached. At this point, 50 µL of the bacterial culture were diluted in 10 mL of NaPi buffer, corresponding to $\approx 2.5 \times 10^6$ CFU mL^{-1} (bacterial working solution). Lyophilized biopolymers, previously sterilized by 0.22 µm filtration, were re-dissolved to a concentration of 100 µM in sterile NaPi to prepare two-fold serial dilutions that were deposited (10 µL per well) in a sterile 96-well polystyrene U-shaped bottom wells microplate (Sarstedt, Numbrecht, Germany).

Right after, 20 µL of bacterial working solution were added per well and incubated for 1 hour at room temperature (21–23 °C). Sterile NaPi buffer was used as the control. Then, 70 µL of 3% (w/v) Mueller–Hinton broth were added to each well to a final volume of 100 µL of 2.1% (w/v) Mueller-Hinton broth (final concentration). The final concentration of the biopolymers ranged from 10 to 0.038 µM and the final seeding density was 5×10^5 CFU mL^{-1}. The microwell plates were incubated at 37 °C for 20 hours, and then they were analyzed at 600 nm in a microplate.

Antimicrobial Activity of HIn Coatings: Coatings were prepared either in the bottom of the well of 24-well tissue culture-treated polystyrene microplates (Sarstedt, Numbrecht, Germany) for assessment of antimicrobial activity, or in 13 mm-diameter sterile plastic coverslips (# 83.1840.002, Sarstedt, Numbrecht, Germany) for SEM analysis. Lyophilized HELP and HIn biopolymers were re-dissolved in water and sterilized by filtration (0.22 µm). Coatings were prepared in the form of thin films by deposition of 50 µL of 2 mg mL^{-1} biopolymer sterile solution, thus covering a surface of 1 cm^2 with 100 µg of biopolymer. Samples were dried allowing water to evaporate at room temperature under a sterile hood.

To evaluate the antimicrobial capacity of the biopolymer coatings, a modification of the antimicrobial assay described above was set up. Briefly, 20 µL of 10 mM NaPi buffer containing approximately $2{,}5 \times 10^6$ CFU mL^{-1} of *P. aeruginosa* ATCC 15 692 strain were deposited within the coated surfaces of the 24-well polystyrene microplate and were incubated for 1 hour at room temperature (21–23 °C). Right after, 300 µL of 2.1% (w/v) Mueller-Hinton broth were added to the wells and the microplate was incubated at 37 °C for 20 h. The bacterial growth was determined by reading 50 µL of each sample in a U-shaped 96-well polystyrene microplate at 600 nm in a microplate reader.

For SEM analysis, *P. aeruginosa* ATCC 15 692 culture was diluted to 2×10^8 CFU mL^{-1} in NaPi buffer, and 20 µL were deposited onto the coated surface of the plastic coverslips and incubated for 1 hour at room temperature. After incubation, the solution was removed by washing twice with 50 µl PBS. The samples were fixed at room temperature for 30 min using 50 µL of 2.5% (v/v) glutaraldehyde in PBS. After glutaraldehyde removal, the coverslips were rinsed again by soaking in PBS. Samples dehydration was performed with increasing concentrations of ethanol/water (30%, 50%, 70%, 90%, and 100%) using for each Step 1 mL of solution and 5 min of incubation. Subsequently, samples were dried under the hood flow, mounted on aluminum stubs covered with a double-sided carbon tape and coated with chromium using a Q150T ES plus sputter coater (Quorum Technologies Ltd., UK). The morphological analysis was then performed with a scanning electron microscope (Gemini 300, Zeiss, Germany) working in secondary electron detection mode. The working distance was set at about 8.5 mm to obtain the appropriate magnifications, and the acceleration voltage was set at 5 kV.

Antimicrobial Capacity Assessment of the HIn Matrix: To assess the antimicrobial activity of the HIn matrix, conditions similar to those described above for the MIC assay were adopted.

HELP and HIn hydrogel matrices were prepared in a sterile 96-wells polystyrene V-shaped bottom microplate (Sarstedt, Numbrecht, Germany). 10 µL of 4% (w/v) sterile aqueous solutions of HELP and HIn

ADVANCED SCIENCE NEWS
www.advancedsciencenews.com

Macromolecular Bioscience
www.mbs-journal.de

were deposited in the well bottom and were enzymatically cross-linked using microbial transglutaminase (N-Zyme Biotec GmbH, Darmstadt, Germany) at a final concentration of 2 μg μL^{-1}. Cross-linking was carried out for 1 hour at room temperature (21–23 °C) and after three washes with excess of water, the matrices were directly lyophilized or treated with Glu-C. For this latter reaction 25 μL of 100 mM ammonium bicarbonate pH 8 with 10 ng μL^{-1} Glu-C were added to each matrix, whereas the control samples were treated with 25 μL of buffer alone and incubated overnight at 37 °C. After this reaction, the microplate was transferred at −80 °C and lyophilized.

Subsequently, each matrix was re-hydrated with 20 μL of bacterial working solution (2.5×10^6 CFU mL^{-1} in 10 mM NaPi buffer) and incubated for 1 h at room temperature before the addition of 100 μL of 2.1% (w/v) Mueller-Hinton broth. The microplate was incubated for 20 h at 37 °C and then the supernatants were transferred in a U-shape microplate to be read at 600 nm.

Specific Release of the In Antimicrobial Domain by Glu-C Endoprotease from the HIn Biopolymer: The reactions with the Glu-C enzyme (New England Biolabs, #P8100S) were set up in parallel with the HELP and the HIn biopolymers at the final concentration of 6 mg mL^{-1} in 100 mM ammonium bicarbonate buffer, pH 8, with of Glu-C 10 ng μL^{-1}. After the incubation at 37 °C for 5 h, 1.5 μL of the reaction were added to the same volume of Laemmli loading buffer for the SDS-PAGE analysis.

To separate the In peptide from the HELP moiety, a purification exploiting the inverse transition cycling was performed, adding to the reaction NaCl to 1.5 M, Triton-X100 to 1% (v/v), and warming at 37 °C for 5 min. After the centrifugation for 5 min at 10 000 rpm. The supernatant and the pellet were separated and subjected to SDS-PAGE analysis.

Specific Release of the In Domain by Glu-C Endoprotease from the HIn Matrix: The In domain was released from the 4% (w/v) HIn matrix by incubation with Glu-C. Matrices of 150 μL each were incubated overnight at 37 °C with 500 μL of 100 mM ammonium bicarbonate buffer pH 8 with 10 ng μL^{-1} of Glu-C enzyme. The control samples were incubated in the buffer alone.

After the overnight incubation, the supernatant was collected. Then, each matrix was washed twice for 1 h with 1 mL of 20% (v/v) acetonitrile in water. A third wash was performed overnight. The washes that showed fluorescence emission were pooled together with the supernatant to be frozen and lyophilized. The lyophilized material was re-suspended in water to be assayed by Bicinchoninic acid assay (Pierce BCA Protein Assay Kit), SDS-PAGE, and ESI mass spectrometry. For the antimicrobial activity assessment, the lyophilized material was re-suspended in NaPi and sterilized by 0.2 μm filtration.

Release of the In Domain from the HIn Biopolymer by Elastolytic Activity: The HIn biopolymer was sterilized by filtration and a 100 μM solution in NaPi buffer was treated with 0.4, 0.2, and 0.1 ng μL^{-1} of elastase (Sigma, elastase from porcine pancreas, #E7885) for 3 h at 37 °C in a final reaction volume of 30 μL. In parallel, the same conditions were adopted to set up equivalent reactions with the bovine serum albumin (BSA) as well as the HELP biopolymer. A 2 μL of each reaction were analyzed in SDS-PAGE. The antimicrobial capacity of 10 μL of the elastase reaction mixtures were assessed towards *P. aeruginosa* ATCC 15 692 as described above.

Release of the In Domain from the HIn Matrix by Elastolytic Activity: 4% (w/v) HIn hydrogel matrices (10 μL each) were prepared in sterile conditions as described above. After the cross-linking, the matrices were extensively washed with sterile NaPi buffer and then incubated with 15 μL of 8 ng μL^{-1} elastase solution in NaPi buffer at 37 °C for 3 h. These reactions were then incubated with 10 μl of *P. aeruginosa* ATCC 15 692 bacterial solution diluted to 5×10^6 CFU mL^{-1} in NaPi buffer for 1 hour at room temperature before the addition of 70 μL of 3% (w/v) Mueller–Hinton broth. The microwell plates were incubated at 37 °C for 20 h, and then they were analyzed at 600 nm in the microplate reader.

Statistical Analysis: One-way analysis of variance (ANOVA) was carried out to compare the means of different data sets within each experiment. A value of $p < 0.05$ was considered statistically significant. All experiments were performed at least in triplicate.

Supporting Information

Supporting Information is available from the Wiley Online Library or from the author.

Acknowledgements

The authors were grateful to Dr. Lucia Corich and Prof. Cristina Lagatolla for providing the bacterial strains used in this study, Prof. Sabina Passamonti for her helpful support, and Dr. Marco Stebel, Dr. Davide Porrelli, and Dr. Fabio Hollan for technical assistance. This work was supported by the Horizon 2020 Innovative Training Network AIMed project under the Marie Skłodowska-Curie, grant agreement No 861138, and the Horizon Europe STOP – Surface Transfer of Pathogens project, grant agreement No 101057961.

Conflict of Interest

The authors declare no conflict of interest.

Data Availability Statement

The data that support the findings of this study are available from the corresponding author upon reasonable request.

Keywords

antimicrobial peptides, hydrogel matrix, recombinant biopolymers, smart materials

Received: May 24, 2023
Revised: August 7, 2023
Published online: September 24, 2023

[1] R. Laxminarayan, *Lancet* **2022**, *399*, 606.
[2] C. J. L. Murray, K. S. Ikuta, F. Sharara, L. Swetschinski, G. Robles Aguilar, A. Gray, C. Han, C. Bisignano, P. Rao, E. Wool, S. C. Johnson, A. J. Browne, M. G. Chipeta, F. Fell, S. Hackett, G. Haines-Woodhouse, B. H. Kashef Hamadani, E. A. P. Kumaran, B. Mcmanigal, S. Achalapong, R. Agarwal, S. Akech, S. Albertson, J. Amuasi, J. Andrews, A. Aravkin, E. Ashley, F.-X. Babin, F. Bailey, S. Baker, et al., *Lancet* **2022**, *399*, 629.
[3] A. Moretta, C. Scieuzo, A. M. Petrone, R. Salvia, M. D. Manniello, A. Franco, D. Lucchetti, A. Vassallo, H. Vogel, A. Sgambato, P. Falabella, *Front Cell Infect Microbiol* **2021**, *11*, 668632.
[4] C. Wang, T. Hong, P. Cui, J. Wang, J. Xia, *Adv Drug Deliv Rev* **2021**, *175*, 113818.
[5] O. Bellotto, S. Semeraro, A. Bandiera, F. Tramer, N. Pavan, S. Marchesan, *Pharmaceutics* **2022**, *14*, 446.
[6] Z. Cui, Q. Luo, M. S. Bannon, V. P. Gray, T. G. Bloom, M. F. Clore, M. A. Hughes, M. A. Crawford, R. A. Letteri, *Biomater. Sci.* **2021**, *9*, 5069.
[7] M. Riool, V. Patrulea, C. Monteiro, *in Pharmaceutics* **2022**, *14*, 2171.
[8] J. Rosenbloom, W. R. Abrams, Z. Indik, H. Yeh, N. Ornstein-Goldstein, M. M. Bashir, *Ciba Found Symp.* **1995**, *192*, 59.
[9] M. Santos, S. Serrano-Dúcar, J. González-Valdivieso, R. Vallejo, A. Girotti, P. Cuadrado, F. J. Arias, *Curr. Med. Chem.* **2019**, *26*, 7117.
[10] L. Colomina-Alfaro, S. Marchesan, A. Stamboulis, A. Bandiera, *Biotechnol. Bioeng.* **2023**, *120*, 323.

ADVANCED SCIENCE NEWS
www.advancedsciencenews.com

Macromolecular Bioscience
www.mbs-journal.de

[11] A. Bandiera, *Prep. Biochem. Biotechnol.* **2010**, *40*, 198.
[12] A. Bandiera, A. Taglienti, F. Micali, B. Pani, M. Tamaro, V. Crescenzi, G. Manzini, *Biotechnol. Appl. Biochem.* **2005**, *42*, 247.
[13] A. Bandiera, *Enzyme Microb. Technol.* **2011**, *49*, 347.
[14] M. E. Selsted, M. J. Novotny, W. L. Morris, Y. Q. Tang, W. Smith, J. S. Cullor, *J. Biol. Chem.* **1992**, *267*, 4292.
[15] J. Batista Araujo, G. Sastre De Souza, E. N. Lorenzon, *World J. Microbiol. Biotechnol.* **2022**, *38*, 39.
[16] N. Shagaghi, E. A. Palombo, A. H. A. Clayton, M. Bhave, *World J. Microbiol. Biotechnol.* **2016**, *32*, 31.
[17] E. Gasteiger, *Nucleic Acids Res.* **2003**, *31*, 3784.
[18] A. Bandiera, Sist, P., Terdoslavich, M., Urbani, R., in *35th Annual Northeast Bioengineering Conference*, IEEE, Boston, MA **2009**.
[19] A. Bandiera, P. Sist, R. Urbani, *Biomacromolecules* **2010**, *11*, 3256.
[20] P. Sist, A. Bandiera, R. Urbani, S. Passamonti, *Biomacromolecules* **2022**, *23*, 3336.
[21] D. W. Urry, D. C. Gowda, T. M. Parker, C.-H. Luan, M. C. Reid, C. M. Harris, A. Pattanaik, R. D. Harris, *Biopolymers* **1992**, *32*, 1243.
[22] K. Trabbic-Carlson, D. E. Meyer, L. Liu, R. Piervincenzi, N. Nath, T. Labean, A. Chilkoti, *Protein Eng. Des. Sel.* **2004**, *17*, 57.
[23] M. Joachim, N. Maguire, J. Schäfer, D. Gerlach, P. Czermak, *Front Bioeng. Biotechnol.* **2019**, *7*, 150.
[24] D. R. Galloway, *Mol. Microbiol.* **1991**, *5*, 2315.
[25] S. Ruden, A. Rieder, I. Chis Ster, T. Schwartz, R. Mikut, K. Hilpert, *Front Microbiol* **2019**, *10*, 2740.
[26] M. Bagheri, M. Beyermann, M. Dathe, *Bioconjug. Chem.* **2012**, *23*, 66.
[27] A. Bandiera, A. Markulin, L. Corich, F. Vita, V. Borelli, *Biomacromolecules* **2014**, *15*, 416.
[28] L. Corich, M. Busetti, V. Petix, S. Passamonti, A. Bandiera, *J. Biotechnol.* **2017**, *255*, 57.
[29] S. Bera, A. Ghosh, S. Sharma, T. Debnath, B. Giri, A. Bhunia, *J. Colloid Interface Sci.* **2015**, *452*, 148.

Chapter 5. Materials derived from the human elastin-like polypeptide fusion with an antimicrobial peptide strongly promote cell adhesion

This chapter introduces a research article already published in the Journal of Material Chemistry B (Royal Society of Chemistry).

Colomina-Alfaro, L., Sist, S., D' Andrea, P., Urbani, R., P., Marchesan, Stamboulis, A., & Bandiera, A. (2024). **Materials derived from the human elastin-like polypeptide fusion with an antimicrobial peptide strongly promote cell adhesion.** *J. Mater. Chem. B, 2024, Advance Article.* https://doi.org/10.1039/D4TB00319E. Reproduced with permission under a Creative Commons Attribution 3.0 Unported Licence. *Copyright © 2024 by the Authors. Journal of Materials Chemistry B published by the Royal Society of Chemistry.*

The third objective of this thesis was to follow the strategy adopted to realise HIn model to produce another HELP fusion construct carrying the β-defensin 1 (hBD1) and to assess its biological properties. hBD1 was successfully fused at the C-terminal of HELP, and the fusion protein was named HhBD1. Specific endoprotease sites within the fusion protein sequence were introduced to release the two most active domains of hBD1. Once more, the fusion protein was produced in *E. coli*, purified following the ITC method and physico-chemically characterised by turbidimetric techniques. The biological characterisation of the biopolymer and its release products reveals that their antimicrobial properties against *E. coli* ATCC 25922 depend on the redox state. Moreover, the cytotoxicity assays of the biopolymer in solution showed a high cytocompatibility towards osteoblastic and fibroblastic cells. In addition, the possibility of developing coatings, thin films, and hydrogel matrices based on this biopolymer was explored, and their adhesion properties were assayed. Unexpectedly, 2D and 3D HhBD1-based materials showed a strong cell pro-adhesive capacity that, to our knowledge, has not been previously described for hBD1.

My contribution to this journal article is as follows: investigation, conceptualisation, methodology, formal data analysis and validation, graphical representation, and original & revised draft writing. The following experiments have been carried out by myself:

- Production of the recombinant HhBD1 fusion biopolymer
    - Cloning, expression, and purification
    - Specific release of hBD1 domains from the HhBD1 fusion biopolymer
- Antimicrobial and biological evaluation of HhBD1
    - Radial diffusion assay
    - Cell culture and viability assay
- HhBD1 3D matrix production and characterisation
    - 3D matrix production
    - Oscillatory rheological analysis
- Cell culture on HhBD1-based substrates
    - Preparation of the coatings
    - Adhesion and viability assays of cells cultured on coatings
    - Cell culture on HELP and HhBD1 matrices
    - Fluorescence analysis

Journal of Materials Chemistry B

ROYAL SOCIETY OF CHEMISTRY

PAPER

View Article Online
View Journal

Cite this: DOI: 10.1039/d4tb00319e

Materials derived from the human elastin-like polypeptide fusion with an antimicrobial peptide strongly promote cell adhesion†

Laura Colomina-Alfaro, [a] Paola Sist, [a] Paola D'Andrea, [a] Ranieri Urbani, [b] Silvia Marchesan, [b] Artemis Stamboulis [c] and Antonella Bandiera *[a]

Protein and peptide materials have attracted great interest in recent years, especially for biological applications, in light of their possibility to easily encode bioactivity whilst maintaining cytocompatibility and biodegradability. Heterologous recombinant expression to produce antimicrobial peptides is increasingly considered a convenient alternative for the transition from conventional methods to more sustainable production systems. The human elastin-like polypeptide (HELP) has proven to be a valuable fusion carrier, and due to its cutting-edge properties, biomimetic materials with antimicrobial capacity have been successfully developed. In this work, we have taken advantage of this platform to produce a difficult-to-synthesise sequence as that of the human β-defensin 1 (hBD1), an amphipathic cationic peptide with structural folding constraints relevant to its bioactivity. In the design of the gene, highly specific endoproteinases recognition sites were introduced to release the active forms of hBD1. After the expression and purification of the new fusion construct, its biological activity was evaluated. It was found that both the fusion biopolymer and the released active forms can inhibit the growth of *Escherichia coli* in redox environments. Remarkably, 2D and 3D materials derived from the biopolymer showed a strong cell adhesion-promoting activity. These results suggest that HELP represents a multitasking platform that not only facilitates the production of bioactive domains and derived materials but could also pave the way for the development of new approaches to study biological interactions at the molecular level.

Received 16th February 2024,
Accepted 15th July 2024

DOI: 10.1039/d4tb00319e

rsc.li/materials-b

1. Introduction

Protein and peptide materials have become very popular over the last decade for a wide variety of biological uses and beyond, thanks to their inherent bioactivity, cytocompatibility, and biodegradability.[1–3] In particular, those containing antimicrobial peptides (AMPs) are highly attractive in light of the emergence of antimicrobial resistance against traditional antibiotics, although their design entails a set of challenges to maintain their bioactivity.[4,5] Recombinant fusion biotechnology has emerged as a promising platform to produce antimicrobial peptides. Standard chemical synthesis encounters several burdens that lead to increased production timelines and costs. These challenges include the hurdle of synthesising difficult sequences or lengthy peptides, inefficient purification processes due to the primary structure of the AMPs, and the need for the proper folding (*e.g.*, the occurrence of disulfide bridges, post-translational modifications, *etc.*) to maintain the antimicrobial efficacy.[6,7] In contrast, the recombinant production in *Escherichia coli* offers cost-effectiveness, scalability, and efficient expression systems, resulting in high yields and establishing the basis for large-scale protein production.[8] To date, many fusion carriers have been developed and used for AMP production. Nevertheless, the elastin-like polypeptides (ELPs) are still the least exploited.[9]

ELPs are a class of recombinant biopolymers inspired by elastin and therefore endowed with the inverse transition property, a thermo-responsive behaviour that allows these components to shift from the solvated form to the suspension state, depending on the temperature of the environment.[10]

The human elastin-like polypeptide (HELP) fusion carrier developed in our laboratory differs from most other ELPs

[a] *Department of Life Sciences, University of Trieste, 34127 Trieste, Italy. E-mail: abandiera.units.it*
[b] *Department of Chemical and Pharmaceutical Sciences, University of Trieste, 34127 Trieste, Italy*
[c] *School of Metallurgy and Materials, Biomaterials Research Group, University of Birmingham, Edgbaston, Birmingham, B15 2TT, UK*

† Electronic supplementary information (ESI) available: HhBD1 cloning and purification; stability of HELP and HhBD1; hBD1 accessible surface area calculation, radial diffusion assays; oscillatory rheology analysis; mass spectrometry; fluorescence analyses of cell cultured on coatings and matrices. See DOI: **https://doi.org/10.1039/d4tb00319e**

described in the literature as it possesses the cross-linking domains characteristic of tropoelastin.[11] These domains can be cross-linked by an enzymatic reaction, resulting in the formation of cytocompatible hydrogel matrices. This mild process does not affect cell viability, allowing its use for cell encapsulation and culture.[12] Notably, the cross-linking domains are also the main target for elastase, an enzyme secreted by activated polymorphonuclear leukocytes during inflammation.[13] Consequently, the presence of elastolytic proteases of different origins can trigger the release of any domain fused to HELP, as well as any compound embedded in the gel matrix.[14] Recently, a HELP-AMP fusion with the antimicrobial peptide indolicidin has been described. In addition to the successful high-yield expression, the HELP-AMP fusion product retained both the HELP thermo-responsive properties and the AMP activity, demonstrating the advantage of using this carrier for the production of AMP domains.[15]

The human β-defensin 1 (hBD1) belongs to the defensins family, a class of small, cationic antimicrobial peptides with a well-defined tertiary structure stabilised by three specific disulfide bridges that are conserved among all β-defensins.[16] hBD1 is constitutively expressed and produced by several types of epithelial cells, such as those of the urinary tract, pancreatic duct, respiratory tract, and intestine, as well as by keratinocytes.[17] Recent evidence suggests that the members of the β-defensin family are multifunctional peptides that not only have functions related to host defence,[18,19] but are also involved in cell proliferation and migration,[20] wound healing, tissue regeneration,[21,22] and tumour inhibition,[23] positioning them as attractive components for translational applications. hBD1 plays a critical role in the innate immune system's defence against microbial infections and constitutes one of the body's first lines of defence against pathogens. It is well-known for its broad-spectrum antimicrobial activity against various bacteria, fungi, and viruses.[24] However, the length of the sequence, the presence of six cysteine residues essential for the correct folding, as well as the need to increase hBD1 availability to produce multifunctional and biomimetic materials are the main challenges for its production by chemical synthesis. This has led us to employ the HELP carrier for the recombinant expression of hBD1 as an alternative and more sustainable route for the synthesis of this peptide.

This work describes the design, the production, the biochemical characterisation of the HELP-hBD1 fusion biopolymer (HhBD1) and the derived hBD1 peptides, as well as the biological assessment of their activity towards model microorganisms and cell lines. Derived materials such as coatings and matrices based on this new fusion biopolymer are evaluated for their interaction with biological systems.

2. Results and discussion

2.1 Production and characterisation of the HELP recombinant fusion with hBD1

hBD1 was employed to functionalise HELP to develop biomimetic components with antimicrobial properties. It has been described that this AMP is physiologically synthesised as a 68-residue prepropeptide (GenBank: CAA63405.1), the product of the *DEFB1* gene.[25] However, this product is further processed to originate functional domains ranging from 36 to 47 amino acids, which differ from each other by N-terminal truncation.[26] Two major fragments endowed with antimicrobial activity have been described; one of 47 amino acids,[27,28] and another one of 36 amino acids, which is described as the most active domain against bacterial cells.[29,30] For this reason, the fragment of 47 amino acids was selected as the fusion partner at the C-terminus of the HELP carrier (Fig. 1). Remarkably, this last sequence does not contain any acidic residue.[11] Thus, the unique aspartic acid at the beginning of the 36-residue hBD1 domain represents a specific target for the Asp-N endoproteinase, allowing the release of this active peptide from the recombinant fusion biopolymer. Following the same strategy, the addition of a triplet encoding a glutamic acid just before the open reading frame of the 47-residue hBD1 domain resulted in the presence of a second specific cleavage site, in this case for the Glu-C endoproteinase, as schematically shown in Fig. 1.

After cloning, the fusion biopolymer, named HhBD1 (HELP-hBD1, M_W 50694.45 Da), was expressed and produced in *E. coli* following a recombinant approach and purified by the inverse transition cycle, taking advantage of the thermo-responsive behaviour of the elastin domain, which is well described for the purification of ELP and ELP-based biopolymers (Fig. S1, ESI†).[33,34] On average, more than 250 mg of pure HhBD1 were obtained per litre of bacterial culture using our lab-scale production system, which is in agreement with yields reported for other ELP-AMP fusions.[35] Electrophoretic analysis of the

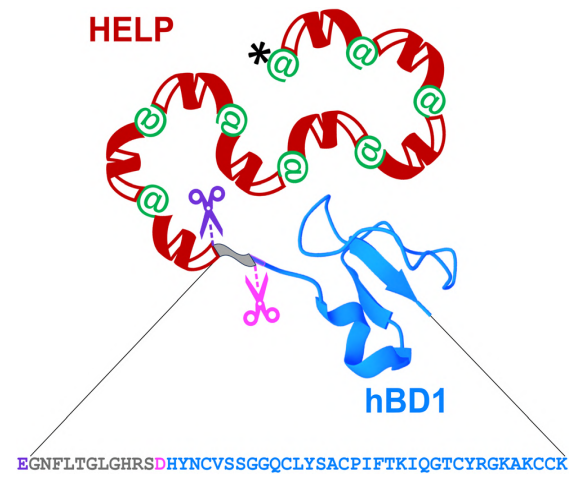

Fig. 1 Schematic representation of the recombinant HhBD1 fusion biopolymer. The hBD1 sequence (grey-blue, 47 amino acids) is fused at the C-terminus of HELP (black, his-tag; green, cross-linking domains; red, hydrophobic domains of the human elastin). The hBD1 sequence is flanked by a glutamic acid residue, the specific proteolytic cleavage site for Glu-C (purple scissors). The 36 amino acids domain (blue) can be obtained by cleavage with the Asp-N specific protease (pink scissors). The image of the hBD1 fusion domain was generated with Mol*Viewer[31] from the PDB entry 1E4S.[32]

pure HhBD1 (Fig. S1, lane 3, ESI†) showed the presence of additional bands that exhibited slower migration than that expected for the HhBD1 monomer, suggesting the presence of multimeric HhBD1 forms due to the formation of interchain disulfide bridges given that the primary structure of hBD1 contains six cysteine residues. The stability of the fusion protein at different pH values (see ESI,† Table S1) and the susceptibility to proteolysis by elastase were tested, and results are reported in Fig. S2 and S3 (ESI†). The HELP biopolymer was unaffected by both acidic and basic conditions. Intriguingly, prolonged incubation of HhBD1 in basic conditions resulted in the formation of a hydrogel-like layer on the bottom of the recipient with the consequent decrease in the concentration of HhBD1 in the supernatant.

As described above, the primary sequence of the HhBD1 biopolymer contains unique glutamic and aspartic acid residues, which are the recognition sites for highly specific endoproteinases. Therefore, the purified HhBD1 was treated with Glu-C and Asp-N to verify the release of the two hBD1 fragments (5069.42 Da and 3934.57 Da, respectively). The electrophoretic analysis (Fig. 2) showed that after the endoproteolytic reactions, most of the HhBD1 signal disappeared, accompanied by the formation of two new bands. The most prominent one migrated at the same level of the HELP band (about 50 kDa) and the other one ran along with the electrophoretic front (Fig. 2, boxed in purple), suggesting that the cleavage converted most of HhBD1 into HELP and hBD1. Both endoproteolytic reactions were performed on HELP as control and no effect on this biopolymer was observed, as expected (Fig. 2).

Turbidimetry analysis of the pure fusion biopolymer showed that, although no temperature-dependent transition

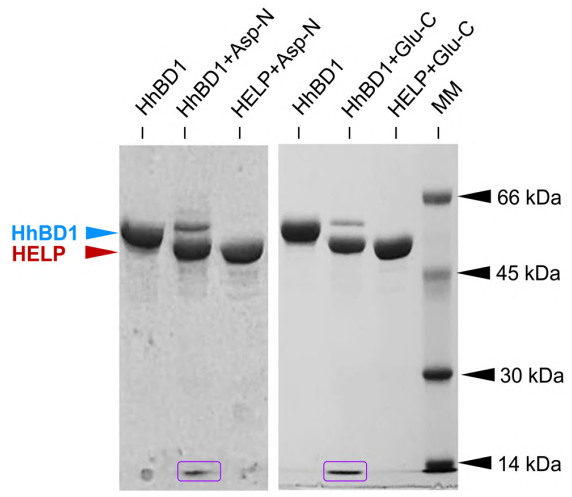

Fig. 2 Representative image of the 10% SDS-PAGE analysis of Glu-C and Asp-N specific cleavage of HhBD1 and HELP biopolymers. The electrophoretic signals corresponding to HhBD1 (blue arrow), HELP (red arrow), and the released hBD1 domains (boxed in purple) are indicated. Molecular mass markers (MM): bovine serum albumin, 66 kDa; ovalbumin, 45 kDa; carbonic anhydrase, 30 kDa and lysozyme, 14 kDa. Coomassie blue staining.

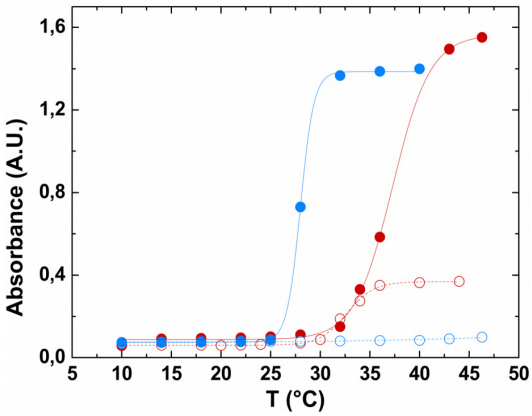

Fig. 3 Turbidimetric analysis of the HELP and HhBD1 biopolymers at 2 mg mL^{-1} as a function of temperature. HELP (red symbols) and HhBD1 (blue symbols) were dissolved in 10 mM Tris (open symbols) and 10 mM Tris/0.15 mM NaCl (filled symbols) buffers, pH 8.

was observed when the biopolymer was dissolved in buffer alone (Fig. 3, blue open symbols), in the presence of a nearly physiological concentration of NaCl, HhBD1 showed a sharper transition at a lower temperature (T_t 28 °C) compared to HELP under the same conditions (T_t 37.3 °C) (Fig. 3, compare red filled with blue filled symbols). This effect was already observed when HELP was fused with indolicidin.[15] It has been described that the fused domains, when folded, may act providing a surface in close proximity to the carrier and that the surface properties, rather than the overall hydrophobicity of the domain, play a dominant role in modulating the Tt of elastin-like carriers.[36] hBD1 exhibits an amphipathic conformation endowed with a predominantly apolar surface area (see ESI,† Table S2). This is consistent with the observed thermo-responsive behaviour of this HELP fusion biopolymer, which exhibits a lower Tt than the HELP carrier alone.

These data showed the successful expression of the HhBD1 fusion biopolymer, which retained the thermo-responsive behaviour of HELP and displayed the expected cleavage pattern established in the design of the synthetic gene.

2.2 Biological activity evaluation of the HhBD1 biopolymer

After the production of purified HhBD1 exploiting the thermo-responsive behaviour of the HELP carrier, the first concern was to verify whether the fusion biopolymer retained the antimicrobial properties of the hBD1 domain. Although it was reported that the minimum inhibitory concentration of hBD1 (MIC) against *Staphylococcus aureus* and *E. coli* strains was 4–8 mg L^{-1} and 16–32 mg L^{-1}, respectively,[30] we could not detect any activity of HhBD1 following this method. Many reasons withstand behind this observation, especially the uncontrolled redox state of the fusion biopolymer in which the disulfide bridge formation is uncontrolled and unspecific and cannot be blocked due to the recombinant nature of HhBD1, and the impossibility of performing MIC assays adding reducing agents to the media, as these are toxic to the bacterial

cells in solution. It has been described that the presence of cysteines is crucial for the antimicrobial activity of hBD1, especially the C-terminal cysteines, and that its antimicrobial capacity is closely related to the reduction of the disulfide bridges, and thus it can be evidenced in reducing environments.[29] Following a modification of the radial diffusion assay described by these authors, in the presence of 2 mM DTT, we were able to detect the antimicrobial activity for the HhBD1 fusion biopolymer towards *E. coli* ATCC 25922 strain when 100 μg of HhBD1 were deposited (containing approximately 10 μg of hBD1). In contrast, no inhibition halos were observed in the absence of the reducing agent (see ESI,† Fig. S4). This activity was also retained after the cleavage of HhBD1 with Glu-C and Asp-N, and no significant differences were observed when comparing the diameters of the inhibition zone of the digestion mixtures with those of the fusion biopolymer (Fig. 4). HELP alone did not show any antimicrobial activity in any of the tested conditions (see ESI,† Fig. S1B and C), confirming that the antimicrobial activity of the HhBD1 fusion biopolymer is due to the presence of the hBD1 domain.

The effect of HhBD1 on the viability of eukaryotic cells was tested using the WST-1 viability assay, in which the metabolic activity of osteoblastic (Fig. 5(A)) and fibroblastic (Fig. 5(B)) cells in the presence of different concentrations of HhBD1 and HELP was assessed. The viability assays did not evidence cytotoxicity on the tested cell lines. Rather, as already reported for HELP,[37] they revealed a moderate pro-proliferative effect of both biopolymers.

The evaluation of the biological activity of the HhBD1 biopolymer revealed that the fusion construct retained the antimicrobial activity, depending on the redox condition of the environment, as already described for hBD1. Furthermore, no cytotoxic effects on eukaryotic cells were detected at any of the concentrations tested (up to 500 μg mL^{-1}).

Taken together, these data point to HhBD1 as a non-cytotoxic candidate component to produce biomaterials and composites endowed with antimicrobial activity that can be specifically triggered in a reducing environment.

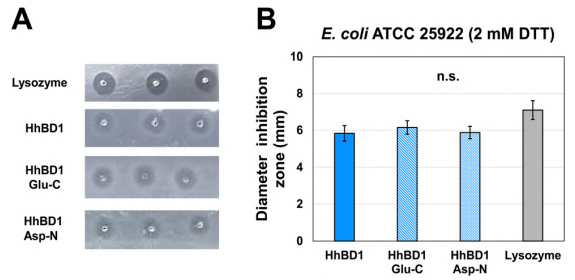

Fig. 4 Antimicrobial activity of HhBD1. (A) Radial diffusion assay performed in the presence of 2 mM DTT by incubating *E. coli* ATCC 25922 strain with the untreated HhBD1 biopolymer and with HhBD1 cleaved with Glu-C and Asp-N. Lysozyme was used as the positive control. (B) The diameter of the inhibition zones was measured and statistically analysed using a one-way ANOVA test. No significant differences (n.s.) were found with $p < 0.05$.

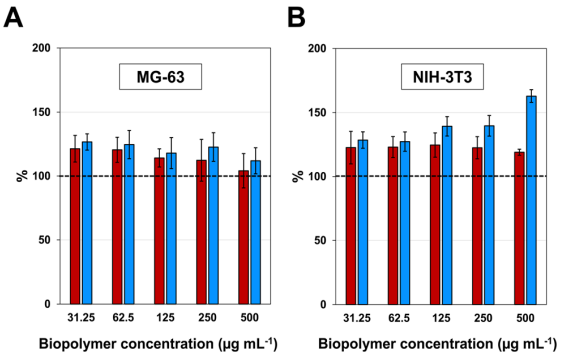

Fig. 5 Viability of (A) MG-63 osteoblast and (B) NIH-3T3 fibroblast cell lines treated with HELP (red bars) and HhBD1 (blue bars) biopolymers at different concentrations. Values were normalised to the untreated control culture (black dotted lines).

2.3 HhBD1-based 3D matrix production and characterisation

The presence of cross-linking domains in the HELP carrier has been demonstrated as a valuable prerequisite for preparing hydrogel matrices endowed with biological functionality.[15] Following an already described enzymatic method,[12] the matrix-forming capacity of HhBD1 was explored and compared with that of HELP. 4% (w/v) aqueous solutions of HhBD1 in the presence of transglutaminase showed a capacity to form a porous, spongy, hydrogel-like matrix indistinguishable from that of HELP, as shown by scanning electron microscopy (SEM) analysis (Fig. 6(A)).

Oscillatory rheology was performed on 4% biopolymer solutions containing 2 μg mL^{-1} transglutaminase to follow the kinetics of the cross-linking reaction (Fig. 6). Although the gelation point is similar for the HELP and HhBD1 systems, the storage modulus of HhBD1 is anticipated compared to HELP, indicating faster enzyme kinetics (Fig. 6(B)). This could be due to the presence of additional glutamine and several lysine residues in the hBD1 domain which may be randomly involved in the cross-linking reaction, or higher solvent exposure of the cross-linking sites for HhBD1 relative to HELP. Both samples displayed elastic (G') and viscous (G'') moduli reaching a plateau after about 90 minutes, resulting in very similar storage moduli (1.0 ± 0.1 kPa) for both matrices. This fact indicates that the HELP cross-linking domains in both biopolymers are the main target of the transglutaminase rather than the hBD1 domain. It is worth noting that the presence of the hBD1 domain lowered the Tt of the HhBD1 fusion biopolymer (Fig. 2(B)), likely favouring the proximity of the HhBD1 chains and resulting in a more efficient cross-linking process, which is in agreement with the faster gelation kinetics. Both HELP and HhBD1 samples formed strong gels, with elastic moduli that were over two orders of magnitude higher than the viscous moduli. The stress sweep analyses supported the main findings of the time sweep tests, with both gels showing a remarkably wide linear viscoelastic range (up to nearly 1 kPa) and with the fracture point of the HELP matrix being slightly anticipated at 1.2 ± 0.3 kPa (Fig. 6(C), red arrow) compared to

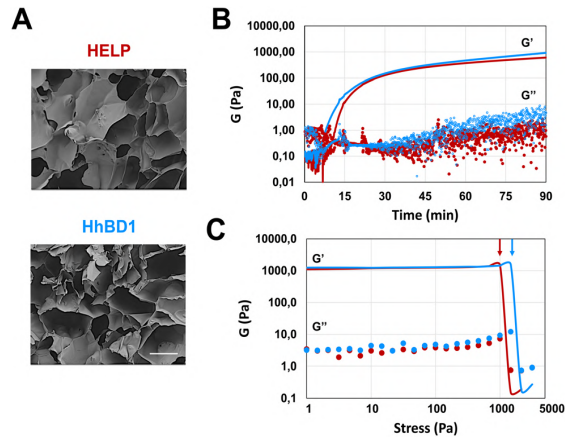

Fig. 6 4% HELP and HhBD1 hydrogel matrices. (A) SEM analysis of the freeze-dried elastin-based hydrogel matrices. The bar is 40 μm. (B) Oscillatory rheological time sweep and (C) frequency sweep analyses of HELP (red) and HhBD1 (blue) matrices. G', elastic or storage modulus; G'', viscous or loss modulus.

that of the HhBD1 gel at 1.8 ± 0.5 kPa (Fig. 6(C), blue arrow), suggesting more cross-linking points in the latter. The stability and nature of the hydrogels were further confirmed by frequency sweep analyses, which showed that the storage and loss moduli of both biopolymers were not affected by the applied frequency (see ESI,† Fig. S5). In summary, SEM and oscillatory rheology analyses evidenced that the HELP and HhBD1 matrices are comparable, although the addition of the antimicrobial domain slightly increased the cross-linking points and strength of the HhBD1 matrix.

The ability of HhBD1 to form a matrix was used as a convenient method to verify the specificity of the endoproteolytic cleavage by Glu-C and Asp-N. As described in the ESI,† each enzymatic reaction was performed on the matrix to cleave the fragments, which became soluble and were then recovered in the supernatant. The supernatant from each reaction was analysed by ESI-MS without further purification. The masses detected were consistent with those calculated for the two expected fragments, confirming the correctness of the amino acid sequence of the peptides and the high specificity of the reactions (see ESI,† Fig. S6A and B for Glu-C and Asp-N released fragments, respectively). Furthermore, these results confirmed the versatility of HELP fusion and the derived matrix to produce bioactive peptides.

2.4 Cell culture on HhBD1-derived substrates

2.4.1 Cell culture on HhBD1-based coatings. Components of the extracellular matrix send signals to cells and influence their ability to survive, divide, and exhibit certain developmental phenotypes. The cytocompatibility of the HELP and its derived materials has already been documented.[12,38] HELP has never shown cytotoxicity towards the tested cells; however, despite supporting cell adhesion, it does not accelerate it.[39] Previous results demonstrated a high cell viability of osteoblast and fibroblast cells in the presence of HhBD1 in the culture media (Fig. 5), thus, we decided to study its effect on cell adhesion and spreading. To evaluate the cell behaviour towards the HhBD1 fusion biopolymer, we prepared different surfaces based on this new construct to compare its effect with that of HELP. To analyse the cell response, HhBD1 and HELP were adsorbed on a substrate that does not support cell culture like the non-treated polystyrene, which here is referred to as NP (see also Experimental Section 4.4). Both MG-63 osteoblast and NIH-3T3 fibroblast cell lines were cultured on the coated and uncoated NP surfaces. Cells were also cultured on the standard tissue-plastic (TP) surface as the 100% adhesion control. Unexpectedly, the observation by optical microscopy showed that HhBD1 coating on NP significantly enhanced osteoblast and fibroblast cell adhesion, at the difference of the HELP coating on NP (Fig. 7(A) and 8(A)). This was confirmed by assessing both cell adhesion and viability of the two cell lines. The adhesion assay on the osteoblast cells showed that coating the NP surface with HELP only slightly improved cell adhesion (less than 20%), while the NP coating with HhBD1 increased adhesion to approximately 60%, demonstrating a remarkable ability to promote cell attachment (Fig. 7(B)). The viability assay showed that the cells that adhered to these surfaces were metabolically active (Fig. 7(C)). A similar effect was observed for the fibroblastic cell cultures. Approximately 90% of the cells remained attached to the HhBD1-coated NP surface (Fig. 8(B)), being metabolically active (Fig. 8(C)). For both cell lines, these assays showed that although the HELP coatings were able to slightly improve cell adhesion respect to the untreated NP surface, the HhBD1-coated surfaces demonstrated a higher capacity to enhance cell adhesion.

To further confirm these observations, thin-film coatings on NP were prepared with HELP and with HhBD1 to ensure a

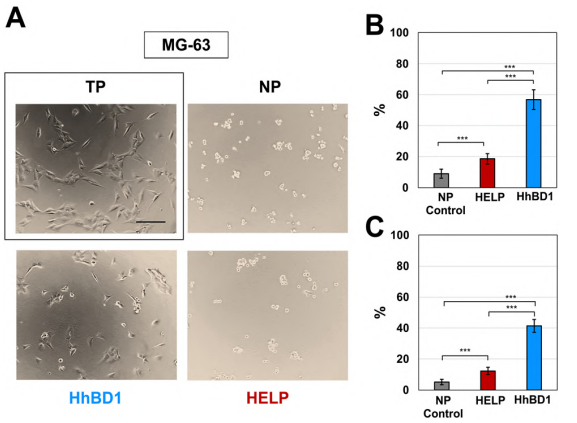

Fig. 7 HhBD1 promoted the adhesion of osteoblastic cells. (A) Representative contrast phase microscopy images of MG-63 cultures on HELP- and HhBD1-coated NP surfaces. Cells cultured on untreated NP and TP (boxed) surfaces were the negative and positive controls for cell adhesion, respectively. (B) Adhesion assay using crystal violet staining and (C) viability assay of the attached cells. Values were normalised to the control cell culture on the TP surface and statistically evaluated using a one-way ANOVA test, ***$p < 0.001$. The bar is 200 nm.

View Article Online
Paper Journal of Materials Chemistry B

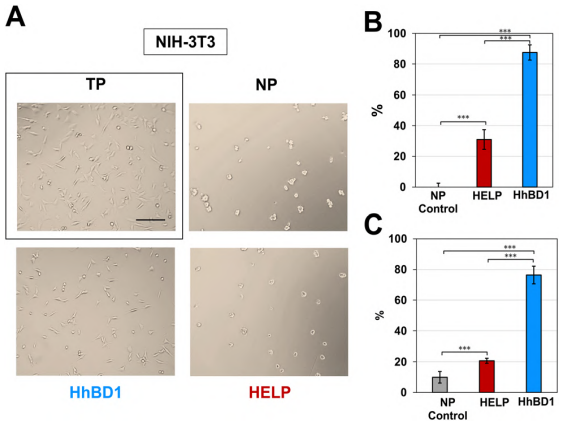

Fig. 8 HhBD1 promotes the adhesion of fibroblastic cells. (A) Representative contrast phase microscopy images of NIH-3T3 cultures on HELP- and HhBD1-coated NP surfaces. Cells cultured on untreated NP and TP (boxed) surfaces were the negative and positive controls for cell adhesion, respectively. (B) Adhesion assay using crystal violet staining and (C) viability assay of the attached cells. Values were normalised to the control cell culture on the TP surface and statistically evaluated using a one-way ANOVA test, ***$p < 0.001$. The bar is 200 nm.

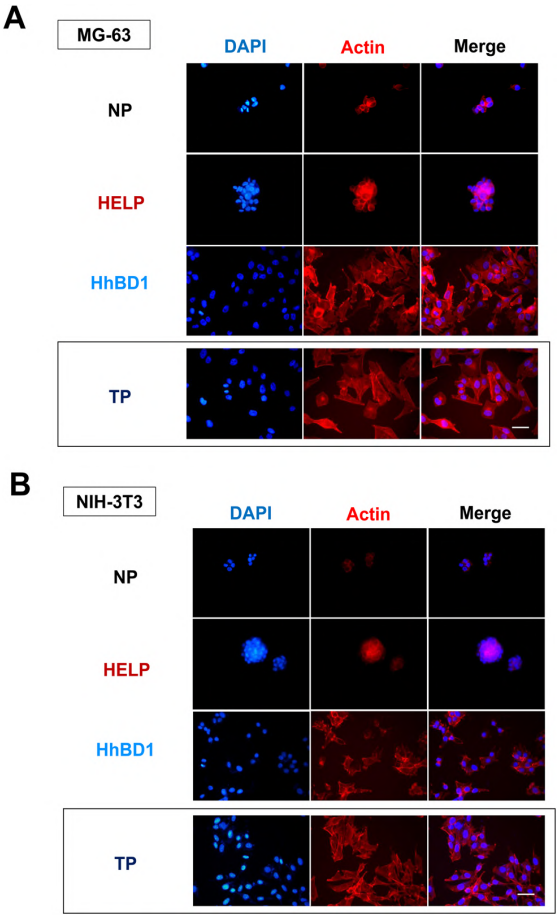

Fig. 9 Fluorescence microscopy analysis of (A) MG-63 osteoblast and (B) NIH-3T3 fibroblast cell lines grown on HhBD1 and HELP thin-film NP coated surfaces. F-actin was labelled with Alexa Fluor 594 phalloidin, and nuclei were counterstained with DAPI. The bar is 50 μm.

controlled coverage of the cell seeding surfaces with the two biopolymers (see Experimental Section 4.4). Fluorescence analysis was performed on the two cell lines cultured on the thin-films (Fig. 9(A) and (B)). To better highlight the pro-adhesive effect, cells were analysed 5 hours after seeding to prevent them from producing their extracellular matrix and starting to adhere to the substrate. Actin filaments were stained with Alexa Fluor 594 phalloidin, and nuclei were counterstained with DAPI. Consistently with previous results, only a few cells showed adhesion to the NP surface and to the HELP thin-film, whereas the HhBD1 thin-film coating strongly promoted cell adhesion to a level comparable to the culture on the TP control surface (Fig. 9(A) and (B)). DAPI staining further evidenced the difference between cultures on HELP and HhBD1 (see ESI,† Fig. S4). These results showed that the presence of the hBD1 domain on the surface has a robust pro-adhesive effect. In both cell lines, the morphology of the cells cultured on HhBD1 thin-films resembled those cultured on the control TP surface (Fig. 9). The cells cultured on the HhBD1 substrate showed highly organised actin meshwork. A slightly lower degree of spreading with respect to the cells cultured on control TP was observed. However, this could be related to irregularities on the surface of the thin-film as well as an uneven distribution of hBD1 on the surface. The cells cultured on HELP showed a different morphology, remaining rounded and showing a tendency to aggregate rather than spread, resembling the cultures on the untreated NP substrate. The DAPI staining emphasised the difference between the cultures on HELP and HhBD1 (see ESI,† Fig. S7).

2.4.2 Cell culture on HhBD1-based 3D matrix. The matrix-forming capacity of HELP could provide further evidence for the observed adhesion capacity conferred by the presence of the hBD1 domain. It was observed that although the HELP matrix is not cytotoxic and can be successfully used to encapsulate cells, proliferation was delayed, and cultures resulted in the formation of islets rather than monolayers.[12] However, it has also been reported that the fusion of adhesion signals to the HELP promotes cell adhesion on the derived hydrogel matrix.[40] To verify whether the hydrogel network derived from HhBD1 could support cell adhesion and growth, 4% HhBD1 matrices were prepared. Before seeding, extensive washing with water was performed to prevent the presence of the enzyme and of the non-crosslinked biopolymer. 24 hours after seeding, the cells cultured on these matrices were stained with toluidine blue (Fig. 10), and the effect of the presence of the hBD1 domain in the matrix became even more evident, especially when the two cultures on HELP and HhBD1 matrices were compared (Fig. 10(A) and Fig. S8A, ESI†). As previously observed,[12] cells seeded on HELP matrices remained round and aggregated, whereas cells cultured on the HhBD1 matrices adopted the morphology already observed for the cultures on TP and on the

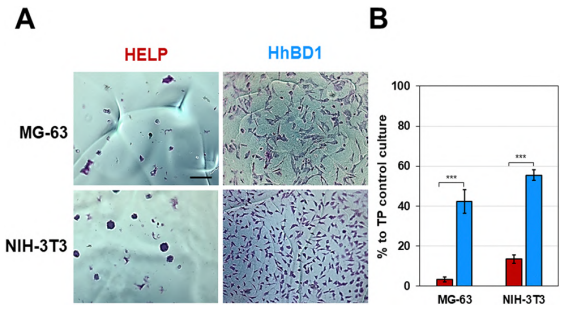

Fig. 10 HhBD1 hydrogel matrices supported cell adhesion of osteoblast and fibroblast. (A) Representative contrast phase images of cells cultured on the hydrogel matrices and stained with toluidine blue. (B) Viability assay of cells cultured on the hydrogel matrices. Values were normalised to the TP cell growth control and statistically evaluated using a one-way ANOVA test, $***p < 0.001$. The bar is 200 nm.

HhBD1 NP coated surfaces. To evaluate the cell adhesion capacity of the matrices, a WST-1 viability assay was employed as an indirect measurement of the number of cells able to attach to the matrices. Thus, before the assay, the samples were washed to remove the cells that were not attached to the matrices. The results further confirmed the remarkable difference between the two culture substrates (Fig. 10(B)).

Fluorescence microscopy analysis was carried out to examine the morphology and cytoarchitecture of the cells cultured on these matrices (Fig. 11 and Fig. S8, ESI†). Only few cell nuclei were visualised on the HELP matrix (Fig. S8B, ESI†), whereas on the HhBD1 matrix, the presence of a high number of stained nuclei was evident, indicating a robust cell adhesion of both osteoblast and fibroblast cells (Fig. S8B, ESI†). Both cell lines cultured on the HhBD1 matrices exhibited cells with a well-organised actin meshwork (Fig. 11), albeit cell dimensions appeared reduced to some extent compared to cells cultured on the standard TP surface (Fig. 9). This slight reduction in spreading may be due to the heterogeneous and irregular surface of the matrix as well as to the different surface stiffness respect that of the TP surface. However, cells were firmly attached and displayed a properly shaped cytoskeleton (Fig. 11).

These data, consistent with previous observations, confirmed that the presence of the hBD1 domain conferred to the HELP matrix a strong signalling effect for cell attachment towards both the tested lines. Interestingly, in contrast to the antimicrobial activity, the pro-adhesive capacity toward eukaryotic cells did not require reducing environmental conditions, suggesting that the peptide conformation may be a crucial factor in modulating its bioactivity. Coatings, thin-films, and hydrogel matrices derived from HhBD1 supported the osteoblasts and fibroblasts adhesion. Overall, these data revealed a pro-adhesive activity of the hBD1 domain, which, to our knowledge, is described for the first time. Although it is known that hBD1, like other β-defensins, is a multifunctional factor,[24,41] a pro-adhesive activity has so far only been demonstrated for hBD5.[42] Notably, it has recently been described that hBD1 can specifically bind to the pore region of the Kv1.3 potassium channel, leading to conformational changes while retaining the activation properties of the channel itself.[43] There is now plenty of evidence that different classes of K^+ channels play a role in integrin-dependent adhesion.[44] It has been demonstrated that these channels can be physically associated with integrins, such that the conformational change of the channel in turn affects the structure of the adjacent integrin subunit, leading to activation of the latter and cell adhesion.[45] Interestingly, these channels are reported to be involved in the regulation of cell size in non-excitable tissues.[46] Our results are consistent with these findings and may even point to a possible unexplored mechanism related to cell adhesion.

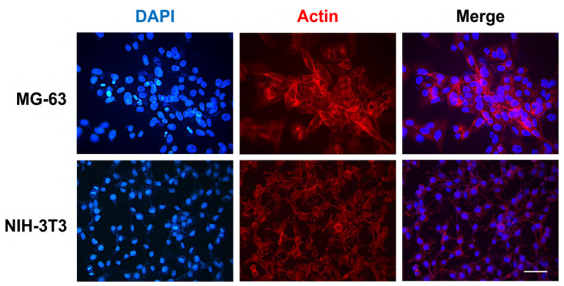

Fig. 11 Fluorescence microscopy analysis of MG-63 and NIH-3T3 cells cultured on HhBD1 hydrogel matrices. F-actin was labelled with Alexa Fluor 594 phalloidin, and nuclei were counterstained with DAPI. The bar is 50 μm.

3. Conclusions

Due to its length and conformation, the hBD1 is considered a difficult-to-synthesise sequence. The HELP carrier has been successfully employed as an alternative and more sustainable system to produce large amounts of this antimicrobial peptide with respect to chemical synthesis. The HhBD1 fusion biopolymer was produced and characterised, verifying the antimicrobial domain(s) release capacity achieved by the appropriate design of the synthetic gene. The analyses confirmed the potential of the new biopolymer, which retained both the thermo-responsive properties and the antimicrobial capacity, holding great promise to produce biocompatible and multifunctional materials. Furthermore, enzymatic crosslinking yielded remarkably strong and stable hydrogels from HhBD1. Unexpectedly, a strong cell adhesion-promoting activity was detected for the surfaces treated with the HhBD1 biopolymer as well as for the derived hydrogel matrix. This finding is consistent with recent data that indicate that hBD1 is a multifaceted factor with still unveiled biological functions and thus harbouring promise for a variety of clinical applications. Despite the development of countless strategies and materials for surface engineering, achieving efficient cell adhesion still represents a challenge. Our data indicates that the novel HhBD1 biopolymer is a versatile component for the fabrication of coatings and scaffolds that promote cell adhesion and that can be safely integrated into biological systems due to their biotic origin. In addition to being an alternative route to produce bioactive

peptides and an effective way to obtain materials that directly integrate the functional domain, the HELP platform turned out to be a valuable system to study, by a reductionist approach, the biological interactions that are still unknown or not fully elucidated at the molecular level. The opportunity to embed a functional peptide in a biomimetic moiety, the availability of a suitable inactive control, as well as the possibility to choose between different configurations, such as the liquid solution and 2D or 3D material settings, are the main features of a powerful tool to decipher the complexity of biological mechanisms.

4. Experimental

4.1 Production of the recombinant HhBD1 fusion biopolymer

Cloning, expression, and purification. The DNA sequence coding for hBD1 (GenBank: AAB21494.1) was cloned at the C-terminal region of the synthetic HELP gene, exploiting the unique restriction sites. The expression and purification of the recombinant HELP and HhBD1 biopolymers were carried out according to established protocols (see ESI†).[15] The purified biopolymer was analysed by 9% acrylamide SDS-PAGE stained with Coomassie blue as previously described.[47] The purified product was freeze-dried and stored at −20 °C for further use.

Physico-chemical characterization. Purified biopolymers were dissolved in 10 mM Tris or 10 mM Tris/0.15 mM NaCl buffer pH 8 to a final concentration of 2 mg mL^{-1}. The solutions were equilibrated at 4 °C for 16 hours before analysis. Turbidimetric analysis was performed by measuring absorbance at λ = 350 nm in a temperature range from 20 to 50 °C at a heating scan rate of 0.2 °C min^{-1} using a Jenway 6300 spectrophotometer (Hong Kong, China). The inverse transition temperature (T_t) was determined as the temperature at which the absorbance value reached 50% of its peak. For each biopolymer, three replicates were performed, and representative data sets were plotted using GraphPad Prism 10.1.0 (270) software (Boston, USA).

Specific release of hBD1 domains from the HhBD1 fusion biopolymer. The reactions with Glu-C (#P8100S, New England Biolabs, Ipswich, USA) and Asp-N (#55576-49-3, Roche, Basel, Switzerland) enzymes were set up for both HhBD1 and HELP biopolymers at a final concentration of 6 mg mL^{-1} in 15 μL of 100 mM ammonium bicarbonate buffer at pH 8. Glu-C reactions were performed at an enzyme concentration of 8.3 ng μL^{-1} for 5 hours at room temperature, while Asp-N reactions were carried out at a final concentration of 2.6 ng μL^{-1} for 18 hours at 37 °C. After the incubation with the specific endoproteinase, 15 μL of Laemmli loading buffer were added to each sample to stop the reaction and 3 μL of this mixture were analysed on 9% SDS-PAGE.

4.2 Antimicrobial and biological evaluation of HhBD1

Radial diffusion assay. Antimicrobial activity was tested for HhBD1 and the products from the reactions with the specific endoproteinase Glu-C and Asp-N described in the previous section. In parallel, control reactions were performed under the same conditions with the HELP biopolymer. All reagents and biopolymers were sterilised by 0.22 μm filtration. The final reaction volume was 500 μL containing 3 mg of biopolymer. After incubation, the reaction mixture was frozen at −80 °C and then freeze-dried. 60 μL of water were added to each freeze-dried reaction sample to concentrate the biopolymer to approximately 50 μg μL^{-1} to perform the killing assay. The antimicrobial activity against *E. coli* ATCC 25922 strain was assessed using a modification of the radial diffusion assay described by Schroeder *et al.*[29] Briefly, a single colony of *E. coli* from a fresh agar plate was used to inoculate 3 mL of 2.1% (w/v) Mueller–Hinton Broth pH 7.3 (Merck Millipore, Massachusetts, USA). 300 μL of the overnight bacterial culture were diluted in 10 mL of 2.1% (w/v) Mueller–Hinton broth and incubated at 37 °C with continuous shaking (150 rpm) for approximately 2–2.5 hours until an optical density (OD) of approximately 0.5 units was reached. At this point, the bacterial cells were harvested, washed three times with ice-cold NaPi buffer (10 mM sodium phosphate pH 7.3) and then diluted in buffer to 0.1 OD units. For the killing assay, 450 μL of this bacterial solution was mixed with 25 mL of NaPi containing 0.21% (w/v) Mueller–Hinton powder, 1% (w/v) low EEO-agarose (Sigma-Aldrich, Missouri, USA) with or without 2 mM dithiothreitol (DTT, Sigma-Aldrich, Missouri, USA). These mixtures were poured onto 10 × 10 cm plates (# 82.9923.422, Sarstedt, Numbrecht, Germany) and then cooled to RT to solidify before holes of approximately 2 mm diameter were punched using a glass Pasteur pipette connected to a vacuum pump. The holes were filled with 2 μL of the solutions prepared as described above containing approximately 100 μg of biopolymer. Lysozyme (2 μg per well) was used as the positive control. The plates were incubated at room temperature for 1 hour to allow the biopolymers to diffuse, and then they were transferred to 37 °C for up to 48 hours. Images were captured, and the diameter of the inhibition zones was measured using ImageJ software.[48] The data were statistically analysed using a one-way analysis of variance with n = 6 and $p < 0.05$.

Cell culture and viability assay. MG-63 and NIH-3T3 cell lines were routinely grown in Dulbecco's modified Eagle's medium (DMEM, Sigma-Aldrich, Missouri, USA) supplemented with 2 mM L-glutamine, 100 μg mL^{-1} streptomycin, and 100 units mL^{-1} penicillin and containing 10% (v/v) heat-inactivated fetal bovine serum. The cells were maintained in 25 cm^2 flasks at 37 °C in an atmosphere with saturated humidity and 5% CO_2. Cells were seeded in a 96-well tissue-culture polystyrene (TP) flat-shaped bottom microplate (Sarstedt, Numbrecht, Germany) at a density of 10^4 cells per cm^2 in 100 μL of supplemented DMEM and cultured under standard conditions for 24 hours. Subsequently, the supernatant was replaced with 100 μL of fresh medium containing 2× serial dilutions starting from 500 μg mL^{-1} of HELP and HhBD1, and the cells were further cultured for 24 hours. 5 μL of WST-1 reagent (Roche, Basel, Switzerland) were added per well and incubated at 37 °C for 60 minutes. Absorbance was measured at 450 nm using a microplate reader (Synergy H1, BioTek, Winooski, USA).

4.3 HhBD1 3D matrix production and characterisation

3D matrix production. Hydrogel matrices were prepared following the enzymatic cross-linking method described previously.[12] 4% (w/v) sterile aqueous solutions of HELP and HhBD1 were mixed with microbial transglutaminase (N-Zyme Biotec GmbH, Germany) to a final concentration of 2 μg μL^{-1} and the cross-linking reaction was carried out at room temperature for 1 hour. After the reaction, the matrices were washed with excess water to remove unreacted components and immediately used or stored at 4 °C.

Scanning electron microscopy. 4% HELP and HhBD1 were prepared as described above. After washing with water, they were frozen at −80 °C and freeze-dried. Slices were carefully cut, mounted on aluminium stubs covered with double-sided carbon tape, and sputter-coated with chromium using a Q150T ES plus coater (Quorum Technologies Ltd, UK). Analysis was performed using a scanning electron microscope (Gemini 300, Zeiss, Oberkochen, Germany) operating in secondary electron detection mode. The working distance was 9.3 mm, and the acceleration voltage was 5 kV.

Oscillatory rheological analysis. 225 μL of 4% (w/v) aqueous solutions of HhBD1 and HELP were mixed, by pipetting upside-down, with 7.5 μL of 60 μg μL^{-1} of transglutaminase and transferred to a flat rheometer plate of 20 mm diameter (Malvern Kinexus Ultra Plus Rheometer, Alfatest, Milan, Italy). The rheometer was then lowered to a gap of 0.6 mm, and a time sweep analysis was performed for 90 minutes (1 Hz, 1 Pa, 25 °C with Peltier temperature controller), followed by a frequency sweep (4 Pa) and a stress sweep (1 Hz). The storage (G') and loss (G'') moduli of the hydrogels were recorded from 0.1 to 10 Hz (stress 4 Pa, within the linear regime). Each test was performed in at least 2 replicates. For the graphical representation of the time and frequency sweeps, the mean value of two representative data sets was plotted, while a representative data set was used for the stress sweep analysis.

4.4 Cell culture on HhBD1-based substrates

Preparation of the coatings. Coatings were prepared either by adsorption or by deposition of the biopolymers to obtain a thin-film. Coatings by adsorption were done in a sterile 96-well nontreated polystyrene (NP) flat-shaped bottom microplate (Vetrotecnica, Padova, Italy). 100 μL of 4 mg mL^{-1} sterile (by 0.2 μm filtration) aqueous solution of each biopolymer were added per well and incubated overnight at 5 °C. Subsequently, the solution was removed, and the wells were washed two times with 200 μL sterile water. After the washes, the microplate was air-dried under a sterile hood.

Thin-film coatings (100 μg of biopolymer per cm^2) were prepared depositing 10 μl (1.25 μg μL^{-1}) of HhBD1 or HELP sterile aqueous solution (0.22 μm filtration) on the bottom (0.125 cm^2) of the microwells of a μ-slide (15-Wells uncoated μ-Slides 3D, #81506, IBIDI, Grafelfing, Germany) and then air-dried under a sterile hood at room temperature.

Adhesion and viability assays of cells cultured on coatings. For cell adhesion assays on HELP and HhBD1 surfaces coated by adsorption, 5000 cells per well were seeded in a final volume of 100 μL of supplemented DMEM. Uncoated tissue-culture-treated (TP) and uncoated NP wells were used as controls. 24 hours after seeding, the cultures were inspected by phase contrast microscopy (Zeiss Primovert contrast phase microscope), and images were acquired using a Zeiss AxioCam 202 mono camera, coupled to Zeiss Zen 3.3 acquisition software (Zeiss, Germany). Before the assays, each well was washed with PBS to remove the unattached cells. Consequently, crystal violet staining and WST-1 cell viability assays were performed on the cells that remained on the surfaces. For the crystal violet assay, the cells were fixed with 50 μL of 100% methanol for 10 minutes on ice. After removing the supernatant, 50 μL of 0.5% crystal violet in 20% methanol were added and incubated for 10 minutes. After extensive washing with water, 50 μL of a 10% acetic acid solution was added to lyse the cells and absorbance was measured at 600 nm. To assess cell viability, 24 hours after seeding the medium was changed and replaced with 100 μL of fresh medium containing 5 μL of WST-1 reagent per well and incubated at 37 °C for 90 minutes. Then, absorbance was measured at 450 nm using a microplate reader.

Cell culture on HELP and HhBD1 matrices. 4% HhBD1 and HELP matrices (w/v) were prepared as described above depositing 10 μL in the bottom of a well of a μ-Slide (15-Wells IbiTreat μ-Slides 3D, #81506, Ibidi, Grafelfing, Germany). The matrices were cross-linked for 1 hour and then washed extensively with sterile water. 5000 cells per well were seeded in a final volume of 50 μL of supplemented DMEM and cultured for 24 hours. The cultures were then inspected by phase contrast microscopy. The wells were washed with PBS. For toluidine blue staining, cells were fixed by adding 30 μL of 2% (v/v) paraformaldehyde in PBS per well and left at room temperature for 15 minutes. After washing twice with PBS, cells were stained with 10 μL of 0.5% (w/v) toluidine blue in 20% ethanol for 10 minutes. After extensive washing with water, the samples were analysed by phase contrast microscopy, and images were acquired. As an alternative to the crystal violet staining, cell adhesion on matrices was indirectly assessed by the WST-1 assay to evaluate the number of attached cells. After washing with PBS to remove the unattached cells, 50 μL of fresh supplemented DMEM containing 5 μL of WST-1 reagent were added per well. After 120 minutes at 37 °C the supernatant was transferred to a microwell plate, and absorbance was measured at 450 nm using a microplate reader.

Fluorescence analysis. Cell morphology was analysed on the cultures on HELP and HhBD1 thin-film coated surfaces as well as on 4% (w/v) matrices. The thin-film coatings were prepared in the μ-slide as described above, and 5000 cells per well were seeded on these coatings in 50 μL of supplemented DMEM. These cultures were carried on for 5 hours. For cell morphology analysis on the HELP and HhBD1 matrices, 10 μL of each 4% (w/v) biopolymer solution were deposited on glass coverslips (#01.4305.19, Vetrotecnica, Padova, Italy), and the cross-linking reaction was carried out as described above. The coverslips were placed in a sterile Petri dish, and 5000 cells in a volume of 20 μL were seeded on each matrix and incubated for

15 minutes. Then, 15 mL of supplemented DMEM were added to the Petri dish and cultured for 24 hours.

All samples were washed three times with an excess of PBS, and cells were fixed by incubation with 4% (v/v) paraformaldehyde in PBS for 15 minutes at room temperature. Samples were then washed with PBS and blocked for 10 minutes with a solution containing 5% normal goat serum and 0.1% Triton X-100 in PBS. Then, 15 μL of blocking solution containing 4′,6-diamidino-2-phenylindole (DAPI; Sigma-Aldrich, Missouri, USA) and Alexa Fluor 594 phalloidin (Molecular Probes, Eugene, USA) at a dilution of 100 ng mL^{-1} and 0.53 U mL^{-1}, respectively were added to each sample and incubated at 4 °C for 2 hours. After washing three times for 10 minutes with 0.1% Triton X-100 in PBS, the μ-slide lid was sealed, and the coverslips were mounted on glass slides. Fluorescently labelled cells were visualised using a fluorescence microscope (Leica DMLS), and images were acquired with a Leica DFC450 C camera coupled to a Leica LAS v4.13 acquisition software (Leica Microsystems, Wetzlar, Germany). Image cropping, superimposition, and analysis were performed using ImageJ software.[48]

Statistical analysis. For graphical representation, the values were represented as the mean ± SD. Unless otherwise indicated, at least three replicas were analysed. One-way analysis of variance (ANOVA) was carried out to compare the means of the different data sets within each experiment.

Data availability

The data supporting this article have been included as part of the ESI.†

Conflicts of interest

There are no conflicts to declare.

Acknowledgements

We thank Prof. Sabina Passamonti for her invaluable support and Dr Marco Stebel, Dr Davide Porrelli, and Dr Fabio Hollan for technical assistance. This work was supported by the H2020 Marie Sklodowska-Curie Action (AIMed project, grant no. 861138), the Horizon Europe STOP project, grant no. 101057961, and the iNEST (Interconnected North-Est Innovation Ecosystem) consortium funded by the European Union NextGenerationEU (PNRR). S.M. acknowledges funding from the Italian Ministry of University and Research through the PRIN program (SHAZAM grant no. 2022XEZK7K) funded by the European Union – Next Generation EU.

References

1 A. C. Conibear, A. Schmid, M. Kamalov, C. F. W. Becker and C. Bello, *Curr. Med. Chem.*, 2020, **27**, 1174–1205.
2 P. J. Jervis, C. Amorim, T. Pereira, J. A. Martins and P. M. T. Ferreira, *Soft Matter*, 2020, **16**, 10001–10012.
3 Y. Yuan, Y. Shi and H. S. Azevedo, *Multifunctional Hydrogels for Biomedical Applications*, 2022, pp. 97–126.
4 A. Rai, R. Ferrão, P. Palma, T. Patricio, P. Parreira, E. Anes, C. Tonda-Turo, M. C. L. Martins, N. Alves and L. Ferreira, *J. Mater. Chem. B*, 2022, **10**, 2384–2429.
5 A. Panjla, G. Kaul, S. Chopra, A. Titz and S. Verma, *ACS Chem. Biol.*, 2021, **16**, 2731–2745.
6 S. Deo, K. L. Turton, T. Kainth, A. Kumar and H. J. Wieden, *Biotechnol. Adv.*, 2022, **59**, 107968.
7 T. Vargues, G. J. Morrison, E. S. Seo, D. J. Clarke, H. L. Fielder, J. Bennani, U. Pathania, F. Kilanowski, J. R. Dorin, J. R. Govan, C. L. Mackay, D. Uhrín and D. J. Campopiano, *Protein Pept. Lett.*, 2009, **16**, 668–676.
8 Y. Li, *Protein Expression Purif.*, 2011, **80**, 260–267.
9 D. Wibowo and C. X. Zhao, *Appl. Microbiol. Biotechnol.*, 2019, **103**, 659–671.
10 R. Lin, S. Wang and W. Liu, *Curr. Pharm. Des.*, 2018, **24**, 3008–3013.
11 A. Bandiera, A. Taglienti, F. Micali, B. Pani, M. Tamaro, V. Crescenzi and G. Manzini, *Biotechnol. Appl. Biochem.*, 2005, **42**, 247–256.
12 A. Bandiera, *Enzyme Microb. Technol.*, 2011, **49**, 347–352.
13 A. Bandiera, A. Markulin, L. Corich, F. Vita and V. Borelli, *Biomacromolecules*, 2014, **15**, 416–422.
14 L. Corich, M. Busetti, V. Petix, S. Passamonti and A. Bandiera, *J. Biotechnol.*, 2017, **255**, 57–65.
15 L. Colomina-Alfaro, P. Sist, S. Marchesan, R. Urbani, A. Stamboulis and A. Bandiera, *Macromol. Biosci.*, 2023, e2300236.
16 D. M. Hoover, O. Chertov and J. Lubkowski, *J. Biol. Chem.*, 2001, **276**, 39021–39026.
17 E. Prado-Montes de Oca, *Int. J. Biochem. Cell Biol.*, 2010, **42**, 800–804.
18 F. Semple and J. R. Dorin, *J. Innate Immun.*, 2012, **4**, 337–348.
19 J. R. Shelley, D. J. Davidson and J. R. Dorin, *Front. Immunol.*, 2020, **11**, 1176.
20 H. Sugiwaki, M. Kotani, A. Fujita and S. Moriwaki, *J. Cosmet., Dermatol.*, 2024, **23**, 676–680.
21 M. Takahashi, Y. Umehara, H. Yue, J. V. Trujillo-Paez, G. Peng, H. L. T. Nguyen, R. Ikutama, K. Okumura, H. Ogawa, S. Ikeda and F. Niyonsaba, *Front. Immunol.*, 2021, **12**, 712781.
22 G. Li, Q. Wang, J. Feng, J. Wang, Y. Wang, X. Huang, T. Shao, X. Deng, Y. Cao, M. Zhou and C. Zhao, *Biomed. Pharmacother.*, 2022, **155**, 113694.
23 C. Q. Sun, R. S. Arnold, C. L. Hsieh, J. R. Dorin, F. Lian, Z. Li and J. A. Petros, *Cancer Biol. Ther.*, 2019, **20**, 774–786.
24 Á. H. Álvarez, M. Martínez Velázquez and E. Prado Montes de Oca, *Int. J. Biochem. Cell Biol.*, 2018, **104**, 133–137.
25 L. K. Ryan and G. Diamond, *Viruses*, 2017, **9**, 153.
26 E. V. Valore, C. H. Park, A. J. Quayle, K. R. Wiles, P. B. McCray, Jr. and T. Ganz, *J. Clin. Invest.*, 1998, **101**, 1633–1642.
27 K. Midorikawa, K. Ouhara, H. Komatsuzawa, T. Kawai, S. Yamada, T. Fujiwara, K. Yamazaki, K. Sayama, M. A. Taubman, H. Kurihara, K. Hashimoto and M. Sugai, *Infect. Immun.*, 2003, **71**, 3730–3739.

28 A. Bolatchiev, V. Baturin, I. Bazikov, A. Maltsev and E. Kunitsina, *Fundam. Clin. Pharmacol.*, 2020, **34**, 102–108.
29 B. O. Schroeder, Z. Wu, S. Nuding, S. Groscurth, M. Marcinowski, J. Beisner, J. Buchner, M. Schaller, E. F. Stange and J. Wehkamp, *Nature*, 2011, **469**, 419–423.
30 A. Bolatchiev, *PeerJ*, 2020, **8**, e10455.
31 D. Sehnal, S. Bittrich, M. Deshpande, R. Svobodová, K. Berka, V. Bazgier, S. Velankar, S. K. Burley, J. Koča and A. S. Rose, *Nucleic Acids Res.*, 2021, **49**, W431–w437.
32 F. Bauer, K. Schweimer, E. Klüver, J. R. Conejo-Garcia, W. G. Forssmann, P. Rösch, K. Adermann and H. Sticht, *Protein Sci.*, 2001, **10**, 2470–2479.
33 D. E. Meyer and A. Chilkoti, *Nat. Biotechnol.*, 1999, **17**, 1112–1115.
34 A. K. Varanko, J. C. Su and A. Chilkoti, *Annu. Rev. Biomed. Eng.*, 2020, **22**, 343–369.
35 L. Colomina-Alfaro, S. Marchesan, A. Stamboulis and A. Bandiera, *Biotechnol. Bioeng.*, 2023, **120**, 323–332.
36 K. Trabbic-Carlson, D. E. Meyer, L. Liu, R. Piervincenzi, N. Nath, T. LaBean and A. Chilkoti, *Protein Eng., Des. Sel.*, 2004, **17**, 57–66.
37 P. D'Andrea, D. Scaini, L. Ulloa Severino, V. Borelli, S. Passamonti, P. Lorenzon and A. Bandiera, *Biomaterials*, 2015, **67**, 240–253.
38 A. Bandiera, R. Urbani and P. Sist, *Annu. Int. Conf. IEEE Eng. Med. Biol. Soc.*, 2010, **2010**, 819–822.
39 A. Bandiera, L. Colomina-Alfaro, P. Sist, G. Gomez d'Ayala, F. Zuppardi, P. Cerruti, O. Catanzano, S. Passamonti and R. Urbani, *Biomacromolecules*, 2023, **24**, 5277–5289.
40 P. D'Andrea, D. Civita, M. Cok, L. Ulloa Severino, F. Vita, D. Scaini, L. Casalis, P. Lorenzon, I. Donati and A. Bandiera, *J. Appl. Biomater. Funct. Mater.*, 2017, **15**, e43–e53.
41 S. K. Ghosh, T. S. McCormick and A. Weinberg, *Front. Oncol.*, 2019, **9**, 341.
42 K. Howell and E. de Leeuw, *Biochem. Biophys. Res. Commun.*, 2018, **502**, 238–242.
43 J. Feng, Z. Xie, W. Yang, Y. Zhao, F. Xiang, Z. Cao, W. Li, Z. Chen and Y. Wu, *Toxicon*, 2016, **113**, 1–6.
44 A. Becchetti, G. Petroni and A. Arcangeli, *Trends Cell Biol.*, 2019, **29**, 298–307.
45 M. Levite, L. Cahalon, A. Peretz, R. Hershkoviz, A. Sobko, A. Ariel, R. Desai, B. Attali and O. Lider, *J. Exp. Med.*, 2000, **191**, 1167–1176.
46 M. T. Pérez-García, P. Cidad and J. R. López-López, *Am. J. Physiol.: Cell Physiol.*, 2018, **314**, C27–c42.
47 A. Bandiera, *Prep. Biochem. Biotechnol.*, 2010, **40**, 198–212.
48 C. A. Schneider, W. S. Rasband and K. W. Eliceiri, *Nat. Methods*, 2012, **9**, 671–675.

Chapter 6. Physicochemical Characterization of a Biomimetic, Elastin-Inspired Polypeptide with Enhanced Thermoresponsive Properties and Improved Cell Adhesion

This chapter introduces a research article published in the Journal of Biomacromolecules (American Chemistry Society)

Bandiera, A., **Colomina-Alfaro, L.**, Sist, P., Gomez d'Ayala, G., Zuppardi, F., Cerruti, P., Catanzano, O., Passamonti, S., & Urbani, R. (2023). **Physicochemical Characterization of a Biomimetic, Elastin-Inspired Polypeptide with Enhanced Thermoresponsive Properties and Improved Cell Adhesion**. *Biomacromolecules*, *24*(11), 5277–5289. https://doi.org/10.1021/acs.biomac.3c00782.

The last aim of the present thesis was to develop a new ELP biopolymer with broadened and enhanced compatibility compared to HELP while maintaining its potential as a fusion carrier. For this purpose, eight vertebrates' elastin aa sequences were aligned, and the most conserved region belonging to the exon 26 of the human homologue was observed. The consensus sequence of 40 aa differed from the human sequence only in 5 aa and evidenced the presence of nonapeptidic repeats composed of pentapeptidic and tetrapeptidic motifs. Based on this observation, and to maintain the same length of the HELP hydrophobic domain, a new elastin-like hydrophobic monomer consisting of 50 aa was designed. In addition, following the HELP structure, eight reiterated monomers were separated by cross-linking domains, and the new biopolymer was named “universal” ELP (UELP). The gene was assembled following the already described strategy; it was cloned in an expression vector and recombinantly produced in *E. coli*. The physico-chemical properties of this polymer were analysed and compared to those of HELP. In addition, the capacity of UELP to promote cell adhesion on non-adhesive surfaces was studied. My contribution to this journal article is as follows: investigation, conceptualisation, methodology, formal data analysis and validation, graphical representation, and original & revised draft writing. The following experiments were carried out by myself:

- UELP biopolymer cloning, expression and purification
- Cell culture. Cytocompatibility evaluation. Adhesion assays
  - Preparation of the coatings
  - Adhesion and viability assays of cells cultured on coatings

BioMACROMOLECULES

pubs.acs.org/Biomac
Article

Physicochemical Characterization of a Biomimetic, Elastin-Inspired Polypeptide with Enhanced Thermoresponsive Properties and Improved Cell Adhesion

Antonella Bandiera,* Laura Colomina - Alfaro, Paola Sist, Giovanna Gomez d'Ayala,* Federica Zuppardi, Pierfrancesco Cerruti, Ovidio Catanzano, Sabina Passamonti, and Ranieri Urbani

Cite This: *Biomacromolecules* 2023, 24, 5277−5289

Read Online

ACCESS | Metrics & More | Article Recommendations | Supporting Information

ABSTRACT: Genetic engineering allows fine-tuning and controlling protein properties, thus exploiting the new derivatives to obtain novel materials and systems with improved capacity to actively interact with biological systems. The elastin-like polypeptides are tunable recombinant biopolymers that have proven to be ideal candidates for realizing bioactive interfaces that can interact with biological systems. They are characterized by a thermoresponsive behavior that is strictly related to their peculiar amino acid sequence. We describe here the rational design of a new biopolymer inspired by elastin and the comparison of its physicochemical properties with those of another already characterized member of the same protein class. To assess the cytocompatibility, the behavior of cells of different origins toward these components was evaluated. Our study shows that the biomimetic strategy adopted to design new elastin-based recombinant polypeptides represents a versatile and valuable tool for the development of protein-based materials with improved properties and advanced functionality.

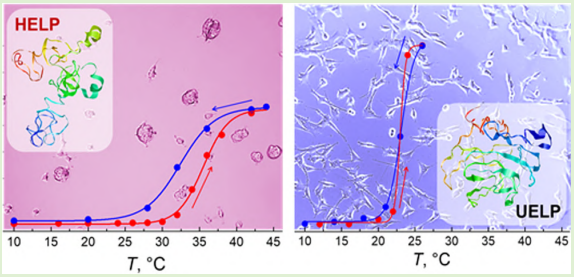

1. INTRODUCTION

Elastin is one of the main structural components of tissues that undergoes countless cycles of expansion and contraction during the lifetime of vertebrates. For this reason, it represents a valuable model to get inspiration for the design and realization of biomaterials with advanced functionality and properties.[1]

Elastin-like polypeptides (ELPs) are recombinant proteins modeled after elastin, mimicking its repetitive structure. Resembling the bovine elastin exon 18 sequence, the ELPs are constituted by long stretches of the regularly repeated VPGVG pentapeptidic motif, which is responsible for the outstanding inverse phase transition behavior that characterizes elastin and these polypeptides.[2]

In the past decade, our group focused on the human elastin homologue that shows a regularly repeated stretch of hexapeptidic rather than pentapeptidic motifs, these last being less represented and interspersed throughout its primary structure. With the aim to realize something between a protein and a polymer, following a biomimetic approach, we adopted the exon 23 and 24 amino acid sequences as the basic monomer to be reiterated. The former corresponds to a cross-linking domain, and the latter consists of the repeated hexapeptidic VAPGVG stretch, resulting in the human elastin-like polypeptide (HELP) family.[3] These versatile biopolymers were described and characterized, and a method to obtain a hydrogel matrix was set up.[4] HELP was also further modified by clonal fusion with different bioactive domains, representing a valuable carrier to increase the yield of difficult-to-express or active peptides.[5] The HELP and its modifications showed no pro-inflammatory activity and good cytocompatibility, especially toward myoblast cells.[5a,6] However, cell-type-dependent adhesion on HELP-based substrates was observed.[6,7] Although the HELP-derived hydrogel matrices showed no cytotoxicity, the cell adhesion on the HELP-based scaffold was improved by the addition of pro-adhesive sequences.[6,8] Moreover, some issues may arise because the HELP elastin-like sequence characterizing the human homologue may elicit an immune response in other organisms, like animal models being used to evaluate the compatibility of biomaterials where this sequence is not present.[9] For example, antibodies that recognize the VAPGVG motif were successfully raised in mice.[10] Last, the chemotactic activity of this same motif is well-known,[11] and this should be considered for the

Received: August 1, 2023
Revised: October 12, 2023
Accepted: October 12, 2023
Published: October 27, 2023

https://doi.org/10.1021/acs.biomac.3c00782
Biomacromolecules 2023, 24, 5277−5289

development of new biomaterials intended for prolonged contact with tissues and organs. The perspective to broaden the compatibility toward as many cell types as possible and, more generally, toward different organisms still maintaining immunotolerance and the potential as carrier fusion partners delineated our approach. Thus, to further extend the properties of the biopolymer and, hence, those of the derived materials, we undertook the assembly of a new ELP biopolymer.

In this paper, we describe the design of the sequence and the production of this construct, as well as its physicochemical characterization. The behavior of this biopolymer was compared with that of the previously described HELP prototype by analyzing it with different techniques, such as turbidimetric analysis, circular dichroism, dynamic light scattering, and nuclear magnetic resonance. The response of cells to surfaces conditioned with these recombinant biopolymers was also evaluated.

2. MATERIAL AND METHODS

2.1. UELP Biopolymer Cloning and Production. The "universal" ELP (UELP) coding sequence was assembled following the same strategy already adopted for the HELP synthetic gene.[12] Briefly, the nucleotidic sequence of 413 bp coding for a tandem repeat of the HELP cross-linking domain and the sequence coding for the nonapeptidic repeats inspired by the human exon 26 were the basic modules constituting the monomer to be reiterated. This sequence, flanked by the *Bam*HI and *BglI* restriction sites at the 5′ and by *DraIII* and *Hin*dIII at the 3′ end, was designed, optimized for *Escherichia coli* expression, and synthesized (Eurofins Genomics). Both the synthetic sequence and the pEX8EL plasmid for HELP expression were digested with *Bam*HI/*HindIII* to replace the HELP gene with the first UELP monomer. This latter was doubled by in-frame inserting another monomer by recombination of *BglI*/*DraIII* ends, cutting the vector with *DraIII*. After one more round of duplication, exploiting the same restriction sites, the UELP gene coding for eight cross-linking domains alternating with 8 hydrophobic domains was obtained and verified by sequencing (Eurofins Genomics).

Expression in *E. coli* C3730 and purification of the recombinant UELP and HELP biopolymers were carried out under standard conditions as previously described.[13]

2.2. Physicochemical Characterization. *2.2.1. Secondary Structure Evaluation.* Using the ProtParam (Expasy) program available on the SIB Swiss Institute of Bioinformatics (https://www.expasy.org/) the grand average of hydropathy value (GRAVY) for proteins was calculated. This parameter was obtained as the sum of hydropathy values of all of the amino acids divided by the number of residues in the sequence.

Prediction of secondary structures of UELP was based on the primary amino acid sequences of the polypeptides by using GOR IV software from the Expasy website (http://www.au.expasy). Moreover, the simulation of the secondary structure of proteins was performed on the I-TASSER-MTD server (multidomain Iterative Threading ASSEmbly Refinement) platform using a hierarchical protocol to predict structures and functions of multidomain (MTD) proteins (https://zhanggroup.org/I-TASSER-MTD/). This protocol predicts the domain boundaries based on the deep-learning contact-map prediction and multiple threading alignments. The individual domain models are assembled into a full-length structure under the guidance of quaternary structural templates and deep-learning distance profiles. The output of the I-TASSER-MTD server includes up to five full-length atomic models (ranked based on the total energy), estimated accuracy of the predicted models (including a confidence score of all models, and root-mean-square deviation (RMSD) for the first model), predicted secondary structures, and predicted solvent accessibility.

2.2.2. Turbidimetric Analysis. The turbidity of UELP and HELP samples was measured as absorbance at λ = 350 nm in the range of 15−50 °C at a heating/cooling scan rate of 0.5 °C·min^{-1} on a Jenway 6300 spectrophotometer. The turbidity was compared to a calibrated zero absorbance measured on the filtered solvent as a blank. Data were fitted by using a Boltzmann sigmoidal function. The inverse transition temperature (T_t) was obtained as the temperature corresponding to 50% of the maximum absorbance value. Purified proteins were dissolved to a final concentration of 2 mg/mL in 10 mM Tris/HCl buffer at pH = 8.0 (Tris) without and with 0.15 M NaCl (Tris/NaCl). Solutions were equilibrated at 4 °C for 16 h before experiments.

2.2.3. Differential Scanning Calorimetry. Thermal properties of lyophilized proteins in solution were evaluated by Differential Scanning Calorimetry (DSC) using a Setaram MicroDSC III DSC model. Stainless steel cells were filled by weight with protein samples (8 mg/mL, in Tris or Tris/NaCl buffer) and then hermetically sealed and equilibrated for 16 h at 4 °C. The calorimeter was pre-equilibrated at 5 °C for 10 min, followed by heating from 5 to 60 °C at a scan rate of 0.5 °C·/ min. The solvent was used as a reference. The inverse T_t was determined as the peak temperature (T_p). The enthalpy (ΔH_t) and entropy (ΔS_t) of the transition were determined by integration of peak area using in-house-developed graphics software. Lysozyme solution was the calibration standard.

2.2.4. Circular Dichroism. Proteins were dissolved at a concentration of 0.1 mg/mL in Tris/NaCl buffer. CD spectra were recorded at different temperatures in a thermostatic cell from 200 to 500 nm on a Jasco J-710 spectrometer under constant nitrogen flux. Data were reported as the mean molar ellipticity $[\theta]$ of the residue (mdeg·cm^2·dmol^{-1}).

2.2.5. Dynamic Light Scattering. The thermoresponsive behavior of human elastin-like polypeptides UELP and HELP was investigated by dynamic light scattering (DLS) using a Malvern Zetasizer Nano ZS instrument (Cambridge, U.K.) equipped with a 4 mV HeNe laser operating at λ = 633 nm, with a measurement angle of 173° backscattering (size diameter range 0.3 nm−10 μm).

DLS was performed on protein solutions at various temperatures and concentrations (2 mg/mL in Tris and Tris/NaCl solutions). The diffusion coefficients D and then the hydrodynamic radius R_h were calculated from intensities (Stokes−Einstein theory) as

$$D = k_B T / 6\pi\eta R_h$$

where k_B is the Boltzmann constant, T is the temperature, and η is the viscosity of the solvent. The intensity, volume, and number distributions were calculated by nonlinear least-squares fitting (NLLS, CONTIN algorithm) of the autocorrelation function measured in the experiment. In the case of broader and multimodal distributions, multiexponential fitting was used.

Through DLS analyses, the inverse transition temperature (T_t) and the hydrodynamic diameter (D_h) of UELP and HELP aggregates in Tris and Tris/NaCl solutions were determined on 2 mg/mL biopolymer solutions. DLS analyses were carried out in a temperature range between 10 and 60 °C, with temperature increments of 2 °C and an equilibration time of 180 s for each temperature increase. The temperature at the curve inflection point (i.e., the temperature above which the transition to 100% of a single large particle occurs) was taken as the inverse transition temperature, T_t.

To evaluate the stability of the self-assembled polypeptide aggregates, particle size measurements were made at a fixed temperature above T_t (40 °C) and repeated every 300 s over a period of 1 h to determine the constancy of the diameters of the particles (Table 1S, Supporting Information).

2.2.6. ^{1}H NMR. The temperature-dependent self-assembly of UELP and HELP was also investigated through variable temperature ^{1}H NMR spectroscopy. Five milligrams per milliliter biopolymer solutions in D_2O were prepared and investigated in the 10−60 °C range with consecutive temperature increments of 10 °C, using a Bruker Avance III 400 MHz spectrometer (90° pulse width 7.5 ms, relaxation delay 1 s, acquisition time 1.4 s, and 128 scans).

2.3. Cell Culture. The MG-63 and NIH3T3 cell lines were routinely grown in Dulbecco's modified Eagle's medium (DMEM, Sigma-Aldrich) supplemented with 2 mM L-glutamine, 100 μg/mL streptomycin, and 100 units/mL penicillin and containing 10% (v/v) heat-inactivated fetal calf serum. Cells were maintained at 37 °C in a

https://doi.org/10.1021/acs.biomac.3c00782
Biomacromolecules 2023, 24, 5277−5289

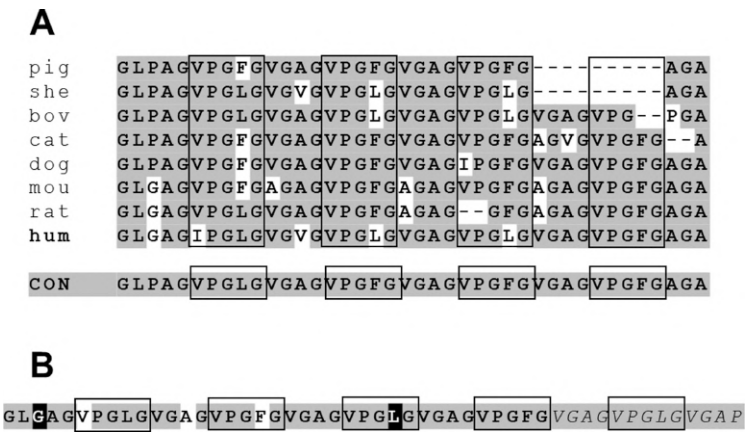

Figure 1. Comparison of part of the exon 26 sequence of elastins from different species. (A) Porcine (XP_020941438.1), ovine (XP_042096308.1), bovine (AAA30505.1), feline (XP_019676153.1), canine (XP_048967017.1), murine (NP_031951.2), rat (NP_036854.1), and human (AAC98395.1) homologues are aligned. In gray are the residues that are the most conserved among these species and that represent the consensus sequence for this region. Boxed, the pentapeptidic motif is followed by a tetrapeptidic block, thus forming the nonapeptidic repeat that characterizes this region. (B) Sequence of UELP hydrophobic domain. Gray, residues corresponding to the consensus; black, residues that are found in the human sequence and were maintained; white, residues that correspond to the consensus and differ from those of the human sequence and that were maintained to enhance the regularity of the repeated sequence; italics, motifs that were repeated to obtain a 50 amino acid domain; boxed, the elastin pentapeptidic repeats.

saturated humidity atmosphere containing 5% CO_2 in 25 cm^2 flasks. To assess the cytocompatibility of recombinant biopolymers, the cells were cultured in a 96-well microplate. Both tissue-culture-treated (TP) and -nontreated (NP) polystyrene plates were used. The wells were filled with 100 μL of a 0.4% (w/v) aqueous solution of each biopolymer that was previously sterilized by 0.22 μm filtration. After overnight incubation at 5 °C, the solution was removed, and the wells were washed two times with 200 μL of sterile water and then air-dried under a sterile hood. Five thousand cells/well were seeded in a final volume of 100 μL. After 24 h, the adhesion assay was performed by crystal violet staining.[14] Briefly, each well was washed with PBS, and the cells were fixed with 50 μL of 2% (v/v) paraformaldehyde/PBS for 20 min. After two washes, cells were stained with a solution of 0.5% crystal violet in 20% ethanol for 10 min. After extensive washing with water, 50 μL of a 10% acetic acid solution was added to lyse cells, and the microplate was analyzed by an UV/vis plate reader at a wavelength of 600 nm.

3. RESULTS AND DISCUSSION

3.1. Structure of the Recombinant Biopolymers Inspired by Human Elastin. The design of new human elastin homologues started almost two decades ago, and it was initiated with a view to prepare materials with advanced functionality based on components, possibly combining some features of the synthetic polymers, like the very regular structure and the controlled composition, with those of the living organisms, like the biotic origin. Back then, collagen was a well-established paradigm, while elastin and the pentapeptidic motif showing temperature-dependent inverse phase transition behavior was an emerging model.[2b15] At the time, most of the studies were undertaken to adopt a "reductionist approach" since each elastin exon encodes an independent domain with its own structure so that it could be studied and characterized by the use of synthetic peptides resembling its sequence.[16] However, the opportunity to reiterate the same domain in long chains offered by genetic engineering allowed us to magnify the physicochemical features of a single domain, especially regarding thermoresponsive behavior.[17]

Thus, following a biomimetic strategy, Bandiera and co-workers focused their attention on the most regularly repeated region of the human elastin homologue. At difference with most of the other elastin-like polypeptides described in the literature at the time, a construct comprising both the cross-linking domains as well as the hydrophobic domains was produced to obtain an ELP biopolymer better resembling the elastin structure. This construct was named HELP (human elastin-like polypeptide).[12] To characterize the physicochemical properties, a second prototype was also produced[3] as a reference more closely related to most of the other described ELPs, which were composed of just long stretches of pentapeptidic repeats without any cross-linking domain.[18] VAPGVG, the hexapeptide-based hydrophobic HELP domain characterizes the primate elastins,[9] and recently, these sequences were described to improve skin elasticity and reduce wrinkles.[19] However, the hexapeptidic motif and its permutations are described as matrikines.[20] Although the HELP turned out to be a valuable component in obtaining hydrogel matrices and a versatile carrier for bioactive domains, this factor may limit, to some extent, the applications of this biopolymer. For this reason, a more accurate analysis of the elastin sequence led to the selection of another monomer to build a construct that overcomes these constraints while maintaining the desired properties. The attention was focused on a regularly repeated as well as much conserved hydrophobic domain among the different organisms in the view of producing a new human-based elastin-like polypeptide with broad compatibility and robust immune tolerance while maintaining the potential as a carrier fusion partner. Aligning several vertebrate elastin amino acid sequences, a highly conserved region is observed, corresponding to part of the exon 26 of the human homologue, which is shown in Figure 1.

Comparing the sequences, a consensus of 40 amino acids, differing in only five positions with respect to the human sequence, can be outlined, evidencing a nonapeptidic repeat composed of the pentapeptidic, VPGL/FG, and the tetrapeptidic, L/VGAG, motifs (Figure 1A). Interestingly,

https://doi.org/10.1021/acs.biomac.3c00782
Biomacromolecules 2023, 24, 5277−5289

exon 26 was described to have a dominant role in the temperature-driven self-assembly of elastin.[21] On this basis, a 50 amino acid repeated sequence identical to the human one except for three positions and one additional nonapeptidic repeat was designed, maintaining the same length of the HELP hydrophobic domain (Figures 1B and 1S). Adopting the same sequence of the HELP cross-linking domains, a new gene that was named "universal" ELP (UELP) with eight reiterated monomers and a length comparable to that of HELP was assembled. In Figure 2A, the schematic primary structures of

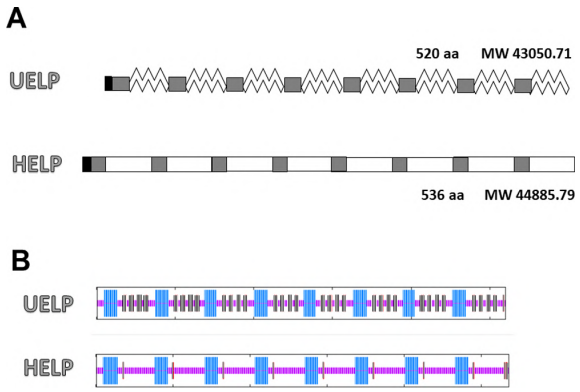

Figure 2. Comparison of the structure of the polypeptides inspired by the elastin human homologue. (A) Schematic representation of the primary structure of the UELP and HELP recombinant proteins. Black, his-tag; gray, cross-linking domains; and white, hydrophobic elastin-like domains. (B) Prediction of the secondary structure of the two biopolymers obtained by I- TASSER simulation. Purple, coil; light blue, helix; and gray, β-strand.

the two recombinant biopolymers derived from human elastin are compared. They represent a system that allows the amino acid sequence (Figure 1S, Supporting Information) to be correlated with the behavior of the biopolymer as well as with the features of the derived materials and with any biological interaction.

3.2. Macromolecular Features of UELP. The distribution of secondary structures in the UELP polypeptide was predicted using GOR IV based on the amino acid sequences. The results, compared with those obtained for HELP, are shown in Figure 2B and Table 1.

An average α-helix content of 25% for the UELP sequence, very close to the corresponding value for the HELP one, was predicted since, in both biopolymers, the polyalanine stretch is present in the cross-linking domains (Figure 1S). Based on the same calculations, the hydrophobic domains of UELP were predicted to have a mixed, partially disordered structure consisting of 24% β-sheet and 51% random coil regions. The β-sheet fraction of the UELP sequence is significantly higher than that calculated for HELP (4%), which rather possesses a higher fraction of random coil sequences (70 vs 51% of UELP). For both biopolymers, it was predicted that β-sheets occur only in the hydrophobic regions (gray fractions in Figure 2B).

Table 1 also shows the distributions of secondary structures for the UELP and HELP biopolymers obtained by deconvolving the spectra of CD measured below the T_t (Figure 3A,B, blue line), showing consistency between theoretical and experimental data.[22] Typical negative bands around 200 and 222 nm ($\pi\pi^*$ and $n\pi^*$ transitions, respectively) were observed. The difference between UELP and HELP in the CD signal, mainly around λ = 207 nm (Figure 3), is likely due to the large positive contribution of the β-structure/β-turns domains of the UELP sequence compared to HELP (Table 1), which resulted in a band with a less negative value (cf. Figure 3A with 3B, blue lines). Interestingly, the UELP biopolymer spectra showed a marked dependence on temperature (Figure 3A) with a significant increase of $[\theta]$ above the T_t temperature (>20 °C). This is likely due to the stabilization of the β-structure assembly after the water removal. On the contrary, this trend is not evident for the HELP biopolymer since, increasing the temperature, the CD spectra remained relatively constant, suggesting a predominantly random coiled structure of the hydrophobic domain (Figure 3B).

A snapshot of the two UELP and HELP protein structures (Figure 4) was generated using multidomain I-TASSER-MTD algorithms on the online platform server.[23] The high-quality three-dimensional (3D) model predictions of the proteins were calculated by deep-learning contact-map prediction and multiple threading alignments starting from the primary structure. Figure 4 clearly shows the larger proportion of β sheet domains of UELP compared to the HELP polypeptide, resulting in a more compact structure, as also supported by the calculated average gyration radii, R_G, from the structures obtained in I-TESSER-MTD simulations, which give R_G = 7.3 and R_G = 9.0 nm for UELP and HELP, respectively.

3.3. Physicochemical Properties of UELP and HELP. *3.3.1. Turbidimetric Analysis.* The inverse thermal transition of UELP in solution was studied by turbidimetric and calorimetric measurements, comparing its behavior with that of the polypeptide HELP in the absence and presence of a nearly physiological salt concentration. It is known that the presence of cross-linking domains among the hydrophobic sequences of elastin strongly influences its thermoresponsive behavior. A near-physiological NaCl concentration is required for optimal coacervation of these types of primary structures.[2b,7,24] On the other hand, for ELPs, which in most cases do not have cross-linking domains, the addition of salt lowers T_t, so this condition is exploited for the purification of these polypeptides.[15,18,24b,25] Thus, salt concentration likely plays an awkward role in modulating the phase transition of polypeptides that have alternating hydrophobic and cross-

Table 1. Comparison of the Main Parameters and Distribution of Secondary Structures of UELP and HELP Biopolymers as Predicted Using GOR IV Based on Amino Acid Sequences

		pI	a.a.	Mw	% polar a.a.	% charged a.a.	α %	β %	rc %
UELP	theor	11.7	520	43050	2	4.5	25	24	51
	CD						17	23	60
HELP	theor	11.7	536	44885	2	4.3	26	4	70
	CD						29	10	61

https://doi.org/10.1021/acs.biomac.3c00782
Biomacromolecules 2023, 24, 5277−5289

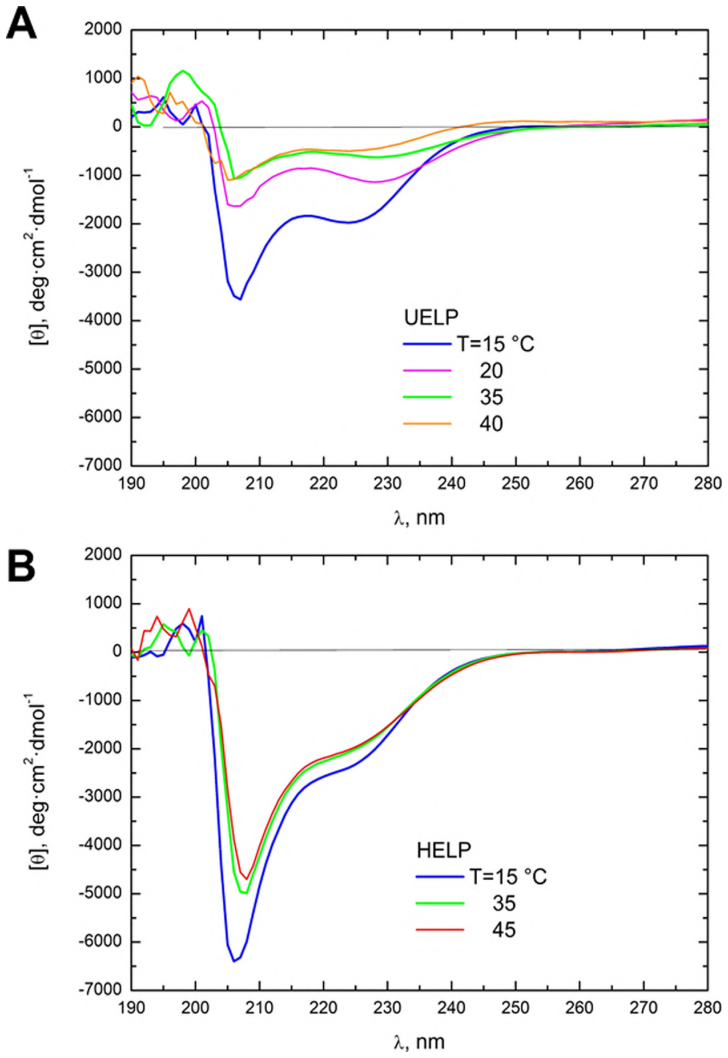

Figure 3. CD spectroscopic analysis of the two elastin-inspired polypeptides UELP (A) and HELP (B) at a concentration of 0.1 mg/mL as a function of temperature: blue line: 15 °C; purple line: 20 °C; green line: 35 °C; orange line: 40 °C; and red line: 45 °C.

linking domains in their sequence, mimicking the primary structure of elastin. The hydrophobic folding and self-assembly processes of UELP and HELP were followed at a specific temperature scanning rate, as described in Section 2. Figure 5 shows the results of the turbidimetric analysis of UELP compared to the biopolymer HELP, which was previously characterized.[7]

Strikingly, in the absence of salt, the 2 mg/mL UELP biopolymer solution (Figure 5A, open symbols) shows a negligible turbidity variation. The T_t of about 27 °C was determined by fitting the transition curve with a Boltzmann sigmoidal function. On the other hand, the HELP sample shows an increase in turbidity of the solution with a T_t of 32 °C under the same conditions (Figure 5B, open symbols).

The addition of 0.15 M NaCl to the UELP biopolymer solutions resulted in a significant and sharp increase in turbidity at a T_t of approximately 22 °C (Figure 5A, filled symbols), indicating full recovery of the transition phase property. In the case of HELP, the addition of a near-physiological salt concentration tended to increase the T_t to about 35 °C (Figure 5B, filled circles).

However, this is consistent with our previous observation on dilute solutions of the biopolymer HELP.[7] A polypeptide consisting of the same HELP hydrophobic hexapeptidic sequences but lacking the cross-linking domains showed significantly higher T_t with respect to HELP and was not affected by the addition of a near-physiological salt concentration.[7] In contrast, the addition of the same salt concentration to the HELP solution resulted in an increase in T_t, suggesting that HELP, once the effect of the presence of the cross-linking domains is attenuated by a near-physiological salt concentration, tends toward the T_t of the sequence without the cross-linking domains.[7]

The behavior of the UELP biopolymer was markedly different from that described above for HELP, suggesting that the presence of the cross-linking domains alternating with the elastin-like regions based on the nonapeptide repeats of exon 26 had a dramatic effect that nearly abolished the ability of UELP to phase transition. However, the addition of salt at

https://doi.org/10.1021/acs.biomac.3c00782
Biomacromolecules 2023, 24, 5277−5289

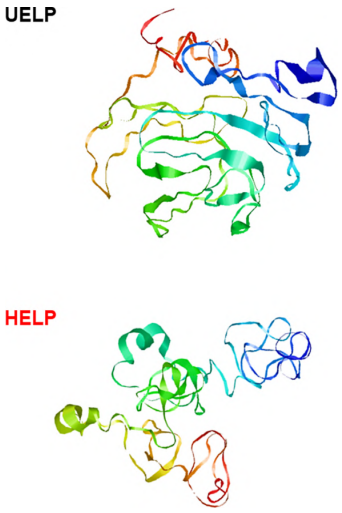

Figure 4. Model of the minimized secondary structure of UELP and HELP obtained by the I-TASSER − MTD simulation.

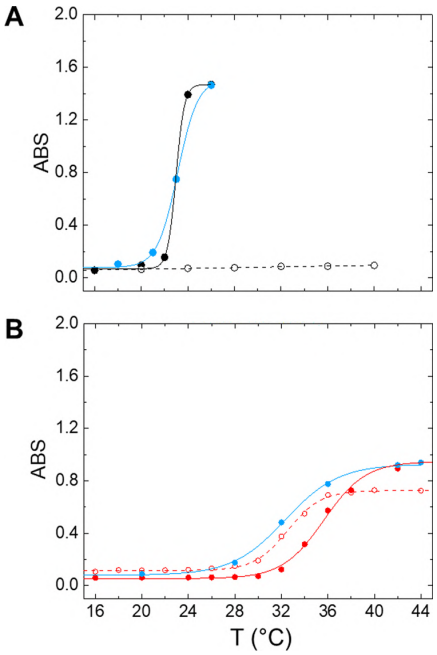

Figure 5. Turbidimetric analysis of the human elastin-derived biopolymers as a function of temperature. UELP (A) and HELP (B) were solved at 2 mg/mL in 10 mM Tris buffer (open symbols) and in Tris/NaCl (solid symbols). Cooling turbidity profiles (in blue) were analyzed in Tris/NaCl buffer.

near-physiological concentrations fully restored the thermoresponsive behavior of the UELP biopolymer, which exhibited a sharper transition at a much lower T_t with respect to that of HELP, confirming that this salt concentration is essential to avoid hampering the temperature transition process of the elastin-like sequences in the presence of the cross-linking domains. The reversibility of the phase transition of UELP and HELP was analyzed in the presence of a near-physiological salt concentration by cooling the samples after the transition. A clear difference between the two biopolymers can also be seen in this process (Figure 5A,B, see the blue lines). In the case of UELP, the curve obtained by cooling almost overlaps with the aggregation curve, while HELP heating and cooling ramps lead to two different, less steep curves that exhibit some hysteresis, suggesting a more stable supramolecular configuration as a function of temperature.

Taken together, these results indicate different self-assembly behaviors of the two biopolymers. The sharper transition of UELP and its prompt reversal compared with the slower HELP turbidity increase with hysteresis during cooling suggested two different aggregation and dissolution mechanisms. The observed different values of the average gyration radii calculated above, which are lower for UELP than for HELP suggest different compaction capacities of the two different hydrophobic sequences. On the other hand, the presence of the cross-linking domains in the biopolymers may also contribute to explaining the different hysteresis observed. Thus, in addition to the interactions among the hydrophobic elastin-like domains, an interplay among the cross-linking domains may be expected.[26] In the case of UELP, the hydrophobic sequences derived from the exon 26 are optimized to strongly promote the self−assembly to a more compact structure,[27] likely overcoming all other possible interactions. Conversely, the delayed HELP coacervation process may allow further interactions beyond the hydrophobic aggregation,[26] leading to a more stable final configuration.

3.3.2. Differential Scanning Calorimetry. DSC experiments were performed to compare and further verify the inverse phase transition properties of UELP and HELP biopolymers. The results are shown in Table 2. The measurements were performed under the same conditions as the turbidimetric analyses, and the behavior of the biopolymers was analyzed in the same Tris buffer solution with and without 0.15 M NaCl. Except for UELP in the absence of salt, an endothermic asymmetric peak was always observed.

Table 2. Thermodynamic Results of the DSC Analysis of 8 mg/mL UELP and HELP in 10 mM Tris Buffer, pH = 8, in the Absence and Presence of 0.15 M NaCl

		T peak	ΔH_{tr} kJ/mol	ΔS_{tr} J/mol K
UELP	TRIS	ND	ND	ND
	TRIS/NaCl	23	29.0	98
HELP	TRIS	29	198.0	655
	TRIS/NaCl	34	35.0	114

According to the turbidimetric analyses, UELP in the presence of NaCl exhibited the lowest peak T_t (23 °C) and showed a greater tendency to transition compared to HELP. As previously reported,[7] ΔH_{tr} can be a useful method for studying the relative hydrophobicity of polypeptides because the lower the transition enthalpy, the lower the hydrophobicity of the polypeptide. Prediction from the sequence data showed that UELP and HELP had similar proportions of polar and charged groups (6.5 and 6.3%, respectively, Table 1), resulting in similar ΔH_{tr} (29 and 35 kJ/mol, respectively) and ΔS_{tr} values (98 and 114 kJ/mol K, respectively), although UELP always had the lowest values, indicating lower hydrophobicity compared with HELP. The DSC data in Table 2 show good agreement between the T_t values and those obtained by turbidimetric analysis under the same conditions (Figure 5). According to these analyses, the data in Table 2 show a significant difference in T_{peak} temperatures between UELP and

https://doi.org/10.1021/acs.biomac.3c00782
Biomacromolecules 2023, 24, 5277−5289

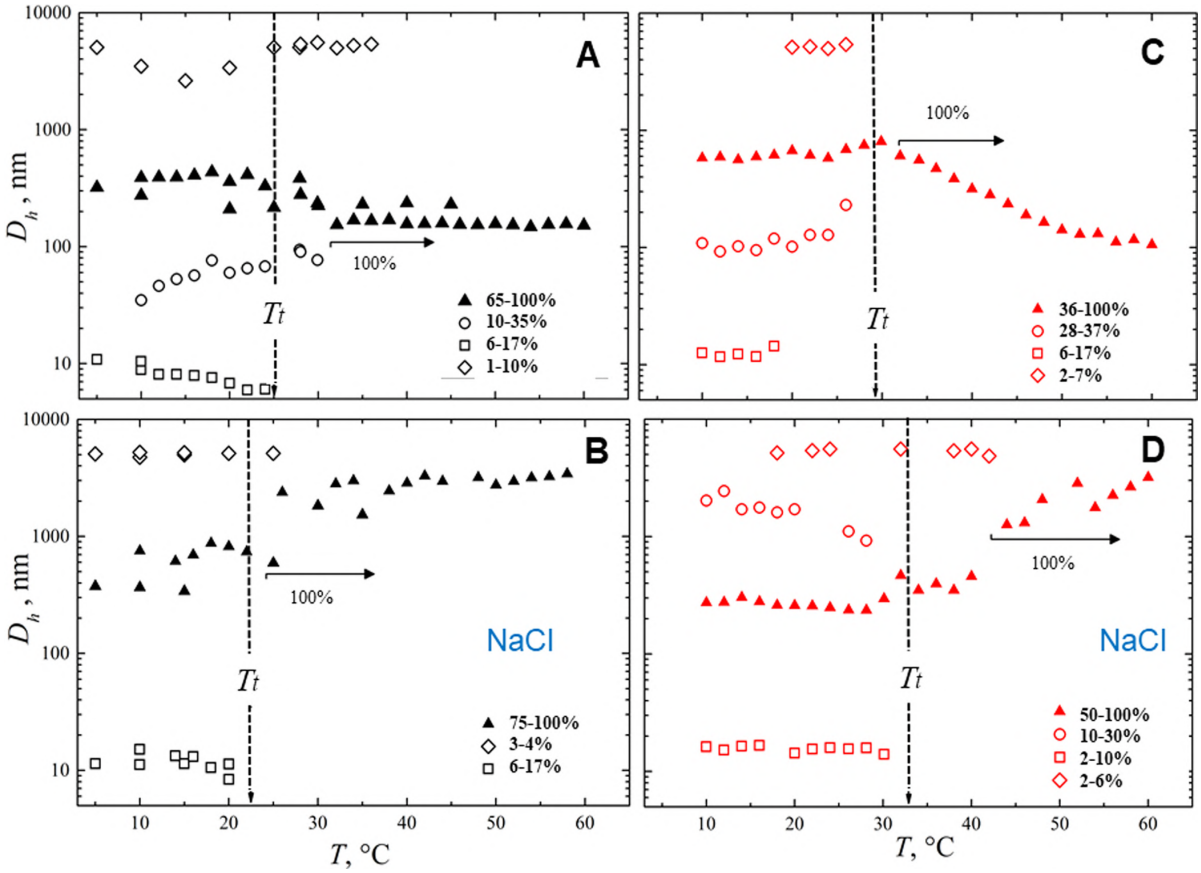

Figure 6. DLS diameters (intensity-based calculated values) for UELP (black symbols) and HELP (red symbols) in 10 mM Tris (A, C, respectively) and in 10 mM Tris/NaCl buffer (B, D) at a concentration of 2 mg/mL as a function of temperature ranging from 10 to 60 °C at a scanning rate of 0.5 °C/min. The vertical dashed bars show the respective T_t values; the horizontal arrows show the predominant size distribution.

HELP proteins, probably due to the higher proportion of β-structures in the UELP sequence. It is likely that, although HELP shows a higher hydrophobicity with respect to UELP, this latter has a higher propensity to adopt the β-structure, making it the most efficient in promoting the hydrophobic interactions and the supramolecular assembly.[27,28]

3.3.3. Dynamic Light Scattering Characterization. By using the DLS technique, we measured the hydrodynamic diameters of the biopolymers in solution and the dimensions of the aggregate sizes as a function of temperature. Figure 2S shows the intensity and volume size distribution of the hydrodynamic diameter (D_h) for UELP and HELP at different salt concentrations at 15 °C. The size distribution, determined as the scattering intensity, showed a multimodal pattern over a wide dimensional range, indicating the presence of particles of various sizes, most of which were centered around 10 nm, as confirmed by the volume size distribution (Figure 2S). This indicates that, below the transition temperature, the smallest biopolymer particles were predominant at room temperature, while the proportion of the largest self-assembled particles was low despite the total scattering intensity being the highest.

Figure 6 shows the average diameter values, D_h, of UELP (Figures 6A,B, black symbols) and HELP (Figure 6C,D, red symbols) in the absence and presence of a near-physiological NaCl concentration as a function of temperature.

The percentages of the peak areas (Figure 6A–D, in the insets), as well as the particle size values, were determined from scattering intensity distribution. T_t was determined at the inflection point of the DLS curve for each sample and is evidenced in Figure 6 (vertical dashed bars).

In the absence of salt and below T_t, a multimodal size distribution was observed for both biopolymers at a concentration of 2 mg/mL (Figure 6A,C). A four-modal size distribution (average D_h of 10, 60, 300, and 3500 nm) was observed for the UELP biopolymer (Figure 6A), with a prevalence (65–100%) of the D_h = 300 nm-sized particles. Under the same conditions, the HELP biopolymer (Figure 6C) showed a similar four-modal size distribution as well, with the main fraction (36–100%) consisting of particles with a D_h = 600 nm. Interestingly, although the two biopolymers showed different behavior above the T_t, both exhibited a monomodal particle size distribution, with an average particle size of about 150 nm at the highest temperature studied (60 °C, Figure 6A,C). However, despite the temperature increase, the UELP particle size remained constant (Figure 6A), whereas the HELP particle size gradually decreased with the temperature rise (Figure 6C). In the presence of 0.15 M NaCl and below T_t, the UELP biopolymer showed a three-modal particle size distribution (Figure 6B), with a prominent fraction of D_h = 600 nm (75%, filled triangles) and two smaller fractions of D_h = 10–15 nm (6–17%, open squares) and D_h = 5000 nm (3–

https://doi.org/10.1021/acs.biomac.3c00782
Biomacromolecules 2023, 24, 5277–5289

4%, open diamonds). Above T_t, again, a monomodal particle size distribution was observed, with a tendency to stabilize aggregates with a D_h of about 3000 nm (Figure 6B, filled triangles with 100% scattered light). Below T_t, the HELP biopolymer (Figure 6D) showed a four-modal distribution with a main fraction (about 50%, filled triangles) with a D_h of 250 nm. Above the T_t, a further temperature increase resulted in a monomodal particle size distribution with a gradually increasing D_h up to about 3000 nm (Figure 6D, filled triangles, 100% of scattered light).

These results show that in the absence of salt and above T_t the HELP sample has a tendency to gradually decrease in particle diameter, suggesting a change from expanded to contracted structures as a function of temperature as previously described for these hexapeptidic sequences.[24b] In contrast, under these conditions, the UELP particle size stabilized around a value that remained constant despite the temperature increase (compare Figure 6A with 6C), suggesting prompt and optimized particle assembly. It can be surmised that for the HELP biopolymer, the structural transition occurred gradually over a temperature range of 30 °C (Figure 6C), which could be due to the higher chain flexibility of the HELP compared to the UELP biopolymer. This is also confirmed by the secondary structure analysis (Figure 2B and Table 1), which shows a higher proportion of random coil sequences in HELP compared with UELP (70 and 51%, respectively). HELP may, therefore, undergo a progressive molecular collapse associated with a realignment of water molecules and a restructuring of hydrogen bonding networks (i.e., peptide−peptide hydrogen bonds replace water−water hydrogen bonds in the nearest solvation shells), gradually displacing water from the hydrophobic moiety and leading to a decrease in particle size.[24b] On the other hand, a significant presence of β-domains in the hydrophobic sequences of UELP is expected (Figure 2B and Table 1), and this likely leads to a more efficient structural collapse process in the local secondary structure and to a rapid rearrangement of water once the critical T_t threshold is reached.[29]

According to our previous observations and the results of turbidimetric analyses, the decrease in T_t of UELP upon addition of salt (Figure 7A) and the previously observed increase in T_t of HELP upon addition of salt (Figure 7B) confirmed the expected critical role of physiological salt concentration in restoring the thermoresponsive properties of elastin-like sequences when inserted between cross-linking domains.

The effect of salt addition not only masks the effect of cross-linking domains but also leads to a different interaction between ions, the hydrophobic thermoresponsive sequence, and water molecules in the nearest hydration shells. Ions diffusing into the nearest hydration shell of the polypeptide can interact strongly with the peptide chain and facilitate the structural folding of the hydrophobic domain.[30] In addition, the ions can disrupt the hydrogen-bonded water network around the protein and promote the formation of hydrogen bonds within the hydrophobic sequence moiety while displacing solvation water molecules from the nearest hydration shell. In the presence of salt and above the T_t, both biopolymers showed the ability to form particles with larger dimensions than in the absence of salt. Above T_t, the UELP biopolymer, during the temperature increase, showed a constant particle size with a large D_h of about 3500 nm during the temperature increase (Figure 6B), while the particles of

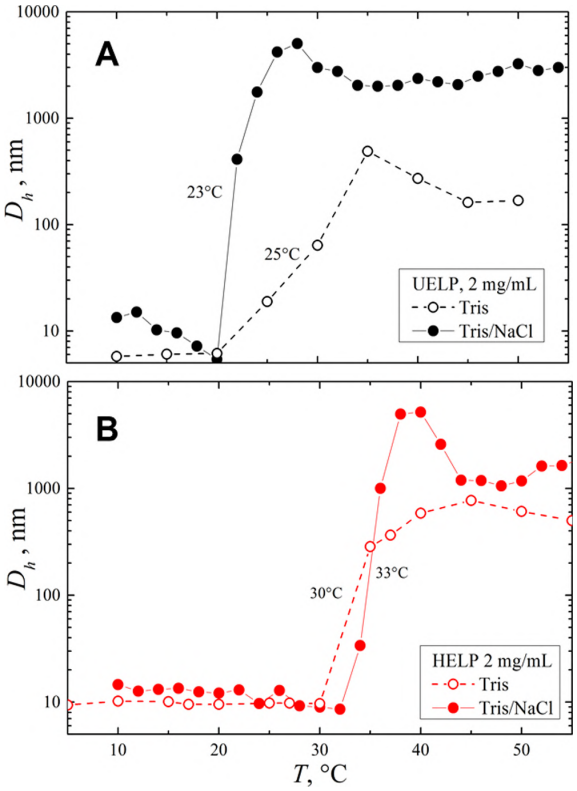

Figure 7. DLS diameter (volume-based calculated values) as a function of temperature. Calculated values of particle distribution in Tris (open symbols) and Tris/NaCl buffer (filled symbols) at a concentration of 2 mg/mL for UELP (A) and for HELP (B).

HELP showed a gradual trend of increasing diameter from about 300 nm up to 4000 nm under the same conditions (Figure 6D), again indicating greater chain flexibility (higher entropy) requiring higher temperature to stabilize the particle size. Figure 7 shows the particle diameters determined by DLS as the percent particle number distribution (N%) for the two biopolymers at a concentration of 2 mg/mL. In the absence of NaCl and below T_t, the particle diameters for the biopolymers were about 6 and 10 nm for UELP and HELP, respectively (Figure 7, open symbols), which most likely corresponds to a single chain size in solution. It is interesting to note that the values of the hydrodynamic diameter D_h, which are calculated from R_G[31] using the equation

$$R_h = D_h/2 = 0.664R_G$$

resulted in a D_h of 9.7 nm and 12.0 nm for UELP and HELP, respectively, thus showing values in agreement with the DLS diameters measured for the temperature below the T_t (Figure 7). In the absence of NaCl and above T_t, the UELP biopolymer formed particles that stabilized at a D_h greater than 200 nm, while HELP formed larger particles 500−800 nm in diameter. The addition of salt at near-physiological concentrations had a remarkable effect on the diameter of UELP particles, which promptly increased from a value of about 6 nm in the absence of salt and near T_t (Figure 7A, open symbols) to about 5000 nm in the presence of NaCl (Figure 7A, filled symbols). This value, which stabilizes as a function of temperature at about 3000 nm, is significantly larger than the

https://doi.org/10.1021/acs.biomac.3c00782
Biomacromolecules 2023, 24, 5277−5289

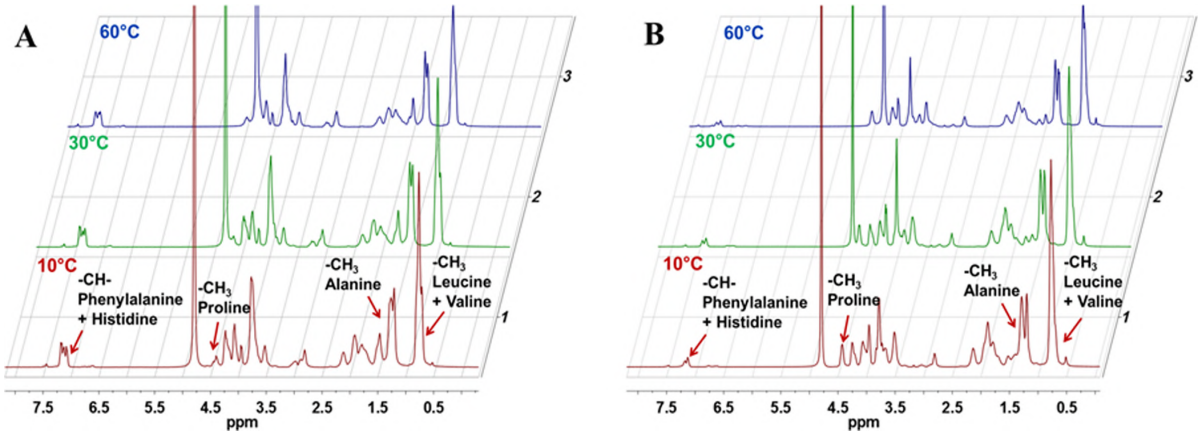

Figure 8. Overlay of ^{1}H NMR spectra of UELP (A) and HELP (B) in D_2O (5 mg/mL) at 10, 30, and 60 °C. Arrows indicate the resonance peaks of the following amino acid residues: leucine + valine, proline, alanine, and phenylalanine + histidine.

Table 3. Total Number of Amino Acid Residues (n res) and Relative Protons (nH) of UELP and HELP[a]

	UELP				HELP			
	theoretical		NMR		theoretical		NMR	
	n res	nH	δ (ppm)	nH	n res	nH	δ (ppm)	nH
L + V	109	654	0.76	658	129	774	0.76	860
A	130	390	1.03−1.38	412	159	477	0.97−1,46	590
P	48	48	4.40	43	72	72	4.42	75
F + H	29	127	6.55−7.54	127	14	52	6.57−7.55	52

[a]Chemical shifts (δ) and proton number (nH) of both biopolymers determined by NMR analysis.

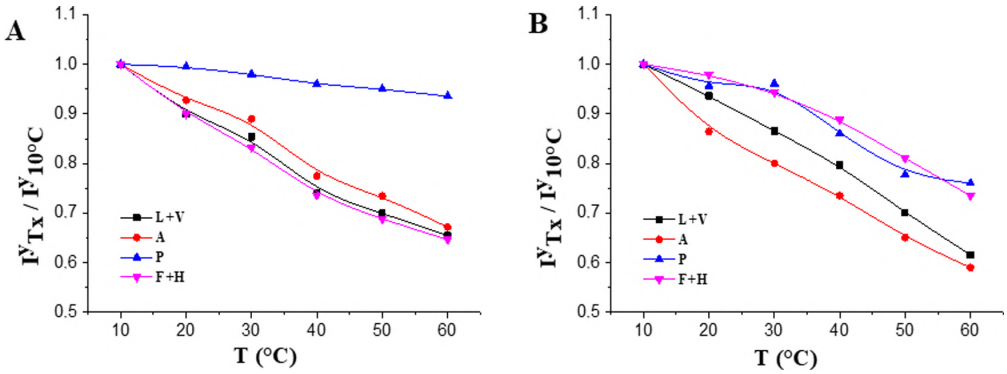

Figure 9. $I^{Y}_{Tx}/I_{10\ °C}{}^{Y}$ as a function of temperature for UELP (A) and HELP (B), as determined by ^{1}H NMR in D_2O (5 mg/mL) in the range between 10 and 60 °C.

value observed in the absence of salt (above 200 nm). In the presence of salt, HELP also showed a remarkable change in particle diameter around T_t, shifting from 10 to 15 to 5000 nm (Figure 7B, filled symbols) but stabilizing at about 1200−1700 nm as a function of temperature. However, in the case of HELP, particle sizes remained comparable in the presence and absence of salt (Figure 7B, see the filled and open symbols).

3.3.4. ^{1}H NMR Spectroscopy. The arrangement of UELP and HELP biopolymers in solution was studied by ^{1}H NMR spectroscopy in D_2O to evaluate differences in the polypeptide supramolecular arrangements occurring upon thermally induced coacervation. Figure 8 shows, as an example, the NMR spectra of HELP and UELP in a D_2O solvent. The characteristic resonances of some protons of the amino acid residues at 10 °C, i.e., under the conditions of maximum solubility, are shown in Table 3. In particular, the signals of $-CH_3$ protons of leucine and valine at 0.76 ppm and $-CH_3$ of alanine were clearly visible (Figure 8).

The formation of supramolecular aggregates by thermally induced self-assembly was studied by ^{1}H NMR at a variable temperature. Upon heating, a significant decrease in the resonance peak areas was observed (Figure 8), along with their downward shift. The latter is clearly visible in Figure 3S, where the chemical shift of the resonance peak was plotted as a function of the temperature for each amino acid residue. A nearly linear trend with an increasing temperature was observed for all proton groups, suggesting that the increase in temperature weakens the hydrogen interactions between the

https://doi.org/10.1021/acs.biomac.3c00782
Biomacromolecules 2023, 24, 5277−5289

polar amino acid groups of the polypeptide and the water and decreases the solvation and electron shielding at the hydrogen nuclei.[32] In addition, the ratio of the absolute integral at a given temperature (T_x) to the integral at 10 °C ($I_{Tx}^{y}/I_{10\ °C}^{y}$) was calculated for each proton resonance peak and plotted as a function of temperature (Figure 9). It can be noticed that most of the peak integrals gradually decreased with temperature increase, with no evidence of sharp transitions associated with the occurrence of T_t. A similar trend in UELP and HELP integrals was observed for the proton peaks of alanine, leucine, and valine, suggesting that these residues exhibit progressively stronger hydrophobic interactions upon heating, reaching a signal decrease of about 33−41% at 60 °C, with a slightly larger decrease for residues in HELP than the analogues in UELP.

Notably, the greatest decrease was observed for UELP phenylalanine and histidine signals (Figure 9A), which may be attributed to the aromatic side chains and the higher proportion of phenylalanine residues in this polypeptide. Interestingly, a striking trend was observed for proline protons. In fact, the intensity ratio of UELP prolines in Figure 9A decreased by only 5% at 60 °C, indicating that strong interactions with water molecules persist when particle aggregation occurs. Since prolines are known to be present mainly in the β-sheet structures, which are generally involved in self-association and subsequent coacervation,[28] this behavior suggests that the UELP β-sheet structures are still stable and solvated after polypeptide self-assembly. In this context, the observed slight decrease in the level of the proline signal is attributed to the rearrangement of the proline residues not involved in the β-sheet structures after self-assembly.

A different trend in the proline signal intensity was observed for HELP. Figure 9B shows a decrease in proline intensity (up to 24%) as a function of temperature, suggesting that in this case, the proline residues are actively involved in the coacervation process of HELP, whereupon they are buried in the hydrophobic moiety. As previously reported,[24b] temperature-driven coacervation of highly hydrophobic elastin-like proteins may occur by decreasing the hydrodynamic radius and expelling water to reduce the hydrophobic-solvent interaction as the temperature increases. From this point of view, proline, as well as other residues belonging to the hydrophobic domains of HELP (alanine, valine, and leucine), could be involved in these temperature-driven structural changes so that their peaks show a larger decrease in HELP.

In summary, NMR analysis is consistent with previous analyses and highlights a different thermally driven coacervation mechanism for the two biopolymers due to the peculiar local secondary structure of their hydrophobic sequences.

3.4. Cytocompatibility Evaluation. HELP biopolymers have been used as substrates for the culture of human cells of various origins. However, it was found that in some cases, cell adhesion after 24 h varied depending on the cell line used and the thickness of the biopolymers on the surface.[6,12,33] To compare the cell adhesion ability of the new UELP versus the biopolymer HELP, tissue-culture-treated polystyrene (TP) was coated with each biopolymer by adsorption, as described in Section 2. MG-63 human osteoblast-like cells and NIH3T3 mouse fibroblasts were seeded, and after 24 h, no significant differences in adhesion were observed for either cell line on each biopolymer coating compared with the TP surface (Figure 10). Interestingly, when the same coating procedure was performed on an untreated polystyrene microtiter plate

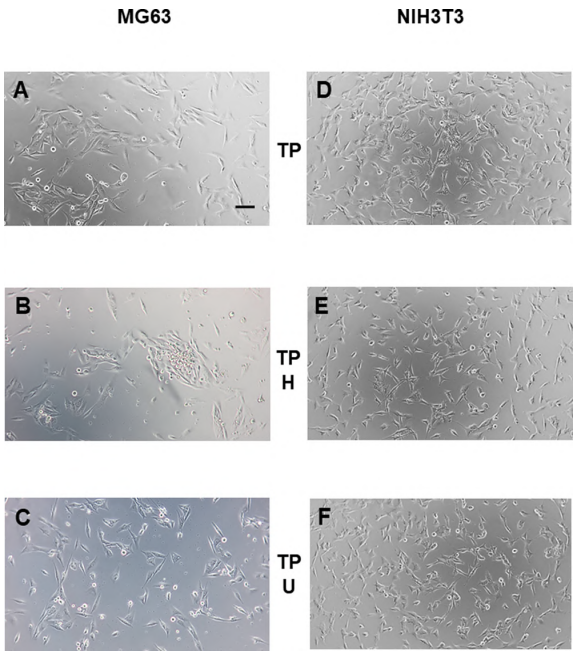

Figure 10. Representative phase-contrast images of cell cultures on coated and uncoated tissue-culture polystyrene wells (TP). MG-63 and NIH3T3 cell lines of human and murine origin, respectively, were seeded on uncoated TP wells (panels A and D) and on TP wells coated with HELP (TP -H, panels B and E) and UELP (TP -U, panels C and F) and grown under standard conditions. Images were acquired 24 h after seeding. The bar is 100 μm.

(NP), a notable difference in adhesion was seen for both cell lines after 24 h (Figure 11). The cells were not able to adhere to the uncoated surface NP as expected (Figure 11, panels A and D). Cells seeded onto the HELP-coated surface NP also behaved similarly to cells observed on the uncoated control surface NP: They showed a rounded morphology and formed small aggregates, suggesting poor adhesion to the surface at this time point (Figure 11, panels B and E). In contrast, cell adhesion on the UELP-coated surfaces of NP in both cell lines was comparable to that observed in the TP control (compare Figure 11, panels C and F, with Figure 10, panels A and D).

The crystal violet adhesion test confirmed this observation (Figure 4S) and confirmed a promoting effect on cell adhesion. However, after a longer time, e.g., 48 or 72 h, depending on the cell line, cells were able to cover all coated surfaces of NP and show their characteristic morphology, indicating that the presence of the biopolymers has no toxic effect (data not shown).

In addition, coatings were prepared by decreasing the concentration of the biopolymer solutions used for adsorption on NP. No significant difference was observed for the HELP-coated surfaces, whereas a dose-dependent cell response was observed on UELP coatings. This effect correlated with the amount of UELP biopolymer present in the solution used to prepare the coatings. Cell metabolic activity was evaluated 24 h after seeding by the WST-1 assay (Figures 5S and 6S). This analysis showed that the UELP and HELP coatings have no toxic effect on both cell lines, and the cell adhesion-promoting effect of UELP was confirmed (see the Supporting Information).

https://doi.org/10.1021/acs.biomac.3c00782
Biomacromolecules 2023, 24, 5277−5289

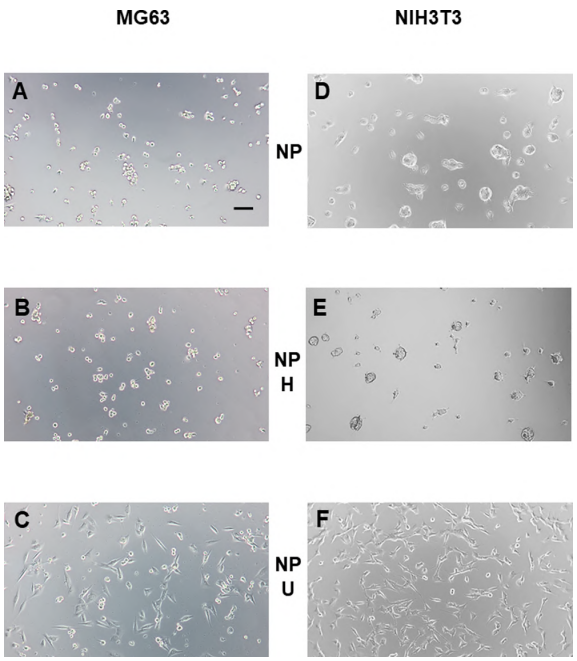

Figure 11. Representative phase-contrast images of cell cultures on coated and uncoated nontissue culture polystyrene (NP). MG-63 and NIH3T3 cell lines of human and murine origin, respectively, were seeded on the uncoated NP wells (panels A and D) and on the NP wells coated with HELP (NP -H, panels B and E) and UELP (NP -U, panels C and F) and grown under standard conditions. Images were acquired 24 h after seeding. The bar is 100 μm.

Remarkably, UELP and HELP have the same structure with alternating elastin-like and cross-linking domains, the same length, and very similar composition, whereas only the amino acid sequence of the elastin-like domain differs (Figure 1). The data presented here suggest that the sequence of the elastin-like domain, the sequence inspired by exon 26 rather than human exon 24, promotes the adhesion of cells of different origins to nonadhesive NP surfaces. Although tropoelastin has long been considered an unstructured protein, the 3D shape of the human homologue has been described using an unconventional approach.[34] According to this model, the region encoded by exon 26 was found to have the highest protease susceptibility, indicating that this sequence is exposed.[34] Thus, this region could also be readily accessible to cells organized in the extracellular matrix of the tissue. This could be one of the possible explanations for why this highly conserved region was well tolerated by the cells and may even represent a point of cell attachment. On the other hand, the exon 24-derived region is also exposed, being located in the so-called "spur" of the tropoelastin structure.[34] However, it can be considered that the sequence of this region, being peculiar to the human, and more in general, primate homologue and also having a recognized signaling role,[20] is less likely to represent a stable adhesion point for the cells within the extracellular matrix.

4. CONCLUSIONS

A new ELP sequence was designed and fabricated to improve cyto- and tissue compatibility and to extend the feasibility of this class of recombinant biopolymers and derived materials to the veterinary field while maintaining typical thermoresponsive properties. The new UELP construct was successfully prepared, and the expression product was characterized, focusing on the comparison of its physicochemical behavior to that of the previously described biopolymer HELP.

Our study highlights the effect of elastin-like sequences mimicking the different hydrophobic domains of human elastin interspersed with the cross-linking domains, leading to the realization of biomimetic elastins that, in addition to phase transition properties, exhibit significantly different features in thermoresponsive behavior. These results indicate that our recombinant platform is a valuable tool to further elucidate the physicochemical properties of elastin and related sequences.

The new UELP polypeptide showed an improved ability to promote the adhesion of cells from different origins to nonadhesive surfaces compared to the biopolymer HELP. Overall, our system, which ensures tight control over the bioinspired structure of the polypeptides, provides a powerful means to analyze how the extracellular environment can influence and potentially control cell response.

These results demonstrate that our approach can lead to the production of biomimetic components that have at least two valuable aspects that can be exploited. One relates to their application for the development of biocompatible materials with advanced functionality, and the other relates to their use as specific and customizable tools to study and elucidate the interaction at the interface of materials and biological systems at the molecular level.

■ ASSOCIATED CONTENT

Supporting Information

The Supporting Information is available free of charge at https://pubs.acs.org/doi/10.1021/acs.biomac.3c00782.

Primary structure of the proteins described in the paper; size distribution of the apparent hydrodynamic diameter of the biopolymers' particles; chemical shift of resonance peaks as a function of temperature; cell adhesion and viability assays (PDF)

■ AUTHOR INFORMATION

Corresponding Authors

Antonella Bandiera − *Department of Life Sciences, University of Trieste, 34127 Trieste, Italy*; orcid.org/0000-0002-0376-9291; Email: abandiera@units.it

Giovanna Gomez d'Ayala − *Institute for Polymers, Composites and Biomaterials (IPCB-CNR), 80078 Pozzuoli, NA, Italy*; Email: Giovanna.gomezdayala@ipcb.cnr.it

Authors

Laura Colomina - Alfaro − *Department of Life Sciences, University of Trieste, 34127 Trieste, Italy*

Paola Sist − *Department of Life Sciences, University of Trieste, 34127 Trieste, Italy*

Federica Zuppardi − *Institute for Polymers, Composites and Biomaterials (IPCB-CNR), 80078 Pozzuoli, NA, Italy*

Pierfrancesco Cerruti − *Institute for Polymers, Composites and Biomaterials (IPCB-CNR), 80078 Pozzuoli, NA, Italy*

Ovidio Catanzano − *Institute for Polymers, Composites and Biomaterials (IPCB-CNR), 80078 Pozzuoli, NA, Italy*; orcid.org/0000-0002-8284-0841

https://doi.org/10.1021/acs.biomac.3c00782
Biomacromolecules 2023, 24, 5277−5289

Sabina Passamonti − *Department of Life Sciences, University of Trieste, 34127 Trieste, Italy;* orcid.org/0000-0001-7876-4666

Ranieri Urbani − *Department of Chemical and Pharmaceutical Sciences, University of Trieste, 34127 Trieste, Italy;* orcid.org/0000-0002-7802-3697

Complete contact information is available at: https://pubs.acs.org/10.1021/acs.biomac.3c00782

Notes

The authors declare no competing financial interest.

■ ACKNOWLEDGMENTS

This work was supported by the Horizon 2020 Innovative Training Network AIMed project under the Marie Skłodowska-Curie, grant agreement No 861138, the Horizon Europe STOP—Surface Transfer of Pathogens project, grant agreement No 101057961, and the PNRR iNEST project, Interconnected Nord-Est Innovation, funded by the EU Recovery fund. This work has been partly funded by a grant from the Italian Ministry of Foreign Affairs and International Cooperation (MAECI), in the frame of the NANOARBO project".

■ REFERENCES

(1) Del Prado Audelo, M. L.; Mendoza-Muñoz, N.; Escutia-Guadarrama, L.; Giraldo-Gomez, D.; González-Torres, M.; Florán, B.; Cortés, H.; Leyva-Gomez, G. Recent Advances in Elastin-Based Biomaterial. *J. Pharm. Pharm. Sci.* **2020**, *23* (1), 314−332.

(2) (a) Rosenbloom, J.; Abrams, W. R.; Indik, Z.; Yeh, H.; Ornstein-Goldstein, N.; Bashir, M. M. Structure of the Elastin Gene. In *Ciba Foundation Symposium 192 - The Molecular Biology and Pathology of Elastic Tissues: The Molecular Biology and Pathology of Elastic Tissues: Ciba Foundation Symposium 192*; Wiley, 1995; Vol. *192*, pp 59−74. (b) Vrhovski, B.; Weiss, A. S. Biochemistry of tropoelastin. *Eur. J. Biochem.* **1998**, *258* (1), 1−18. (c) Chow, D.; Nunalee, M. L.; Lim, D. W.; Simnick, A. J.; Chilkoti, A. Peptide-based Biopolymers in Biomedicine and Biotechnology. *Mater. Sci. Eng. R Rep.* **2008**, *62* (4), 125−155.

(3) Bandiera, A. Assembly and Optimization of Expression of Synthetic Genes Derived from the Human Elastin Repeated Motif. *Prep. Biochem. Biotech.* **2010**, *40* (3), 198−212.

(4) Bandiera, A. Transglutaminase-catalyzed preparation of human elastin-like polypeptide-based three-dimensional matrices for cell encapsulation. *Enzyme Microb. Technol.* **2011**, *49* (4), 347−352.

(5) (a) D'Andrea, P.; Sciancalepore, M.; Veltruska, K.; Lorenzon, P.; Bandiera, A. Epidermal Growth Factor - based adhesion substrates elicit myoblast scattering, proliferation, differentiation and promote satellite cell myogenic activation. *Biochim. Biophys. Acta Mol. Cell Res.* **2019**, *1866* (3), 504−517. (b) Bandiera, A.; Corich, L.; Tommasi, S.; De Bortoli, M.; Pelizzo, P.; Stebel, M.; Paladin, D.; Passamonti, S. Human elastin-like polypeptides as a versatile platform for exploitation of ultrasensitive bilirubin detection by UnaG. *Biotechnol. Bioeng.* **2020**, *117* (2), 354−361.

(6) D'Andrea, P.; Scaini, D.; Ulloa Severino, L.; Borelli, V.; Passamonti, S.; Lorenzon, P.; Bandiera, A. In vitro myogenesis induced by human recombinant elastin-like proteins. *Biomaterials* **2015**, *67*, 240−253.

(7) Bandiera, A.; Sist, P.; Urbani, R. Comparison of thermal behavior of two recombinantly expressed human elastin-like polypeptides for cell culture applications. *Biomacromolecules* **2010**, *11* (12), 3256−3265.

(8) D'Andrea, P.; Civita, D.; Cok, M.; Severino, L. U.; Vita, F.; Scaini, D.; Casalis, L.; Lorenzon, P.; Donati, I.; Bandiera, A. Myoblast adhesion, proliferation and differentiation on human elastin-like polypeptide (HELP) hydrogels *J. Appl. Biomater. Funct. Mater.* 2017; Vol. *15* 1 DOI: 10.5301/jabfm.5000331.

(9) Ciofani, G.; Genchi, G. G.; Mattoli, V.; Mazzolai, B.; Bandiera, A. The potential of recombinant human elastin-like polypeptides for drug delivery. *Expert Opin. Drug Delivery* **2014**, *11* (10), 1507−1512.

(10) Wrenn, D. S.; Griffin, G. L.; Senior, R. M.; Mecham, R. P. Characterization of biologically active domains on elastin: identification of a monoclonal antibody to a cell recognition site. *Biochemistry* **1986**, *25* (18), 5172−5176.

(11) Senior, R. M.; Griffin, G. L.; Mecham, R. P. Chemotactic activity of elastin-derived peptides. *J. Clin. Invest.* **1980**, *66* (4), 859−862.

(12) Bandiera, A.; Taglienti, A.; Micali, F.; Pani, B.; Tamaro, M.; Crescenzi, V.; Manzini, G. Expression and characterization of human-elastin-repeat-based temperature-responsive protein polymers for biotechnological purposes. *Biotechnol. Appl. Biochem.* **2005**, *42*, 247−256.

(13) Corich, L.; Busetti, M.; Petix, V.; Passamonti, S.; Bandiera, A. Evaluation of a biomimetic 3D substrate based on the Human Elastin-like Polypeptides (HELPs) model system for elastolytic activity detection. *J. Biotechnol.* **2017**, *255*, 57−65.

(14) Humphries, M. J. Cell-Substrate Adhesion Assays. *Curr. Protoc. Cell Biol.* **1998**, *00* (1), 9−1.

(15) Urry, D. W.; Parker, T. M. Mechanics of elastin: molecular mechanism of biological elasticity and its relationship to contraction. *J. Muscle Res. Cell Motil.* **2002**, *23* (5−6), 543−559.

(16) (a) Luan, C. H.; Harris, R. D.; Prasad, K. U.; Urry, D. W. Differential scanning calorimetry studies of the inverse temperature transition of the polypentapeptide of elastin and its analogues. *Biopolymers* **1990**, *29* (14), 1699−1706. (b) Pepe, A.; Guerra, D.; Bochicchio, B.; Quaglino, D.; Gheduzzi, D.; Pasquali Ronchetti, I.; Tamburro, A. M. Dissection of human tropoelastin: Supramolecular organization of polypeptide sequences coded by particular exons. *Matrix Bio.* **2005**, *24* (2), 96−109. (c) Tamburro, A. M.; Bochicchio, B.; Pepe, A. Dissection of human tropoelastin: exon-by-exon chemical synthesis and related conformational studies. *Biochemistry* **2003**, *42* (45), 13347−13362.

(17) (a) Chilkoti, A.; Dreher, M. R.; Meyer, D. E. Design of thermally responsive, recombinant polypeptide carriers for targeted drug delivery. *Adv. Drug Delivery Rev.* **2002**, *54* (8), 1093−1111. (b) Miao, M.; Bellingham, C. M.; Stahl, R. J.; Sitarz, E. E.; Lane, C. J.; Keeley, F. W. Sequence and structure determinants for the self-aggregation of recombinant polypeptides modeled after human elastin. *J. Biol. Chem.* **2003**, *278* (49), 48553−48562.

(18) Chilkoti, A.; Christensen, T.; MacKay, J. A. Stimulus responsive elastin biopolymers: Applications in medicine and biotechnology. *Curr. Opin. Chem. Biol.* **2006**, *10* (6), 652−657.

(19) Wu, K.; Liu, Z.; Wang, W.; Zhou, F.; Cheng, Q.; Bian, Y.; Su, W.; Liu, B.; Zha, J.; Zhao, J.; et al. An artificially designed elastin-like recombinant polypeptide improves aging skin. *Am. J. Transl Res.* **2022**, *14* (12), 8562−8571.

(20) Duca, L.; Floquet, N.; Alix, A. J. P.; Haye, B.; Debelle, L. Elastin as a matrikine. *Crit. Rev. Oncol. Hematol.* **2004**, *49* (3), 235−244.

(21) Jensen, S. A.; Vrhovski, B.; Weiss, A. S. Domain 26 of Tropoelastin Plays a Dominant Role in Association by Coacervation. *J. Biol. Chem.* **2000**, *275* (37), 28449−28454.

(22) Miles, A. J.; Ramalli, S. G.; Wallace, B. A. DichroWeb, a website for calculating protein secondary structure from circular dichroism spectroscopic data. *Protein Sci.* **2022**, *31* (1), 37−46.

(23) Zhou, X.; Zheng, W.; Li, Y.; Pearce, R.; Zhang, C.; Bell, E. W.; Zhang, G.; Zhang, Y. I-TASSER-MTD: a deep-learning-based platform for multi-domain protein structure and function prediction. *Nat. Protoc.* **2022**, *17* (10), 2326−2353.

(24) (a) Vrhovski, B.; Jensen, S.; Weiss, A. S. Coacervation Characteristics of Recombinant Human Tropoelastin. *Eur. J. Biochem.* **1997**, *250* (1), 92−98. (b) Greenland, K. N.; Carvajal, M. F. C. A.; Preston, J. M.; Ekblad, S.; Dean, W. L.; Chiang, J. Y.; Koder, R. L.; Wittebort, R. J. Order, Disorder, and Temperature-Driven Compaction in a Designed Elastin Protein. *J. Phys. Chem. B* **2018**, *122* (10),

2725−2736. (c) Miao, M.; Cirulis, J. T.; Lee, S.; Keeley, F. W. Structural Determinants of Cross-linking and Hydrophobic Domains for Self-Assembly of Elastin-like Polypeptides. *Biochemistry* **2005**, *44* (43), 14367−14375.
(25) Christensen, T.; Trabbic-Carlson, K.; Liu, W.; Chilkoti, A. Purification of recombinant proteins from *Escherichia coli* at low expression levels by inverse transition cycling. *Anal. Biochem.* **2007**, *360* (1), 166−168.
(26) Reichheld, S. E.; Muiznieks, L. D.; Stahl, R.; Simonetti, K.; Sharpe, S.; Keeley, F. W. Conformational transitions of the cross-linking domains of elastin during self-assembly. *J. Biol. Chem.* **2014**, *289* (14), 10057−10068.
(27) Jensen, S. A.; Vrhovski, B.; Weiss, A. S. Domain 26 of tropoelastin plays a dominant role in association by coacervation. *J. Biol. Chem.* **2000**, *275* (37), 28449−28454.
(28) Maeda, I.; Fukumoto, Y.; Nose, T.; Shimohigashi, Y.; Nezu, T.; Terada, Y.; Kodama, H.; Kaibara, K.; Okamoto, K. Structural requirements essential for elastin coacervation: favorable spatial arrangements of valine ridges on the three-dimensional structure of elastin-derived polypeptide (VPGVG)n. *J. Pept. Sci.* **2011**, *17* (11), 735−743.
(29) Prhashanna, A.; Taylor, P. A.; Qin, J.; Kiick, K. L.; Jayaraman, A. Effect of Peptide Sequence on the LCST-Like Transition of Elastin-Like Peptides and Elastin-Like Peptide-Collagen-Like Peptide Conjugates: Simulations and Experiments. *Biomacromolecules* **2019**, *20* (3), 1178−1189.
(30) Tamburro, A. M.; Pepe, A.; Bochicchio, B. Localizing alpha-helices in human tropoelastin: assembly of the elastin ″puzzle″. *Biochemistry* **2006**, *45* (31), 9518−9530.
(31) Kok, C. M.; Rudin, A. Relationship between the hydrodynamic radius and the radius of gyration of a polymer in solution. *Die Makromol. Chem., Rapid Commun.* **1981**, *2* (11), 655−659.
(32) Faggio, N.; Zuppardi, F.; Staiano, C.; Poggetto, G. D.; Gomez d'Ayala, G.; Cerruti, P. Removal of anionic and cationic dyes from aqueous solution using thermo- and pH-responsive amphiphilic copolymers. *J. Water Process. Eng.* **2022**, *49*, No. 103107.
(33) Çelebi, B.; Cloutier, M.; Balloni, R.; Mantovani, D.; Bandiera, A. Human Elastin-Based Recombinant Biopolymers Improve Mesenchymal Stem Cell Differentiation. *Macromol. Biosci.* **2012**, *12* (11), 1546−1554.
(34) Baldock, C.; Oberhauser, A. F.; Ma, L.; Lammie, D.; Siegler, V.; Mithieux, S. M.; Tu, Y.; Chow, J. Y.; Suleman, F.; Malfois, M.; et al. Shape of tropoelastin, the highly extensible protein that controls human tissue elasticity. *Proc. Natl. Acad. Sci. U.S.A.* **2011**, *108* (11), 4322−4327.

https://doi.org/10.1021/acs.biomac.3c00782
Biomacromolecules 2023, 24, 5277−5289

Chapter 7. General Discussion

In this chapter, the findings and insights from Chapters 3, 4, 5, and 6 will be summarised, integrated and briefly discussed, identifying future research development.

The research undertaken in this thesis was carried out in the frame of the Horizon 2020 MSCA-ITN project "Antimicrobial integrated methodologies for orthopaedic application". Within this initiative, fifteen early-stage researchers (ESRs) directed their efforts toward developing antimicrobial materials and surfaces with potential applications in the orthopaedic contexts. Consequently, different approaches were used to modify implant materials to grant them with bacterial-killing activities. While some ESRs focused on surface modification by physical treatments, others pursued functionalisation strategies that employed AMPs. Notably, the work conducted at UniTS was devoted to the recombinant production, in *E. coli*, of AMPs fused to HELP carrier and to the exploration of the capabilities of the developed biopolymers to realise 2D and 3D materials that can confer antimicrobial properties to the surfaces, while remaining cytocompatible.

The production of heterologous proteins and peptides in bacterial expression systems has gained particular interest in recent years since they are obtained through simple, well-established, scalable and cost-effective platforms capable of meeting large-scale manufacturing requirements. Unlike chemical synthesis, recombinant production involves more sustainable methods that avoid using harmful reagents or generating toxic end products.[184] However, AMP production in bacterial expression systems poses challenges due to their inherent toxicity to the host cells and susceptibility to protease degradation, which negatively affect production yields. To overcome these drawbacks, AMPs are often produced as fusion proteins employing carriers that mitigate their toxicity and shield them from protease activity.[195, 204] Several carriers have been described; among them, ELPs have garnered considerable attention for producing heterologous proteins since, besides being excellent fusion partners, they can also be employed as purification tags, streamlining downstream processes and further reducing production costs.[184, 291] Their peculiar thermo-responsive properties enable easy and efficient separation of the fusion protein from the total host proteins through effective and straightforward ITC methodology (described on pages 37 and 38) that avoids chromatography steps and yields high-purity materials.[257, 290, 291] Furthermore, due to their biotic origin, low risk of generating toxic by-products and intrinsic self-assembly abilities in response to diverse stimuli, ELPs hold great promise for developing biomaterials that may easily integrate into biological environments.[257, 279] In our laboratory, an ELP based on the human elastin sequence (HELP) has been designed and successfully characterised.[329] Notably, the main characteristic that distinguishes this biopolymer from most of the other ELPs, which are mainly composed of the typical hydrophobic elastin-derived sequences, is the presence of the cross-linking domains, which allows for the formation of a stable hydrogel matrix in the presence of a transglutaminase enzyme.[332] Moreover, these domains make HELP and HELP-derived biopolymers particularly susceptible to elastolytic activity, which can degrade the HELP moiety, releasing any fusion domain.[330] Thus, the versatile HELP platform has been successfully employed to produce bioactive domains and derived materials in recent years.[338, 339, 341] Nevertheless, it has not yet been exploited for AMP production. Thus, in the view of realising biomimetic components endowed with antimicrobial properties, we explored the opportunity of using HELP as the carrier to produce AMPs. Further, the fusion proteins were employed to produce biocompatible materials and surfaces intrinsically containing the functional antimicrobial domains, which can be released upon adequate stimuli.

Thus, at the beginning of the project, literature research was conducted to analyse the strategies already described for producing, through recombinant technologies, AMPs fused to ELP carriers. In addition, approaches describing recombinant ELPs chemically functionalised with AMPs were also considered. In total, 20 ELP-based constructs were identified; 18 were produced through bacterial or plant expression platforms, while the other two used EDC/NHS and click chemistry to conjugate AMPs to ELPs. Diverse antimicrobial domains were fused, with a broad variability of charge and size, and they were positioned at the ELP C- or N-terminal or between two ELP blocks. Interestingly, some fusion proteins retained the AMP antimicrobial capacity while others needed to be released and purified from the carrier to exert their activity. Thus, the AMPs were released by intein self-cleavage or chemical (CNBr, hydroxylamine and formic acid) and enzymatic (enterokinase) methods. Nevertheless, none of the constructs exploited the potential susceptibility of some ELP carriers to elastase degradation for the smart release of the bioactive domains. Furthermore, most approaches utilised the recombinant platform to produce functional-free AMPs rather than to create antimicrobial components and biomaterials. Thus, the employment of the ELP fusion proteins for delivering AMPs and producing antimicrobial coatings, matrices, and biomimetic materials is still limited. The information obtained from this analysis allowed us to set a starting point for designing HELP fusion proteins carrying AMP domains. We considered this work potentially useful for other researchers in the field; thus, the results were collected and organised in a mini-review publication that schematically resumes the state-of-the-art of the existing ELP carrier fusions with AMPs.

The main objective at this point was to realise a model construct for guiding further HELP functionalisation with AMPs of interest and developed by our Consortium Partners. Since ELP-indolicidin fusion has not been described before, we selected this short, cationic and extensively characterised AMP[93] as the bioactive antimicrobial domain to be produced as a HELP fusion. The indolicidin sequence was cloned in-frame to the HELP C-terminal, resulting in the HIn fusion protein. In addition, a linker encoding a cross-linking domain and a unique glutamic acid residue was introduced between the carrier and the AMP coding region. Thus, the sequence was designed to trigger the release of the functional domain by incubation with elastase or with the Glu-C, a highly specific endoprotease. The employment of the HELP carrier successfully sheltered indolicidin toxicity towards *E. coli* host cells, and the fusion protein retained the typical elastin thermo-responsive properties, enabling its purification following the ITC method and yielding over 200 mg of the fusion protein per litre of bacterial culture. The antimicrobial characterisation against model bacterial strains commonly implicated in orthopaedic infections revealed potent inhibition of *P. aeruginosa* by the fusion protein, with a MIC in agreement with that reported in the literature for indolicidin,[93] keeping into account that the AMP represents about one-thirty of the HIn construct. Conversely, no significant activity of the biopolymer in solution was detected towards *S. aureus* growth and mild activity was observed against *E. coli*. Moreover, thin-film coatings made of this biopolymer partially inhibited the growth of *P. aeruginosa* and SEM analysis evidenced extensive membrane blebbing and cell disruption. Under certain growth conditions, *P. aeruginosa* can produce elastase enzymes,[346] potentially degrading HELP moiety and releasing the AMP, which could partially account for the observed strong activity of HIn towards this microorganism.

Moreover, the presence of the AMP did not affect the preparation of HIn matrices through the enzymatic cross-linking method already described for HELP.[332] Thus, HIn matrices were successfully produced, and their antimicrobial characterisation revealed that the biopolymer cross-linking caused the loss of the AMP activity, with matrices unable to inhibit bacterial growth, indicating that tethering within 3D structure rendered the AMP inactive. However, in the design of the fusion protein, a Glu-C recognition site was positioned just before the indolicidin

sequence, allowing the AMP release by the incubation with this endoprotease. Intriguingly, when HIn matrices were treated with Glu-C, they resulted active towards all the microorganisms tested, indicating that the peptide should be released to interact with its target actively. Indolicidin exerts its antimicrobial potential by interacting with intracellular targets and affecting nucleic acid and protein synthesis;[93] thus, covalently linked indolicidin needs to be released from the hydrogel matrix to be able to penetrate the bacterial membrane and reach its cellular targets. This likely explains, at least in part, the result obtained. Therefore, intact HIn matrices were inert, and no antimicrobial activity was observed. Nevertheless, their antimicrobial capacity was restored after the treatment with the specific endoprotease that triggered the indolicidin release. This observation rendered HIn-based matrices particularly compelling for producing materials with smart, on-demand release of the bioactive domains, wherein specific stimuli can serve as switchers between inactive and active configurations. For instance, when integrated into biological systems, HIn matrices may behave as passive materials under physiological conditions, thereby preventing prolonged exposure of the surrounding tissues to the bioactive domain, which in some cases may be toxic to eukaryotic cells and mitigating the risks of developing resistance. However, if the matrix environment changes and the proper stimulus is generated, indolicidin can be selectively released and able to reach its targets. Further, the susceptibility of the HELP cross-linking domains to elastase may allow for the release of any fused domain. Besides being produced by certain microorganisms like, for example, *P. aeruginosa*, elastase is also secreted during inflammation processes, such as in response to infections.[345] Therefore, elastase production under pathogenic conditions could serve as the stimulus that triggers the AMP release. In consequence, the activity of the AMP will counteract the mechanisms responsible for elastase production, thus attenuating the process and providing a dynamic and controlled response.[330] In this view, the matrix's ability to release the antimicrobial domain upon elastolytic stimulus was *in vitro* assessed by employing a commercial elastase to simulate the response of the matrices that can be expected *in vivo*, under infection conditions, for instance. Therefore, mixtures of the products derived from elastase digestion of the HIn matrices resulted in active towards *P. aeruginosa*, indicating that the AMP domain was preserved and that the cleavage restored its potency. This result evidenced the potential of the HELP-AMP fusion for producing biomimetic components endowed with sustained antimicrobial activity.

Following the design principles established for the HIn construct, we validated the potential of the HELP system to produce and characterise AMPs with a more complex structure. Specifically, hBD1 was chosen as a functional domain, motivated by the fact that it is a long AMP and contains 6 cysteine residues,[77, 78] making this sequence challenging to synthesise by chemical methods[178] and prompting our exploration of alternative production avenues relying on recombinant platforms. In the literature, two main active hBD1 domains have been described;[71, 79] thus, similarly to the HIn construct, the HhBD1 coding sequence was designed to allow the specific release of the bioactive domains using specific endoproteases. Hence, the HhBD1 biopolymer was successfully produced and purified using the HELP recombinant platform, achieving fusion protein yields of up to 250 mg per litre of bacterial culture, thus reinforcing our hypothesis on recombinant technologies as a more efficient and cost-effective route for producing difficult-to-synthesise sequences.

The initial characterisation of the antimicrobial properties of the HhBD1 biopolymer in solution did not evidence any antibacterial capacity of this molecule. Considering that hBD1 is constitutively expressed and produced across several epithelial cells where hypoxia and reducing conditions dominate,[77, 78] our laboratory setups may not adequately reflect the physiological environment where hBD1 exerts its antimicrobial potential. Indeed, in

laboratory conditions, hBD1 has a weak antimicrobial activity compared to other human AMPs, particularly towards Gram-positive bacteria.[71, 82] It has been reported that the activity of this AMP is significantly influenced by its redox state. [83, 84] *In vitro*, the Trx system can reduce hBD1, and Trx co-localises with reduced hBD1 in human epithelia,[83] and even though cysteines are essential for its activity, redhBD1 shows a more potent antibacterial activity than oxhBD1. Thus, a radial diffusion assay under reducing conditions was more appropriate for evaluating the antimicrobial properties of the biopolymer developed.[83] This assay confirmed that the bacterial killing activity of HhBD1 strongly depended on the redox state, with the reduced biopolymer being able to inhibit *E. coli* cell growth. Notably, the radial diffusion assay under reduced conditions did not evidence any significant difference between the diameters of inhibition of the fusion biopolymer and the release products obtained by incubation with specific endoproteinases.

Besides developing and characterising the antimicrobial fusion biopolymer, we ascertained its biocompatibility towards eukaryotic cells, and no toxic effects were found at the tested concentration. Indeed, a moderate pro-proliferative activity was observed, as already described for HELP.[338] Intriguingly, when characterising HhBD1-based materials, a strong cell pro-adhesive effect was unequivocally observed due to the presence of the hBD1 domain since cells are unable to attach on HELP alone, and delayed adhesion and proliferation have been observed when cells have been cultured on HELP-based substrates.[332] Coatings, thin films, and matrices containing HhBD1 remarkably promoted osteoblasts and fibroblasts adhesion. Contrast phase and fluorescence microscopy analyses showed that cells cultured on HhBD1 substrates attached and spread with well-defined cytoarchitecture, acquiring the expected morphology of the tested cell lines. To our knowledge, our findings reveal a novel function of hBD1, previously unreported. While hBD1 is known for its multifunctionality, a pro-adhesive activity has only been associated with hBD5 until now. Recently, it has been demonstrated that hBD1 can bind to potassium channels, causing conformational changes without affecting the activation state of the channels.[446] In addition, potassium channels are physically associated with integrins;[447] thus, conformational changes triggered by hBD1 may influence integrin-dependent adhesion, a process in which these channels play a role.[448] Therefore, our results may point to an unexplored mechanism related to cell adhesion; nevertheless, future studies are needed to corroborate this hypothesis. In addition, herein, only the effect of hBD1 on cell adhesion was reported; hence, subsequent investigations will further characterise the long-term behaviour of primary hMSCs cultured onto HhBD1 substrates regarding cell morphology, proliferation, and differentiation.

In addition, rheological analysis of the HhBD1 matrices indicated their suitability for producing scaffolds for tissue engineering applications. Therefore, this biopolymer holds great promise in producing biocompatible materials with enhanced cell adhesion and antimicrobial properties.

Compared to the other ELP platforms employed for AMP production, the only limitation observed for the HELP system was the inability to purify the AMP domain by exploiting the thermo-responsive HELP properties once released from the elastin carrier. Indolicidin and hBD1 were successfully purified from the HELP moiety by the ITC method, only when it was carried out in the presence of detergents, otherwise the co-precipitation of the AMPs with the HELP domain occurred. However, this condition interferes with the antimicrobial assays. Nevertheless, the most interesting findings of our system were obtained by employing the fusion protein rather than the free, released AMP domain. Furthermore, the main strengths of our approach are the ability to develop coatings and matrices granted with antimicrobial activity and effectively stimulating cell adhesion, as evidenced by the characterisation of HIn and HhBD1 biopolymers, respectively. As evidenced in the mini-review publication

presented in Chapter 3, almost all the systems described for ELP-AMP production using ELPs as carriers mainly focused on producing the AMPs as free or fusion peptides rather than for developing functional biomaterials. Further studies could explore the possibility of realising materials combining both HELP-based fusion biopolymers and evaluate how they perform, for instance, in co-cultures between bone-derived cells and bacteria. Another research line may consider the employment of these biopolymers to coat surfaces. Indeed, these biopolymers and the derived materials hold great promise for surface functionalisation to confer antimicrobial properties without inducing resistance.

During the work carried out in this thesis, a new construct based on mammalian elastin was developed to improve and broaden the biocompatibility and cytocompatibility of the carrier itself. Comparing and aligning the sequence of the exon 26 of elastin from 8 mammalian species, a consensus of 40 aa, differing in only 5 positions with respect to the human elastin, was obtained. Thus, a new ELP was assembled, following the structure of HELP, where eight elastin hydrophobic domains are alternated with the hydrophilic cross-linking domains.[329] The gene was expressed in *E. coli,* and the new UELP protein was purified using the ITC method. The physico-chemical characterisation of UELP in solution showed very different thermo-responsive behaviour with respect to HELP, especially referring to the transition temperature in physiological conditions. UELP showed a sharper transition at a lower Tt (23 °C) than HELP (34 °C), with a more than 10 °C difference. Thus, in physiological conditions and at room temperature, UELP is in an aggregated state while HELP is still soluble. Intriguingly, the biological assessment of UELP-based substrates unveiled their cell adhesion properties. Compared to HELP-treated surfaces, where the cells scarcely adhere, the UELP-based substrates promoted cell adhesion and spreading, showing the expected morphological features of the tested cell lines. UELP and HELP have the same structure with alternating elastin-like and cross-linking domains, the same length, and very similar composition. They differ only in the amino acid sequence of the elastin-like domain; UELP is inspired by a vertebrate's consensus sequence of the exon 26, while HELP is based on the human exon 24.[329] Thus, our findings suggest that the elastin sequence of exon 26 likely promotes cell adhesion. This sequence is described to be exposed in the tropoelastin 3D structure, as evidenced by its high susceptibility to protease degradation; thus, it may be accessible and represent points for cell attachment signals.[449] On the other hand, in the human homologue, the sequence encoded by the exon 24 is also exposed; still, it is less probable to represent stable adhesion points since this region has been demonstrated to have other signalling functions.[450]

The biomimetic strategy adopted for developing UELP led to a novel ELP biopolymer with enhanced thermo-responsive properties, which is expected to further improve the yield of the derived fusion constructs. This improved thermo-responsive properties of UELP, compared to HELP, could provide significant advantages for the purification steps. Nevertheless, when using this biopolymer, it has to be taken into account that, at working temperatures, the aggregated state is favoured, thus affecting, for instance, the functional domain activity in solution and other reactions. On the other hand, the new biopolymer is better tolerated by the cells, favouring their adhesion. Hence, this macromolecule holds promise for developing biomaterials for tissue engineering and wound healing. The UELP temperature-dependent properties may be tuned, for instance, by reducing the size of the biopolymer[264, 269, 274] yet maintaining the cell adhesion capabilities. Future developments of this work may address the production of a shorter UELP macromolecule to obtain a carrier with an optimised temperature-dependent behaviour for the desired application, like the functionalisation with AMPs. For example, following the indolicidin model design, the potential of this new carrier for AMP production could be tested.

Summarising, through this work, several aspects of the recombinant HELP/UELP fusion carriers for producing AMPs, or in general any protein or peptide, were evidenced:

- they are recombinantly produced in *E. coli* as soluble proteins, with the advantage of an expression system that avoids the formation of inclusion bodies and, hence, the employment of denaturant conditions for their extraction from the biomass. This allows their purification in native conditions without affecting the bioactive domain structure and function;
- the thermo-responsive behaviour characterising the elastin-based biopolymers is exploited for their high-grade purification, ensuring a high-yield and cost-effective process that does not rely on costly and complex chromatographic separation;
- AMP domains up to 50 aa have been successfully fused to the HELP moiety, maintaining both the carrier and the AMP functionalities;
- the design of the fusion construct is customisable, and multiple functionalities can be integrated within the same biopolymer to meet the requirements of the desired application. Thus, in addition to the AMP domains, linkers, as well as specific endoproteinase recognition sites, may be introduced, expanding the biological activity of the fusion protein and allowing for the release of the fused AMPs;
- HELP and the potential UELP carriers, unlike other elastin-like carriers described in the literature, possess elastin-derived cross-linking domains. These can be enzymatically cross-linked to form hydrogel-like matrices that carry the fusion domain. This allows for obtaining biocompatible and functional materials that can be integrated into biological systems;
- the cross-linking domains within the carrier sequence are the main target for elastase, an enzyme that, by its degradation activity, triggers the release of the fused domain;
- so far, several cell lines have been cultured on HELP-based substrates; however, poor cell adhesion adhesion has been observed. The biopolymer is not toxic since the cells are viable and can proliferate, although with a slight delay. However, they remain rounded, growing as clusters or islets. Intriguingly, UELP coatings promoted cell attachment, opening the door for its employment as a carrier for AMP production and for developing biocompatible materials with enhanced cell adhesion properties;
- integration of hBD1 at the C-terminal of HELP conferred cell adhesion properties. To our knowledge, this functionality has been observed for the first time for hBD1, underscoring the capabilities of the HELP platforms to investigate biological interactions.

Future research may explore further functionalisation of the HELP and UELP-based materials, fine-tuning thermo-responsive properties, and investigating additional biological interactions. Furthermore, integrating multiple functionalities within the fusion constructs opens opportunities for creating advanced biomimetic materials with tailored properties.

Chapter 8. Conclusions

- An extensive analysis of reported strategies for producing antimicrobial peptides fused or conjugated to ELPs has evidenced that the use of these peculiar carriers for AMP production is still limited. Nevertheless, diverse approaches have been developed, employing a diverse range of AMPs and ELPs, and different fusion configurations and expression systems have been explored.
- The successful design, production, and functional testing of the HIn fusion construct demonstrated the viability of the HELP system as a multifunctional and antimicrobial delivery platform. The ability to produce 2D and 3D materials with sustained antimicrobial activity highlighted its potential for smartly releasing antimicrobial domains upon proper stimuli.
- Subsequent to the HIn construct, the HELP platform was further employed to produce a fusion construct carrying the hBD1. This difficult-to-synthesize sequence was successfully incorporated into the HELP system and recombinantly produced in *E. coli*, demonstrating its adaptability and potential for producing a wide range of bioactive antimicrobial materials. Its demonstrated capabilities in promoting cell adhesion and sustaining antimicrobial activity underscored this biopolymer's versatility and utility in producing biomaterials.
- UELP biopolymer was developed following a biomimetic strategy, and its physico-chemical and biological characterisation revealed enhanced thermal properties and improved cell adhesion compared to HELP. These results suggest promising applications of UELP-based materials in various fields, including antimicrobial coatings, tissue engineering scaffolds, and wound healing.
- Several advantages of the recombinant HELP/UELP platform for AMP production were underscored. These include soluble expression in *E. coli*, simple purification methods, customisable fusion construct design, and the potential for creating biocompatible materials with diverse functionalities.
- The HELP/UELP carriers are versatile platforms, enabling the production of bioactive domains and derived materials and offering new avenues for investigating biological interactions at the molecular level. They allow for the incorporation of functional peptides into biomimetic structures, with the advantage of providing suitable unfunctionalised controls. Moreover, the flexibility to choose between various configurations, including aqueous solution, 2D, or 3D material settings, enhances the potential of these platforms for producing biomaterials and composites with antimicrobial properties.

In summary, the findings presented in this thesis contribute to advancing the understanding and application of ELP-based biomaterials for biomedical applications, paving the way for future innovations in the field of antimicrobial materials and beyond.

References

1. A. R. Collaborators., *Lancet*, 2022, **399**, 629-655.
2. K. I. Mohr, *Curr Top Microbiol Immunol*, 2016, **398**, 237-272.
3. A. Gelpi, A. Gilbertson and J. D. Tucker, *Sex Transm Infect*, 2015, **91**, 68-69.
4. A. Fleming, *Bull World Health Organ*, 2001, **79**, 780-790.
5. H. Otten, *J Antimicrob Chemother*, 1986, **17**, 689-696.
6. R. Gaynes, in *Emerg Infect Dis*, 2017, vol. 23, pp. 849-853.
7. R. P. Lange, H. H. Locher, P. C. Wyss and R. L. Then, *Curr Pharm Des*, 2007, **13**, 3140-3154.
8. A. Fleming, *Journal*, 1945.
9. J. Davies, *Can J Infect Dis Med Microbiol*, 2006, **17**, 287-290.
10. T. Pulingam, T. Parumasivam, A. M. Gazzali, A. M. Sulaiman, J. Y. Chee, M. Lakshmanan, C. F. Chin and K. Sudesh, *Eur J Pharm Sci*, 2022, **170**, 106103.
11. N. Rosenblatt-Farrell, in *Environ Health Perspect*, United States, 2009, vol. 117, pp. A244-250.
12. R. J. Fair and Y. Tor, *Perspect Medicin Chem*, 2014, **6**, 25-64.
13. E. C. f. D. P. a. Control, The bacterial challenge: time to react, https://www.ecdc.europa.eu/en/publications-data/ecdcemea-joint-technical-report-bacterial-challenge-time-react, (accessed February 13, 2024).
14. P. H. England, Health matters: antimicrobial resistance, https://www.gov.uk/government/publications/health-matters-antimicrobial-resistance, (accessed February 13, 2024).
15. J. O'Neill, 2016.
16. L. Czaplewski, R. Bax, M. Clokie, M. Dawson, H. Fairhead, V. A. Fischetti, S. Foster, B. F. Gilmore, R. E. Hancock, D. Harper, I. R. Henderson, K. Hilpert, B. V. Jones, A. Kadioglu, D. Knowles, S. Ólafsdóttir, D. Payne, S. Projan, S. Shaunak, ... and J. H. Rex, *Lancet Infect Dis*, 2016, **16**, 239-251.
17. P. Cardoso, H. Glossop, T. G. Meikle, A. Aburto-Medina, C. E. Conn, V. Sarojini and C. Valery, *Biophys Rev*, 2021, **13**, 35-69.
18. M. Mahlapuu, J. Håkansson, L. Ringstad and C. Björn, *Front Cell Infect Microbiol*, 2016, **6**, 194.
19. G. Wang, *Protein Sci*, 2023, **32**, e4778.
20. R. L. Gallo, *Exp Dermatol*, 2013, **22**, 517.
21. R. J. Dubos, *J Exp Med*, 1939, **70**, 1-10.
22. R. J. Dubos, *J Exp Med*, 1939, **70**, 11-17.
23. A. Lewies, L. H. Du Plessis and J. F. Wentzel, *Probiotics Antimicrob Proteins*, 2019, **11**, 370-381.
24. G. Wang, *Methods Enzymol*, 2022, **663**, 1-18.
25. J. Niggemann, P. Bozko, N. Bruns, A. Wodtke, M. T. Gieseler, K. Thomas, C. Jahns, M. Nimtz, I. Reupke, T. Brüser, G. Auling, N. Malek and M. Kalesse, *Chembiochem*, 2014, **15**, 1021-1029.
26. A. Zipperer, M. C. Konnerth, C. Laux, A. Berscheid, D. Janek, C. Weidenmaier, M. Burian, N. A. Schilling, C. Slavetinsky, M. Marschal, M. Willmann, H. Kalbacher, B. Schittek, H. Brötz-Oesterhelt, S. Grond, A. Peschel and B. Krismer, *Nature*, 2016, **535**, 511-516.
27. K. A. Brogden, A. J. De Lucca, J. Bland and S. Elliott, *Proc Natl Acad Sci U S A*, 1996, **93**, 412-416.
28. G. Wang, X. Li and Z. Wang, *Nucleic Acids Res*, 2016, **44**, D1087-1093.
29. A. Bin Hafeez, X. Jiang, P. J. Bergen and Y. Zhu, *Int J Mol Sci*, 2021, **22**.
30. R. E. Hancock and D. S. Chapple, *Antimicrob Agents Chemother*, 1999, **43**, 1317-1323.
31. G. Wang, *Methods Mol Biol*, 2015, **1268**, 43-66.
32. L. E. Uggerhøj, T. J. Poulsen, J. K. Munk, M. Fredborg, T. E. Sondergaard, N. Frimodt-Moller, P. R. Hansen and R. Wimmer, *Chembiochem*, 2015, **16**, 242-253.
33. N. Chen and C. Jiang, *Eur J Med Chem*, 2023, **255**, 115377.
34. H. Gu, T. Kato, H. Kumeta, Y. Kumaki, T. Tsukamoto, T. Kikukawa, M. Demura, H. Ishida, H. J. Vogel and T. Aizawa, *ACS Omega*, 2022, **7**, 31924-31934.
35. Y. Huang, J. Huang and Y. Chen, *Protein Cell*, 2010, **1**, 143-152.
36. P. M. Hwang, N. Zhou, X. Shan, C. H. Arrowsmith and H. J. Vogel, *Biochemistry*, 1998, **37**, 4288-4298.
37. F. Bauer, K. Schweimer, E. Klüver, J. R. Conejo-Garcia, W. G. Forssmann, P. Rösch, K. Adermann and H. Sticht, *Protein Sci*, 2001, **10**, 2470-2479.
38. A. Rozek, C. L. Friedrich and R. E. Hancock, *Biochemistry*, 2000, **39**, 15765-15774.
39. H. Nar, A. Schmid, C. Puder and O. Potterat, *ChemMedChem*, 2010, **5**, 1689-1692.
40. V. Nizet, *J Allergy Clin Immunol*, 2007, **120**, 13-22.
41. B. Bechinger and K. Lohner, *Biochim Biophys Acta*, 2006, **1758**, 1529-1539.
42. S. R. Dennison, L. H. Morton, F. Harris and D. A. Phoenix, *Biophys Chem*, 2007, **129**, 279-283.
43. T. A. E. Ahmed and R. Hammami, *J Food Biochem*, 2019, **43**, e12546.
44. Y. Luo and Y. Song, *Int J Mol Sci*, 2021, **22**.
45. P. Kumar, J. N. Kizhakkedathu and S. K. Straus, *Biomolecules*, 2018, **8**.
46. A. Ghosh, R. K. Kar, J. Jana, A. Saha, B. Jana, J. Krishnamoorthy, D. Kumar, S. Ghosh, S. Chatterjee and A. Bhunia, *ChemMedChem*, 2014, **9**, 2052-2058.
47. C. B. Park, H. S. Kim and S. C. Kim, *Biochem Biophys Res Commun*, 1998, **244**, 253-257.
48. J. L. Vizán, C. Hernández-Chico, I. del Castillo and F. Moreno, *Embo j*, 1991, **10**, 467-476.

49. A. Patrzykat, C. L. Friedrich, L. Zhang, V. Mendoza and R. E. Hancock, *Antimicrob Agents Chemother*, 2002, **46**, 605-614.
50. Y. H. Ho, T. C. Sung and C. S. Chen, *Mol Cell Proteomics*, 2012, **11**, M111.014720.
51. H. Gusman, J. Travis, E. J. Helmerhorst, J. Potempa, R. F. Troxler and F. G. Oppenheim, *Infect Immun*, 2001, **69**, 1402-1408.
52. H. R. Chileveru, S. A. Lim, P. Chairatana, A. J. Wommack, I. L. Chiang and E. M. Nolan, *Biochemistry*, 2015, **54**, 1767-1777.
53. E. F. Haney, S. K. Straus and R. E. W. Hancock, *Front Chem*, 2019, **7**, 43.
54. K. A. Brogden, *Nat Rev Microbiol*, 2005, **3**, 238-250.
55. A. M. Aerts, I. E. François, B. P. Cammue and K. Thevissen, *Cell Mol Life Sci*, 2008, **65**, 2069-2079.
56. M. E. Klotman and T. L. Chang, *Nat Rev Immunol*, 2006, **6**, 447-456.
57. G. Diamond, N. Beckloff, A. Weinberg and K. O. Kisich, *Curr Pharm Des*, 2009, **15**, 2377-2392.
58. N. Ganesan, B. Mishra, L. Felix and E. Mylonakis, *Microbiol Mol Biol Rev*, 2023, **87**, e0003722.
59. J. Xie, Y. Li, X. Guo, J. Rao, T. Yan, L. Mou, X. Wu, X. Xie, W. Yang and B. Zhang, *Biochimie*, 2020, **176**, 1-11.
60. J. R. Shartouny and J. Jacob, *Semin Cell Dev Biol*, 2019, **88**, 147-155.
61. M. de Amaral and J. Ienes-Lima, *Virus Res*, 2022, **315**, 198769.
62. J. Kim, B. H. Cho and Y. S. Jang, *J Microbiol Biotechnol*, 2023, **33**, 288-298.
63. W. Lu, *Semin Cell Dev Biol*, 2019, **88**, 105-106.
64. G. López-García, O. Dublan-García, D. Arizmendi-Cotero and L. M. Gómez Oliván, *Molecules*, 2022, **27**.
65. E. E. Avila, *Curr Protein Pept Sci*, 2017, **18**, 1098-1119.
66. T. Ganz, M. E. Selsted and R. I. Lehrer, *Eur J Haematol*, 1990, **44**, 1-8.
67. E. V. Valore and T. Ganz, *Blood*, 1992, **79**, 1538-1544.
68. G. Zhang and L. T. Sunkara, *Pharmaceuticals (Basel)*, 2014, **7**, 220-247.
69. M. Pazgier and J. Lubkowski, *Protein Expr Purif*, 2006, **49**, 1-8.
70. T. Ganz and R. I. Lehrer, *Curr Opin Immunol*, 1998, **10**, 41-44.
71. M. Pazgier, D. M. Hoover, D. Yang, W. Lu and J. Lubkowski, *Cell Mol Life Sci*, 2006, **63**, 1294-1313.
72. A. Vankeerberghen, O. Scudiero, K. De Boeck, M. Macek, Jr., P. F. Pignatti, N. Van Hul, H. Nuytten, F. Salvatore, G. Castaldo, D. Zemkova, V. Vavrova, J. J. Cassiman and H. Cuppens, *Genomics*, 2005, **85**, 574-581.
73. R. I. Lehrer, A. M. Cole and M. E. Selsted, *J Biol Chem*, 2012, **287**, 27014-27019.
74. Y. Q. Tang, J. Yuan, G. Osapay, K. Osapay, D. Tran, C. J. Miller, A. J. Ouellette and M. E. Selsted, *Science*, 1999, **286**, 498-502.
75. A. E. Garcia, G. Osapay, P. A. Tran, J. Yuan and M. E. Selsted, *Infect Immun*, 2008, **76**, 5883-5891.
76. D. Yang, Z. H. Liu, P. Tewary, Q. Chen, G. de la Rosa and J. J. Oppenheim, *Curr Pharm Des*, 2007, **13**, 3131-3139.
77. H. Álvarez Á, M. Martínez Velázquez and E. Prado Montes de Oca, *Int J Biochem Cell Biol*, 2018, **104**, 133-137.
78. E. Prado-Montes de Oca, *Int J Biochem Cell Biol*, 2010, **42**, 800-804.
79. E. V. Valore, Park, C. H., Quayle, A. J., Wiles, K. R., & Ganz, T., *Journal of Clinical Investigation*, 1998, **101(8)**.
80. M. Pazgier, A. Prahl, D. M. Hoover and J. Lubkowski, *J Biol Chem*, 2007, **282**, 1819-1829.
81. D. M. Hoover, O. Chertov and J. Lubkowski, *J Biol Chem*, 2001, **276**, 39021-39026.
82. O. Scudiero, S. Galdiero, M. Cantisani, R. Di Noto, M. Vitiello, M. Galdiero, G. Naclerio, J. J. Cassiman, C. Pedone, G. Castaldo and F. Salvatore, *Antimicrob Agents Chemother*, 2010, **54**, 2312-2322.
83. B. O. Schroeder, Wu, Z., Nuding, S., Groscurth, S., Marcinowski, M., Beisner, J., Buchner, J., Schaller, M., Stange, E.F., Wehkamp, J., . . , .. , *Nature*, 2011, **469**, 419–423.
84. J. Raschig, D. Mailänder-Sánchez, A. Berscheid, J. Berger, A. A. Strömstedt, L. F. Courth, N. P. Malek, H. Brötz-Oesterhelt and J. Wehkamp, *PLoS Pathog*, 2017, **13**, e1006261.
85. M. J. Goldman, G. M. Anderson, E. D. Stolzenberg, U. P. Kari, M. Zasloff and J. M. Wilson, *Cell*, 1997, **88**, 553-560.
86. P. K. Singh, H. P. Jia, K. Wiles, J. Hesselberth, L. Liu, B. A. Conway, E. P. Greenberg, E. V. Valore, M. J. Welsh, T. Ganz, B. F. Tack and P. B. McCray, Jr., *Proc Natl Acad Sci U S A*, 1998, **95**, 14961-14966.
87. A. Bolatchiev, V. Baturin, I. Bazikov, A. Maltsev and E. Kunitsina, *Fundam Clin Pharmacol*, 2020, **34**, 102-108.
88. A. Bolatchiev, *PeerJ*, 2020, **8**, e10455.
89. S. U. Jaeger, B. O. Schroeder, U. Meyer-Hoffert, L. Courth, S. N. Fehr, M. Gersemann, E. F. Stange and J. Wehkamp, *Mucosal Immunol*, 2013, **6**, 1179-1190.
90. B. F. Kraemer, R. A. Campbell, H. Schwertz, M. J. Cody, Z. Franks, N. D. Tolley, W. H. Kahr, S. Lindemann, P. Seizer, C. C. Yost, G. A. Zimmerman and A. S. Weyrich, *PLoS Pathog*, 2011, **7**, e1002355.
91. J. Wendler, B. O. Schroeder, D. Ehmann, L. Koeninger, D. Mailänder-Sánchez, C. Lemberg, S. Wanner, M. Schaller, E. F. Stange, N. P. Malek, C. Weidenmaier, S. LeibundGut-Landmann and J. Wehkamp, *Sci Rep*, 2019, **9**, 3640.
92. M. Zanetti, *J Leukoc Biol*, 2004, **75**, 39-48.
93. J. Batista Araujo, G. Sastre de Souza and E. N. Lorenzon, *World J Microbiol Biotechnol*, 2022, **38**, 39.
94. S. Nagpal, K. J. Kaur, D. Jain and D. M. Salunke, *Protein Sci*, 2002, **11**, 2158-2167.
95. A. P. Podorieszach and H. E. Huttunen-Hennelly, *Org Biomol Chem*, 2010, **8**, 1679-1687.
96. J. C. Hsu and C. M. Yip, *Biophys J*, 2007, **92**, L100-102.
97. J. Vergis, S. V. S. Malik, R. Pathak, M. Kumar, R. Sunitha, S. B. Barbuddhe and D. B. Rawool, *Probiotics Antimicrob Proteins*, 2020, **12**, 705-715.
98. E. Mataraci and S. Dosler, *Antimicrob Agents Chemother*, 2012, **56**, 6366-6371.
99. E. de Alteriis, V. Maselli, A. Falanga, S. Galdiero, F. M. Di Lella, R. Gesuele, M. Guida and E. Galdiero, *Infect Drug Resist*, 2018, **11**, 915-925.
100. L. R. Haines, R. E. Hancock and T. W. Pearson, *Vector Borne Zoonotic Dis*, 2003, **3**, 175-186.

101. S. Ron-Doitch, B. Sawodny, A. Kühbacher, M. M. N. David, A. Samanta, J. Phopase, A. Burger-Kentischer, M. Griffith, G. Golomb and S. Rupp, *J Control Release*, 2016, **229**, 163-171.
102. T. J. Falla and R. E. Hancock, *Antimicrob Agents Chemother*, 1997, **41**, 771-775.
103. A. Rozek, J. P. Powers, C. L. Friedrich and R. E. Hancock, *Biochemistry*, 2003, **42**, 14130-14138.
104. H. S. Sader, K. A. Fedler, R. P. Rennie, S. Stevens and R. N. Jones, *Antimicrob Agents Chemother*, 2004, **48**, 3112-3118.
105. T. Niemeyer-van der Kolk, H. van der Wall, G. K. Hogendoorn, R. Rijneveld, S. Luijten, D. van Alewijk, E. H. A. van den Munckhof, M. L. de Kam, G. L. Feiss, E. P. Prens, J. Burggraaf, R. Rissmann and M. B. A. van Doorn, *Clin Transl Sci*, 2020, **13**, 994-1003.
106. M. Vaara, *Curr Opin Pharmacol*, 2009, **9**, 571-576.
107. C. Y. Chang, C. W. Lin, S. K. Chiang, P. L. Chen, C. Y. Huang, S. J. Liu, P. Chong and M. H. Huang, *ACS Med Chem Lett*, 2013, **4**, 522-526.
108. S. M. Kim, J. M. Kim, B. P. Joshi, H. Cho and K. H. Lee, *Biochim Biophys Acta*, 2009, **1794**, 185-192.
109. D. I. Andersson, D. Hughes and J. Z. Kubicek-Sutherland, *Drug Resist Updat*, 2016, **26**, 43-57.
110. S. Maria-Neto, K. C. de Almeida, M. L. Macedo and O. L. Franco, *Biochim Biophys Acta*, 2015, **1848**, 3078-3088.
111. K. E. Ridyard and J. Overhage, *Antibiotics (Basel)*, 2021, **10**.
112. H.-S. Joo, C.-I. Fu and M. Otto, *Philosophical Transactions of the Royal Society B: Biological Sciences*, 2016, **371**, 20150292.
113. A. Schmidtchen, I. M. Frick, E. Andersson, H. Tapper and L. Björck, *Mol Microbiol*, 2002, **46**, 157-168.
114. M. Sieprawska-Lupa, P. Mydel, K. Krawczyk, K. Wójcik, M. Puklo, B. Lupa, P. Suder, J. Silberring, M. Reed, J. Pohl, W. Shafer, F. McAleese, T. Foster, J. Travis and J. Potempa, *Antimicrob Agents Chemother*, 2004, **48**, 4673-4679.
115. R. Belas, J. Manos and R. Suvanasuthi, *Infect Immun*, 2004, **72**, 5159-5167.
116. M. Mattiuzzo, C. De Gobba, G. Runti, M. Mardirossian, A. Bandiera, R. Gennaro and M. Scocchi, *J Microbiol Biotechnol*, 2014, **24**, 160-167.
117. M. H. Braff, A. L. Jones, S. J. Skerrett and C. E. Rubens, *J Infect Dis*, 2007, **195**, 1365-1372.
118. M. Duperthuy, *Microorganisms*, 2020, **8**.
119. E. Llobet, J. M. Tomás and J. A. Bengoechea, *Microbiology (Reading)*, 2008, **154**, 3877-3886.
120. Y. Kai-Larsen, P. Lüthje, M. Chromek, V. Peters, X. Wang, A. Holm, L. Kádas, K. O. Hedlund, J. Johansson, M. R. Chapman, S. H. Jacobson, U. Römling, B. Agerberth and A. Brauner, *PLoS Pathog*, 2010, **6**, e1001010.
121. H. Mulcahy, L. Charron-Mazenod and S. Lewenza, *PLoS Pathog*, 2008, **4**, e1000213.
122. F. Guilhelmelli, N. Vilela, P. Albuquerque, S. Derengowski Lda, I. Silva-Pereira and C. M. Kyaw, *Front Microbiol*, 2013, **4**, 353.
123. G. Shi, X. Kang, F. Dong, Y. Liu, N. Zhu, Y. Hu, H. Xu, X. Lao and H. Zheng, *Nucleic Acids Res*, 2022, **50**, D488-d496.
124. N. Cortes-Penfield, N. T. Oliver, A. Hunter and M. Rodriguez-Barradas, *Infect Dis (Lond)*, 2018, **50**, 643-647.
125. K. D. Leuthner, A. Yuen, Y. Mao and A. Rahbar, *Expert Rev Anti Infect Ther*, 2015, **13**, 149-159.
126. G. G. Zhanel, D. Calic, F. Schweizer, S. Zelenitsky, H. Adam, P. R. Lagacé-Wiens, E. Rubinstein, A. S. Gin, D. J. Hoban and J. A. Karlowsky, *Drugs*, 2010, **70**, 859-886.
127. D. Münch, I. Engels, A. Müller, K. Reder-Christ, H. Falkenstein-Paul, G. Bierbaum, F. Grein, G. Bendas, H. G. Sahl and T. Schneider, *Antimicrob Agents Chemother*, 2015, **59**, 772-781.
128. M. J. Rybak, *Clin Infect Dis*, 2006, **42 Suppl 1**, S35-39.
129. R. L. Soon, R. L. Nation, S. Cockram, J. H. Moffatt, M. Harper, B. Adler, J. D. Boyce, I. Larson and J. Li, *J Antimicrob Chemother*, 2011, **66**, 126-133.
130. S. N. Avedissian, J. Liu, N. J. Rhodes, A. Lee, G. M. Pais, A. R. Hauser and M. H. Scheetz, *Antibiotics (Basel)*, 2019, **8**.
131. G. Pavithrra and R. Rajasekaran, *Interdiscip Sci*, 2019, **11**, 575-583.
132. T. Mogi and K. Kita, *Cell Mol Life Sci*, 2009, **66**, 3821-3826.
133. C. Lang and C. Staiger, *Pharmazie*, 2016, **71**, 299-305.
134. Q.-Y. Zhang, Z.-B. Yan, Y.-M. Meng, X.-Y. Hong, G. Shao, J.-J. Ma, X.-R. Cheng, J. Liu, J. Kang and C.-Y. Fu, *Military Medical Research*, 2021, **8**, 1-25.
135. A. K. Marr, W. J. Gooderham and R. E. Hancock, *Curr Opin Pharmacol*, 2006, **6**, 468-472.
136. M. Bacalum and M. Radu, *International Journal of Peptide Research and Therapeutics*, 2015, **21**, 47-55.
137. G. S. Dijksteel, M. M. W. Ulrich, E. Middelkoop and B. Boekema, *Front Microbiol*, 2021, **12**, 616979.
138. J. Xuan, W. Feng, J. Wang, R. Wang, B. Zhang, L. Bo, Z.-S. Chen, H. Yang and L. Sun, *Drug Resistance Updates*, 2023, **68**, 100954.
139. R. Bessalle, H. Haas, A. Goria, I. Shalit and M. Fridkin, *Antimicrob Agents Chemother*, 1992, **36**, 313-317.
140. S. R. Dennison, F. Harris and D. A. Phoenix, *Protein Pept Lett*, 2005, **12**, 27-29.
141. G. Wang, *Curr Biotechnol*, 2012, **1**, 72-79.
142. T. Unger, Z. Oren and Y. Shai, *Biochemistry*, 2001, **40**, 6388-6397.
143. M. Dathe, H. Nikolenko, J. Klose and M. Bienert, *Biochemistry*, 2004, **43**, 9140-9150.
144. O. Scudiero, E. Nigro, M. Cantisani, I. Colavita, M. Leone, F. A. Mercurio, M. Galdiero, A. Pessi, A. Daniele, F. Salvatore and S. Galdiero, *Int J Nanomedicine*, 2015, **10**, 6523-6539.
145. X. Li, Y. Li, H. Han, D. W. Miller and G. Wang, *J Am Chem Soc*, 2006, **128**, 5776-5785.
146. H. C. Chen, J. H. Brown, J. L. Morell and C. M. Huang, *FEBS Lett*, 1988, **236**, 462-466.
147. S. Nabizadeh, L. Rahbarnia, J. Nowrozi, S. Farajnia and F. Hosseini, *J Biomol Struct Dyn*, 2023, 1-9.

148. S. K. Carvajal, Y. Vargas-Casanova, H. M. Pineda-Castañeda, J. E. García-Castañeda, Z. J. Rivera-Monroy and C. M. Parra-Giraldo, *Antibiotics (Basel)*, 2022, **11**.
149. T. Silva, B. Claro, B. F. B. Silva, N. Vale, P. Gomes, M. S. Gomes, S. S. Funari, J. Teixeira, D. Uhríková and M. Bastos, *Langmuir*, 2018, **34**, 2158-2170.
150. H. M. Jindal, K. Zandi, K. C. Ong, R. D. Velayuthan, S. M. Rasid, C. Samudi Raju and S. D. Sekaran, *PeerJ*, 2017, **5**, e3887.
151. S. Jung, J. Mysliwy, B. Spudy, I. Lorenzen, K. Reiss, C. Gelhaus, R. Podschun, M. Leippe and J. Grötzinger, *Antimicrob Agents Chemother*, 2011, **55**, 954-960.
152. P. Méndez-Samperio, *Infect Drug Resist*, 2014, **7**, 229-237.
153. J. M. Sierra and M. Viñas, *Expert Opin Drug Discov*, 2021, **16**, 601-604.
154. A. J. Karlsson, W. C. Pomerantz, K. J. Neilsen, S. H. Gellman and S. P. Palecek, *ACS Chem Biol*, 2009, **4**, 567-579.
155. N. Molchanova, P. R. Hansen and H. Franzyk, *Molecules*, 2017, **22**.
156. Y. Hu, X. Li, S. M. Sebti, J. Chen and J. Cai, *Bioorg Med Chem Lett*, 2011, **21**, 1469-1471.
157. N. Srinivas, P. Jetter, B. J. Ueberbacher, M. Werneburg, K. Zerbe, J. Steinmann, B. Van der Meijden, F. Bernardini, A. Lederer, R. L. Dias, P. E. Misson, H. Henze, J. Zumbrunn, F. O. Gombert, D. Obrecht, P. Hunziker, S. Schauer, U. Ziegler, A. Käch, ... and J. A. Robinson, *Science*, 2010, **327**, 1010-1013.
158. V. V. Iyer, *Curr Med Chem*, 2016, **23**, 3025-3043.
159. R. Bellavita, S. Braccia, S. Galdiero and A. Falanga, *Pharmaceuticals (Basel)*, 2023, **16**.
160. R. Dwivedi, P. Aggarwal, N. S. Bhavesh and K. J. Kaur, *Amino Acids*, 2019, **51**, 1443-1460.
161. R. Lei, J. Hou, Q. Chen, W. Yuan, B. Cheng, Y. Sun, Y. Jin, L. Ge, S. A. Ben-Sasson, J. Chen, H. Wang, W. Lu and X. Fang, *ACS Nano*, 2018, **12**, 5284-5296.
162. R. Cao, L. Li, Z. Xu, J. Li, D. Wu, Y. Wang and H. Zhu, *Bioorg Med Chem Lett*, 2023, **90**, 129322.
163. J. C. Moreira Brito, L. R. Carvalho, A. Neves de Souza, G. Carneiro, P. P. Magalhães, L. M. Farias, N. R. Guimarães, R. M. Verly, J. M. Resende and M. Elena de Lima, *Front Mol Biosci*, 2022, **9**, 1001508.
164. M. H. Cardoso, R. Q. Orozco, S. B. Rezende, G. Rodrigues, K. G. N. Oshiro, E. S. Cândido and O. L. Franco, *Front Microbiol*, 2019, **10**, 3097.
165. W. F. Porto, I. C. M. Fensterseifer, S. M. Ribeiro and O. L. Franco, *Biochim Biophys Acta Gen Subj*, 2018, **1862**, 2043-2052.
166. C. Loose, K. Jensen, I. Rigoutsos and G. Stephanopoulos, *Nature*, 2006, **443**, 867-869.
167. C. D. Fjell, H. Jenssen, W. A. Cheung, R. E. Hancock and A. Cherkasov, *Chem Biol Drug Des*, 2011, **77**, 48-56.
168. Y. LeCun, Y. Bengio and G. Hinton, *Nature*, 2015, **521**, 436-444.
169. Y. C. Lo, S. E. Rensi, W. Torng and R. B. Altman, *Drug Discov Today*, 2018, **23**, 1538-1546.
170. K. Yin, W. Xu, S. Ren, Q. Xu, S. Zhang, R. Zhang, M. Jiang, Y. Zhang, D. Xu and R. Li, *Interdiscip Sci*, 2024.
171. E. F. Haney, Y. Brito-Sánchez, M. J. Trimble, S. C. Mansour, A. Cherkasov and R. E. W. Hancock, *Sci Rep*, 2018, **8**, 1871.
172. N. S. Parachin, K. C. Mulder, A. A. Viana, S. C. Dias and O. L. Franco, *Peptides*, 2012, **38**, 446-456.
173. B. H. Gan, J. Gaynord, S. M. Rowe, T. Deingruber and D. R. Spring, *Chem Soc Rev*, 2021, **50**, 7820-7880.
174. S. Deo, K. L. Turton, T. Kainth, A. Kumar and H. J. Wieden, *Biotechnol Adv*, 2022, **59**, 107968.
175. D. Goodwin, P. Simerska and I. Toth, *Curr Med Chem*, 2012, **19**, 4451-4461.
176. S. Wegmuller and S. Schmid, *Current Organic Chemistry*, 2014, **18**, 1005-1019.
177. R. B. Merrifield, *Journal of the American Chemical Society*, 1963, **85**, 2149-2154.
178. V. Mäde, S. Els-Heindl and A. G. Beck-Sickinger, *Beilstein J Org Chem*, 2014, **10**, 1197-1212.
179. J. P. da Costa, M. Cova, R. Ferreira and R. Vitorino, *Appl Microbiol Biotechnol*, 2015, **99**, 2023-2040.
180. M. Kordi, P. G. Talkhounche, H. Vahedi, N. Farrokhi and M. Tabarzad, *Protein J*, 2024.
181. C. Li, H.-M. Blencke, V. Paulsen, T. Haug and K. Stensvåg, *Bioengineered Bugs*, 2010, **1**, 217-220.
182. A. J. Otero-Gonzáiez, B. S. Magalhaes, M. Garcia-Villarino, C. López-Abarrategui, D. A. Sousa, S. C. Dias and O. L. Franco, *The FASEB journal*, 2010, **24**, 1320-1334.
183. M. Haji Abbasi Somehsaraie, V. Fathi Vavsari, M. Kamangar and S. Balalaie, *Iran J Pharm Res*, 2022, **21**, e123879.
184. D. Wibowo and C. X. Zhao, *Appl Microbiol Biotechnol*, 2019, **103**, 659-671.
185. A. Mazurkiewicz-Pisarek, J. Baran and T. Ciach, *Int J Mol Sci*, 2023, **24**.
186. R. Roca-Pinilla, L. Lisowski, A. Arís and E. Garcia-Fruitós, *Microb Cell Fact*, 2022, **21**, 267.
187. H. Chen, Z. Xu, N. Xu and P. Cen, *J Biotechnol*, 2005, **115**, 307-315.
188. H. Chen, Z. Xu and P. Cen, *Protein Pept Lett*, 2006, **13**, 155-162.
189. Z. Xu, H. Chen, X. Yin, N. Xu and P. Cen, *Appl Biochem Biotechnol*, 2005, **127**, 53-62.
190. S. K. Niazi and M. Magoola, *Biologics*, 2023, **3**, 380-401.
191. G. L. Rosano and E. A. Ceccarelli, *Frontiers in microbiology*, 2014, **5**, 79503.
192. L. Peng, Z. Xu, X. Fang, F. Wang, S. Yang and P. Cen, *Protein and Peptide Letters*, 2004, **11**, 339-344.
193. L. L. Corrales-Garcia, L. D. Possani and G. Corzo, *Amino Acids*, 2011, **40**, 5-13.
194. K. L. Piers, M. H. Brown and R. E. Hancock, *Gene*, 1993, **134**, 7-13.
195. Y. Li, *Biotechnol Appl Biochem*, 2009, **54**, 1-9.
196. A. Schütz, F. Bernhard, N. Berrow, J. F. Buyel, F. Ferreira-da-Silva, J. Haustraete, J. van den Heuvel, J. E. Hoffmann, A. de Marco, Y. Peleg, S. Suppmann, T. Unger, M. Vanhoucke, S. Witt and K. Remans, *STAR Protoc*, 2023, **4**, 102572.
197. A. M. Azevedo, P. A. Rosa, I. F. Ferreira and M. R. Aires-Barros, *Trends in biotechnology*, 2009, **27**, 240-247.
198. C. X. Zhao, M. D. Dwyer, A. L. Yu, Y. Wu, S. Fang and A. P. Middelberg, *Biotechnology and Bioengineering*, 2015, **112**, 957-964.
199. K. Yang, Y. Su, J. Li, J. Sun and Y. Yang, *Protein Expr Purif*, 2012, **85**, 200-203.

200. D. A. Sousa, K. C. Mulder, K. S. Nobre, N. S. Parachin and O. L. Franco, *Journal of biotechnology*, 2016, **234**, 83-89.
201. D. Wibowo, C.-X. Zhao and A. P. Middelberg, *Langmuir*, 2015, **31**, 1999-2007.
202. A. López-Cano, M. Martínez-Miguel, J. Guasch, I. Ratera, A. Arís and E. Garcia-Fruitós, *Microbial cell factories*, 2022, **21**, 77.
203. R. Roca-Pinilla, A. López-Cano, C. Saubi, E. Garcia-Fruitós and A. Arís, *Microbial Cell Factories*, 2020, **19**, 122.
204. Y. Li, *Protein Expr Purif*, 2011, **80**, 260-267.
205. S. A. Kozlov, A. A. Vassilevski and E. V. Grishin, *Recent Patents on Inflammation & Allergy Drug Discovery*, 2008, **2**, 58-63.
206. M. Joachim, N. Maguire, J. Schäfer, D. Gerlach and P. Czermak, *Front Bioeng Biotechnol*, 2019, **7**, 150.
207. Y. Li, *Protein Expression and Purification*, 2013, **87**, 72-78.
208. J. Bogomolovas, B. Simon, M. Sattler and G. Stier, *Protein expression and purification*, 2009, **64**, 16-23.
209. B. Bommarius, H. Jenssen, M. Elliott, J. Kindrachuk, M. Pasupuleti, H. Gieren, K.-E. Jaeger, R. Hancock and D. Kalman, *Peptides*, 2010, **31**, 1957-1965.
210. I. Čipáková, E. Hostinová, J. Gašperík and V. r. Velebný, *Protein expression and purification*, 2004, **37**, 207-212.
211. S. Maiti, S. Patro, S. Purohit, S. Jain, S. Senapati and N. Dey, *Antimicrobial agents and chemotherapy*, 2014, **58**, 6896-6903.
212. L. Huang, J. Wang, Z. Zhong, L. Peng, H. Chen, Z. Xu and P. Cen, *Biotechnol Lett*, 2006, **28**, 627-632.
213. L. Huang, Z. Xu, Z. Zhong, L. Peng, H. Chen and P. Cen, *Applied biochemistry and biotechnology*, 2007, **142**, 139-147.
214. X. C. Rao, S. Li, J. C. Hu, X. L. Jin, X. M. Hu, J. J. Huang, Z. J. Chen, J. M. Zhu and F. Q. Hu, *Protein Expr Purif*, 2004, **36**, 11-18.
215. J. Lee, J. Kim, S. Hwang, W. Lee, H. Yoon, H. Lee and S. Hong, *Biochemical and Biophysical Research Communications*, 2000, **277**, 575-580.
216. X. Li, Y. Jiang and Y. Lin, *Journal of Biotechnology*, 2022, **347**, 49-55.
217. H. Diao, C. Guo, D. Lin and Y. Zhang, *Biochemical and biophysical research communications*, 2007, **357**, 840-846.
218. S. A. Jang, B. H. Sung, J. H. Cho and S. C. Kim, *Applied and Environmental Microbiology*, 2009, **75**, 3980-3986.
219. T. Deng, H. Ge, H. He, Y. Liu, C. Zhai, L. Feng and L. Yi, *Protein Expression and Purification*, 2017, **140**, 52-59.
220. S. Baghbeheshti, S. Hadadian, A. Eidi, L. Pishkar and H. Rahimi, *International Journal of Peptide Research and Therapeutics*, 2021, **27**, 457-462.
221. Z. Xu, F. Wang, L. Peng, X. Fang and P. Cen, *Applied biochemistry and biotechnology*, 2005, **120**, 1-13.
222. Z. Xu, L. Peng, Z. Zhong, X. Fang and P. Cen, *Biotechnology progress*, 2006, **22**, 382-386.
223. K. Morin, S. Arcidiacono, R. Beckwitt and C. Mello, *Applied microbiology and biotechnology*, 2006, **70**, 698-704.
224. Y. Yang, D. Wu, C. Wang, A. Shan, C. Bi, Y. Li and W. Gan, *International Journal of Molecular Sciences*, 2020, **21**, 1470.
225. P. Magalhães, A. Lopes, P. Mazzola, C. Rangel-yagui and T. Penna, *Pharm. Sci*, 2011, **10**, 1-15.
226. H. Schwarz, J. Gornicec, T. Neuper, M. A. Parigiani, M. Wallner, A. Duschl and J. Horejs-Hoeck, *Scientific reports*, 2017, **7**, 44750.
227. J. M. Cregg, I. Tolstorukov, A. Kusari, J. Sunga, K. Madden and T. Chappell, *Methods in enzymology*, 2009, **463**, 169-189.
228. T. Vogl and A. Glieder, *New biotechnology*, 2013, **30**, 385-404.
229. L. Byrne, K. O'Callaghan and M. Tuite, *Methods in Molecular Biology: Humana Press New Jersey*, 2005, 51-64.
230. H. Müller, D. Salzig and P. Czermak, *Biotechnol Prog*, 2015, **31**, 1-11.
231. D. Mattanovich, P. Branduardi, L. Dato, B. Gasser, M. Sauer and D. Porro, *Methods Mol Biol*, 2012, **824**, 329-358.
232. I. Cipakova and E. Hostinová, *Protein and Peptide Letters*, 2005, **12**, 551-554.
233. T. S. Møller, J. Hay, M. J. Saxton, K. Bunting, E. I. Petersen, S. Kjærulff and C. J. Finnis, *Microb Cell Fact*, 2017, **16**, 11.
234. Z. Chen, D. Wang, Y. Cong, J. Wang, J. Zhu, J. Yang, Z. Hu, X. Hu, Y. Tan, F. Hu and X. Rao, *Appl Microbiol Biotechnol*, 2011, **89**, 281-291.
235. K. H. Hsu, C. Pei, J. Y. Yeh, C. H. Shih, Y. C. Chung, L. T. Hung and B. R. Ou, *J Gen Appl Microbiol*, 2009, **55**, 395-401.
236. M. Lübeck and P. S. Lübeck, *Microorganisms*, 2022, **10**.
237. B. Shanmugaraj, C. J. I. Bulaon, A. Malla and W. Phoolcharoen, *Molecules*, 2021, **26**, 4032.
238. F. Nazarian-Firouzabadi, M. T. Torres and C. de la Fuente-Nunez, *Biotechnol Adv*, 2024, **71**, 108296.
239. E. M. Porter, L. Liu, A. Oren, P. A. Anton and T. Ganz, *Infect Immun*, 1997, **65**, 2389-2395.
240. E. V. Valore, E. Martin, S. S. Harwig and T. Ganz, *J Clin Invest*, 1996, **97**, 1624-1629.
241. A. Y. Liu, D. Destoumieux, A. V. Wong, C. H. Park, E. V. Valore, L. Liu and T. Ganz, *J Invest Dermatol*, 2002, **118**, 275-281.
242. W. Weber and M. Fussenegger, in *Cell and Tissue Reaction Engineering: With a Contribution by Martin Fussenegger and Wilfried Weber*, Springer Berlin Heidelberg, Berlin, Heidelberg, 2009, pp. 263-277.
243. J. Zitzmann, G. Sprick, T. Weidner, C. Schreiber and P. Czermak, *New insights into cell culture technology*, 2017, 43-97.
244. L. Ikonomou, Y. J. Schneider and S. N. Agathos, *Appl Microbiol Biotechnol*, 2003, **62**, 1-20.
245. Y. c. HU, *Acta Pharmacologica Sinica*, 2005, **26**, 405-416.
246. R. O'Flaherty, A. Bergin, E. Flampouri, L. M. Mota, I. Obaidi, A. Quigley, Y. Xie and M. Butler, *Biotechnol Adv*, 2020, **43**, 107552.

247. M. Taniguchi, A. Ochiai, H. Kondo, S. Fukuda, Y. Ishiyama, E. Saitoh, T. Kato and T. Tanaka, *J Biosci Bioeng*, 2016, **121**, 591-598.
248. M. Taniguchi, A. Ochiai, S. Fukuda, T. Sato, E. Saitoh, T. Kato and T. Tanaka, *J Biosci Bioeng*, 2016, **122**, 385-392.
249. K. A. Martemyanov, A. S. Spirin and A. T. Gudkov, *Biotechnology Letters*, 1996, **18**, 1357-1362.
250. D. M. Kim and C. Y. Choi, *Biotechnol Prog*, 1996, **12**, 645-649.
251. C. E. Hodgman and M. C. Jewett, *Biotechnol Bioeng*, 2013, **110**, 2643-2654.
252. B. J. Des Soye, S. R. Davidson, M. T. Weinstock, D. G. Gibson and M. C. Jewett, *ACS Synth Biol*, 2018, **7**, 2245-2255.
253. H. Xu, W. Q. Liu and J. Li, *Methods Mol Biol*, 2022, **2433**, 89-103.
254. R. Kelwick, A. J. Webb, J. T. MacDonald and P. S. Freemont, *Metab Eng*, 2016, **38**, 370-381.
255. R. W. Martin, N. I. Majewska, C. X. Chen, T. E. Albanetti, R. B. C. Jimenez, A. E. Schmelzer, M. C. Jewett and V. Roy, *ACS Synth Biol*, 2017, **6**, 1370-1379.
256. S. Liu, J. M. Yu, Y. C. Gan, X. Z. Qiu, Z. C. Gao, H. Wang, S. X. Chen, Y. Xiong, G. H. Liu, S. E. Lin, A. McCarthy, J. V. John, D. X. Wei and H. H. Hou, *Mil Med Res*, 2023, **10**, 16.
257. J. Bhattacharyya, J. J. Bellucci and A. Chilkoti, *Biomaterials from Nature for Advanced Devices and Therapies*, 2016, 106-126.
258. J. R. Cabello, I. De Torre, F. Cipriani and L. Poocza, in *Peptides and proteins as biomaterials for tissue regeneration and repair*, Elsevier, 2018, pp. 309-327.
259. B. Vrhovski and A. S. Weiss, *European Journal of Biochemistry*, 1998, **258**, 1-18.
260. J. Kristensen and M. Karsdal, in *Biochemistry of Collagens, Laminins and Elastin*, Elsevier, 2016, pp. 197-201.
261. H. Vindin, S. M. Mithieux and A. S. Weiss, *Matrix biology*, 2019, **84**, 4-16.
262. J. H. Kristensen and M. A. Karsdal, in *Biochemistry of Collagens, Laminins and Elastin*, 2016, pp. 197-201.
263. W. R. Gray, L. B. Sandberg and J. A. Foster, *Nature*, 1973, **246**, 461-466.
264. D. W. Urry, D. C. Gowda, T. M. Parker, C. H. Luan, M. C. Reid, C. M. Harris, A. Pattanaik and R. D. Harris, *Biopolymers: Original Research on Biomolecules*, 1992, **32**, 1243-1250.
265. J. Despanie, J. P. Dhandhukia, S. F. Hamm-Alvarez and J. A. MacKay, *J Control Release*, 2016, **240**, 93-108.
266. T. Kowalczyk, K. Hnatuszko-Konka, A. Gerszberg and A. K. Kononowicz, *World Journal of Microbiology and Biotechnology*, 2014, **30**, 2141-2152.
267. D. E. Meyer and A. Chilkoti, *Biomacromolecules*, 2002, **3**, 357-367.
268. E. Garanger and S. Lecommandoux, *Advanced Drug Delivery Reviews*, 2022, **191**, 114589.
269. D. W. Urry, *J Protein Chem*, 1988, **7**, 1-34.
270. D. Urry, R. Shaw and K. Prasad, *Biochemical and biophysical research communications*, 1985, **130**, 50-57.
271. D. Urry, W. Cunningham and T. Ohnishi, *Biochemistry*, 1974, **13**, 609-616.
272. D. W. Urry, B. Starcher and S. Partridge, *Nature*, 1969, **222**, 795-796.
273. D. Urry, M. Long, B. Cox, T. Ohnishi, L. Mitchell and M. Jacobs, *Biochimica et Biophysica Acta (BBA)-Protein Structure*, 1974, **371**, 597-602.
274. D. W. Urry, *Journal of protein chemistry*, 1988, **7**, 81-114.
275. D. W. Urry, H. Sugano, K. U. Prasad, M. M. Long and R. S. Bhatnagar, *Biochemical and Biophysical Research Communications*, 1979, **90**, 194-198.
276. D. W. Urry, C. H. Luan, T. M. Parker, D. C. Gowda, K. U. Prasad, M. C. Reid and A. Safavy, *Journal of the American Chemical Society*, 1991, **113**, 4346-4348.
277. D. W. Urry, *Journal*, 1997, **101**, 11007-11028.
278. D. López Barreiro, I. J. Minten, J. C. Thies and C. M. Sagt, *ACS Biomaterials Science & Engineering*, 2021, **9**, 3796-3809.
279. A. K. Varanko, J. C. Su and A. Chilkoti, *Annu Rev Biomed Eng*, 2020, **22**, 343-369.
280. K. Trabbic-Carlson, D. E. Meyer, L. Liu, R. Piervincenzi, N. Nath, T. LaBean and A. Chilkoti, *Protein Eng Des Sel*, 2004, **17**, 57-66.
281. T. Christensen, W. Hassouneh, K. Trabbic-Carlson and A. Chilkoti, *Biomacromolecules*, 2013, **14**, 1514-1519.
282. D. Chow, M. L. Nunalee, D. W. Lim, A. J. Simnick and A. Chilkoti, *Materials Science and Engineering: R: Reports*, 2008, **62**, 125-155.
283. J. A. MacKay, D. J. Callahan, K. N. FitzGerald and A. Chilkoti, *Biomacromolecules*, 2010, **11**, 2873-2879.
284. D. Urry and T. Ohnishi, *Biopolymers: Original Research on Biomolecules*, 1974, **13**, 1223-1242.
285. D. T. McPherson, C. Morrow, D. S. Minehan, J. Wu, E. Hunter and D. W. Urry, *Biotechnology progress*, 1992, **8**, 347-352.
286. C. Guda, X. Zhang, D. McPherson, J. Xu, J. Cherry, D. Urry and H. Daniell, *Biotechnology Letters*, 1995, **17**, 745-750.
287. J. R. McDaniel, J. A. MacKay, F. G. Quiroz and A. Chilkoti, *Biomacromolecules*, 2010, **11**, 944-952.
288. L. F. Lima, M. G. D. C. Sousa, G. R. Rodrigues, K. B. S. de Oliveira, A. M. Pereira, A. da Costa, R. Machado, O. L. Franco and S. C. Dias, *Frontiers in Nanotechnology*, 2022, **4**, 874790.
289. Y. Guo, S. Liu, D. Jing, N. Liu and X. Luo, *Journal of Nanobiotechnology*, 2023, **21**, 418.
290. D. T. McPherson, J. Xu and D. W. Urry, *Protein Expr Purif*, 1996, **7**, 51-57.
291. D. E. Meyer and A. Chilkoti, *Nat Biotechnol*, 1999, **17**, 1112-1115.
292. J. van Strien, O. Escalona-Rayo, W. Jiskoot, B. Slütter and A. Kros, *Journal of Controlled Release*, 2023, **353**, 713-726.
293. Y. Cho, Y. Zhang, T. Christensen, L. B. Sagle, A. Chilkoti and P. S. Cremer, *The Journal of Physical Chemistry B*, 2008, **112**, 13765-13771.
294. A. Phour, V. Gaur, A. Banerjee and J. Bhattacharyya, *Adv Drug Deliv Rev*, 2022, **190**, 114544.

295. S. R. MacEwan and A. Chilkoti, *Journal of Controlled Release*, 2014, **190**, 314-330.
296. S. Roberts, M. Dzuricky and A. Chilkoti, *FEBS letters*, 2015, **589**, 2477-2486.
297. A. Yeboah, R. I. Cohen, C. Rabolli, M. L. Yarmush and F. Berthiaume, *Biotechnology and bioengineering*, 2016, **113**, 1617-1627.
298. A. Jiang, X. Guan, L. He and X. Guan, *Frontiers in Pharmacology*, 2023, **13**, 1113079.
299. D. M. Floss, M. Sack, E. Arcalis, J. Stadlmann, H. Quendler, T. Rademacher, E. Stoger, J. Scheller, R. Fischer and U. Conrad, *Plant biotechnology journal*, 2009, **7**, 899-913.
300. U. Conrad, I. Plagmann, S. Malchow, M. Sack, D. M. Floss, A. A. Kruglov, S. A. Nedospasov, S. Rose-John and J. Scheller, *Plant biotechnology journal*, 2011, **9**, 22-31.
301. M. Amiram, K. M. Luginbuhl, X. Li, M. N. Feinglos and A. Chilkoti, *Proceedings of the National Academy of Sciences*, 2013, **110**, 2792-2797.
302. C. A. Gilroy, K. M. Luginbuhl and A. Chilkoti, *Journal of Controlled Release*, 2016, **240**, 151-164.
303. W. Liu, J. A. MacKay, M. R. Dreher, M. Chen, J. R. McDaniel, A. J. Simnick, D. J. Callahan, M. R. Zalutsky and A. Chilkoti, *Journal of controlled Release*, 2010, **144**, 2-9.
304. W. Liu, J. McDaniel, X. Li, D. Asai, F. G. Quiroz, J. Schaal, J. S. Park, M. Zalutsky and A. Chilkoti, *Cancer research*, 2012, **72**, 5956-5965.
305. W. Liu, M. R. Dreher, D. Y. Furgeson, K. V. Peixoto, H. Yuan, M. R. Zalutsky and A. Chilkoti, *Journal of controlled release*, 2006, **116**, 170-178.
306. W. Liu, M. R. Dreher, D. C. Chow, M. R. Zalutsky and A. Chilkoti, *Journal of controlled release*, 2006, **114**, 184-192.
307. W. Hassouneh, T. Christensen and A. Chilkoti, *Current protocols in protein science*, 2010, **61**, 6.11. 11-16.11. 16.
308. S. R. MacEwan, W. Hassouneh and A. Chilkoti, *JoVE (Journal of Visualized Experiments)*, 2014, e51583.
309. F. Leonhardt, A. Gennari, G. B. Paludo, C. Schmitz, F. X. da Silveira, D. C. D. A. Moura, G. Renard, G. Volpato and C. F. Volken de Souza, *3 Biotech*, 2023, **13**, 186.
310. J. J. Bellucci, M. Amiram, J. Bhattacharyya, D. McCafferty and A. Chilkoti, *Angewandte Chemie (International ed. in English)*, 2013, **52**, 3703.
311. D. Lan, G. Huang, H. Shao, L. Zhang, L. Ma, S. Chen and A. Xu, *Anal Biochem*, 2011, **415**, 200-202.
312. A. Mullerpatan, D. Chandra, E. Kane, P. Karande and S. Cramer, *Journal of biotechnology*, 2020, **309**, 59-67.
313. A. Mullerpatan, E. Kane, R. Ghosh, A. Nascimento, H. Andersen, S. Cramer and P. Karande, *Biotechnology and Bioengineering*, 2020, **117**, 3775-3784.
314. C. Sweet, A. Aayush, L. Readnour, K. V. Solomon and D. H. Thompson, *Biomacromolecules*, 2021, **22**, 1990-1998.
315. J. Han, S. Fang, X. He, L. Wang, C. Li, J. Wu, Y. Cai and Y. Wang, *Food Chemistry*, 2022, **373**, 131543.
316. J. Bhattacharyya, J. J. Bellucci, I. Weitzhandler, J. R. McDaniel, I. Spasojevic, X. Li, C.-C. Lin, J.-T. A. Chi and A. Chilkoti, *Nature Communications*, 2015, **6**, 7939.
317. J. Andrew MacKay, M. Chen, J. R. McDaniel, W. Liu, A. J. Simnick and A. Chilkoti, *Nature Materials*, 2009, **8**, 993-999.
318. M. Dzuricky, S. Xiong, P. Weber and A. Chilkoti, *Nano letters*, 2019, **19**, 6124-6132.
319. B. Bulutoglu, A. Acun, S. L. Deng, S. Mert, E. Lupon, A. G. Lellouch, C. L. Cetrulo Jr, B. E. Uygun and M. L. Yarmush, *Advanced healthcare materials*, 2022, **11**, 2102795.
320. H. Zhao, V. Ibrahimova, E. Garanger and S. Lecommandoux, *Angewandte Chemie International Edition*, 2020, **59**, 11028-11036.
321. S. Acosta, L. Quintanilla-Sierra, L. Mbundi, V. Reboto and J. C. Rodríguez-Cabello, *Advanced Functional Materials*, 2020, **30**, 1909050.
322. D. W. Nelson and R. J. Gilbert, *Advanced healthcare materials*, 2021, **10**, 2101329.
323. D. L. Nettles, A. Chilkoti and L. A. Setton, *Advanced drug delivery reviews*, 2010, **62**, 1479-1485.
324. M. J. Glassman, R. K. Avery, A. Khademhosseini and B. D. Olsen, *Biomacromolecules*, 2016, **17**, 415-426.
325. C. Hrabchak, J. Rouleau, I. Moss, K. Woodhouse, M. Akens, C. Bellingham, F. Keeley, M. Dennis and A. Yee, *Acta Biomaterialia*, 2010, **6**, 2108-2115.
326. M. K. McHale, L. A. Setton and A. Chilkoti, *Tissue engineering*, 2005, **11**, 1768-1779.
327. A. Girotti, J. Gonzalez-Valdivieso, M. Santos, L. Martin and F. J. Arias, *International Journal of Biological Macromolecules*, 2020, **164**, 1640-1648.
328. S. R. MacEwan and A. Chilkoti, *Peptide Science: Original Research on Biomolecules*, 2010, **94**, 60-77.
329. A. Bandiera, A. Taglienti, F. Micali, B. Pani, M. Tamaro, V. Crescenzi and G. Manzini, *Biotechnol Appl Biochem*, 2005, **42**, 247-256.
330. A. Bandiera, A. Markulin, L. Corich, F. Vita and V. Borelli, *Biomacromolecules*, 2014, **15**, 416-422.
331. L. Corich, M. Busetti, V. Petix, S. Passamonti and A. Bandiera, *J Biotechnol*, 2017, **255**, 57-65.
332. A. Bandiera, *Enzyme Microb Technol*, 2011, **49**, 347-352.
333. A. Bandiera, *Prep Biochem Biotechnol*, 2010, **40**, 198-212.
334. A. Bandiera, P. Sist and R. Urbani, *Biomacromolecules*, 2010, **11**, 3256-3265.
335. G. Ciofani, G. G. Genchi, I. Liakos, A. Athanassiou, V. Mattoli and A. Bandiera, *Acta biomaterialia*, 2013, **9**, 5111-5121.
336. B. Çelebi, M. Cloutier, R. Balloni, D. Mantovani and A. Bandiera, *Macromolecular bioscience*, 2012, **12**, 1546-1554.
337. S. Bozzini, L. Giuliano, L. Altomare, P. Petrini, A. Bandiera, M. T. Conconi, S. Fare and M. C. Tanzi, *Journal of Materials Science: Materials in Medicine*, 2011, **22**, 2641-2650.
338. P. D'Andrea, D. Scaini, L. Ulloa Severino, V. Borelli, S. Passamonti, P. Lorenzon and A. Bandiera, *Biomaterials*, 2015, **67**, 240-253.

339. P. D'Andrea, D. Civita, M. Cok, L. Ulloa Severino, F. Vita, D. Scaini, L. Casalis, P. Lorenzon, I. Donati and A. Bandiera, *J Appl Biomater Funct Mater*, 2017, **15**, e43-e53.
340. P. D'Andrea, M. Sciancalepore, K. Veltruska, P. Lorenzon and A. Bandiera, *Biochimica et Biophysica Acta (BBA)-Molecular Cell Research*, 2019, **1866**, 504-517.
341. A. Bandiera, L. Corich, S. Tommasi, M. De Bortoli, P. Pelizzo, M. Stebel, D. Paladin and S. Passamonti, *Biotechnology and Bioengineering*, 2020, **117**, 354-361.
342. P. Sist, F. Tramer, A. Bandiera, R. Urbani, S. Redenšek Trampuž, V. Dolžan and S. Passamonti, *International Journal of Molecular Sciences*, 2023, **24**, 16289.
343. P. Sist, A. Bandiera, R. Urbani and S. Passamonti, *Biomacromolecules*, 2022, **23**, 3336-3348.
344. G. Ciofani, G. G. Genchi, P. Guardia, B. Mazzolai, V. Mattoli and A. Bandiera, *Macromolecular bioscience*, 2014, **14**, 632-642.
345. A. Heinz, *Critical reviews in biochemistry and molecular biology*, 2020, **55**, 252-273.
346. D. R. Galloway, *Mol Microbiol*, 1991, **5**, 2315-2321.
347. A. Bandiera, O. Catanzano, P. Bertoncin, C. Bergonzi, R. Bettini and L. Elviri, *Biotechnology and Applied Biochemistry*, 2022, **69**, 1793-1804.
348. S. Corvec, M. E. Portillo, B. M. Pasticci, O. Borens and A. Trampuz, *Int J Artif Organs*, 2012, **35**, 923-934.
349. G. Subbiahdoss, R. Kuijer, D. W. Grijpma, H. C. van der Mei and H. J. Busscher, *Acta Biomater*, 2009, **5**, 1399-1404.
350. C. Cyteval and A. Bourdon, *Diagnostic and interventional imaging*, 2012, **93**, 547-557.
351. S. Akay and A. Yaghmur, *Molecules*, 2024, **29**, 1172.
352. D. Campoccia, L. Montanaro and C. R. Arciola, *Biomaterials*, 2006, **27**, 2331-2339.
353. X. Li, L. Sun, P. Zhang and Y. Wang, *Coatings*, 2021, **11**, 294.
354. J. Cobo and J. L. Del Pozo, *Expert Rev Anti Infect Ther*, 2011, **9**, 787-802.
355. U. Filipović, R. G. Dahmane, S. Ghannouchi, A. Zore and K. Bohinc, *Adv Colloid Interface Sci*, 2020, **283**, 102228.
356. J. Barros, L. Grenho, C. M. Manuel, C. Ferreira, L. F. Melo, O. C. Nunes, F. J. Monteiro and M. P. Ferraz, *Int Microbiol*, 2013, **16**, 191-198.
357. A. G. Gristina, P. Naylor and Q. Myrvik, *Med Prog Technol*, 1988, **14**, 205-224.
358. M. S. Dhillon, A. Hooda, T. F. Moriarty and S. Sharma, *Indian J Orthop*, 2023, **57**, 44-51.
359. T. Bjarnsholt, O. Ciofu, S. Molin, M. Givskov and N. Høiby, *Nat Rev Drug Discov*, 2013, **12**, 791-808.
360. F. Reffuveille, C. de la Fuente-Núñez, S. Mansour and R. E. Hancock, *Antimicrob Agents Chemother*, 2014, **58**, 5363-5371.
361. M. Colilla, I. Izquierdo-Barba and M. Vallet-Regí, *Medicines*, 2018, **5**, 125.
362. S. Ferraris and S. Spriano, *Materials Science and Engineering: C*, 2016, **61**, 965-978.
363. S. B. Goodman, Z. Yao, M. Keeney and F. Yang, *Biomaterials*, 2013, **34**, 3174-3183.
364. A. Nouri, A. Shirvan, Y. Li and C. Wen, *Journal*, 2022.
365. C. L. Romanò, S. Scarponi, E. Gallazzi, D. Romanò and L. Drago, *J Orthop Surg Res*, 2015, **10**, 157.
366. A. Ghimire and J. Song, *ACS Appl Mater Interfaces*, 2021, **13**, 20921-20937.
367. X. Teng, C. Yao, C. P. McCoy and S. Zhang, *ACS Biomater Sci Eng*, 2024, **10**, 1162-1172.
368. X. Chen, J. Zhou, Y. Qian and L. Zhao, *Mater Today Bio*, 2023, **19**, 100586.
369. Z. Wu, B. Chan, J. Low, J. J. H. Chu, H. W. D. Hey and A. Tay, *Bioact Mater*, 2022, **16**, 249-270.
370. E. Fadeeva, V. K. Truong, M. Stiesch, B. N. Chichkov, R. J. Crawford, J. Wang and E. P. Ivanova, *Langmuir*, 2011, **27**, 3012-3019.
371. K. Bartlet, S. Movafaghi, L. P. Dasi, A. K. Kota and K. C. Popat, *Colloids Surf B Biointerfaces*, 2018, **166**, 179-186.
372. V. K. Manivasagam, G. Perumal, H. S. Arora and K. C. Popat, *J Biomed Mater Res A*, 2022, **110**, 1314-1328.
373. R. Fraioli, P. M. Tsimbouri, L. E. Fisher, A. H. Nobbs, B. Su, S. Neubauer, F. Rechenmacher, H. Kessler, M. P. Ginebra, M. J. Dalby, J. M. Manero and C. Mas-Moruno, *Sci Rep*, 2017, **7**, 16363.
374. J. Buxadera-Palomero, C. Calvo, S. Torrent-Camarero, F. J. Gil, C. Mas-Moruno, C. Canal and D. Rodríguez, *Colloids Surf B Biointerfaces*, 2017, **152**, 367-375.
375. O. P. Edupuganti, V. Antoci, Jr., S. B. King, B. Jose, C. S. Adams, J. Parvizi, I. M. Shapiro, A. R. Zeiger, N. J. Hickok and E. Wickstrom, *Bioorg Med Chem Lett*, 2007, **17**, 2692-2696.
376. V. Antoci, Jr., C. S. Adams, J. Parvizi, H. M. Davidson, R. J. Composto, T. A. Freeman, E. Wickstrom, P. Ducheyne, D. Jungkind, I. M. Shapiro and N. J. Hickok, *Biomaterials*, 2008, **29**, 4684-4690.
377. R. Vaishya, M. Chauhan and A. Vaish, *J Clin Orthop Trauma*, 2013, **4**, 157-163.
378. L. Drago, W. Boot, K. Dimas, K. Malizos, G. M. Hänsch, J. Stuyck, D. Gawlitta and C. L. Romanò, *Clin Orthop Relat Res*, 2014, **472**, 3311-3323.
379. G. Giavaresi, E. Meani, M. Sartori, A. Ferrari, D. Bellini, A. C. Sacchetta, J. Meraner, A. Sambri, C. Vocale, V. Sambri, M. Fini and C. L. Romanò, *Int Orthop*, 2014, **38**, 1505-1512.
380. C. Zoccali, G. Scoccianti, R. Biagini, P. A. Daolio, F. L. Giardina and D. A. Campanacci, *Eur J Orthop Surg Traumatol*, 2021, **31**, 1647-1655.
381. L. Zhao, P. K. Chu, Y. Zhang and Z. Wu, *J Biomed Mater Res B Appl Biomater*, 2009, **91**, 470-480.
382. H. S. Ryu, Y. I. Kim, B. S. Lim, Y. J. Lim and S. J. Ahn, *J Periodontol*, 2015, **86**, 1268-1275.
383. S. Ding, H. Hong, L. Xu, X. Wang, W. Zhang, X. Li, Y. Wang and J. Chen, *Zhongguo Xiu Fu Chong Jian Wai Ke Za Zhi*, 2022, **36**, 335-342.
384. M. Naveed, V. Hejazi, M. Abbas, A. A. Kamboh, G. J. Khan, M. Shumzaid, F. Ahmad, D. Babazadeh, X. FangFang, F. Modarresi-Ghazani, L. WenHua and Z. XiaoHui, *Biomed Pharmacother*, 2018, **97**, 67-74.
385. T. Wu, Q. Zhou, G. Hong, Z. Bai, J. Bian, H. Xie and C. Chen, *Colloids Surf B Biointerfaces*, 2023, **230**, 113484.
386. N. Vakili and A. Asefnejad, *Biomed Tech (Berl)*, 2020, **65**, 621-630.

387. T. Zhang, X. Qin, Y. Gao, D. Kong, Y. Jiang, X. Cui, M. Guo, J. Chen, F. Chang, M. Zhang, J. Li and P. Yin, *Front Bioeng Biotechnol*, 2023, **11**, 1118487.
388. M. Stevanović, M. Đošić, A. Janković, V. Kojić, M. Vukašinović-Sekulić, J. Stojanović, J. Odović, M. Crevar Sakač, K. Y. Rhee and V. Mišković-Stanković, *ACS Biomater Sci Eng*, 2018, **4**, 3994-4007.
389. V. Zarghami, M. Ghorbani, K. P. Bagheri and M. A. Shokrgozar, *J Mater Sci Mater Med*, 2022, **33**, 46.
390. S. Asadi, B. Mortezagholi, A. Hadizadeh, V. Borisov, M. J. Ansari, H. Shaker Majdi, A. Nishonova, H. Adelnia, B. Farasati Far and C. Chaiyasut, *Pharmaceutics*, 2022, **14**.
391. Y. Dong, L. Liu, J. Sun, W. Peng, X. Dong, Y. Gu, Z. Ma, D. Gan and P. Liu, *J Mater Chem B*, 2021, **9**, 8321-8329.
392. L. Xing, H. Song, J. Wei, X. Wang, Y. Yang, P. Zhe, M. Luan and J. Xu, *Molecules*, 2023, **28**.
393. Y. Liu, T. Dong, Y. Chen, N. Sun, Q. Liu, Z. Huang, Y. Yang, H. Cheng and K. Yue, *ACS Appl Mater Interfaces*, 2023, **15**, 11507-11519.
394. B. Costa, G. Martínez-de-Tejada, P. A. C. Gomes, L. M. MC and F. Costa, *Pharmaceutics*, 2021, **13**.
395. M. Gabriel, K. Nazmi, E. C. Veerman, A. V. Nieuw Amerongen and A. Zentner, *Bioconjug Chem*, 2006, **17**, 548-550.
396. B. e. Nie, H. Ao, C. Chen, K. Xie, J. Zhou, T. Long, T. t. Tang and B. Yue, *RSC Advances*, 2016, **6**, 46733-46743.
397. B. Mishra and G. Wang, *Biofouling*, 2017, **33**, 544-555.
398. S. Acosta, A. Ibañez-Fonseca, C. Aparicio and J. C. Rodríguez-Cabello, *Biomater Sci*, 2020, **8**, 2866-2877.
399. M. Hoyos-Nogués, F. Velasco, M. P. Ginebra, J. M. Manero, F. J. Gil and C. Mas-Moruno, *ACS Appl Mater Interfaces*, 2017, **9**, 21618-21630.
400. R. Chen, M. D. Willcox, K. K. Ho, D. Smyth and N. Kumar, *Biomaterials*, 2016, **85**, 142-151.
401. S. Makihira, T. Shuto, H. Nikawa, K. Okamoto, Y. Mine, Y. Takamoto, M. Ohara and K. Tsuji, *Int J Mol Sci*, 2010, **11**, 1458-1470.
402. M. Godoy-Gallardo, C. Mas-Moruno, K. Yu, J. M. Manero, F. J. Gil, J. N. Kizhakkedathu and D. Rodriguez, *Biomacromolecules*, 2015, **16**, 483-496.
403. D. T. Yucesoy, M. Hnilova, K. Boone, P. M. Arnold, M. L. Snead and C. Tamerler, *Jom (1989)*, 2015, **67**, 754-766.
404. H. Yazici, M. B. O'Neill, T. Kacar, B. R. Wilson, E. E. Oren, M. Sarikaya and C. Tamerler, *ACS Appl Mater Interfaces*, 2016, **8**, 5070-5081.
405. M. Drexelius, R. Arnold, D. Meinberger, M. Wilhelm, S. Mathur and I. Neundorf, *J Pept Sci*, 2023, **29**, e3481.
406. R. Fateme, G. Fatemeh, S. Sima, A. Moshaverinia and S. Hasannia, *International Journal of Peptide Research and Therapeutics*, 2020, **26**, 1629-1639.
407. Z. B. Huang, X. Shi, J. Mao and S. Q. Gong, *Sci Rep*, 2016, **6**, 38410.
408. D. Xu, W. Yang, Y. Hu, Z. Luo, J. Li, Y. Hou, Y. Liu and K. Cai, *Colloids Surf B Biointerfaces*, 2013, **110**, 225-235.
409. B. Nie, H. Ao, J. Zhou, T. Tang and B. Yue, *Colloids Surf B Biointerfaces*, 2016, **145**, 728-739.
410. B. Nie, H. Ao, T. Long, J. Zhou, T. Tang and B. Yue, *Colloids Surf B Biointerfaces*, 2017, **150**, 183-191.
411. Y. Wang, J. Zhang, T. Gao, N. Zhang, J. He and F. Wu, *Colloids Surf B Biointerfaces*, 2021, **202**, 111697.
412. G. Gao, K. Yu, J. Kindrachuk, D. E. Brooks, R. E. Hancock and J. N. Kizhakkedathu, *Biomacromolecules*, 2011, **12**, 3715-3727.
413. G. Gao, D. Lange, K. Hilpert, J. Kindrachuk, Y. Zou, J. T. Cheng, M. Kazemzadeh-Narbat, K. Yu, R. Wang, S. K. Straus, D. E. Brooks, B. H. Chew, R. E. Hancock and J. N. Kizhakkedathu, *Biomaterials*, 2011, **32**, 3899-3909.
414. C. Monteiro, H. Fernandes, D. Oliveira, N. Vale, M. Barbosa, P. Gomes and L. M. MC, *Molecules*, 2020, **25**.
415. F. Costa, S. Maia, J. Gomes, P. Gomes and M. C. Martins, *Acta Biomater*, 2014, **10**, 3513-3521.
416. F. M. Costa, S. R. Maia, P. A. Gomes and M. C. Martins, *Biomaterials*, 2015, **52**, 531-538.
417. P. Sahariah, K. K. Sørensen, M. Hjálmarsdóttir, E. Sigurjónsson Ó, K. J. Jensen, M. Másson and M. B. Thygesen, *Chem Commun (Camb)*, 2015, **51**, 11611-11614.
418. M. Barbosa, F. Costa, C. Monteiro, F. Duarte, M. C. L. Martins and P. Gomes, *Acta Biomater*, 2019, **84**, 242-256.
419. T. Li, N. Wang, S. Chen, R. Lu, H. Li and Z. Zhang, *Int J Nanomedicine*, 2017, **12**, 2995-3007.
420. M. Ma, M. Kazemzadeh-Narbat, Y. Hui, S. Lu, C. Ding, D. D. Chen, R. E. Hancock and R. Wang, *J Biomed Mater Res A*, 2012, **100**, 278-285.
421. M. Pihl, S. Galli, R. Jimbo and M. Andersson, *J Biomed Mater Res B Appl Biomater*, 2021, **109**, 1787-1795.
422. M. Kazemzadeh-Narbat, B. F. Lai, C. Ding, J. N. Kizhakkedathu, R. E. Hancock and R. Wang, *Biomaterials*, 2013, **34**, 5969-5977.
423. A. Volejníková, P. Melicherčík, O. Nešuta, E. Vaňková, L. Bednárová, J. Rybáček and V. Čeřovský, *J Med Microbiol*, 2019, **68**, 961-972.
424. H. P. Stallmann, C. Faber, E. T. Slotema, D. M. Lyaruu, A. L. Bronckers, A. V. Amerongen and P. I. Wuisman, *J Antimicrob Chemother*, 2003, **52**, 853-855.
425. H. P. Stallmann, C. Faber, A. L. Bronckers, A. V. Nieuw Amerongen and P. I. Wuisman, *J Antimicrob Chemother*, 2004, **54**, 472-476.
426. C. Faber, H. P. Stallmann, D. M. Lyaruu, U. Joosten, C. von Eiff, A. van Nieuw Amerongen and P. I. Wuisman, *Antimicrob Agents Chemother*, 2005, **49**, 2438-2444.
427. H. P. Stallmann, R. de Roo, C. Faber, A. V. Amerongen and P. I. Wuisman, *J Orthop Res*, 2008, **26**, 531-538.
428. M. Kazemzadeh-Narbat, J. Kindrachuk, K. Duan, H. Jenssen, R. E. Hancock and R. Wang, *Biomaterials*, 2010, **31**, 9519-9526.
429. M. Kazemzadeh-Narbat, S. Noordin, B. A. Masri, D. S. Garbuz, C. P. Duncan, R. E. Hancock and R. Wang, *J Biomed Mater Res B Appl Biomater*, 2012, **100**, 1344-1352.
430. P. Melicherčík, O. Nešuta and V. Čeřovský, *Pharmaceuticals (Basel)*, 2018, **11**.
431. M. Mateescu, S. Baixe, T. Garnier, L. Jierry, V. Ball, Y. Haikel, M. H. Metz-Boutigue, M. Nardin, P. Schaaf, O. Etienne and P. Lavalle, *PLoS One*, 2015, **10**, e0145143.

432. H. Cheng, K. Yue, M. Kazemzadeh-Narbat, Y. Liu, A. Khalilpour, B. Li, Y. S. Zhang, N. Annabi and A. Khademhosseini, *ACS Appl Mater Interfaces*, 2017, **9**, 11428-11439.
433. A. de Breij, M. Riool, P. H. Kwakman, L. de Boer, R. A. Cordfunke, J. W. Drijfhout, O. Cohen, N. Emanuel, S. A. Zaat, P. H. Nibbering and T. F. Moriarty, *J Control Release*, 2016, **222**, 1-8.
434. A. L. Rodríguez López, M. R. Lee, B. J. Ortiz, B. D. Gastfriend, R. Whitehead, D. M. Lynn and S. P. Palecek, *Acta Biomater*, 2019, **93**, 50-62.
435. A. I. Stavrakis, S. Zhu, A. H. Loftin, X. Weixian, J. Niska, V. Hegde, T. Segura and N. M. Bernthal, *Biomed Res Int*, 2019, **2019**, 1638508.
436. A. I. Stavrakis, S. Zhu, V. Hegde, A. H. Loftin, A. G. Ashbaugh, J. A. Niska, L. S. Miller, T. Segura and N. M. Bernthal, *J Bone Joint Surg Am*, 2016, **98**, 1183-1189.
437. V. Hegde, H. Y. Park, E. Dworsky, S. D. Zoller, W. Xi, D. O. Johansen, A. H. Loftin, C. D. Hamad, T. Segura and N. M. Bernthal, *Spine (Phila Pa 1976)*, 2020, **45**, E305-e311.
438. J. Chen, X. Shi, Y. Zhu, Y. Chen, M. Gao, H. Gao, L. Liu, L. Wang, C. Mao and Y. Wang, *Theranostics*, 2020, **10**, 109-122.
439. Y. Zhang, K. Hu, X. Xing, J. Zhang, M. R. Zhang, X. Ma, R. Shi and L. Zhang, *Macromol Biosci*, 2021, **21**, e2000194.
440. T. Liu, S. Yan, R. Zhou, X. Zhang, H. Yang, Q. Yan, R. Yang and S. Luan, *ACS Appl Mater Interfaces*, 2020, **12**, 42576-42585.
441. L. E. Alksne and S. J. Projan, *Curr Opin Biotechnol*, 2000, **11**, 625-636.
442. J. Zhan, L. Wang, Y. Zhu, H. Gao, Y. Chen, J. Chen, Y. Jia, J. He, Z. Fang, C. Mao, L. Ren and Y. Wang, *ACS Appl Mater Interfaces*, 2018, **10**, 35830-35837.
443. X. Shen, F. Zhang, K. Li, C. Qin, P. Ma, L. Dai and K. Cai, *Materials & Design*, 2016, **92**, 1007-1017.
444. S. Yan, H. Shi, L. Song, X. Wang, L. Liu, S. Luan, Y. Yang and J. Yin, *ACS Appl Mater Interfaces*, 2016, **8**, 24471-24481.
445. X. Wang, S. Yan, L. Song, H. Shi, H. Yang, S. Luan, Y. Huang, J. Yin, A. F. Khan and J. Zhao, *ACS Appl Mater Interfaces*, 2017, **9**, 40930-40939.
446. J. Feng, Z. Xie, W. Yang, Y. Zhao, F. Xiang, Z. Cao, W. Li, Z. Chen and Y. Wu, *Toxicon*, 2016, **113**, 1-6.
447. M. Levite, L. Cahalon, A. Peretz, R. Hershkoviz, A. Sobko, A. Ariel, R. Desai, B. Attali and O. Lider, *J Exp Med*, 2000, **191**, 1167-1176.
448. A. Becchetti, G. Petroni and A. Arcangeli, *Trends Cell Biol*, 2019, **29**, 298-307.
449. C. Baldock, A. F. Oberhauser, L. Ma, D. Lammie, V. Siegler, S. M. Mithieux, Y. Tu, J. Y. Chow, F. Suleman, M. Malfois, S. Rogers, L. Guo, T. C. Irving, T. J. Wess and A. S. Weiss, *Proc Natl Acad Sci U S A*, 2011, **108**, 4322-4327.
450. D. Laurent, F. Nicolas, J. P. A. Alain, H. Bernard and D. Laurent, *Critical Reviews in Oncology/Hematology*, 2004, **49**, 235-244.

Annex I. Supporting Information Chapter 4

HIn primary structure

Domain	Theoretical MW	aa sequence
His-tag	1629.74 Da	MRGSHHHHHHGSAAA
HELP	43117.88 Da	(AAAAAAKAAAKAAQFGLVPGVGVAPGVGVAPGVGVAPGVGLAPGVGVAPGVGVAPGVGVAPGIAP)8
Linker	2558.92 Da	GGLAAAAAAAAAKAAAKAAQGGLPGIPGRE
AMP (In)	1907.30 Da	ILPWKWPWWPWRR

Cloning of HIn. To obtain the HIn construct, the coding sequence of the linker and of the indolicidin, flanked by *DraIII* sites was purchased from Eurofins Genomics and ligated into the pEX8EL vector exploiting the unique *DraIII* site at the HELP orf C-terminus, described in Bandiera, A., *et al.,* (2005).[1] After transformation of *Escherichia coli C3037I* (New England Biolabs), positive clones were selected and verified by sequencing (Eurofins Genomics). The expression strain was transformed with the plasmid carrying the new HIn construct.

Expression of HIn. Selected clones of *E. coli* C3037I strain transformed with the plasmid carrying the new HIn construct were grown in Luria Bertani medium (LB, 10 g/L tryptone, 5 g/L sodium chloride and 5 g/L yeast extract, pH 7.2) supplemented with 50 µg/mL of ampicillin and 70 µg/mL of chloramphenicol. Typically, a starter culture of 120 mL of the same medium after overnight growth at 37°C was used to inoculate 1.2 L of Terrific Broth (TB, 12 g/L tryptone and 24 g/L yeast extract) supplemented with phosphate-buffered glycerol (PGB, 2.3 g/L potassium phosphate monobasic, 12.5 g/L potassium phosphate dibasic, and 4 mL/L glycerol). Bacterial cells were grown at 37 °C under shaking conditions until turbidity at 600 nm reached about 1 O.D. unit. The culture was then induced with Isopropyl β- d-1- thiogalactopyranoside to a final concentration of 0.1 mM and allowed to further grow for 5h. Then, bacterial cells were collected by centrifugation at 8000 rpm for 20 min at 10°C (Beckman–Coulter, J-26 XP). The pellets were stored at -20°C for further processing.

Extraction and ITC purification of HIn product. The protocol exploited the thermo-responsive behaviour of HIn and was based on the Inverse Transition Cycling (ITC) first described by Meyer, D., and Chilkoti, A. (1999).[2] The pellet obtained from 1.2 L of IPTG-induced bacterial culture was re-suspended in 400 mL of extraction buffer (50 mM Tris/HCl pH = 8, 250 mM NaCl, 0,1 mM EDTA, 0,1% Triton X-100, 1 mM PMSF) and disrupted using a high pressure homogenizer (Panda NS1001L, GEA Niro Soavi, Italy). The recovered suspension was cooled on ice, 2-mercaptoethanol was added to 20 mM and centrifuged at 10000 rpm, for 30 min at 8 °C (Beckman–Coulter, J-26 XP). Supernatant was properly diluted adding fresh extraction buffer and precipitated adding NaCl to a final concentration of 1.5 M at 37 °C. The aggregated polypeptide particles were separated by centrifugation at 7000 rpm, 37 °C for 30 min. The pellet was re-dissolved in cold water, non-soluble material was discarded after cold centrifugation and solution was precipitated again by NaCl addition and rising temperature to 37 °C. Three ITCs yield pure recombinant protein. After the last temperature-dependent transition cycle the material was lyophilized for long-term storage and a solution 2 mg/mL was prepared to analyze by SDS-PAGE.

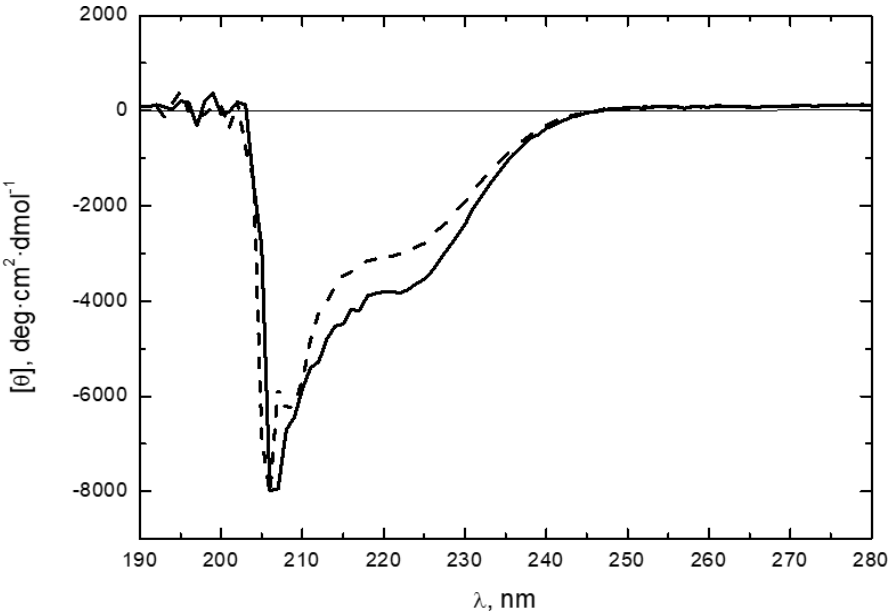

Figure 1S: Circular dichroism (CD) spectra of HIn (black line) compared with that of the HELP biopolymer (dashed line). Spectra were recorded on protein solutions with a concentration of 0.1 mg/mL in NaPi / NaCl (10 mM sodium phosphate/ 0.15M NaCl pH = 6.8) buffer. The CD Spectra were recorded at 25 °C in a 200- to 500-nm thermostatic cell on a Jasco J-710 spectrometer under constant nitrogen flow, and the data were expressed as the mean molar ellipticity [θ] of the residue (mdeg-cm2-dmol-1).

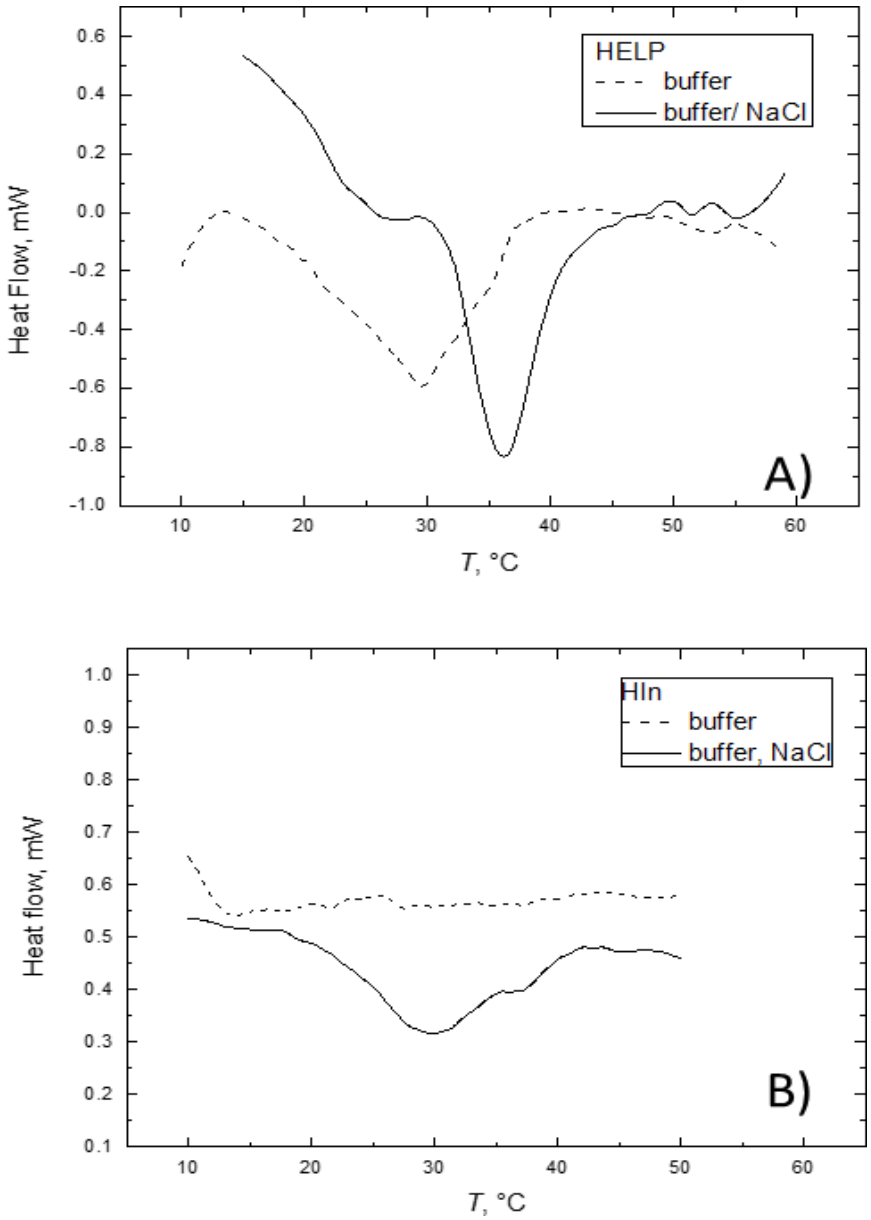

Figure 2S: DSC thermograms of A) HELP and B) HIn biopolymers 4 mg/mL in NaPi (10 mM sodium phosphate pH = 6.8, dotted line) and NaPi / NaCl (10 mM sodium phosphate/ 0.15M NaCl pH = 6.8, black line) buffers. Stainless steel cells were filled by weight with protein samples and then hermetically sealed and equilibrated for 16 h at 4 °C. The calorimeter was pre-equilibrated at 5°C for 10 min, followed by heating from 5 to 70 °C at a scan rate of 0.5 °C/min. The solvent was used as a reference. The onset and the peak inverse transition temperature (Tt) were determined.

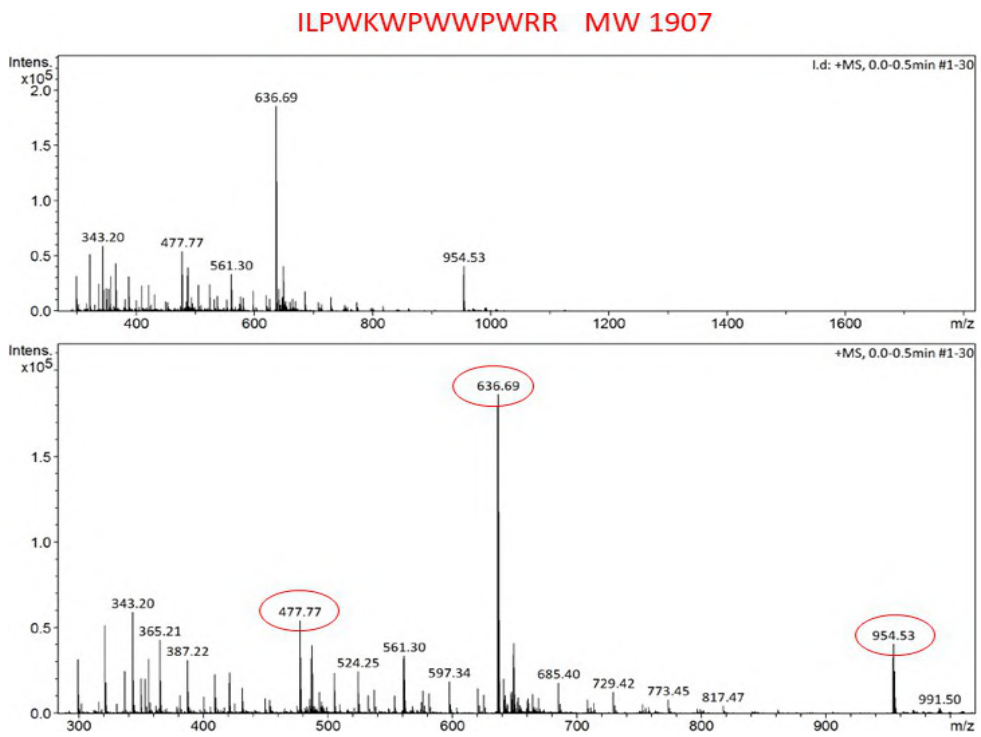

Figure 3S: Electrospray ionization Mass Spectrometry analysis of the indolicidin domain obtained by specific Glu-C cleavage of a 4% HIn matrix. A 150 µL matrix was incubated overnight at 37˚C with 500 µL of 100 mM ammonium bicarbonate buffer pH 8 with 10 ng/µL of Glu-C enzyme. After the reaction, the supernatant was collected, added by 0.1% TFA and injected with a syringe infusion pump at 2 µl/min, scanning at m/z 300/1800. Positive-ion detection was performed at an orifice potential of 75 V.

Table 1S: Theoretical masses of the expected ions predicted by PeptideMass (Expasy Server, https://web.expasy.org/peptide_mass/)

The peptide masses from your sequence are:

[Theoretical pI: 12.01 / Mw (average mass): 1907.30 / Mw (monoisotopic mass): 1906.03]

mass	position	#MC	modifications	peptide sequence
954.0226	1-13	0		ILPWKWPWWPWRR

100.0% of sequence covered (you may modify the input parameters to display also peptides < 500 Da or > 100000000000 Da):

```
        10
ILPWKWPWWP WRR
```

The peptide masses from your sequence are:

[Theoretical pI: 12.01 / Mw (average mass): 1907.30 / Mw (monoisotopic mass): 1906.03]

mass	position	#MC	modifications	peptide sequence
636.3508	1-13	0		ILPWKWPWWPWRR

100.0% of sequence covered (you may modify the input parameters to display also peptides < 500 Da or > 100000000000 Da):

```
        10
ILPWKWPWWP WRR
```

References

1. D. E. Meyer and A. Chilkoti, *Nat Biotechnol*, **1999**, 17, 1112-1115.
2. Bandiera, A. Taglienti, F. Micali, B. Pani, M. Tamaro, V. Crescenzi and G. Manzini, *Biotechnol Appl Biochem*, **2005**, 42, 247-256.

Annex II. Supporting Information Chapter 5

HhBD1 cloning, expression, extraction, and purification

Cloning. The coding sequence of hBD1, flanked by *DraIII and HindIII* sites, was purchased from Eurofins Genomics (Milan, Italy) and ligated into the pEX8EL vector, exploiting the unique *DraIII and HindIII* sites in the vector for the in-frame fusion if the coding sequence of hBD1nat the C-terminus of HELP according to the already described methodology.[1] Chemically competent *Escherichia coli* C3037I cells (New England Biolabs, Massachusetts, USA) were transformed with the ligation mixture, and positive clones were selected and verified by sequencing (Eurofins Genomics).

Expression. Positive clones of *E. coli* C3037I strain transformed with the plasmid carrying the HhBD1 construct were grown in Luria-Bertani medium (LB, 10 g L^{-1} tryptone, 5 g L^{-1} sodium chloride and 5 g L^{-1} yeast extract, pH 7.2) supplemented with 50 µg mL^{-1} of ampicillin and 70 µg mL^{-1} of chloramphenicol. A starter culture of 120 mL in the same medium after overnight growth at 37 °C was used to inoculate 1.2 L of Terrific Broth (TB, 12 g L-1 tryptone and 24 g L-1 yeast extract) supplemented with phosphate-buffered glycerol (PGB, 2.3 g L^{-1} monobasic potassium phosphate, 12.5 g L^{-1} dibasic potassium phosphate, and 4 mL L^{-1} monobasic glycerol). Bacterial cells were grown at 37 °C under shaking conditions until turbidity at 600 nm reached about 1 OD unit. HhBD1 expression was then induced by adding isopropyl β-d-1-thio galacto pyranoside to a final concentration of 0.1 mM, and the bacteria were further cultured for 5 hours. Then, the bacterial mass was harvested by centrifugation at 8000 rpm for 20 minutes at 10 °C (Beckman-Coulter, J-26 XP, California, USA), and the pellets were stored at -20 °C for further processing.

Extraction. The pellets obtained from the expression cultures were resuspended in 400 mL of extraction buffer (50 mM Tris/HCl pH 8, 250 mM NaCl, 0.1 mM EDTA, 0,1% Triton X-100, and 1 mM PMSF) and disrupted using a high-pressure homogeniser (Panda NS1001L, GEA Niro Soavi, Parma, Italy) by 4 cycles at 1280 bar. Then, 2-mercaptoethanol was added to a final concentration of 20 mM, the bacterial lysate was cooled on ice and centrifuged at 10000 rpm for 30 minutes at 8 °C (Beckman–Coulter, J-26 XP, California, USA), and the cellular debris was discarded, and the supernatant was stored at -20°C.

Purification. The HhBD1 purification procedure was based on the thermo-responsive properties of the HELP domain following a method known as Inverse Transition Cycling (ITC).[2] Briefly, the supernatant from the extraction procedure described above was precipitated by adding NaCl to a final concentration of 1.5 M and warmed to 37 °C in a water bath. The aggregated polypeptide particles were collected by centrifugation at 7000 rpm at 37 °C for 30 minutes. The resulting pellet was redissolved in cold water; the insoluble material was removed after cold centrifugation. The supernatant was precipitated again by NaCl addition and raising temperature to 37 °C. Three successive ITC cycles ensured the production of highly pure recombinant fusion protein. After the last temperature-dependent transition cycle, the material was frozen and lyophilised for long-term storage.

A solution of 0.5 mg mL-1 concentration was prepared for SDS-PAGE analysis.

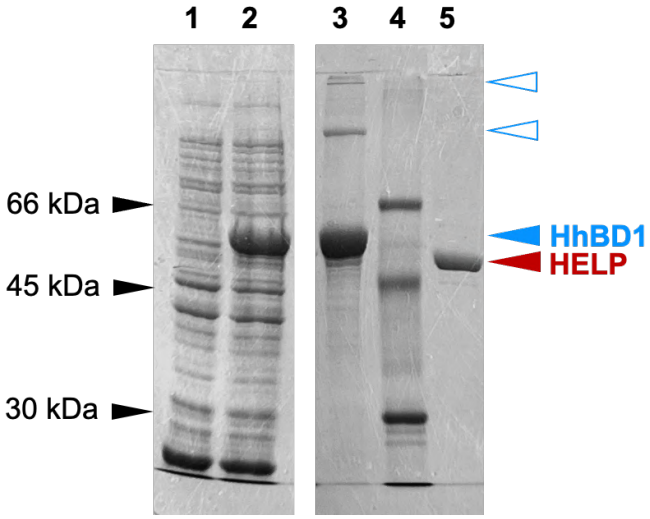

Figure S1: Representative 10 % SDS-PAGE analysis of the production and purification of the HhBD1 biopolymer. Lane 1, total protein content of the lysate of the expression culture before IPTG induction; lane 2, total protein content of the bacterial lysate 5 hours after IPTG induction; lane 3, recombinant HhBD1 fusion biopolymer purified by ITC. The main HhBD1 band (solid blue arrow) corresponded to an apparent mass of about 55 kDa. Minor, slower migrating bands are visible in the upper part of the lane, likely due to HhBD1 multimers formation (open blue arrows). Lane 4, molecular mass markers, and lane 5, purified HELP biopolymer as the reference. Molecular mass markers: bovine serum albumin, 66 kDa; ovalbumin, 45 kDa; carbonic anhydrase, 30 kDa. Coomassie blue staining.

Stability of HELP and HhBD1

Effect of pH. HELP and HhBD1 pH stability were tested by incubating 1mL of each biopolymer at the concentration of 2 mg mL^{-1} in 5 mM of HCl and 5 mM of NaOH. In parallel, aqueous solutions of the biopolymers were prepared as controls. The solutions were then incubated without stirring for 16 hours at 25°C.

Table S1. pH values of HhBD1 and HELP solutions in acid and basic conditions. The pH values of the solutions were measured at the beginning of the experiment (T_0) and after 16 hours of incubation (T_{end}).

	pH			
	HELP		**HhBD1**	
	T_0	**T_{end}**	**T_0**	**T_{end}**
H_2O	6.3	6.7	6.2	6.9
5 mM NaOH	12	11.9	12	11.9
5 mM HCl	2.3	2.3	2.3	2.2

At the same time points, 10 µL from each sample were collected and mixed (1:1) with Laemmli loading buffer for SDS-PAGE analysis. 4 µL (4 µg) were loaded per well to analyse the biopolymer stability using an SDS-PAGE.

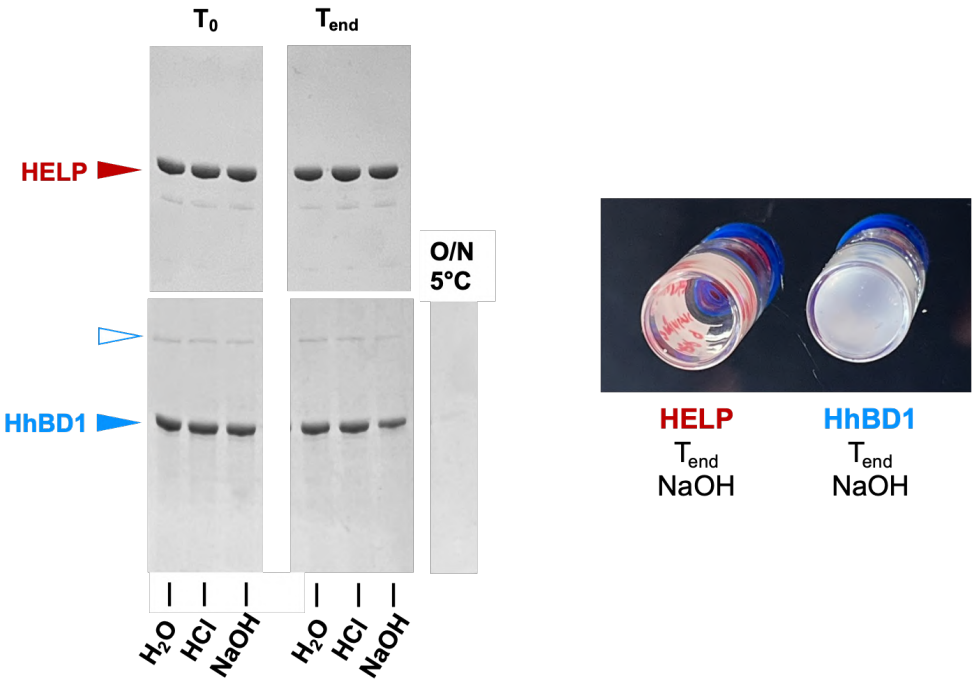

Figure S2: HELP and the HhBD1 biopolymers' stability in acidic and basic conditions. 9% SDS-PAGE analysis (on the left). After the run (V=160 v, 1 hour), the gel was stained with Coomassie blue. Red arrow, HELP electrophoretic band, solid blue arrow, HhBD1 electrophoretic band, open blue arrow, HhBD1 multimer. All the samples except the HhBD1 in 5 mM NaOH remained unaffected by the treatments. A concentration decrease was detectable by SDS PAGE analysis in the HhBD1 sample after incubation in basic conditions with the simultaneous formation of a clearly visible hydrogel-like layer on the tube bottom (on the right). This layer proved to be stable after cold water rinsing and subsequent overnight incubation at 5°C in 1 mL of water. No protein signal was detected by SDS-PAGE analysis of this sample.

Susceptibility to elastase. Aqueous solutions of HELP and HhBD1 biopolymers (6 mg mL^{-1}) in 10 mM NaPi buffer pH 6.8 were incubated with 0.2 (100X), 0.02 (10X) ng μL^{-1} of elastase (Sigma, #E7885) for 3 h at 37 °C in a final reaction volume of 50 µL. In parallel, control reactions were set up under the same condition without the elastase (CTRL). The same reactions were prepared with bovine serum albumin (BSA) in the absence and in the presence of the highest final concentration (0.2 ng μL^{-1}) of elastase. To stop the reactions, 50 µL of Laemli loading buffer were added to each sample, and 1.5 µL of this mixture, corresponding to 4.5 µg, were analysed in 9% SDS-PAGE. As shown in Figure S3, BSA was not degraded by the enzyme, whereas, as expected, HhBD1 showed the same elastase susceptibility of HELP, holding the potential for the smart release of the bioactive domain upon elastolytic stimuli.[3]

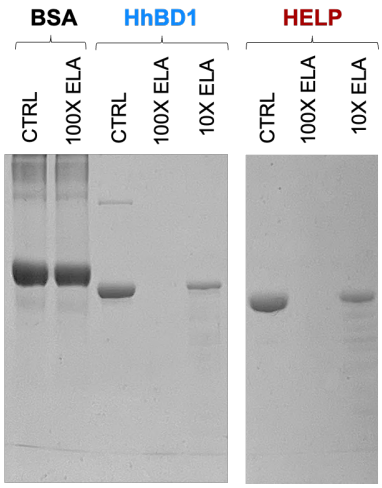

Figure S3: 9% SDS-PAGE analysis of HELP and HhBD1 biopolymers' susceptibility to elastase degradation.

Accessible surface area calculation of the 36 amino acids domain of hBD1

The PDB file of the 36 amino acids structure of hBD1 from PDB entry 1E4S (see **Fig. 1** in the main manuscript) was used to estimate the solvent-accessible surface area using the online software GETAREA (https://curie.utmb.edu/getarea.html).[4]

Table S2: Theoretical solvent accessibility surface area of hBD1

POLAR area/energy = 962.47

APOLAR area/energy = 1921.08

UNKNOW area/energy = 0.00

Total area/energy = 2883.55

Radial diffusion assays

Radial diffusion assays were performed as described in the main manuscript (**Experimental section 4.2**) in the absence or presence of 2 mM DTT.

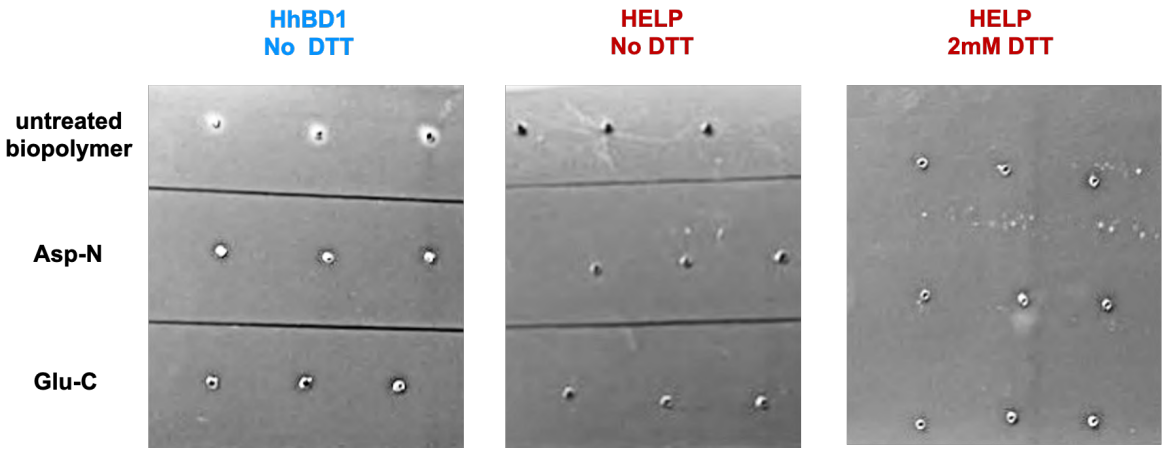

Figure S4: Representative images of the radial diffusion assays in the absence and presence of 2 mM DTT. No inhibition halos were observed.

Oscillatory rheology analysis

Frequency sweep analysis. Oscillatory rheology analysis was performed as described in the main manuscript (**Experimental section 4.3**) using a Malvern Kinexus Ultra Plus rheometer (Alfatest, Milan, Italy). The frequency sweep analysis was performed after the time sweep. The storage (G') and loss (G") moduli of the hydrogels were recorded from 0.1 to 10 Hz (stress 4 Pa, within the linear regime). For the graphical representation, the mean value of two representative data sets was plotted.

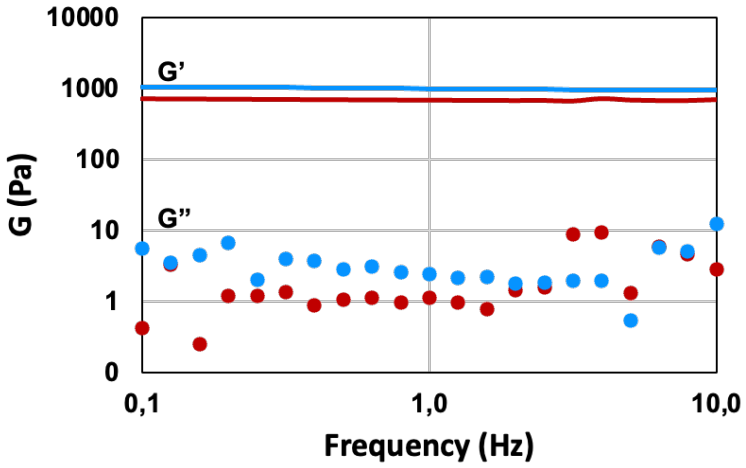

Figure S5: Frequency sweep analysis of HELP (red) and HhBD1 (blue) matrices. G′ is the elastic or storage modulus and G″ is the viscous or loss modulus.

Mass spectrometry

The hBD1 domains released from the matrix were analysed by electrospray ionisation mass spectrometry (ESI-MS). Specific cleavage of 4% (w/v) HhBD1 matrix was achieved by carrying out the reactions with Glu-C and Asp-N enzymes under the same conditions reported in the main manuscript (**Experimental section 4.3**). The matrices were prepared by depositing 10 µl of 4% HhBD1 aqueous solution per well in a 96-well polystyrene V-shaped bottom microplate (Sarstedt, Numbrecht, Germany). After extensive washing with water, the matrices were incubated with 25 µL of 100 mM ammonium bicarbonate buffer pH 8, containing 8.3 ng μL^{-1} or 2.6 ng μL^{-1} of Glu-C and Asp-N, respectively. In total, 8 replicates for each enzymatic reaction were set up. After the reaction, the supernatants of the matrices digested with Glu-C were pulled, as well as those of the matrices treated with Asp-N. For ESI-MS analysis, the pulled supernatants were supplemented with 50% acetonitrile/0.1% TFA and injected with a syringe infusion pump at a flow rate of 2 µl min^{-1}, with a scanning range of m/z 300/1800. Detection was carried out in positive ion mode with an orifice potential set at 75 V.

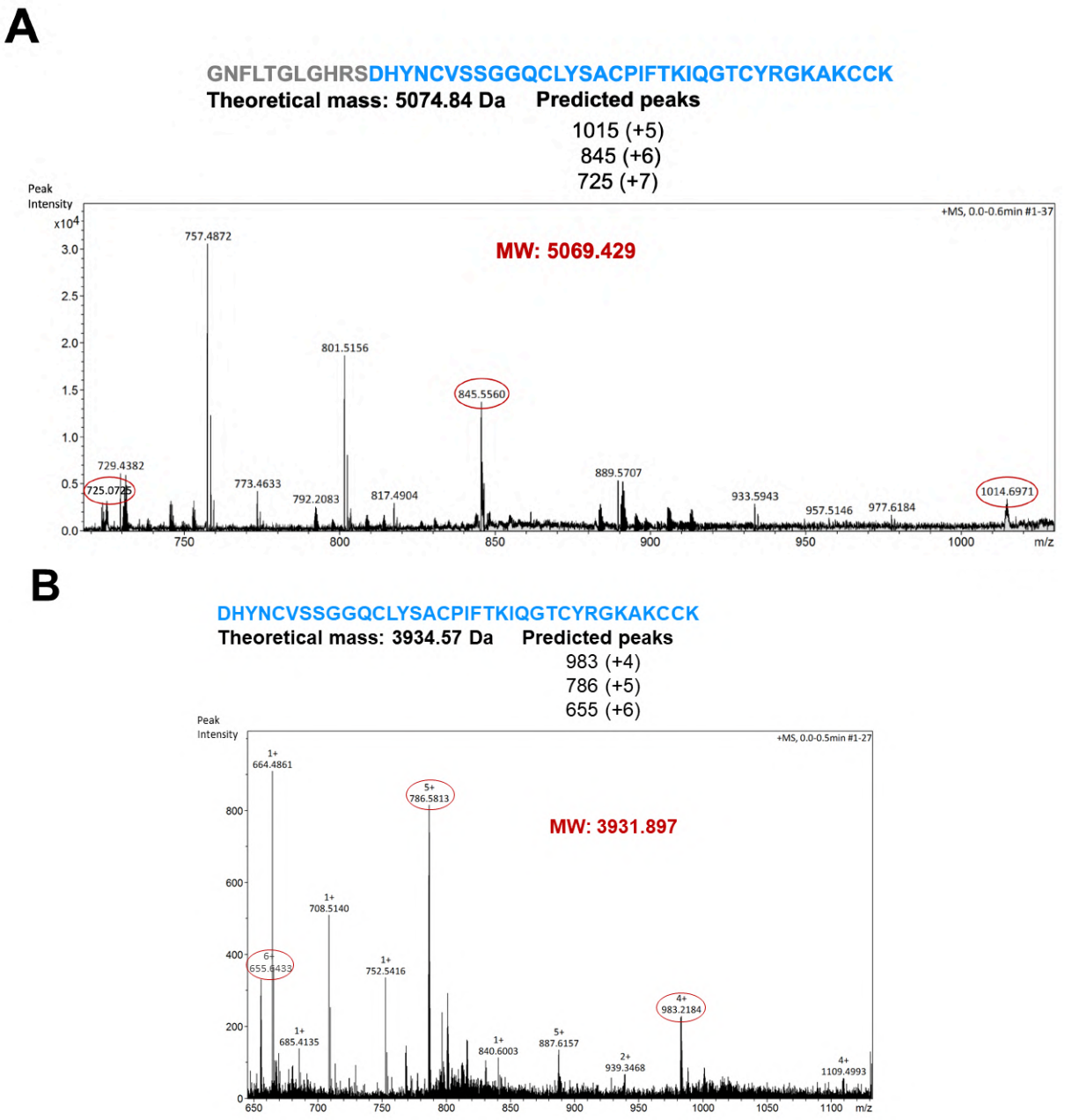

Figure S6: Mass spectrometry analysis of the peptides derived from the treatment of HhBD1 matrices with A) Glu-C and B) Asp-N endoproteinases.

Analysis of cells cultured on HELP and HhBD1 thin-film coatings

Fluorescence microscopy analysis was performed on cells seeded on the HhBD1 and HELP thin-films. Thin-film preparation, cell seeding, and fluorescence staining were performed as described in the main manuscript (**Experimental section 4.4**).

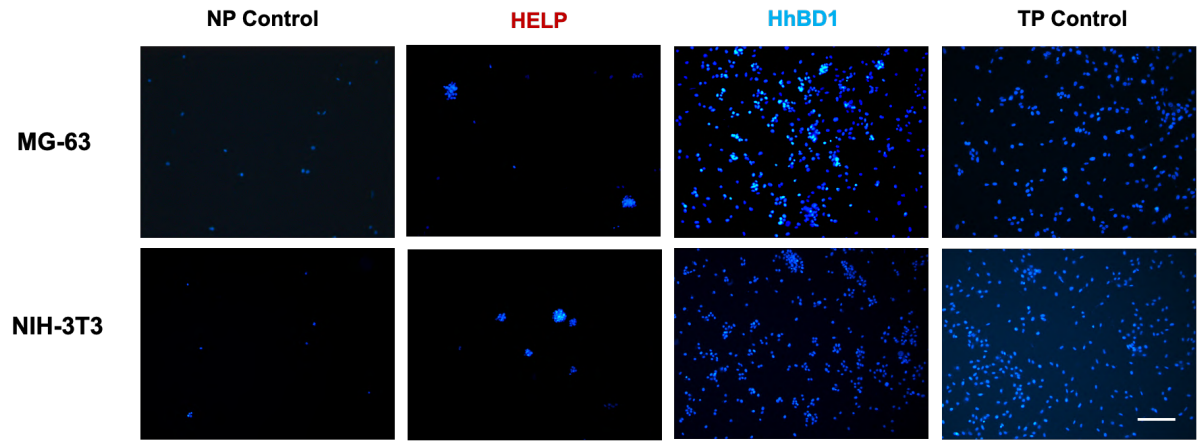

Figure S7: Fluorescence microscopy analysis of osteoblastic and fibroblastic cell adhesion on HELP and HhBD1 thin films (100 µg per 1 cm^2). Nuclei were stained with DAPI. The bar is 200 nm.

Analysis of cells seeded on HELP and HhBD1 matrices

Phase contrast and fluorescence microscopy analyses were performed on cells seeded on the HhBD1 and HELP matrices. Matrix preparation, cell seeding, and fluorescence staining were performed as described in the main manuscript (**Experimental section 4.4**).

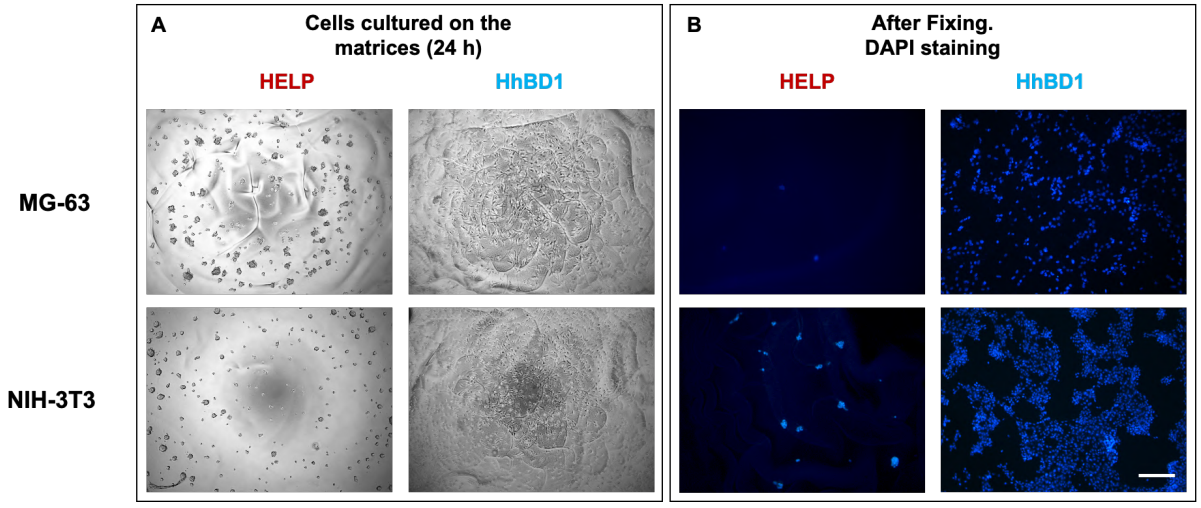

Figure S8: Fibroblast and osteoblast cell cultures on the HELP-based matrices. A) Representative contrast phase microscopy images of cell adhesion on HELP and HhBD1 matrices 24 hours after seeding. B) Fluorescence microscopy images of the nuclei of the cells attached to the matrices stained with DAPI. The bar is 200 nm.

References

1. A. Bandiera, A. Taglienti, F. Micali, B. Pani, M. Tamaro, V. Crescenzi and G. Manzini, *Biotechnol Appl Biochem,* 2005, **42**, 247-256.
2. D. E. Meyer and A. Chilkoti, *Nat Biotechnol*, 1999, **17**, 1112-1115.
3. A. Bandiera, A. Markulin, L. Corich, F. Vita, V. Borelli, *Biomacromolecules*, 2014, **15**, 416-422.
4. R. Fraczkiewicz and W. Braun *Journal of Computational Chemistry*, 1998, **19**, 319-333.

Annex III. Supporting Information Chapter 6

Table 1S: Transition temperature (T_t) and hydrodynamic diameter (D_h) of 2 mg/mL solutions at 40°C. To verify the particle diameter stability, the measurements were repeated at 1 hour intervals at constant temperature.

		T_t (°C)	D_h (T= 40°C) /nm
UELP	TRIS	25	178
	TRIS/NaCl	23	1930
HELP	TRIS	29	204
	TRIS/NaCl	33	439

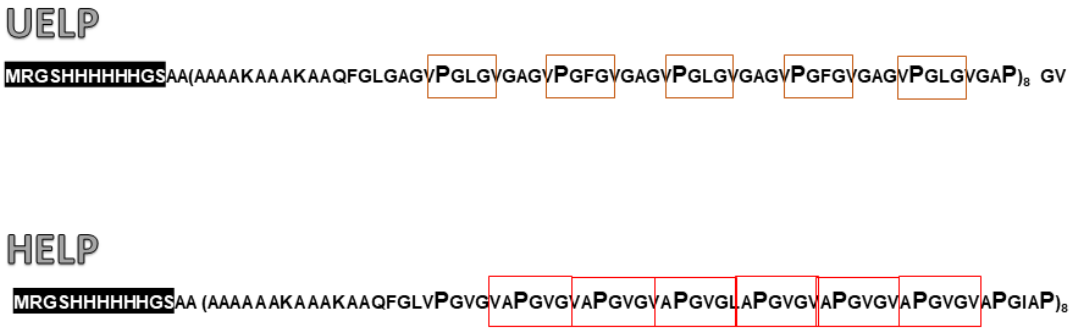

Figure 1S: Primary structure of the three human elastin-like polypeptides described in this paper. The monomers (in brackets) are repeated eight times in the final construct. In black, the his-tag at the N-terminus is evidenced. Boxed, the pentapeptidic (orange) and the hexapeptidic (red) repeats.

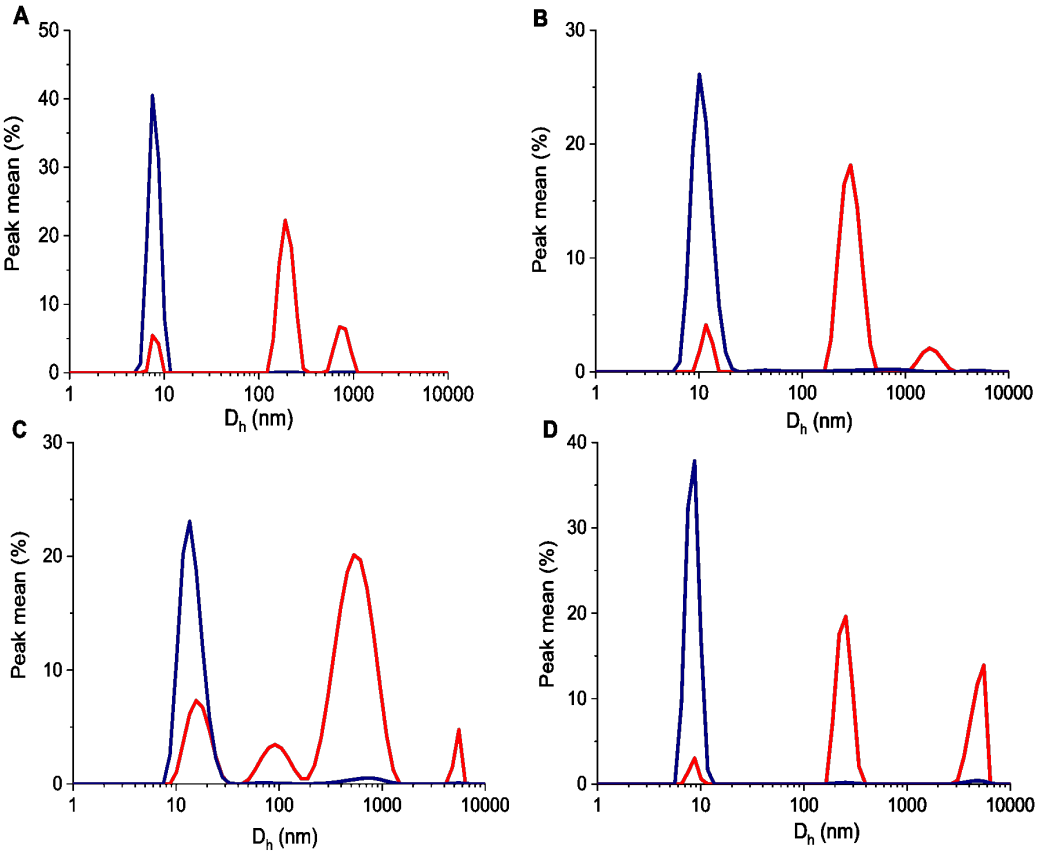

Figure 2S*:* Size distribution of the apparent hydrodynamic diameter (D_h) determined as scattering intensity (red line) and volume (blue line) at 15 °C for the following 2 mg/ml biopolymer solutions: (A) HELP Tris buffer pH 8; (B) HELP Trisl/NaCl 0.15 M buffer pH 8; (C) UELP Tris buffer pH8; (D) Tris/NaCl 0.15 M pH 8.

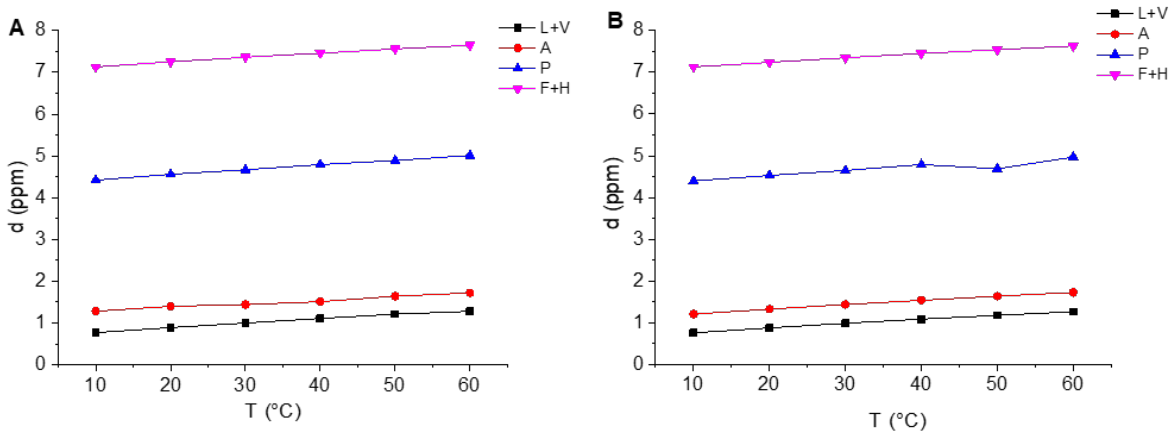

Figure 3S: Chemical shift of resonance peaks as a function of temperature for the different amino acidic residues of HELP (A) and UELP (B).

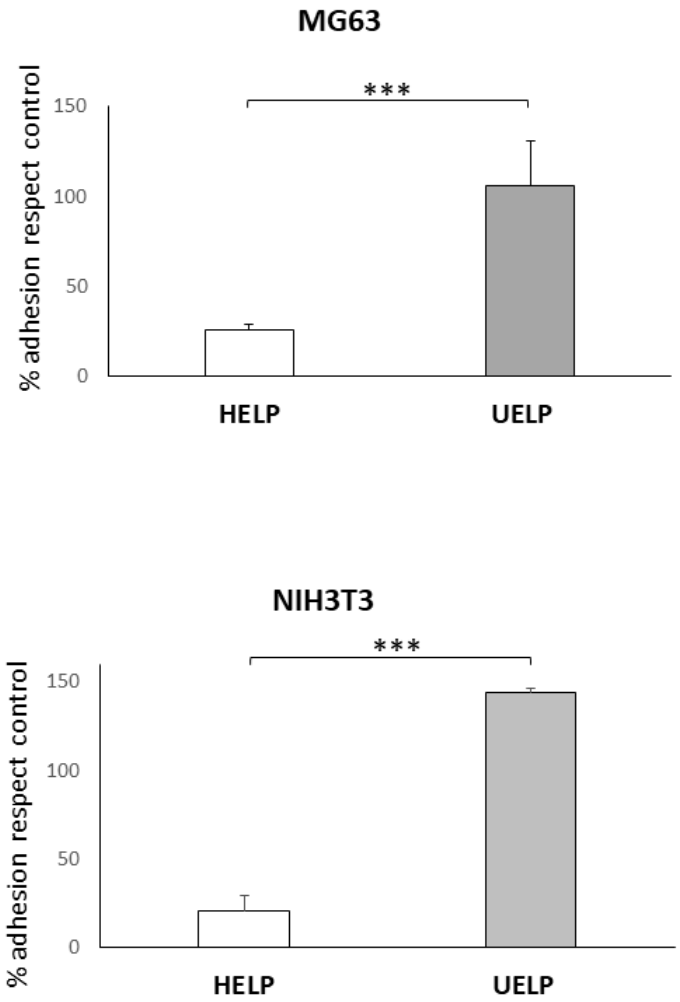

Figure 4S: Crystal violet adhesion assays of MG63 (upper panel) and NIH3T3 (lower panel) cells at 24 hours after seeding. Non-adhesive tissue culture polystyrene wells were left uncoated (control) or were coated HELP and UELP, respectively, like in Figure 10 and Figure 11. The control was the culture on tissue culture treated polystyrene. *** $p < 0.0001$; $n = 5$ via one-way ANOVA.

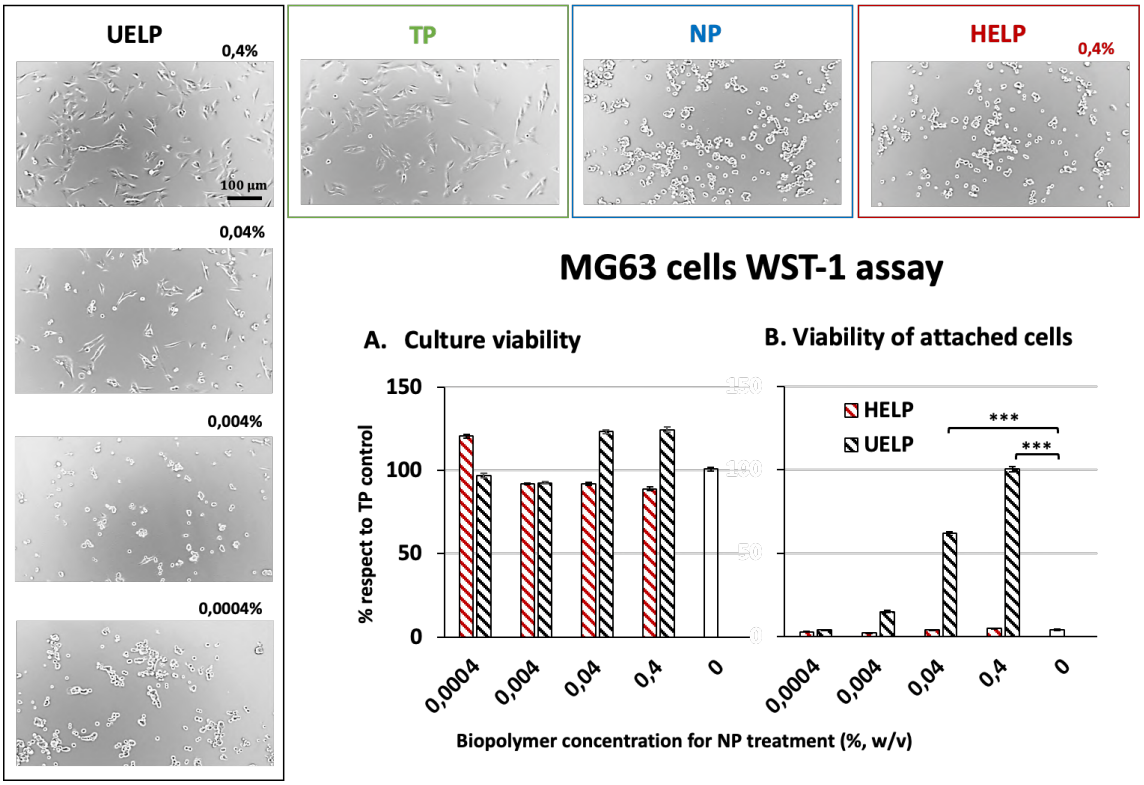

Figure 5S: Representative phase contrast images of MG63 osteoblastic cells of human origin cultured on non-treated polystyrene (NP) surfaces coated by incubation with aqueous solutions with different concentrations of UELP biopolymer (on the left, boxed in black). On the top, representative images of control cultures on tissue culture treated polystyrene (TP, green box), on NP without any coating (blue box) as well as cultures on NP coated with HELP (red box) are shown.

The coatings were prepared in a non-treated 96-well microplate by adding 100 µl of 0.22 µm -filtered aqueous solutions of biopolymer at 0.0004, 0.004, 0.04, and 0.4% (w/v) per well. After overnight incubation at 5°C, the solution was removed, and the wells were washed twice with 200 µL of sterile water and then air-dried. 100 µL of supplemented DMEM containing 5000 cells were seeded in each well. After 24 hours. The cultures were inspected by phase contrast microscopy and the images were acquired.

Cell viability after 24 hours was assessed by the WST-1 metabolic assay. Depending on the coating, after 24 hours, two different cell morphologies were observed in the cultures: unattached, rounded cells and flat and spread cells, attached to the surface. Thus, the assay was performed under two conditions, one to assess the viability of the culture (attached and unattached cells) and the other to assess the viability of the attached cells only.

A - Culture viability: 24 hours after seeding, 5 µL of WST-1 reagent were directly added to the 100 µL of culture medium in each well. After 90 min of incubation at 37°C, the absorbance was measured at 450 nm by a microplate reader.

B - Viability of the attached cells: 24 hours after seeding, the culture medium was removed and the cells were washed with 100 µL of sterile PBS to remove all non-attached cells. Then, 100 µL of supplemented DMEM containing 5 µL of WST-1 reagent were added per well. After 90 min of incubation at 37°C, the absorbance was measured at 450 nm by a microplate reader. Values were normalised to the TP control cultures.*** $p < 0.0001$; $n = 8$ via one-way ANOVA.

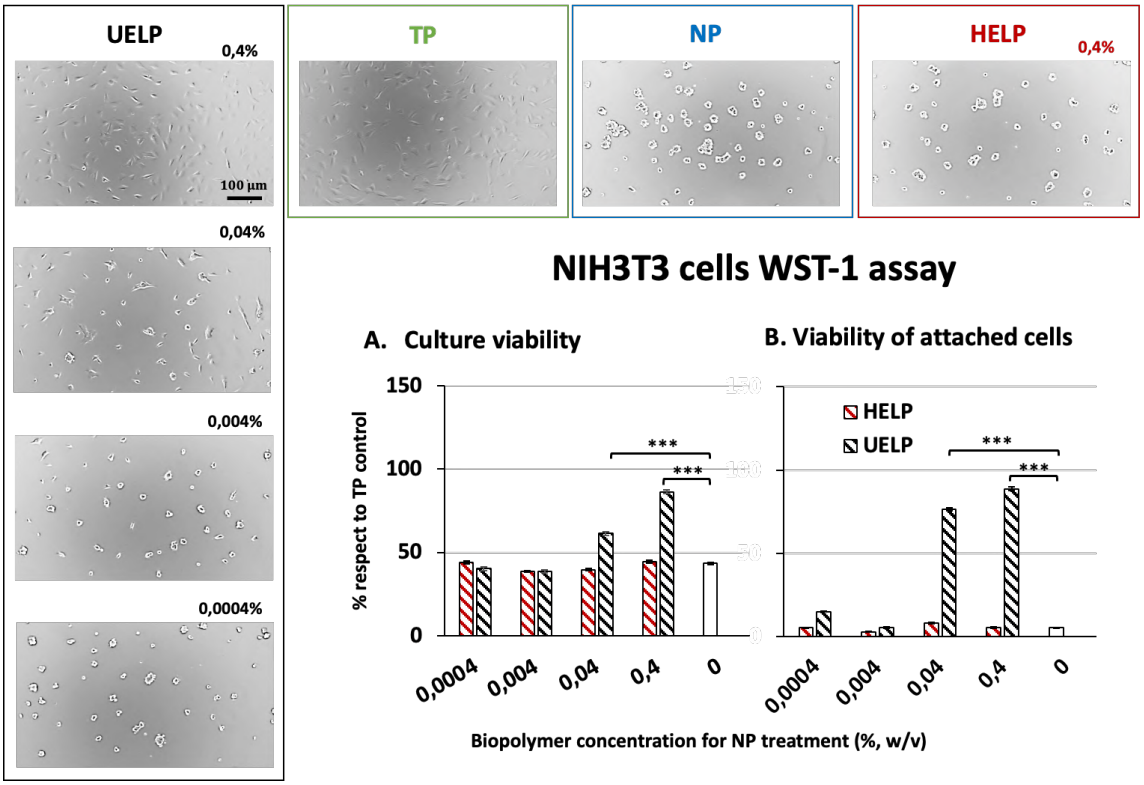

Figure 6S: Representative phase contrast images of NIH3T3 cells cultured on non-treated polystyrene (NP) surfaces coated by incubation with aqueous solutions with different concentrations of UELP biopolymer (on the left, boxed in black). On the top, representative images of control cultures on tissue culture treated polystyrene (TP, green box), on NP without any coating (blue box) as well as cultures on NP coated with HELP (red box) are shown.

A - Culture viability

B - Viability of the attached cells

Values were normalised to the TP control cultures.*** $p < 0.0001$; $n = 8$ via one-way ANOVA.

The same conditions and procedures already described for the cultures shown in the previous Figure 5S were employed for the NIH3T3 murine fibroblasts.